

PID-ACO VIBRATION CONTROLLER WITH
MAGNETORHEOLOGICAL DAMPER FOR WIND TURBINE
TOWER

MAHMUDUR RAHMAN

FACULTY OF ENGINEERING
UNIVERSITY OF MALAYA
KUALA LUMPUR

2019

PID-ACO VIBRATION CONTROLLER WITH
MAGNETORHEOLOGICAL DAMPER FOR WIND TURBINE
TOWER

MAHMUDUR RAHMAN

**THESIS SUBMITTED IN FULFILMENT OF THE
REQUIREMENTS FOR THE DEGREE OF DOCTOR OF
PHILOSOPHY**

**FACULTY OF ENGINEERING
UNIVERSITY OF MALAYA
KUALA LUMPUR**

2019

UNIVERSITY OF MALAYA
ORIGINAL LITERARY WORK DECLARATION

Name of Candidate: Mahmudur Rahman

Registration/Matric No: KHA140079

Name of Degree: Doctor of Philosophy

Title of Project Paper/Research Report/Dissertation/Thesis ("this Work"):

PID-ACO Vibration Controller with Magnetorheological Damper for Wind
Turbine Tower

Field of Study: Engineering Design

I do solemnly and sincerely declare that:

- (1) I am the sole author/writer of this Work;
- (2) This Work is original;
- (3) Any use of any work in which copyright exists was done by way of fair dealing and for permitted purposes and any excerpt or extract from, or reference to or reproduction of any copyright work has been disclosed expressly and sufficiently and the title of the Work and its authorship have been acknowledged in this Work;
- (4) I do not have any actual knowledge, nor do I ought reasonably to know that the making of this work constitutes an infringement of any copyright work;
- (5) I hereby assign all and every right in the copyright to this Work to the University of Malaya ("UM"), who henceforth shall be owner of the copyright in this Work and that any reproduction or use in any form or by any means whatsoever is prohibited without the written consent of UM having been first had and obtained;
- (6) I am fully aware that if in the course of making this Work I have infringed any copyright whether intentionally or otherwise, I may be subject to legal action or any other action as may be determined by UM.

Candidate's Signature

Date:

Subscribed and solemnly declared before,

Witness's Signature

Date:

Name:

Designation:

PID-ACO VIBRATION CONTROLLER WITH MAGNETORHEOLOGICAL DAMPER FOR WIND TURBINE TOWER

ABSTRACT

Vibration in the wind turbine tower disturbs the reliability and increase the possibility of structural damage. Therefore, researchers are very attracted to find suitable solution to minimize vibration in wind turbine tower. Two common vibration control approaches, i.e. passive and active control have the limitations to adapt low frequency, varying loading, and frequency conditions vibrations. It is thus resulted in high external energy consumption in supplying controllable current. Previous studies showed that different controllers for wind turbine vibration control are less effective when the frequency or type of disturbances vary and thus require several tuning processes. In addition, previous research works suggested that it is less effective in vibration reduction when the damper is installed at the top or at the bottom of the tower. Therefore, this research proposes a semi-active vibration control approach for wind turbine tower with optimal tuning of proportional integral derivative (PID) through ant colony optimization (ACO) algorithm and by installing a magnetorheological (MR) damper at the mid-point of the tower to overcome the limitations mentioned above. At first, appropriate dynamic model is estimated using finite difference method (FDM) and system identification process. The FDM dynamic model is found 100% fit to estimated data with reasonably good value of mean squared error (MSE) and Cross Signature Assurance Criterion (CSAC). Next, PID control parameters are optimized with ACO method based on the vibration displacement as objective function to achieve the optimal damping force which is used to encounter vibrations under different excitation frequencies and loading conditions. The placement of MR damper on the tower is then investigated to ensure structural balance and vibration mitigation at all points of the wind turbine tower. It is found that wind turbine tower vibration is reduced up 72% when the damper is placed at middle of the tower and the

selection of this optimal location is also based on considerations such as design complexity and maintenance cost. When the proposed optimized PID-ACO controller is tested under different excitations frequencies and loading conditions, results show that the semi-active PID-ACO controller reduces the tower vibration up to 83% and 68% under harmonics excitation at tower 1st mode and random disturbances respectively without the needs of re-tuning the PID parameters. This is effective in preventing structural damage of the wind turbine tower due to unexpected disturbances. This research validates the simulation results with real implementation of lab-scaled wind turbine tower under various loadings such as harmonics excitation at tower 1st mode, sweep frequencies, and random excitations under four damping environments, 1) without damper, 2) passive damper, (i.e. 0 ampere current to MR damper), 3) optimal input current to MR damper, and 4) Locked state, (i.e. high input current to MR damper). It is observed that the real implementation semi-active PID-ACO control system with MR damper reduces up to 73% and 40% of vibration displacement under harmonics excitation at tower 1st mode and random disturbances respectively.

Keywords: Ant colony optimization; Magnetorheological damper; PID controller optimization; Vibration control; Wind turbine tower

PENGAWAL GETARAN PID-ACO DENGAN MENGGUNAKAN PEREDAM MAGNETORHEOLOGI UNTUK MENARA TURBIN ANGIN

ABSTRAK

Getaran yang terhasil dalam menara turbin angin boleh mengurangkan ketahanan dan meningkatkan kemungkinan kerosakan pada struktur. Oleh itu, para penyelidik sangat tertarik dalam mencari penyelesaian yang sesuai untuk mengurangkan getaran yang terhasil dalam menara turbin angin. Dua pendekatan yang biasa digunakan dalam kawalan getaran, iaitu kawalan pasif dan kawalan aktif terbatas dalam menyelesaikan masalah dengan kekerapan yang rendah, bebanan yang berubah dan getaran dalam keadaan frekuensi. Oleh sebab itu, ia mengakibatkan penggunaan tenaga luaran yang tinggi dalam membekalkan arus elektrik yang boleh dikawal. Kajian terdahulu menunjukkan bahawa pengawal berbeza bagi kawalan getaran turbin angin dilihat kurang berkesan apabila kekerapan atau jenis gangguan berubah-ubah dan memerlukan beberapa proses penalaan. Di samping itu, kerja-kerja penyelidikan terdahulu mendapati bahawa pengurangan getaran kurang berkesan apabila peredam dipasang di bahagian atas atau di bahagian bawah menara turbin angin. Oleh itu, kajian ini mencadangkan pendekatan kawalan getaran separuh aktif untuk menara turbin angin yang menggunakan kaedah penalaan optimum turunan integral berkadar (PID) melalui algoritma pengoptimuman koloni semut (ACO) dan dengan memasang peredam magnetorheologi pada bahagian tengah menara untuk mengatasi batasan yang telah disebutkan di atas. Model dinamik yang sesuai dianggarkan terlebih dahulu dengan menggunakan kaedah perbezaan terhingga (FDM) dan proses pengenalan sistem. Model dinamik FDM didapati 100% sesuai dengan data anggaran yang mempunyai nilai kuadrat kuadrat kesilapan (MSE) dan Kriteria Penandatanganan Tanda Tangan (CSAC) yang cukup baik. Seterusnya, parameter kawalan PID dioptimumkan dengan kaedah ACO berdasarkan anjakan getaran sebagai fungsi objektif bagi mencapai daya redaman optimum yang digunakan dalam mengenalpasti getaran di bawah frekuensi pengujaan dan bebanan yang berbeza. Kemudian, kedudukan

peredam MR di menara turbin angin dikaji bagi memastikan keseimbangan struktur dan pengaliran getaran di semua bahagian menara turbin angin. Ujikaji ini mendapati bahawa getaran menara turbin angin berjaya dikurangkan sehingga 72% apabila peredam diletakkan di bahagian tengah menara dan pemilihan lokasi optimum ini juga adalah berdasarkan pertimbangan seperti kerumitan reka bentuk dan kos penyelenggaraan. Apabila pengawal PID-ACO yang dioptimumkan diuji pada frekuensi pengujian dan keadaan bebanan yang berbeza, hasil menunjukkan pengawal PID-ACO separuh aktif berjaya mengurangkan getaran menara turbin angin sehingga 83% dan 68% bagi pengujian harmonik pada mod pertama menara dan gangguan rawak tanpa perlunya penalaan semula pada parameter PID. Penemuan ini amat berkesan dalam mencegah kerosakan struktur menara turbin angin yang disebabkan oleh gangguan yang tidak dijangka. Ujikaji ini mengesahkan hasil yang diperolehi daripada simulasi dengan melaksanakan ujikaji keatas menara turbin angin di dalam makmal pada keadaan yang berbeza seperti pengujian harmonik pada mod pertama menara, frekuensi sapu, dan pengujian rawak dengan empat keadaan redaman yang berbeza, 1) tanpa peredam, 2) peredam pasif, (iaitu 0 ampere arus elektrik kepada peredam MR), 3) arus elektrik optimum kepada peredam MR, dan 4) keadaan terkunci, (iaitu semasa arus elektrik tinggi kepada peredam MR). Ujikaji ini menunjukkan pengurangan anjakan getaran sehingga 73% dan 40% bagi pengujian harmonik pada mod pertama menara dan gangguan rawak melalui penggunaan sistem kawalan PID-ACO separuh aktif beserta peredam MR.

Kata kunci: Algoritma koloni semut; Peradam magnetorheologi; Pengoptimuman pengawal PID; Kawalan getaran; Menara turbin angin

ACKNOWLEDGEMENTS

First, praise to Allah (swt), for His blessing to give me the ability and knowledge to complete the research work fruitfully.

I would like to express my deepest gratitude to my supervisor Ir. Dr. Ong Zhi Chao, for his effort, guidance, and support throughout the project. He is an expert in my research area and supervise me very closely to achieve the research objectives. Also, I must thank him for his kindness to take me as a research assistant.

Also, I must mention my co-supervisor Assoc. Prof. Chong Wen Tong and Dr. Sabariah Julai for their extensive guidance and support, without them the project would have not been successful to achieve the objectives of this research.

Thanks to all lectures who have taught me and guide to successfully finish the research. Also, I must remember all my friends and colleagues for their ideas and support.

Finally, I proudly mention my parents and family members who are always there for me when matters most, especially my mother for her love and inspiration throughout my study.

TABLE OF CONTENTS

Abstract	iii
Abstrak	v
Acknowledgements	vii
Table of Contents	viii
List of Figures	xii
List of Tables.....	xvii
List of Symbols and Abbreviations.....	xviii
List of Appendices	xxii
CHAPTER 1: INTRODUCTION.....	1
1.1 Background.....	1
1.2 Problem statement and motivation	4
1.3 Objectives	5
1.4 Contributions and significance of the research.....	6
1.5 Research flow and scope	7
1.6 Outline of the thesis	11
CHAPTER 2: LITERATURE REVIEW.....	12
2.1 Introduction.....	12
2.2 General background.....	12
2.3 Vibration control strategies.....	18
2.3.1 Passive control.....	19
2.3.2 Active control	21
2.3.3 Semi-active control.....	23
2.4 Vibration control dampers	25

2.4.1	Tuned mass damper	25
2.4.2	Tuned liquid damper	28
2.4.3	Controllable fluid damper.....	31
2.4.4	Other vibration control dampers.....	33
2.5	Modeling of wind turbine tower	34
2.5.1	Finite difference method	38
2.5.2	Finite element method	40
2.6	Magnetorheological fluid damper.....	46
2.6.1	Operating principles and classifications of MR fluid damper.....	48
2.6.2	MR damper models	52
2.7	Control scheme	54
2.7.1	Proportional integral derivative controller	56
2.7.2	Ant colony optimization method	58
2.8	Damper positioning in semi-active vibration control of wind turbine	60
2.9	Summary.....	61
CHAPTER 3: METHODOLOGY		65
3.1	Introduction.....	65
3.2	Modeling and control system of semi-active wind turbine tower	66
3.2.1	Modeling of wind turbine tower.....	67
3.2.2	Modeling of MR damper	70
3.2.3	Control scheme.....	72
	3.2.3.1 PID controller design and optimization	72
	3.2.3.2 Current controller	78
3.3	Simulation procedures	80
3.4	Equipment and experimental set up.....	81
3.4.1	MR damper and its controller.....	82

3.4.2	Optimal placement of MR damper	86
3.4.3	Sensory information and data acquisition system	87
3.4.4	Vibration test system	89
3.4.5	Experimental test rig	90
3.4.5.1	Experimental set-up for MR damper model validation.....	90
3.4.5.2	Experimental set-up for wind turbine tower vibration control..	91
3.5	Experimental procedures	92
3.5.1	Characteristics of MR damper	93
3.5.2	Semi-active vibration control of wind turbine tower	93
CHAPTER 4: RESULTS AND DISCUSSION		95
4.1	Introduction.....	95
4.2	Simulation Results	95
4.2.1	Modeling of wind turbine tower.....	95
4.2.2	Simulation model of MR damper	102
4.2.3	Optimized PID controller with ACO.....	103
4.2.4	Optimal placement of MR damper	108
4.2.5	Effectiveness of optimized PID-ACO controller under different loadings	
111		
4.2.6	Current controller	116
4.2.7	Semi-Active control response with controllable MR damper under different excitations.....	117
4.3	Experimental validation.....	132
4.3.1	Model validation.....	132
4.3.1.1	Validation of wind turbine tower model	132
4.3.1.2	Validation of MR damper model	134

4.3.2	Simulation results for wind turbine vibration control using PID-ACO control with MR damper under different loadings	138
4.3.3	Experimental results for wind turbine vibration control using PID-ACO control with MR damper under different loadings	142
4.3.4	Comparison between simulation and experimental result.....	144
CHAPTER 5: CONCLUSION AND RECOMMENDATION		147
5.1	Conclusions	147
5.2	Recommendations.....	149
	References	150
	List of Publications and Papers Presented	170
	Appendix A	171
	Appendix B	174

LIST OF FIGURES

Figure 1.1: Research flow chart	10
Figure 2.1: Content structure of the review	18
Figure 2.2: (a) Structure with Passive Energy Dissipation (PED) (T T Soong & Spencer Jr, 2002) and (b) Typical construction of passive control device	20
Figure 2.3: (a) Structure with active Control (T T Soong & Spencer Jr, 2002) and (b) Typical construction of active control device	22
Figure 2.4: (a) Structure with semi-active Control (T T Soong & Spencer Jr, 2002) and (b) Typical construction of semi-active control	24
Figure 2.5: Construction of TMD in wind turbine (Lackner & Rotea, 2011b).....	26
Figure 2.6: Comparison of wind turbine tower response between passive control and active TMD control system (Rotea et al., 2010)	27
Figure 2.7: (a) Schematic diagram of wind turbine with TLCDs, (b) TLCD model (Mensah & Dueñas-Osorio, 2014)	29
Figure 2.8: Reductions in (a) tip displacement and (b) bending moment of wind turbine tower using TLCD (Mensah & Dueñas-Osorio, 2014).....	30
Figure 2.9: Schematic diagram of VAWT with TMD/TLCD.....	31
Figure 2.10: Schematic of controllable fluid damper (Stewart, 2012).....	32
Figure 2.11: (a) The BVA and (b) Top displacement of wind tower with and without BVA (J. Li et al., 2012)	34
Figure 2.12: Free body diagram of beam with forces and moments.....	36
Figure 2.13: Multi-degree of freedom of discrete system.....	38
Figure 2.14: Cantilever Beam	38
Figure 2.15: A beam element	41
Figure 2.16: MRF magnetic particles chain-like formation with the applied magnetic field.	47

Figure 2.17: Typical MR damper configuration	49
Figure 2.18: Basic operating principle of MR dampers. Reprinted from (Geldhof, 2013)	49
Figure 2.19: MR damper modes: (a) Valve mode (b) Direct shear (c) Squeeze mode....	50
Figure 2.20: MR damper classification	51
Figure 2.23: Wind turbine vibration control response using (a) H-infinity (Karimi et al., 2010) and (b) Robust MPC controller (Staino & Basu, 2013b).....	55
Figure 2.24: Structure of PID controller	56
Figure 2.25: State space graph for ACO	59
Figure 2.26: Flowchart of ACO method	60
Figure 3.1: Block diagram of semi-active control system	65
Figure 3.2: Flow chart of research methodology	66
Figure 3.3: Schematic of the wind turbine tower as cantilever beam	68
Figure 3.4: Structure of Modified Bouc-Wen model	70
Figure 3.5: Block diagram of PID controller optimization	72
Figure 3.6: Flow chart of PID parameter optimization process	74
Figure 3.7: Block diagram of control system with and without PID controller in SIMULINK	77
Figure 3.8: Current controller	79
Figure 3.9: MR damper RD-8041-1	83
Figure 3.10: MR damper assembly drawing (courtesy: LORD technical data sheet for RD- 8041-1)	84
Figure 3.11: Wonder Box Device Controller- RD-3002-03	85
Figure 3.12: Voltage and current relationship (Measured) in the Wonder Box Device Controller- RD-3002-03	86
Figure 3.13: Placement of MR damper	87

Figure 3.14: Data acquisition hardware	89
Figure 3.15: Vibration test system	90
Figure 3.16: Experimental setup for characteristic testing of MR damper	91
Figure 3.17: Experimental setup for wind turbine tower vibration control	92
Figure 4.1: Frequency response function of wind turbine tower	96
Figure 4.2: Input force and uncontrolled response of the tower under harmonic excitation	97
Figure 4.3: (a) Frequency response function and (b) pole-zero map of estimated models using FDM	99
Figure 4.4: (a) Frequency response function and (b) pole-zero map of estimated models using FEM	101
Figure 4.5: Force characteristics under different current inputs (0-1A)	103
Figure 4.6: Input force and uncontrolled response of the tower	104
Figure 4.7: (a) Error, (b) Computational time, (c) Control force, and (d) Uncontrolled and controlled response using Z-N, PSO and ACO tuned parameter at 20 th element of the tower.....	107
Figure 4.8: Desired force at 5 th , 10 th , and 15 th elements of the tower	109
Figure 4.9: Tower Response at 20 th elements for damper at 5 th , 10 th , and 15 th elements of the tower.....	110
Figure 4.10: Uncontrolled, passive, and PID-ACO control response of 20th element of the tower for sinusoidal disturbance at 1 st mode.....	113
Figure 4.11: Uncontrolled, passive, and PID-ACO control response of 20th element of the tower for random disturbance	115
Figure 4.12: Semi-active vibration control response of wind turbine tower	120
Figure 4.13: Required current for MR damper when input force at (a) 50N, (b) 80N and (c) 100N	122

Figure 4.14: Force vs Displacement for input force at (a) 50N, (b) 80N, and (c) 100N	123
Figure 4.15: Desired and actual control force for input force at (a) 50N, (b) 80N, and (c) 100N	123
Figure 4.16: Controlled and Uncontrolled responses for input force at (a) 50N, (b) 80N, and (c) 100N	124
Figure 4.17: Required current for MR damper when input force at 2Hz, 4.68Hz, and 6Hz	125
Figure 4.18: Force vs Displacement (Input force at 2Hz, 4.68Hz, 6Hz)	126
Figure 4.19: Desired and actual control force for input force at (a) 2Hz, (b) 4.68Hz, and (c) 6Hz	127
Figure 4.20: Controlled and Uncontrolled responses for input force (2Hz, 4.68Hz, 6Hz)	127
Figure 4.21: Semi-active vibration control response of wind turbine tower under random excitation	131
Figure 4.22: Experimental and Simulation result: force vs displacement under different current inputs	134
Figure 4.23: Experimental and Simulation result: force vs time under different current inputs	135
Figure 4.24: Energy dissipation of MR damper for different current inputs	137
Figure 4.25: (a) Current; (b) Desired vs Actual force of MR damper	139
Figure 4.26: Simulation result: Tower response at 20 th elements under sinusoidal force @1 st mode at Controlled, passive, and locked state	139
Figure 4.27: Simulation result: Tower response at 20 th elements under chirp force (1-10Hz) at Controlled, passive, and locked state	140

Figure 4.28: Simulation result: Tower response at 20 th elements under random force at Controlled, passive, locked, and uncontrolled state	141
Figure 4.29: Experimental result: Tower response at 20 th elements under sinusoidal force @1 st mode at Controlled, passive, and locked state	143
Figure 4.30: Experimental result: Tower response at 20 th elements under chirp force (1-10Hz) at Controlled, passive, and locked state	143
Figure 4.31: Experimental result: Tower response at 20 th elements under random force at Controlled, passive, locked, and uncontrolled state	143

LIST OF TABLES

Table 2.1: Comparison between HAWT and VAWT	15
Table 2.2: Various MR damper designs and working principles	52
Table 2.3: Calculated error for MR damper models(J. B. F. Spencer et al., 1996)	54
Table 2.4: Effect of increasing the PID parameters	58
Table 2.5: Research gap and proposed study	63
Table 3.1: Properties of Cantilever Beam	68
Table 3.2: MR damper parameters	71
Table 3.3: Input parameters of ACO algorithm for tuning PID controller	77
Table 3.4: List of Instruments	82
Table 3.5: Typical properties of RD-8041-1 MR damper (courtesy: LORD Corporation technical data sheet for RD-8041-1)	84
Table 3.6: Electrical properties of RD-8041-1 MR damper (courtesy: LORD technical data sheet for RD-8041-1).....	85
Table 4.1: Modal properties of the structure	96
Table 4.2: Evaluation of transfer functions of wind turbine tower modeled by FDM....	98
Table 4.3: Evaluation of transfer functions of wind turbine tower modeled by FEM ..	100
Table 4.4: Comparison of FDM and FEM modeling	102
Table 4.5: PID parameters and outputs of Z-N, ACO and PSO tuning method	105
Table 4.6: Consistency test of PID parameters using ACO method	108
Table 4.7: Comparison between uncontrolled and controlled system	132
Table 4.8: Comparison between experimental and simulation models.....	133
Table 4.9: Comparison between simulation and experimental result	145

LIST OF SYMBOLS AND ABBREVIATIONS

Symbols

m	:	Mass
c	:	Damping co-efficient
x	:	Displacement in x-axis
$F(t)$:	External force
E	:	Modulus of elasticity
I	:	Moment of Inertia
ρ	:	Density
l	:	Beam height
S	:	Cross section area
k	:	Spring co-efficient
t	:	Time
V	:	Shear force
M	:	Bending moment
p	:	Transverse load
ω_n	:	Natural frequency
y	:	Displacement in y-axis
L	:	Length of the beam
θ	:	Angle
N	:	No of elements
C	:	Linear rigidity
H	:	Shape function
$[M]$:	Mass matrix
$[K]$:	Stiffness matrix
$[\zeta]$:	Damping ratio matrix

U	:	Rotational displacement
Λ	:	Strain energy
D	:	Second Derivative
Π	:	Total potential energy
T	:	Kinetic energy
γ	:	Mass per unit length
x_0	:	Initial displacement
α	:	Evolutionary coefficient
β, n, A, γ	:	Adjustable parameters for hysteresis loop
c_1	:	Dashpot
c_0	:	Viscous damping
K_p	:	Proportional control parameters of PID
K_i	:	Integral control parameters of PID
K_d	:	Derivative control parameters of PID
e	:	Error
$u(t)$:	Control force
X	:	Optimization parameters
W	:	Subspace
W_{ant}	:	Total no of Ants
T	:	Single ant
h	:	Length of subspace
P_{ij}	:	Probability
τ_{ij}	:	Amount of pheromone
ρ	:	Decay Parameter
Q	:	Quantity of pheromone

f_{best}	:	Objective function
τ_0	:	Initial value of pheromone
F_{exc}	:	Excitation force
F_{act}	:	Actuating control force
$H_f^X(\omega)$:	Experimental frequency response function
$H_f^A(\omega)$:	Numerical frequency response function
i	:	Current
α, c_0, c_1	:	Current dependent MR damper parameters
F_d	:	Desired force
F_a	:	Actual force
Tf	:	Transfer Function

Abbreviations

ACO	:	Ant Colony Optimization
BVA	:	Ball Vibration Absorber
CSAC	:	Cross Signature Assurance Criterion
DAC	:	Disturbance Accommodating Control
DAQ	:	Data Acquisition
EMA	:	Experimental Modal Analysis
ER	:	Electrorheological
FDM	:	Finite Difference Method
FEM	:	Finite Element Method
FRF	:	Frequency Response Function

HAWT	:	Horizontal Axis Wind Turbine
LQG	:	Linear Quadrative Gaussian
LQR	:	Linear Quadrative Regulator
MIMO	:	Multiple Input Multiple Output
MPC	:	Model Predictive Control
MR	:	Magnetorheological
MRF	:	Magnetorheological Fluid
MSE	:	Mean Squared Error
MTLCD	:	Multiple Tuned Liquid Column Damper
MTMD		Multiple Tuned Mass Damper
PDE	:	Partial Differential Equation
PI	:	Proportional Integral
PID	:	Proportional Integral Derivative
PSO	:	Particle Swarm Optimization
RMS	:	Root Mean Square
SATMD	:	Semi-active Tuned Mass Damper
STLCD	:	Single Tuned Liquid Column Damper
TF	:	Transfer Function
TLCD	:	Tuned Liquid Column Damper
TLD	:	Tuned Liquid Damper
TMD	:	Tuned Mass Damper
UTM	:	Universal Testing Machine
VAWT	:	Vertical Axis Wind Turbine
WT	:	Wind Turbine
Z-N	:	Ziegler-Nichols

LIST OF APPENDICES

Appendix A: Effectiveness of PID-ACO controller for vibration control of wind turbine tower under different loadings.....	168
Appendix B: Experimental result for nonlinear characteristics of MR damper under different stroke lengths and velocities.....	171

University of Malaya

CHAPTER 1: INTRODUCTION

1.1 Background

Wind turbine (WT) energy generation technology is one of the feasible and fastest growing renewable energy sources at present. Electricity generation using wind turbines is an active research field and it is becoming more promising and acceptable method. Wind turbines are widely utilized to generate electricity using global wind resource with technology advancements. Many types of wind turbines are developed to harvest wind energy. To enhance the performance of wind turbine power production, reliability and longer lifetime needs to be ensured. One of the factors reducing efficiency of wind turbines is structural vibration. The vibration in the wind turbines not only leading to structural damage but also increasing operating and maintenance cost which limits the power output significantly. Wind turbine tower responses are analyzed due to wind loading at (Chen et al., 2009) and maximum displacement is found at the top of the tower. Vibration in the wind turbine tower mainly occurs due to additional weight on top of the tower, disturbance from rotating blades and non-determinant wind excitations. Vibration of a system cannot be destroyed but can be reduced or converted to energy using appropriate strategies. Vibration control system improves structural response of wind turbines and reliability which has impact on lifetime of the components. Lowering the vibration amplitude of a system will provide a lesser amount of noise, assure user, and operating comfort, maintain the high performance and production efficiency. These will assist the system to prolong the lifetime of an industrial structure or machinery. Also, vibration control enhances the performance of wind turbines providing suitable work environment without external disturbance. Different types of control approach, (i.e. passive, active, or semi-active (Housner et al., 1997)) are investigated in the last years to solve the vibration problems of wind turbines. Different types of devices and their control techniques are also presented to implement the above-mentioned control approaches.

Different vibration control approaches, actuating devices, and actuating force controllers which are proposed to reduce vibration of wind turbines in the past. Fitzgerald and Basu presented a numerical analysis of active control system of wind turbine tower/nacelle vibration using tuned mass damper (TMD) (B. Fitzgerald & Basu, 2016). The TMD is placed inside the turbine nacelle which is controlled with linear quadratic regulator (LQR) controller. The wind turbine model also includes soil-structure interaction and the excitation is subjected to gravity and turbulent aerodynamic loadings. The result shows that the peak to peak displacement is reduced by 83% compared to the uncontrolled and passive control system. Brodersen et al. presented an investigation of TMD as an active control for tower displacement control of wind turbine (Brodersen et al., 2017). A frequency tuning method is introduced to control the active TMD. Murtagh et al. also investigated a TMD but as passive control approach by placing the damper at top of the wind turbine tower for vibration mitigation under drag based loadings. The result shows that the peak displacement is reduced by 20% compared to the uncontrolled case.

Tuned liquid column damper (TLCD) is also a useful damping device which is previously implemented for wind turbine vibration control. Mensah and Dueñas-Osorio implemented a TLCD on top of the tower with the nacelle to control the vibration amplitude which shows a reduction of 53% reduction of peak displacement of the tower (Mensah & Dueñas-Osorio, 2014). Colwell and Basu investigated the TLCD on a multiple-degree-of-freedom wind turbine model to mitigate vibration under large wind and wave excitations and the result shows a reduction up to 55% in the peak response of the tower compared to the system without TLCD (Colwell & Basu, 2009). Rotational spring was used in these studies to describe SSI in wind turbine models and a TMD was attached inside turbine nacelle to minimize vibration of wind turbine tower. TLCD is also

implemented in wind turbine blades for mitigating edgewise vibration (Z. Zhang et al., 2015). Karimi et al. also investigated TLCD as semi-active damping device for wind turbine tower vibration control (Karimi et al., 2010). A feedback control system with H_∞ control method is used in the study to achieve the desired reduction of vibration on the tower. In another study, Karimi et al. also investigated modern control such as linear quadratic regulator (LQR) and linear quadratic Gaussian (LQG) for wind turbine vibration control applications (Eide & Karimi, 2009).

Zhang et al. investigated another effective damper which is called as ball vibration absorber (BVA) (Z.-L. Zhang et al., 2013) to suppress wind turbine vibration through shake table test on a 1/13 scaled wind turbine model theoretically and experimentally. The experimental result shows that 39% of displacement is reduced by using BVA (J. Li et al., 2012). A passive system equipped with rolling-ball damper is investigated at (J.L. Chen & C. T. Georgakis, 2013) to a 1/20 scaled wind tower model. The proposed damper is investigated under three different loading cases such as over speed, extreme operating gust, and parking.

Smart material dampers like magnetorheological (MR) damper is popular in vibration control for automotive applications but its use in a wind turbine is limited. Kirkegaard et al. presented simulation and experimental study of semi-active vibration control of wind turbine tower using MR damper (Kirkegaard et al., 2002). In this study, the control gain is computed with the H_2 /LQG controller and the required voltage for MR damper is computed with an optimal control algorithm. Recently, Martynowicz investigated MR damper as semi-active vibration control of wind turbine tower by placing the MR tuned vibration absorber on top of the tower (P. Martynowicz, 2015). For experimental study, the modified ground-hook control is implemented to find required voltage of MR damper.

1.2 Problem statement and motivation

Different solutions are implemented for vibration control of wind turbine tower and blades in past. In these studies, different types of control algorithm are used to find desired control force to counter vibration amplitudes. Among them, PID, LQR/LQG controllers are mostly implemented, however, the controller gains are generally tuned with trial and error methods. Also, the effectiveness of these controllers at different frequencies and amplitudes is not provided. This is important for vibration control problems for structures like wind turbines where high vibration may occur at different excitation frequencies. Therefore, it is required to investigate whether the controller reduces vibration when the excitation frequency/amplitudes varies. PID controller is easy to implement but effective in vibration control problems where the controller gains are required to be tuned properly. However, it is previously investigated that this controller cannot adapt when the excitation frequency varies.

Placement of MR damper on the vibrating system is another important factor in semi-active vibration control method which ensures maximum vibration reduction with minimum input current. Previous studies showed that for wind turbines dampers are placed either on top of the tower as tuned mass damper (P. Martynowicz, 2016) or at the ground (Caterino et al., 2016). Damper on top of tower produces extra mass inside nacelle of HAWT where generators, control box etc. are installed. Moreover, in the case of heavy wind or small earthquake, vibration occurs throughout all the points of the tower including base. In this circumstance, damper on top cannot provide required counter force to reduce vibration efficiently. On the other hand, damper installed at the base can efficiently reduce the base displacement due to external disturbances, however, for tall horizontal axis wind turbines, vibration occurs from top/base and transfers to other points of the tower. Also, vibration on top of the tower due to disturbances from blades, generators cannot be reduced efficiently if the damper is installed at the base. Therefore,

an optimal position of MR damper should be investigated for enhancement of vibration reduction of wind turbine tower from top to base. Therefore, based on the previous studies, research gaps are identified based on vibration control under different excitation frequencies, tuning process of vibration controller, and position of MR damper. Various control policies have been investigated for wind turbine vibration control such as PID, LQR, H-infinity etc. However, the effectiveness of these controllers at different frequencies (including natural frequency) is not provided. Various tuning processes have been investigated for vibration controller such as Ziegler-Nichols, Cohen Coon etc. The controller gains are generally tuned with trial and error methods. Also, for tuning process, step input excitation is used for tracking the error between the reference and actual input. Tuning process using for harmonic force with natural frequency has not been investigated. The investigation for optimal positioning of MR damper is limited. The MR damper at mid-point of the tower has not been investigated previously. Therefore, this research proposed to fulfil the need to improve the wind turbine structure with the aim of maximum vibration reduction based on the identified research gaps.

1.3 Objectives

The main purpose of this study is to investigate semi-active MR damper to mitigate wind turbine tower vibration with naturally optimized PID controller which can offer maximum vibration reduction under different excitation frequencies, including natural frequency, and different types of loadings. This research project aims to address the stated research problems in some areas as described next.

1. To model and estimate the appropriate dynamic transfer function of a semi-active vibration control system of wind turbine tower with finite difference method and system identification process.

2. To design and optimize PID controller using the nature-inspired algorithm, i.e. ACO for semi-active vibration control system with MR damper under different excitation frequency and different types of loadings.
3. To investigate the optimal position of MR damper on wind turbine tower.
4. To experimental validate the simulation performance of the proposed semi-active vibration control approach under optimal placement of MR damper on a constructed wind turbine test rig.

1.4 Contributions and significance of the research

- i. In the first objective, Finite difference method (FDM) is used to solve the partial differential equations of wind turbine tower since it is simple and easy to model but provide a better model of the structure for transverse vibration application. The modeling of the beam using FDM is compared with finite element model (FEM) result to show the effectiveness of the modeling and it is also verified using system identification process. System identification process is utilized to find a proper dynamic model of wind turbine tower to implement control methods. Identified models from FDM results are compared to get the best-fitted model.
- ii. In the second objective, desired force response to counter vibration amplitude and suitable current input signal for MR damper are achieved using PID and PI controller respectively. ACO algorithm is implemented in this study to optimize PID parameters. The effectiveness of ACO algorithm is validated by comparing its performance with Ziegler-Nichols (Z-N) and particle swarm optimization (PSO). The parameters of ACO are identified properly to adapt with wind turbine environment. The proposed PID-ACO controller provides optimal control parameters can overcome the limitation of low vibration

reduction under excitation force at natural frequency where resonance may occur and limitation of low adaptability when excitation frequency varies.

- iii. In the third objective, the optimal position of MR damper on the wind turbine tower is investigated based on the vibration reduction rate, design complexity, and maintenance cost. The control force for damper, and wind turbine tower responses are achieved for three different positions of MR damper such as at the top, at mid-point and at the base. The responses are compared to find suitable position of MR damper. This research investigates the MR damper at mid-point of wind turbine tower as optimal position of MR damper.
- iv. In the fourth objective, simulation results of the proposed vibration control approach are validated using a constructed wind turbine test rig. The wind turbine tower responses are observed under harmonic excitation (@ 1st mode) to encounter the concept of resonance, chirp excitation to verify the proposed PID-ACO controller's effectiveness for different frequencies, and random excitation for any possible external disturbances such as wind/wave loadings. The wind turbine model is validated with an experimental model. The MR damper model is also validated with experimental characteristic analysis of MR damper. The wind turbine tower response is also observed under three types of damping environments: 1) Passive damper (0 ampere current to MR damper), 2) Optimal input current, and 3) Locked state (high input current to MR damper).

1.5 Research flow and scope

This research deals with designing and developing semi-active vibration control of wind turbines. Three important phases of this research are modelling semi-active vibration

control system, development of controllable semi-active control system with MR fluid damper and development of an experimental model of wind turbines integrated with proposed vibration control system. The flowchart of the research is presented in Figure 1.1.

Previous studies on wind turbine vibration control, proposed control system and damping devices are analyzed to design a new and effective control method for maximum vibration control under various disturbance and damping environments. MATLAB, a numerical computing environment, is utilized for system modeling, system identification, control system design and simulation of the proposed system. The modeling of the beam using FDM is compared with FEM result to show the effectiveness of the modeling and it is also verified using system identification process. System identification process is utilized to find a proper dynamic model of wind turbine tower to implement control methods. Selected model of wind turbine tower is simulated under different loads to analyze and design a controller for the actuator.

Suitable controller design is very important for vibration control problems for structures like wind turbines where high vibration may occur for excitation frequencies. Therefore, it is required to investigate whether the controller can reduce vibration when the excitation frequency varies. PID controller is easy to implement but effective in vibration control problems where the controller gains are required to be tuned properly. However, it is previously investigated that this controller cannot adapt when the excitation frequency varies. In this study, optimal control parameters of PID are acquired using the evolutionary algorithm, ACO to achieve desired vibration control force. For tuning process, step input excitation is used for tracking the error between the reference and actual input. But, sinusoidal input force at 1st mode is used in this study so that best control parameters are achieved to counter the high vibration amplitudes. The proposed

PID-ACO control system is compared with passive control and uncontrolled system to verify its effectiveness under different loadings.

The position of the external damper is another important design factor to ensure maximum vibration reduction with low input current and low maintenance cost. This study will also investigate the different position of MR damper on the tower to provide optimal force to the tower to reduce vibration. The proposed control method can increase the power production capability of the wind turbine by controlling vibration significantly on the tower due to external disturbances from blades, generator, and heavy winds.

The PID-ACO controller provides optimal control force to ensure maximum vibration reduction. The proposed controller controls the tower vibration when the excitation frequency varies. This is important to investigate because this type of excitation force is very suitable for vibration control of variable speeds system like wind turbine. Proposed control method is investigated under different excitation frequencies and amplitudes. The effectiveness of the proposed semi-active PID-ACO controller is also investigated under different loading conditions such as sinusoidal and random excitation force to ensure that the controller can reduce vibration for any possible disturbances to tower.

A lab-scaled wind turbine tower vibration control system with MR damper is built to validate the simulation results. Aluminum beam is used to represent wind turbine tower. A vertical axis wind turbine is placed on top of the tower. The MR damper is installed at the middle of the tower.

Experimental model analysis (EMA) is conducted to find the modal properties of the tower. The natural frequencies, damping ratio and uncontrolled responses are compared with simulated model. The model parameters are modified based on the experimental data. The MR damper model is also validated using the experimental characteristic analysis of MR damper using universal testing machines.

Different types of excitation forces such as sinusoidal, chirp and random etc. are implemented on wind turbine tower to investigate the performance of the proposed vibration control method. The simulation results under these excitations are validated with experimental results. The result of the proposed control system is also compared with ‘uncontrolled’, ‘passive control’, and ‘locked’ states of MR damper.

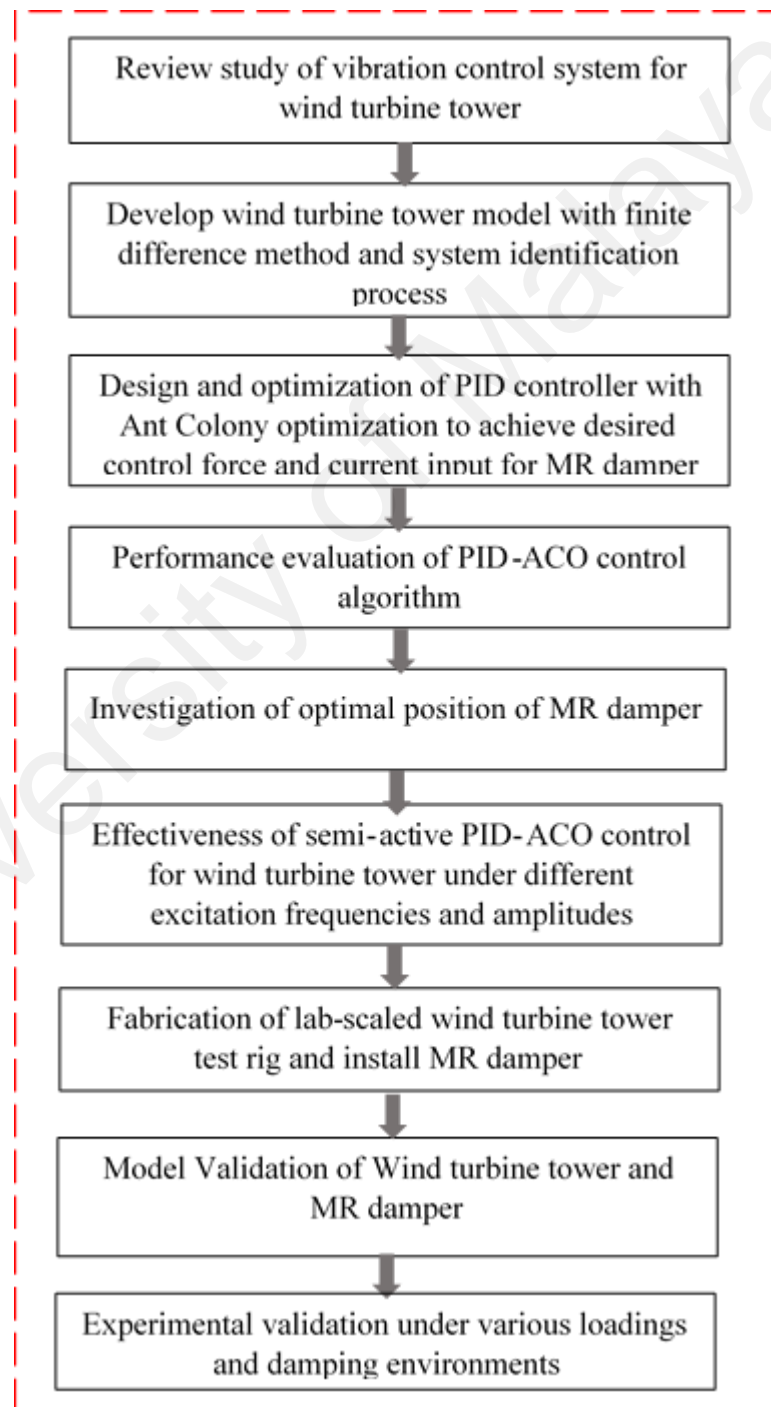


Figure 1.1: Research flow chart

1.6 Outline of the thesis

This thesis is subdivided into five chapters.

A brief background and outlines are provided in **chapter one**. An overview of this research work and some keywords of this research are focused in this chapter. The research gaps and the proposed studies are presented in this section. At the end, the objectives, research flow and scope of this research are elaborated.

Previous studies on wind turbine vibration control are presented and analyzed in **chapter two**. An overview of MR fluid and its applications are discussed in this chapter. Different types of damper and control algorithms which are proposed previously are critically analyzed to find the find a novel solution to fulfil the research gap.

Chapter three explains the research methodology of the research which includes modeling of semi-active wind turbine tower vibration control system with optimal control algorithm to suit different loading conditions and maximum vibration reduction, and experimental set up of lab-scaled wind turbine model. Also, the design and optimization of suitable control methods are discussed in this chapter.

In **chapter four**, simulation and experimental results are discussed. Both the wind turbine model and the MR damper model are validated using the experimental results. The performance of the proposed vibration control method is analyzed with respect to the objectives set.

Chapter five is the last chapter of this research which explains contributions, outcomes, and limitations of this research. To end the chapter, recommendations for future work in semi-active vibration control fields are presented.

CHAPTER 2: LITERATURE REVIEW

2.1 Introduction

In this chapter, the background and the literature review of this research are presented. At the beginning of the chapter different types of wind turbine structures and vibration problem are described. Then the main vibration control strategies such as Passive, Active, and Semi-active control systems are compared and discussed. Next, MR fluid and its applications are explained. Then it directs to the presentation of different MR damper models which will allow selecting an appropriate model to use for this research. These steps follow the wind turbine tower modeling represented by the cantilever beam. System identification process will be presented for finding a dynamic model of wind turbine tower. The mathematical theories for different modelling methods of wind turbine tower are also presented in this chapter. This discussion will then move to implement control schemes on wind turbine tower. The chapter will conclude with the description of proposed controllers for implementation.

2.2 General background

Power generation using wind turbines is an effective and potential source to meet the electricity requirement in all over the world nowadays. Wind energy is utilized for different purposes such as rural electrification, street lamp post, to charge electric vehicles and even to operate wind turbines to generate electricity. Wind energy is widely used in rural electrification mainly at and less developed country and low-income households. Several studies presented utilizations of wind energy as a renewable energy source for rural electrification (Bekele & Tadesse, 2012; Lahimer et al., 2013; Leary et al., 2012; Werapun et al., 2014). Wind energy is also suggested to be used to charge electric vehicles in Netherlands in 2020 (Bellekom et al., 2012). Wind energy was also used for outdoor/street lighting system (Malaya, 2014). There are many different types of wind

turbines were proposed and developed in the past depending on the orientations of the blade and configurations. But they can be grouped into two as named as horizontal axis wind turbines (HAWTs) and vertical axis wind turbines (VAWTs) based on the orientation of their axis of blade rotation. HAWTs have been most implemented wind turbines technology since few decades; however, VAWTs have also become very prominent in this technology in the recent decades. The initial development of HAWTs and VAWTs were studied in (Shikha et al., 2005). The blades of the HAWTs rotate horizontally and perpendicular to the wind. Researchers proposed different types of HAWTs based on different methods and configurations to enhance its efficiency (Bai et al., 2013; Bofares & Elmnefi, 2014; Fischer et al., 2014; Goundar & Ahmed, 2013; Lignarolo et al., 2014; Sedaghat & Mirhosseini, 2012; Velázquez et al., 2014). HAWTs are typically tall which assists the system to face much higher and strong winds to generate power effectively. However, installation and maintenance cost of HAWTs is relatively high because the installation kits were placed on the top of the tower inside the nacelle. So, it becomes difficult and costly when it needs to be repaired. On the other hand, VAWTs consist of blades with the vertical axis of rotation and they do not have to be arranged to any specific direction to face the wind. Another advantage of the VAWTs is that the installation box which includes generator, gearbox etc. can be placed in the basement of the tower. It makes the maintenance and repair work easy and simple. The advantages, different designs, and optimizations of VAWT were presented in several research papers (Chong et al., 2013; Scheurich & Brown, 2013; Vita et al., 2013; Z. J. Yang et al., 2014). Different designs and configurations of VAWTs were also reviewed in (Aslam Bhutta et al., 2012; Borg et al., 2014). Darrieus type wind turbine has the highest value of efficiency although problems of low starting torque and poor building integration are the major drawbacks of the system. This type of wind turbine is called as 'lift type' wind turbine where lift forces on the blades result the rotor to rotate and produce

electricity. Savonius rotor type wind turbine is another type of VAWT which has less efficiency value than darrieus type and not used for high power applications. However, the self-starting capability is the important advantage of savonius type wind turbine compared to lift-type wind turbines. Four aerodynamic models for VAWT were analyzed at (Borg et al., 2014) to highlight the performances as well as advantages and disadvantages. The blade element momentum and cascade models have good power predictions capability and fast computational times but may fail to predict instantaneous blade forces. Whereas, vortex and panel models can simulate the wake of the VAWT and have the capability to model a rotor which consists multiple rotating bodies. The rotation axis for a horizontal wind turbine is horizontal or parallel to the ground. For big wind areas, HAWTs are very popular and produces more energy. However, HAWTs need big space and are generally heavier which are not efficient enough in turbulent winds. HAWTs are generally installed in high wind areas, especially in sea areas. The rotation axis of a vertical wind turbine is perpendicular to the ground and mostly used in residential applications. VAWTs work well under turbulent wind conditions, thus VAWTs are efficient where the wind is not consistent. VAWTs can generate power from low wind and they are generally positioned in the low wind urban environment. Likewise, HAWT, VAWT do not have a tower and situated on the ground where the wind is low and turbulent. Also, the direction of blade rotation encourages the structure to be at low wind environment for better performance. There are several other factors that affect the efficiency of HAWTs and VAWTs. Few factors and possible solutions for them were presented in (Ahmed & Cameron, 2014). Several challenges have been highlighted for performance degradation of wind turbine technology which are maintaining performance efficiency, intermittent nature of wind supply, global industrialization, fossil fuel energy market, social acceptability of on-shore wind power, cost, technical and climate change of off-shore wind power, competition from other clean energy competitors, policy

instability etc. The possible solutions were suggested in the study to enhance the performance of wind turbines and some of the important solutions are proper maintaining of different machining parts such as blades, gearbox, bearing etc. to ensure good performance, ensuring adequate nature wind supply, reducing noise of heavyweight wind turbines, reducing cost, and solve technical issues such as place of installation, designs etc. Furthermore, the HAWTs need higher wind speeds for generating a smaller amount of electricity and thus it becomes less important in the urban environment. HAWTs and VAWTs have different efficiency level based on their direction of rotation, configurations and they were compared in (S Eriksson et al., 2008; Ishugah et al., 2014; Pope et al., 2010b). Table 2.1 shows the comparison between HAWT and VAWT to highlight their advantages and disadvantages based on configurations and efficiency.

Table 2.1: Comparison between HAWT and VAWT

HAWT	VAWT
Rotating axis of the wind turbine remains horizontal, or parallel with the ground	Rotating axis remains vertical, or perpendicular to the ground
It can produce more electricity from a given amount of wind	It produces up to 50% more electricity on an annual basis versus conventional turbines with the same swept area
It is suitable for big wind application	It is suitable for small wind projects and residential applications
Comparatively heavier and not suitable for turbulent winds	Lighter and produce well in tumultuous wind conditions
HAWT only are powered by the wind of specific direction	Vertical axis turbines are powered by wind coming from all 360°, and even turbines are powered when the wind blows from top to bottom
Not suitable to generate electricity from the wind speed below 6 m/s and generally cut out speed 25 m/s	Generates electricity in winds as low as 2 m/s and continues to generate power in wind speeds up to 65 m/s based on the model
They cannot withstand extreme weather conditions due to frost, freezing rain or heavy snow plus heavy winds more than 50 m/s	Withstands extreme weather such as frost, ice, sand, salt, humidity, and very high wind conditions more than 60 m/s
Birds are injured or killed by the propellers since they are not solid objects, so the birds fly into the blades	Does not harm wildlife as birds can detect a solid object and can be seen on aircraft radar
Most are self-starting	Low starting torque and may require energy to start turning
Difficult to transport and install	Lower construction and transportation costs

Control system, generator, and gearbox are positioned at the top of the tower at around 100 m above the ground which require larger and stronger structures.	Transmission and generation systems are positioned at the bottom of the structures which requires small support
Environment is quite noisy because of larger structures	VAWT has less noise while in operation compared to HAWT

From the comparison, it can be concluded that HAWT are generally installed in high wind areas and VAWT in urban and low wind environments. HAWT have larger structures and more production efficiency. While VAWT installation and maintenance cost is low compared to HAWT because of small structure and operating components placed in the ground. The actual examples of these types of wind turbines with different performance analysis were presented in refs (S. Eriksson et al., 2008; Ishugah et al., 2014; Islam et al., 2013; Pope et al., 2010a). When wind turbine technology becomes one of most used technology for power generation, researchers have indicated few limitations of wind turbines technology based on the dynamics, structure, and control systems. Therefore, research focus on wind turbine technology has been increased to improve the productivity and effectiveness. One of the major limitations of this technology is the structural complexity. One of the main reasons of this complexity is exciting force of the wind turbines which involves different levels of vibration in the system. Based on the above research papers and study, the dynamic behavior of HAWTs and VAWTs are analyzed. Because of the tall towers and high wind speed, high vibration occurs in the HAWTs towers and blades. HAWTs also experience vibration problem because of the heavy loads on the top the tower which includes generator, gearbox, and other installation kits. VAWTs also affected by vibration because the ground air flow creates turbulent flow. Vibration in the wind turbines system reduces efficiency and thus requires implementing vibration control system. The level of vibration is then controlled with design optimization using different vibration control methods. Wind excitation, earthquake excitation and waves (for offshore turbines) are the major sources of structural

vibration of wind turbine blades and tower. Significant interest has been shown to research and development to overcome the vibration problem in recent years in wind turbine technology. As a consequent, the main vibration control devices such as passive, active, and semi-active devices have been implemented with huge interest. Definitions and applications of these three major classes of vibration control devices in structures were reviewed in (Symans & Constantinou, 1999). Passive control system can enhance the structural damping, stiffness, and strength. Active and semi-active control systems employed external controllable force devices with integrated sensors, controllers and signal processing (T Soong & Spencer Jr, 2002) . The goal of these control methods is to maximize the performance of wind turbine energy generation by minimizing the vibrations of the wind turbine drive train and tower. For energy dissipation, damping devices is generally used in the system to provide necessary damping forces. There are different types of damping devices that has been implemented for structural vibration control such as tuned mass dampers, tuned liquid mass damper, controllable fluid dampers etc. The use and effectiveness of these dampers in wind turbine structures are reviewed in this study. System controllers play an important role to maximize the performance of the system. Therefore, different control policies applied for mitigating vibration in wind turbines are also reviewed. The content structure of this review is shown in Figure 2.1.

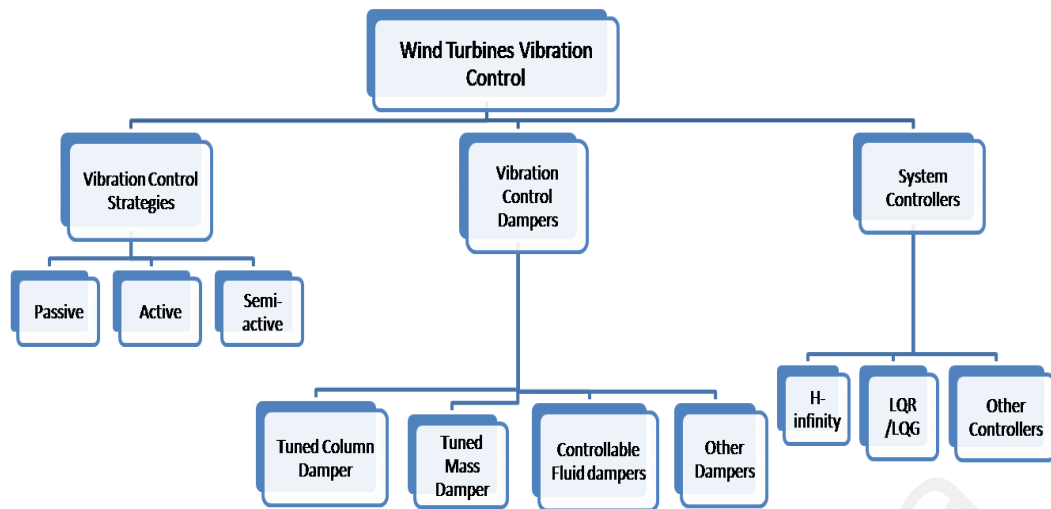


Figure 2.1: Content structure of the review

To prepare this study, an extensive review of the previous research works on wind turbine technology and its vibration control method is conducted.

2.3 Vibration control strategies

There are several areas can be improved to enhance the wind turbine technology, an important area is structural control of the turbine blades, tower, and other supporting components. Several vibration control approaches have been developed and implemented in the past on different structures such as tall buildings, long bridges, and wind turbines to reduce vibration for different external excitations. The necessity and applications of structural control approaches were presented in (Roderick, 2012). Three important vibration control techniques which are being used frequently in the structures are mentioned below:

- Passive Control
- Active Control
- Semi-active Control

2.3.1 Passive control

The passive control method is simple and reliable. This control method does not require an external force (C. Li et al., 2017). The passive control method is easy to implement to reduce the structural vibration and it is widely used in wind turbine technology for enhancement. A conventional vibration control technique consists of springs and dampers only, is referred as a passive control device. The working principle of the springs and dampers in a passive control device is to either absorb vibration energy or loading the transmission path of the disturbing vibration. Good vibration control of the structure is the impact of this device. Basic principles of passive control method were presented in (T Soong & Spencer Jr, 2002). The passive control system may include sensors to measure the excitation amplitude. Since there are no external control forces, the vibration amplitude was minimized by controlling internal forces provided by the motion of the points of attachment (Constantinou et al., 1998). System controllers are also designed to control the input forces. Several researchers adopted passive control system in various applications for vibration control for its simplicity and efficiency (Y. Hu et al., 2014; Sales et al., 2013; Yu et al., 2013). Figure 2.2 shows the basic structure of passive vibration control approach where no external forces are required. The parameters k and c represent spring and damping coefficient respectively for a single-degree-of-freedom structural model.

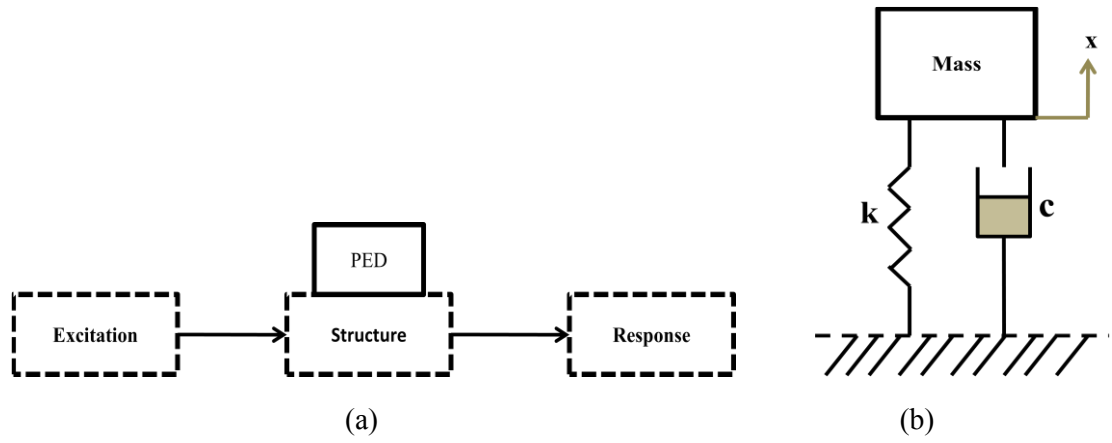


Figure 2.2: (a) Structure with Passive Energy Dissipation (PED) (T Soong & Spencer Jr, 2002) and (b) Typical construction of passive control device

Passive control approach is simple and effective, it was extensively used in structural loading and vibration control (Buckle, 2000; Kulkarni et al., 2012; Symans et al., 2008). Passive control devices were developed and implemented in wind turbines with a large number for performance enhancement. A passive control method was presented by (P J Murtagh et al., 2005) to mitigate the vibration of the blades and tower. A tuned mass damper (TMD) was used for energy dissipation and Fourier transform approach was implemented to find the displacement at the top of the tower. To improve the structural response of wind turbines, passive control approach was presented in (Lackner & Rotea, 2011a). Also, this study presented a calculation of optimal parameters using parametric study for passive control method. In another study, passive structural responses at offshore wind turbines were simulated (Colwell & Basu, 2009). The wind turbines are modeled as multiple-degree-of-freedom structure and simulated subjected to both strong and moderate wind and wave loadings. Passive structural control was also presented at (Enevoldsen & Mørk, 1996). In this study, the effect of passive damping on a 40m high and 500kW pitch regulated three-bladed horizontal wind turbine was investigated.

2.3.2 Active control

The active control system provides enhanced the structural behavior of a system and it consists of force delivery devices, real-time data processors, and sensors. Active control devices employ one or more actuators which apply torques or forces to the structure according to a control law. External actuators provide required forces to mitigate the structural vibration. Real-time data processors process measured information and calculate the necessary forces to counter the measured vibration amplitude. Sensors were used to measure excitation amplitude, structural response amplitudes etc.(Chu et al., 2005). The input control forces are provided based on the acquired information from sensors that measure the excitation input and the response of the system structure. The control forces are generated by electro-hydraulic actuators which require large power sources. Active control systems enhance the performance in response control with the capacity of control using actuators. Researchers applied active control system to various applications to mitigate vibration of the system (Dubay et al., 2014; Thenozhi & Yu, 2014; Wu et al., 2014; H. Zhang et al., 2014). Figure 2.3 shows the basic structure of active vibration control approach where external control actuating force (U) is applied. The parameters k and c represent spring and damping coefficient respectively for a single-degree-of-freedom structural model. Under excitation, the structural behavior is measured through sensors and the processors provide the required force to control actuator. Then the control actuator inputs required force to minimize the unwanted amplitude of the structure.

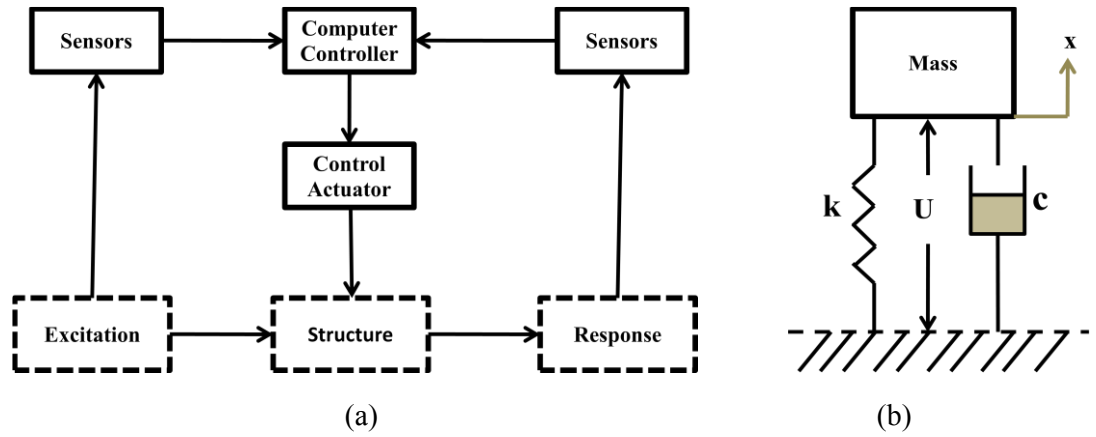


Figure 2.3: (a) Structure with active Control (T Soong & Spencer Jr, 2002) and (b) Typical construction of active control device

The implementation of active control approach has received significant attention in recent years to deal with structural vibration due to different excitation. The design, installation, and performance of the active control techniques on a full-scale structure were presented at (T.T. Soong et al., 1992). Some recent investigations on active control approach for different structural vibration control were presented in (Ma et al., 2018; Taskin et al., 2017; Z. Wang & Keogh, 2018; Xue et al., 2017). Passive vibration control can be combined with active vibration control and an integrated passive-active vibration control system is evaluated to reduce vibratory power transmission for a rigid body connected to a plate structure at (Sun et al., 2015).

Active control approach is another useful and widely used optimization method in wind turbines to control structural vibration. Staino and Basu (2013a) proposed a modeling and control of wind turbine vibrations due to the change of rotational speed of the blades. An active controller was presented by (Krenk et al., 2012) to reduce wind-induced edgewise vibrations and the simulations of this method show the improvement of the blade response in terms of vibration. Active vibration control method is also applied to three-bladed wind turbine rotors with 42m blades where actuator-sensor pairs are implemented to each blade. The actuators are tuned to supply resonant damping of the collective and whirling modes by using separate resonance characteristics of both modes.

In another study, an aerodynamic device, synthetic jet actuator for active vibration control approach was investigated to control the vibration of wind turbine blades (Taylor et al., 2015).

2.3.3 Semi-active control

To achieve the full advantages of passive and active control approaches in structural control applications, a new control technique has been introduced in recent years. Semi-active control approach extracts some best features from passive and active control approaches to providing best possible structural vibration control. Compared to the passive control method where the control forces are developed from the motion of the structure itself, appropriate adjustable mechanical devices are used to provide control forces for the semi-active method. The semi-active approach has become attractive for structural vibration control applications due to controllable damping and low power requirement for operating damping devices. Several studies presented semi-active vibration control method for different applications (Okubo et al., 2014; Su et al., 2014; Zhao et al., 2013). Figure 2.4 shows the basic structure of semi-active vibration control approach where controllable damping device is implemented. The structure of a semi-active control system is quite same as active control system except for the external control force. Semi-active control system consists of external devices capable of providing adjustable control forces. Therefore, semi-active devices are often called as controllable passive devices (Chu et al., 2005).

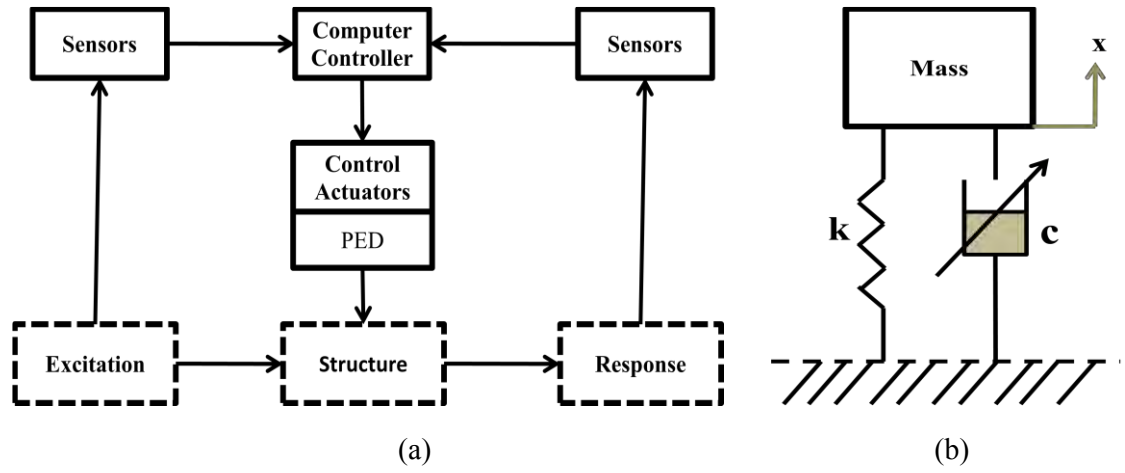


Figure 2.4: (a) Structure with semi-active Control (T Soong & Spencer Jr, 2002) and (b) Typical construction of semi-active control

A lot of research proposed semi-active vibration control to automotive applications (B. K. Song et al., 2017; Tang et al., 2017; A. S. Yildiz & Sivrioglu, 2016). However, for the first time in the field of structural engineering, semi-active structural control approach was proposed subjected to environmental loads by (Hrovat et al., 1983) a few decades ago. From then, this approach became very attractive for structural vibration control where vibration occurs due to earthquakes and heavy wind loads. Researchers found semi-active vibration control as a low cost and effective control strategy with controllable damping devices (Braz-Cesar & Barros, 2018; G. L. Hu et al., 2017; Huang et al., 2018; Miah et al., 2015).

Wind turbines technology is effective to generate power but sometimes vibration occurred in the system affects its effectiveness. The effectiveness of wind turbines decreases when power requirement is high to control the vibration. Semi-active control approach is an effective solution to control the vibration level with low power consumption which makes the wind turbine more effective. Semi-active vibration control approach was investigated to mitigate wind turbines vibration by many researchers. Karimi et al. (2010) investigated semi-active control device to mitigate the vibration of offshore wind turbine tower. Tuned liquid column damper was used with a controllable valve as an external damping device to deal with wind turbine vibrations due to wind load

and earthquake excitations. Kirkegaard et al. (2002) also applied the semi-active system to wind turbine tower to reduce the vibration numerically and experimentally. The wind turbine response was measured using a shaking table experimental model with a controllable fluid damper attached as damping device. Semi-active control approach appears to be most attractive nowadays for its nature of structure which offers the reliability of passive and adaptability of active devices.

2.4 Vibration control dampers

Vibration control dampers are very important to dissipate energy from a structure. A wide range of vibration control damping device has been developed to control unwanted vibration in the structure. Among them, few devices such as a tuned mass damper, tuned liquid damper, and controllable fluid dampers have become very popular for their capability of improving structural response. These dampers are implemented in the structure as passive, active, and semi-active damping devices. The applications and effectiveness of these damping devices in structural vibration control are discussed in this section.

2.4.1 Tuned mass damper

The concept of tuned mass-damper (TMD) was first presented in the 1940s by (Den Hartog, 1947). TMD consists of a secondary mass placed top of the primary structure with spring and damping elements. It provides a frequency-dependent hysteresis characteristic that increases damping in the main structure. The efficiency of TMD in reducing structural vibrations is now well established and is widely used in tall buildings, bridges, and towers for vibration control purpose. It is also a well-known strategy for optimizing wind turbine power generation efficiency by mitigation vibration. TMD can be used as a simple passive device; however, the effectiveness of the passive TMD can

also be improved using external actuator force (called as active TMD) or controllable force (called as semi-active TMD). A TMD was constructed in the wind turbine nacelle in (Lackner & Rotea, 2011b) to mitigate the vibration of the tower. Generally, a TMD, represent with spring damper system, is placed on top of the main structure to counteract, and reduce extraneous vibration. The construction of TMD for vibration control of wind turbine tower is shown in Figure 2.5.

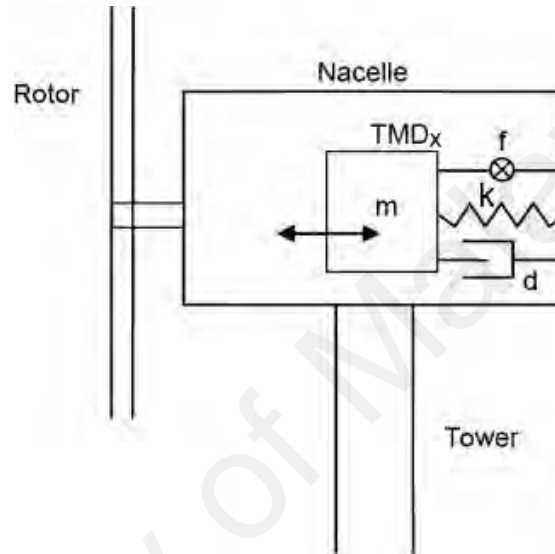


Figure 2.5: Construction of TMD in wind turbine (Lackner & Rotea, 2011b)

Recently, wind turbine tower vibration control using passive and active TMD was investigated in (Lackner & Rotea, 2011a) and (Rotea et al., 2010) respectively. In the first paper, Lackner & Rotea performed a parametric study to achieve optimal parameters of passive TMD and then simulated wind turbine models with equipped TMD. The results showed the improvement in the response of the offshore wind turbine technology and demonstrate the potential of the active TMD in wind turbines. Rotea et al. designed and constructed active TMD for wind turbine structural control in another study. The simulation study showed a clear improvement of response using active TMD compared to passive control. The responses of wind turbine tower using TMD for passive and active control approach are compared in Figure 2.6.

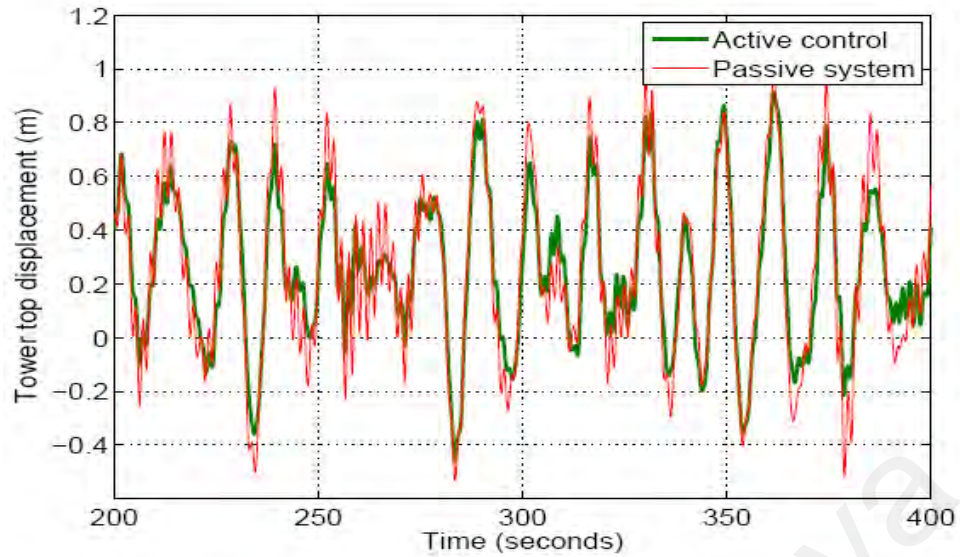


Figure 2.6: Comparison of wind turbine tower response between passive control and active TMD control system (Rotea et al., 2010)

Another paper investigated the along-wind forced vibration control system using passive TMD for a simplified wind turbine system (P.J Murtagh et al., 2008). Recently, TMD has been used in floating wind turbine model by national renewable energy laboratory to control deflections of tower and blades (He et al., 2014). Using this method, the reduction rate of deflections at tower and blades are 50% and 40% respectively. There are two main types of vibration occurs in the wind turbine blades. Edgewise vibration is vibration occurs in the plane of rotation of the blades, whereas Flap wise vibration is out of the rotation of the blades. Fitzgerald et al. investigated the use of active TMD for mitigation of both edgewise (B Fitzgerald et al., 2013) and flap wise (B. Fitzgerald & Basu, 2013) vibration of the wind turbine blades. A Euler-Lagrangian wind turbine mathematical model has been implemented for this purpose by considering the structural dynamic system and the interaction between in-plane and out-of-plane vibrations. Recently, semi-active tuned mass damper (STMD) was proposed to control flap wise vibrations in wind turbine blades and simulation results show that STMD successfully reduced the response of the wind turbine due to wind-induced excitation (Arrigan & Pakrashi, 2011). However, based on the effectiveness of TMD for structural vibration

control, researchers proposed an optimization method of TMD which was named as multiple tuned mass dampers (MTMD) to improve the vibration control system. Collins et al. investigated multiple tuned mass dampers (MTMD) to optimize wind turbine system where multiple mass damping system was connected with the turbine towers (Collins et al., 2005). The use of MTMD was also investigated for mitigation of edgewise vibration of tower/nacelle and spar of the spar-type floating wind turbine (Dinh & Basu, 2014). The results showed that this method with passive control approach can reduce the nacelle sway displacement up to 50% compared to TMD which can reduce up to 40%. As of today, the use of TMD in wind turbine technology becomes very popular because of its simplicity and effectiveness, thus remains an important issue to study.

2.4.2 Tuned liquid damper

Another important and commonly used damping device for structural vibration control is tuned liquid damper (TLD). A TLD is also used to design passive, active and semi-active device for structural vibration control. Among different types of TLD, Tuned Liquid Column Damper (TLCD) is most feasible and efficient damper to solve vibration problem due to high excitation force. A TLCD is generally modeled as U-shape tube which is partially filled with a volume of liquid and it acts as a mass of the damper. When a TLCD is attached to a structure and structure is excited, the liquid of TLCD oscillates through the column and re-establish the system to equilibrium. A TLCD is typically placed on top of the structures. Two decades ago, Sakai et al. (1989) proposed a TLCD to suppress wind-induced horizontal motion of high rise buildings. The performances of single-tuned liquid column damper (STLCD) were investigated in (Won et al., 1997), whereas multiple-tuned liquid column damper (MTLCD) were investigated for wind applications in (Chang et al., 1998; Gao et al., 1999). A hybrid tuned liquid damper was also proposed for structural vibration control in (Haroun et al., 1996). Other than U-tube

shape, rectangular and crossed tube-like containers were also proposed for tuned liquid damper (TLD) for structural vibration control in (Fujino et al., 1988) and (X. T. Zhang et al., 1993) respectively. Different types of TLDs and their applications in structural vibration were studied in (Rao, 2013). The use of TLD for the building has been adopted to control vibration at wind turbine because of its success in structural engineering. Figure 2.7 shows the schematic diagram of a wind turbine vibration control method by using TLCD where two TLCDs are applied.

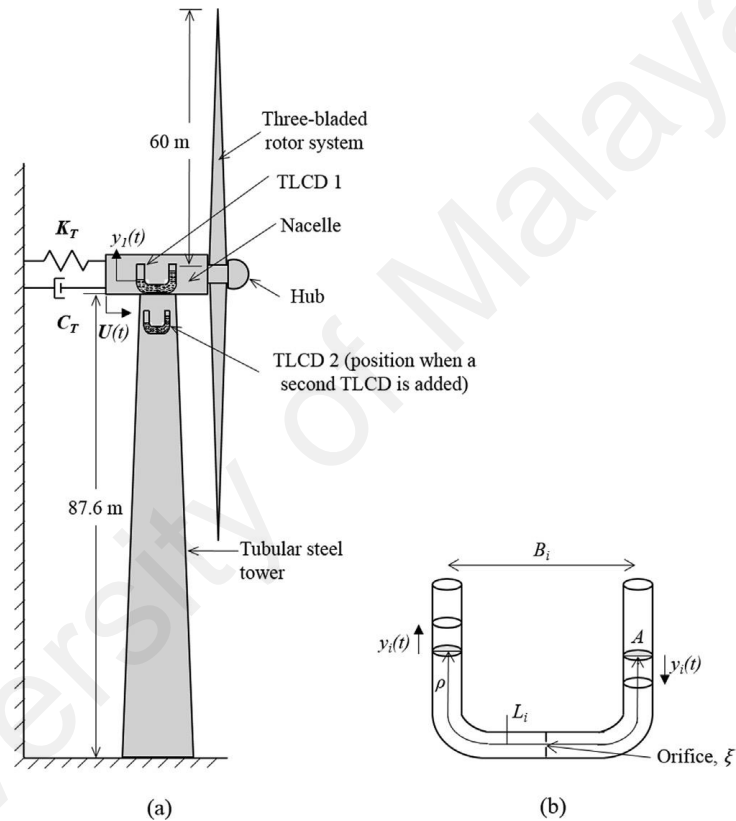


Figure 2.7: (a) Schematic diagram of wind turbine with TLCDs, (b) TLCD model (Mensah & Dueñas-Osorio, 2014)

The effectiveness of TLD in reducing the structural response of wind turbines under and random excitations was investigated in (Ghaemmaghami et al., 2013). Annular TLD was proposed in this study and simulation was done based on single-degree of freedom hybrid wind turbine model. This study found that the used TLD method is effective for the small amplitude of excitations. For large amplitude of excitations, TLCD damper was investigated in many studies for structural vibration control. Colwell and Basu (2009)

investigated TLCD on multiple-degree-of-freedom offshore wind turbine system to suppress the vibration subjected to both ‘moderate and strong’ wind and wave loadings. This study found that TLCD is effective for the large amplitude of excitations and can reduce vibration up to 55% of peak response of wind turbines compared to the same system without TLCD. TLCD has also been studied to control the structural response of wind turbines at (Wilmink & Hengeveld, 2005). The study found that TLCD enables significant damping to the wind turbine system and thus offers cost reduction to increase the efficiency of the system. Structural response minimization, reliability improvement of wind turbine technology using TLCD were presented in (Mensah & Dueñas-Osorio, 2014). The study simulated a wind turbine model with TLCD and the results show significant reductions in tip displacement and bending moment which is shown in Figure 2.8.

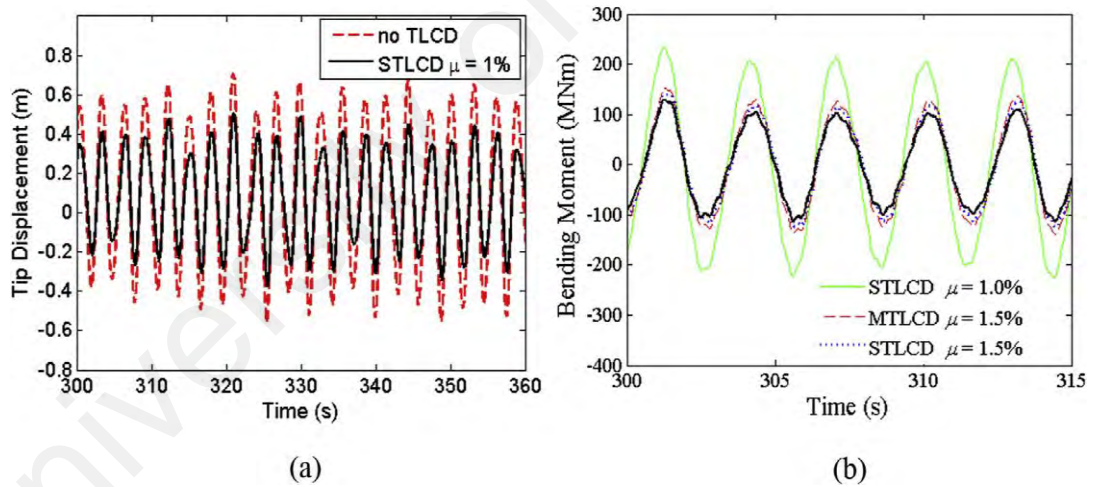


Figure 2.8: Reductions in (a) tip displacement and (b) bending moment of wind turbine tower using TLCD (Mensah & Dueñas-Osorio, 2014)

Chen and Georgakis proposed a spherical TLD for vibration control in wind turbines (J.L. Chen & C.T. Georgakis, 2013). The spherical TLD consists of two layers of hemispherical shape containers which are partially filled with water. The radius of spherical containers is determined by its frequency and the mass of the sloshing water. The dynamic responses were reduced significantly using shake table test for different excitation loads. The dynamic behavior and vibration control response of wind turbine

blades were investigated using passive TLCD in (Arrigan & Basu, 2007). The effectiveness of using TLCD on wind turbine blades in stationary horizontal position was presented to achieve desired vibration control response. Recently, Zhang et al investigated the edgewise vibration control of wind turbine blades using TLCD (Z. Zhang et al., 2014) and achieved improved results.

The study found that TMD and TLCD are mostly implemented in HAWTs, but they can also be implemented in VAWTs. A schematic diagram of vertical axis wind turbine is shown in Figure 2.9 which presents an idea for the implementation of TMD or TLCD. The wind flow direction for VAWT is not uniform, therefore, the direction of the external force either needs to be fixed or the position of the dampers needs to be changed for the implementation of TMD or TLCD in VAWTs.

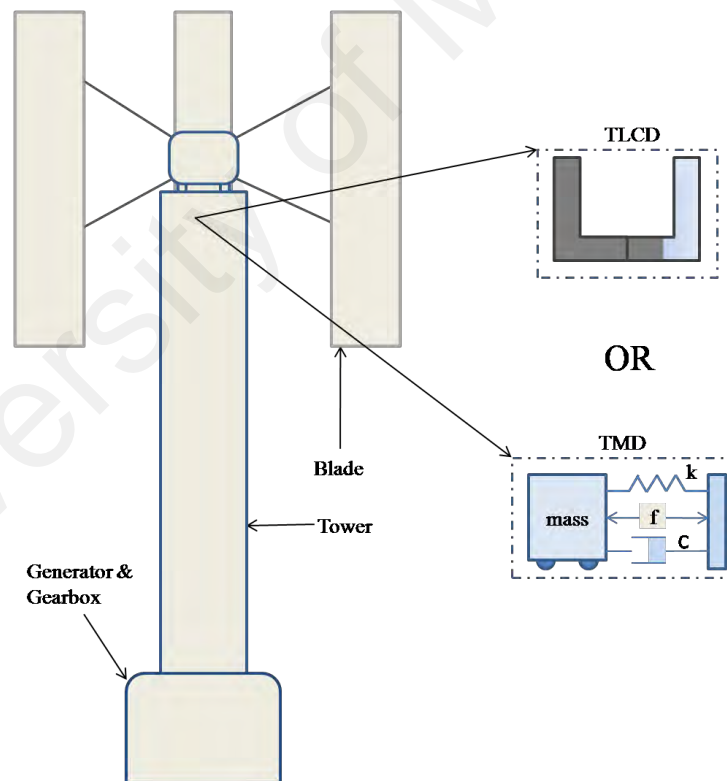


Figure 2.9: Schematic diagram of VAWT with TMD/TLCD

2.4.3 Controllable fluid damper

The controllable fluid damper is a class of semi-active devices which uses controllable fluids inside the damper. Electrorheological (ER) and Magnetorheological

(MR) fluid dampers are the two most commonly implemented controllable semi-active devices for structural vibration control. These types of dampers are very reliable because they contain no moving parts except piston. Controllable fluids of ER/MR damper can change from free-flowing state to semi-solid state when it comes to an electric (ER) or magnetic (MR) field. The input current and force characteristics of MR damper were evaluated using different damper models by (B. F. Spencer et al., 1997). The schematic diagram of controllable damper filled with ER/MR fluid is shown in Figure 2.10.

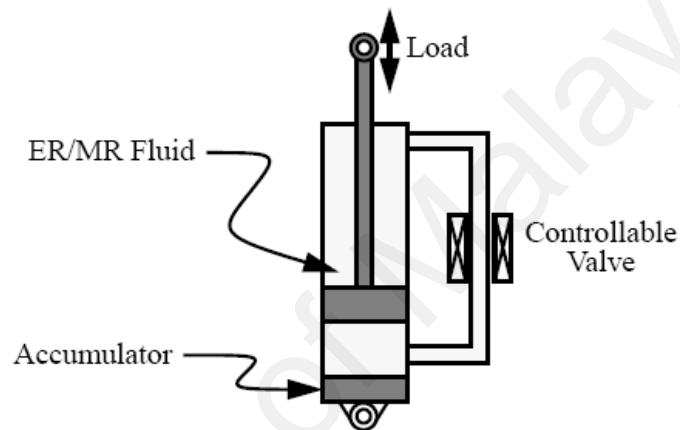


Figure 2.10: Schematic of controllable fluid damper (Stewart, 2012)

The contribution of ER/MR damper in structural vibration control is significant (Contreras-Lopez et al., 2016; Lin et al., 2017; Nguyen et al., 2017; Z. H. Wang et al., 2018). The usefulness of these damping devices has also influenced the researchers to implement them in wind turbine technology for optimization purpose. Kirkegaard et al. (2002) investigated semi-active vibration control of wind turbine tower using MR damper. In this study, wind turbine tower was modeled as a two-degree-of-freedom system and MR damper was used as external damping device. Shaking table scaled model has been used as a wind turbine for experimental verification and MR damper is placed between the shaking table and top of the frame structure. The results showed an improved response in terms of vibration reduction using MR damper compared to passive damping. MR fluid was also implemented to design semi-active TLCD in (Luo et al., 2012) to overcome the shortcoming of the passive system and to enhance the reliability of the

system. MR fluid was used in this study to design a controllable valve for semi-active TLCD. Recently, magnetorheological vibration absorber was implemented to design the wind turbine tower-nacelle model for the purpose of vibration suppression (P Martynowicz & Szydlo, 2013). At present, the controllable fluid dampers such as ER/MR damper become much-desired damping device in structural control applications because of its reliability, versatility, and adaptability.

2.4.4 Other vibration control dampers

Some other important dampers were proposed in the past in structural vibration control. These types of dampers also play important roles to deal with structural vibration due to the wind, wave, and earthquake excitations. Pendulum damper is one kind of passive TMD which was utilized in many structural vibration control applications (Gerges & Vickery, 2005; Oliveira et al., 2013; Setareh et al., 2006). Pendulum damper is modeled with a large mass that is hung in an oil bath. When the base is excited, the mass is released to swing at the opposite motion of the structure to provide counterforce. The use of pendulum damper is not limited to tall buildings but also effective for wind turbines. A pendulum damper was modelled for vibration control of wind turbine towers in (Avila et al., 2009) and it is simulated under white noise wind effect. In another study, the reduction of fatigue loading in wind turbine was investigated with a pendulum TMD in (Argyriadis & Hille, 2004). A simple two-mass model was used in this study. Another important damping device is ball vibration absorber (BVA) which was first investigated by (Pirner, 2002) on two television towers. Recently Zhang et al. investigated the ball vibration absorber through a series of shake table test for wind turbines vibration suppression theoretically and experimentally (Z.-L. Zhang et al., 2013). The BVA consists of a steel ball, an arc path and two steel plates which prevent the ball slides aside. When the base structure is excited, the ball rolls along the arc path and thus counters the

excitation force by absorbing energy. Experimental result found that vibration response was reduced to 39% of the displacement with the use of BVA (J. Li et al., 2012). The structure of the BVA and the displacement response of the wind turbine tower with and without BVA are shown in Figure 2.11.

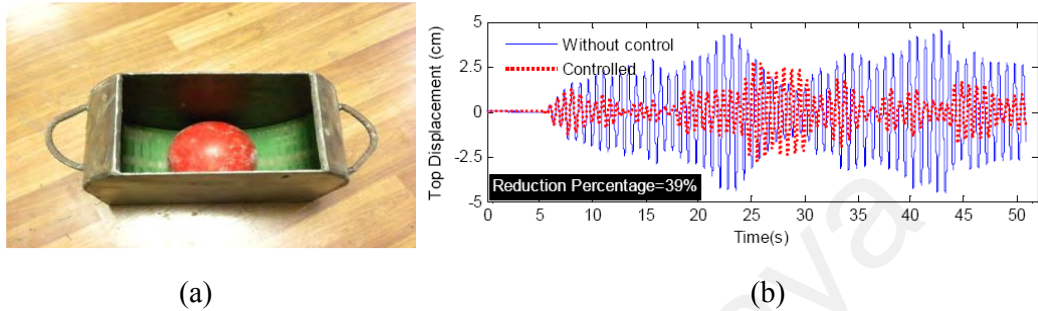


Figure 2.11: (a) The BVA and (b) Top displacement of wind tower with and without BVA (J. Li et al., 2012)

Another contributing damping device is tuned rolling-ball damper which is quite like the TLCD in shape. Tuned rolling damper consists of one or multiple steel balls in place of liquid compared to TLCD. (J.L. Chen & C. T. Georgakis, 2013) studied tuned rolling ball damper modeled with one-layer (spherical) and two-layer (hemispherical) containers for wind turbine shake table scaled model. This study presented vibration control response of developed wind turbine test model for different excitation load and several balls in the container.

2.5 Modeling of wind turbine tower

Modeling of wind turbine tower is very important to analyze the vibration under different conditions and apply the vibration control system appropriately. It is vital for real implementations and the model should be validated with actual wind turbine tower. With proper modeling, material or boundary conditions, changes in geometry, can be projected. For wind turbine tower modeling, numerical method is most common. In computational physics website, the wind turbine is modeled as a beam by using finite difference method (Nicholas & Nakanishi, 2015). For structural design and vibration

analysis, wind turbine tower is mostly presented with cantilever beam (fixed-free) (Adhikari & Bhattacharya, 2012; Katsanis, 2013; Negm & Maalawi, 2000) because of its simplicity and ability to effectively represent the wind turbine tower. Modeling and different control systems of cantilever beam vibration using active control approach are reviewed by (Ros et al., 2015). Literature of this review found that most common modeling method of the beam is FEM. Equations of cantilever beam are complex, therefore, numerical methods such as FEM and FDM are often used to solve these equations to find natural frequencies and dynamic response of wind turbine model represented in cantilever beam (Asareh et al., 2016; Gwon, 2011; Rajagopalan & Fanucci, 1985). In the study of (Genov et al., 2010), the wind turbine is modeled as a cantilever beam with distributed mass, elastic and damping properties which is fixed at the bottom with a concentrated mass at the tip and the tip is subjected to wind load. The governing equation used is

$$m \frac{\partial^2 y}{\partial t^2} + 2cm \frac{\partial y}{\partial t} + \frac{\partial^2}{\partial x^2} \left(EI \frac{\partial^2 y}{\partial x^2} \right) = \delta(x - l)F(t) \text{ for } x \in [0, l] \text{ and } t \geq 0 \quad (2.1)$$

where $m = \rho S$ – linear mass, kg/m (ρ – density and S – cross section area)

c is the damping coefficient, E is the modulus of elasticity, I is the area moment of inertia, $\delta(x - l)$ is delta function of l , l is the beam height, $F(t)$ is the external force.

In this study, numerical approaches, finite difference method, and finite element method, are used for governing equation of wind turbine model. Before solving the governing equation of wind turbine model, it is necessary to understand flexible beam system. In many engineering applications, uniform beam elements are always assumed and utilized. To obtain a mathematical model of the wind turbine as a cantilever beam, the Euler-Bernoulli equation is used.

The equation of the cantilever beam can be derived with Euler-Bernoulli beam equation. Figure 2.12 shows a uniformly distributive cantilever beam for transverse

vibration with element length dx . A free body diagram of the beam shear forces, V and bending moments, M acting on the beam element are also shown.

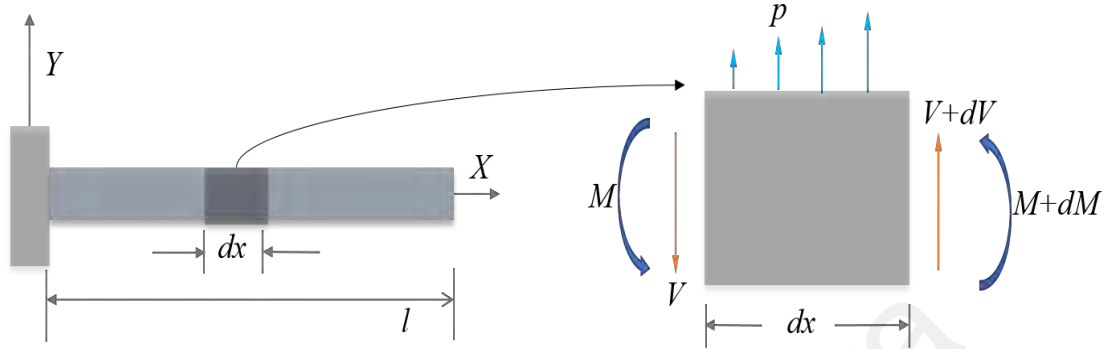


Figure 2.12: Free body diagram of beam with forces and moments

According to the free body diagram, the total shear force in the Y direction is

$$dV - p(x)dx = 0 \quad (2.2)$$

and the total moment at the right face of the element is

$$dM - Vdx - \frac{1}{2}p(x)(dx)^2 = 0 \quad (2.3)$$

It is assumed that dx is very small, therefore, the equations of total shear force and moment can be simplified and generates as

$$\frac{dV}{dx} = p(x), \quad \frac{dM}{dx} = V \quad (2.4)$$

Then the equation then can be written as

$$\frac{d^2M}{dx^2} = \frac{dV}{dx} = p(x) \quad (2.5)$$

According to mechanics of materials, the bending moment is related to beam deflection by

$$M = EI \frac{d^2y}{dx^2} \quad (2.6)$$

where E is the Young's modulus of elasticity, I is the cross-sectional moment of inertia, $I = bh^3/12$ (b is width, h is height of cross-sectional of the beam). The product of modulus of elasticity, E with moment of inertia, I is the flexural rigidity of beam.

By substituting M into the Equation (2.5), it is found that

$$\frac{d^2}{dx^2} \left[EI \frac{d^2 y}{dx^2} \right] = p(x) \quad (2.7)$$

Since inertia force is in the same direction as $p(x)$

$$p(x) = \rho S \omega^2 y \quad (2.8)$$

where ρ is the density of the beam, S is the cross-sectional area of the beam

Substituting formula of $p(x)$ into the Equation (2.5), it is found that

$$\frac{d^2}{dx^2} \left[EI \frac{d^2 y}{dx^2} \right] - \rho S \omega^2 y = 0 \quad (2.9)$$

If the flexural rigidity, EI is constant, then the equation can be expressed as

$$\frac{d^2}{dx^2} \left[\frac{d^2 y}{dx^2} \right] - \frac{\rho S \omega^2 y}{EI} = 0 \quad (2.10)$$

By substituting $\beta^4 = \rho S \frac{\omega^2}{EI}$ into the equation, it produces a fourth-order differential equation for lateral displacement of beam.

$$\frac{d^4 y}{dx^4} - \beta^4 y = 0 \quad (2.11)$$

The general solution of equation is

$$y = A \cosh \beta x + B \sinh \beta x + C \cos \beta x + D \sin \beta x \quad (2.12)$$

where A, B, C and D are constant of integration.

The natural frequencies are formulated as

$$\omega_n = \beta_n \sqrt{\frac{EI}{\rho S}} \quad (2.13)$$

where β is the characteristic roots and i is the corresponding mode shapes.

The equation of motion for a uniform beam element expressed by a PDE is

$$\frac{EI}{\rho S} \frac{\partial^4 y(x,t)}{\partial x^4} + \frac{\partial^2 y(x,t)}{\partial t^2} = \frac{1}{m} F(x, t) \quad (2.14)$$

where m is the beam mass and F is the applied lateral force.

If the damping is added to the structure and simplify, the equation becomes

$$\frac{EI}{\rho S} \frac{\partial^4 y(x,t)}{\partial x^4} + 2c \frac{\partial y}{\partial t} + \frac{\partial^2 y(x,t)}{\partial t^2} = \frac{1}{m} F(x, t) \quad (2.15)$$

2.5.1 Finite difference method

A free body diagram of a discrete cantilever beam is shown in Figure 2.13. The discrete system is a multi-degree of freedom system that made up of N masses and $N+2$ spiral springs. C_r represents the linear rigidities of r^{th} spiral spring. In the system, the springs are attached to identical bars of length l , which are assumed to be massless, not infinitely rigid and are an elastic material which may be slightly deformed. The momentum M_r of the r^{th} spiral spring is formulated as, $M_r = -C_r^l \theta$ as presented in (Eddanguir et al., 2012)

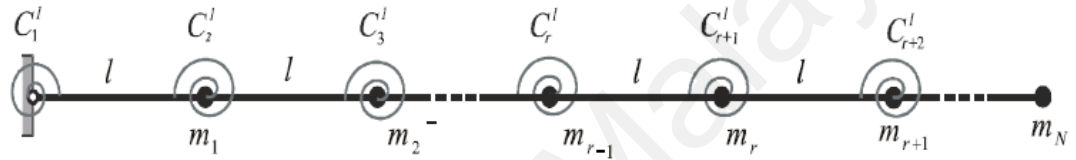


Figure 2.13: Multi-degree of freedom of discrete system

Also, the linear potential energy stored in each spiral spring is

$$V_l = \frac{1}{2} \sum_{i=1}^N C_r^l (\theta_i - \theta_{i-1})^2 \quad (2.16)$$

Now, consider transverse vibration of the cantilever beam that shown in Figure 2.14. The cantilever beam has the characteristics of: Young's modulus, E , length of beam, L , cross-sectional area, S , second moment of area of the cross-section, I , transverse or vertical displacement of the beam and it is equal to $y(x) \sin \omega t$, $y(x, t)$,

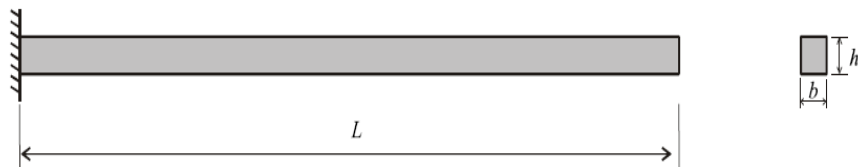


Figure 2.14: Cantilever Beam

For a continuous beam, the linear potential energy due to the bending is

$$V_l = \frac{1}{2} EI \int_0^L \left(\frac{d^2 y}{dx^2} \right)^2 dx \quad (2.17)$$

By using the finite difference method, the second derivative of y can be converted as shown

$$\frac{d^2y}{dx^2} = \frac{\frac{dy}{dx}|_i - \frac{dy}{dx}|_{i-1}}{l} = \frac{\theta_i - \theta_{i-1}}{l} \quad (2.18)$$

By substituting Equation (2.16) into Equation (2.17),

$$V_l = \frac{1}{2} EI \sum_{i=1}^N (\theta_i - \theta_{i-1})^2 \quad (2.19)$$

Both linear potential energy in Equation (2.16) and Equation (2.19) are compared, and thus the rigidities of the spiral spring can be expressed as

$$C_r^l = \frac{EI}{l} = \frac{N}{L} EI, (2 \leq i \leq N + 1) \quad (2.20)$$

In order to determine the linear rigidity matrix or stiffness matrix, k_{ij} of cantilever beam, the expressions established in (Eddanguir et al., 2012), Equations (2.16-2.20), are recalled,

$$k_{rr} = \frac{1}{l^2} (C_r^l + 4C_{r+1}^l + C_{r+2}^l) = \frac{I}{l^3} (E_r + 4E_{r+1} + E_{r+2}), r = 1, 2, 3, \dots N \quad (2.21)$$

$$k_{rr+1} = -\frac{2}{l^2} (C_{r+1}^l + C_{r+2}^l) = -\frac{2I}{l^3} (E_r E_{r+1} + E_{r+2}), r = 1, 2, 3, \dots N - 1 \quad (2.22)$$

$$k_{rr+2} = \frac{C_{r+2}^l}{l^2} = \frac{E_{r+2}I}{l^3}, r = 1, 2, 3, \dots N - 2 \quad (2.23)$$

And for the mass matrix, M_{ij} , is expressed as

$$[M_{ij}] = \frac{\rho SL}{N} [m_{ij}] \quad (2.24)$$

And for the stiffness matrix, the rigidity matrix, K_{ij} is expressed as

$$[K_{ij}] = \frac{N^3 EI}{L^3} [k_{ij}] \quad (2.25)$$

For obtaining the linear stiffness matrix of a cantilever beam, the following values are required,

- a. $C_l = 3C_i$ and $C_{n+2} = 0$
- b. $m_i = m$ for $(1 \leq i \leq N - 1)$ and $m_N = 0.5m$ with $m = \rho SL/N$

The eigenvalue problem that describing the linear system is

$$[K_{ij}]\{X\} = \omega^2 [M_{ij}]\{X\} \quad (2.26)$$

The Equation (2.23) and Equation (2.24) are substituting into Equation (2.25),

$$[k_{ij}]\{X\} = \omega^2 \frac{\rho SL^4}{EIN^4} [m_{ij}]\{X\} \quad (2.27)$$

It is noted that

$$\lambda_n = \frac{\rho SL^4}{EIN^4} \quad (2.28)$$

For a uniform beam,

$$\beta_n^4 = \rho S \frac{\omega_n^2}{EI} \quad (2.29)$$

Thus, Equation (2.27) and Equation (2.28) can form an expression that related each other

$$(L\beta_n)^4 = \lambda_n N^4 \quad (2.30)$$

Also, the mass matrix and stiffness matrix are as shown

$$[K_{ij}] = \frac{N^3 EI}{L^3} \begin{bmatrix} 8 & -4 & 1 & 0 & \cdots & \cdots & 0 \\ -4 & 6 & -4 & 1 & 0 & & \vdots \\ 1 & -4 & 6 & \ddots & \ddots & \ddots & \vdots \\ 0 & 1 & \ddots & \ddots & -4 & 1 & 0 \\ \vdots & \ddots & \ddots & -4 & 6 & -4 & 1 \\ \vdots & & \ddots & 1 & -4 & 5 & -2 \\ 0 & \cdots & \cdots & 0 & 1 & -2 & 1 \end{bmatrix} \quad (2.31)$$

and

$$[M_{ij}] = \frac{\rho SL}{N} \begin{bmatrix} 1 & 0 & \cdots & \cdots & 0 \\ 0 & 1 & \ddots & \ddots & \vdots \\ \vdots & \ddots & \ddots & \ddots & \vdots \\ \vdots & & \ddots & 1 & 0 \\ 0 & \cdots & \cdots & 0 & 0.5 \end{bmatrix}, \text{ for } 1 \leq i, j \leq N \quad (2.32)$$

The damping ratio, however, is assumed to be

$$[\zeta] = [0.01 \quad \cdots \quad 0.01], \text{ for } 1 \leq i \leq N \quad (2.33)$$

2.5.2 Finite element method

In this method, beam element is needed to be determined. A simple beam element is illustrated Figure 2.15. As shown in the figure, a simple beam element consists of two nodes and there are two degrees of freedom at each node which are vertical displacement and rotation angle. Thus, a total of four nodal values is associated with a beam element.

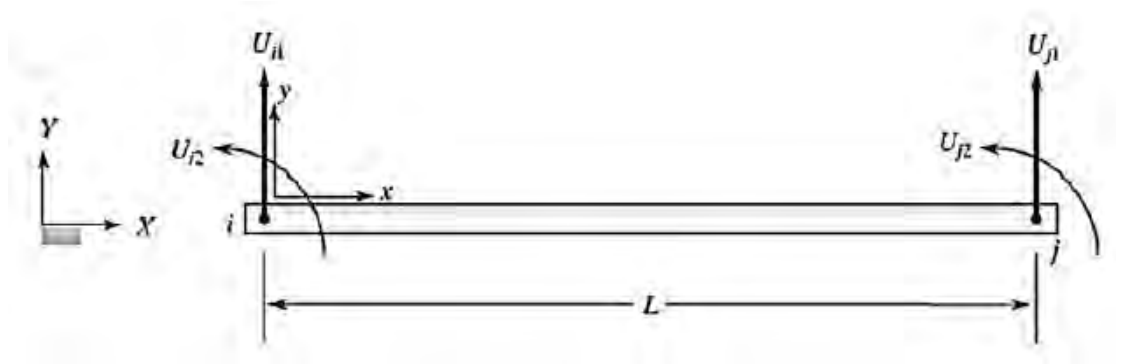


Figure 2.15: A beam element

A displacement can be represented by third order polynomial with four unknown coefficients,

$$y = c_1 + c_2x + c_3x^2 + c_4x^3 \quad (2.34)$$

The end conditions of an element are as followed,

- At node i , the vertical displacement at $x = 0$ is $y = c_1 = U_{i1}$
- At node i , the slope at $x = 0$ is $\left. \frac{dy}{dx} \right|_{x=0} = c_2 = U_{i2}$
- At node j , the vertical displacement at $x = L$ is $y = c_1 + c_2L + c_3L^2 + c_4L^3 = U_{j1}$
- At node j , the slope at $x = L$ is $\left. \frac{dy}{dx} \right|_{x=L} = c_2 + 2c_3L + 3c_4L^2 = U_{j2}$

Now, there are four equations with four unknowns. To solve c_1, c_2, c_3 and c_4 , they are substituted into Equation (2.33). The result is

$$y = H_{i1}U_{i1} + H_{i2}U_{i2} + H_{j1}U_{j1} + H_{j2}U_{j2} \quad (2.35)$$

where the shape functions are

$$H_{i1} = 1 - \frac{3x^2}{L^2} + \frac{2x^3}{L^3} \quad (2.36)$$

$$H_{i2} = x - \frac{2x^2}{L} + \frac{x^3}{L^2} \quad (2.37)$$

$$H_{j1} = \frac{3x^2}{L^2} - \frac{2x^3}{L^3} \quad (2.38)$$

$$H_{j2} = -\frac{x^2}{L} + \frac{x^3}{L^2} \quad (2.39)$$

Then, in the following derivative of the stiffness matrix, the contribution of shear stresses to the strain energy is neglected. Therefore, the strain energy for a beam element is

$$\Lambda^{(e)} = \int_Y \frac{\sigma \varepsilon}{2} dY = \int_y \frac{E \varepsilon^2}{2} dV = \frac{E}{2} \int_Y \left(-y \frac{d^2 y}{dx^2}\right)^2 dY = \frac{E}{2} \int_0^L \left(\frac{d^2 y}{dx^2}\right)^2 dx \int_S y^2 dS \quad (2.40)$$

The $\int_S y^2 dS$ is the second moment of the area of I , then

$$\Lambda^{(e)} = \frac{EI}{2} \int_0^L \left(\frac{d^2 y}{dx^2}\right)^2 dx \quad (2.41)$$

Next, the displacement, v is replaced with the shape functions and the nodal values.

It can be evaluated as following

$$\frac{d^2 y}{dx^2} = \frac{d^2}{dx^2} [H_{i1} \quad H_{i2} \quad H_{j1} \quad H_{j2}] \begin{Bmatrix} U_{i1} \\ U_{i2} \\ U_{j1} \\ U_{j2} \end{Bmatrix} \quad (2.42)$$

For the next few steps, matrix notations are used for simplifications and to prevent unnecessary mathematical operations.

The second derivative of the shape functions are defined as following

$$D_{i1} = \frac{d^2 H_{i1}}{dx^2} = -\frac{6}{L^2} + \frac{12x}{L^3} \quad (2.43a)$$

$$D_{i2} = \frac{d^2 H_{i2}}{dx^2} = -\frac{4}{L} + \frac{6x}{L^2} \quad (2.43b)$$

$$D_{j1} = \frac{d^2 H_{j1}}{dx^2} = \frac{6}{L^2} - \frac{12x}{L^3} \quad (2.43c)$$

$$D_{j2} = \frac{d^2 H_{j2}}{dx^2} = -\frac{2}{L} + \frac{6x}{L^2} \quad (2.43d)$$

Thus, the Equation (2.42) can be written as

$$\frac{d^2 y}{dx^2} = [D]\{U\} \quad (2.44)$$

where $[D] = [D_{i1} \quad D_{i2} \quad D_{j1} \quad D_{j2}]$ and $\{U\} = \begin{Bmatrix} U_{i1} \\ U_{i2} \\ U_{j1} \\ U_{j2} \end{Bmatrix}$

Please be noted that $\left(\frac{d^2 y}{dx^2}\right)^2$ can be represented as

$$\left(\frac{d^2y}{dx^2}\right)^2 = ([D]\{U\})([D]\{U\}) = \{U\}^T [D]^T [D] \{U\} \quad (2.45)$$

Substitute Equation (2.44) into Equation (2.41),

$$\Lambda^{(e)} = \frac{EI}{2} \int_0^L \{U\}^T [D]^T [D] \{U\} dx \quad (2.46)$$

Since the total potential energy, Π for a body is defined as the difference between the total strain energy and the work done by the external forces, then

$$\Pi = \Sigma \Lambda^{(e)} - \Sigma F U \quad (2.47)$$

Also, the minimum total potential energy principle states that for a stable system, the displacement at the equilibrium position occurs. Thus,

$$\frac{\partial \Pi}{\partial U_k} = \frac{\partial}{\partial U_k} \Sigma \Lambda^{(e)} - \frac{\partial}{\partial U_k} \Sigma F U = 0 \text{ for } k = 1, 2, 3, 4 \quad (2.48)$$

where U_k takes on the values of the modal degrees of freedom $U_{i1}, U_{i2}, U_{j1}, U_{j2}$

It is noted that in Equation (2.46), there are two major parts which are strain energy and work done by external forces. The differentiation of strain energy with respect to nodal degrees of freedom will lead to the formulation of beam stiffness matrix whereas the differentiation of the work done by external forces leads to load matrix. By minimizing the strain energy with respect to $U_{i1}, U_{i2}, U_{j1}, U_{j2}$, the stiffness matrix is obtained

For the strain energy part,

$$\frac{\partial \Lambda^{(e)}}{\partial U_k} = EI \int_0^L [D]^t [D] dx \{U\} \quad (2.49)$$

By evaluating Equation (2.48),

$$EI \int_0^L [D]^t [D] dx \{U\} = \frac{EI}{L^3} \begin{bmatrix} 12 & 6L & -12 & 6L \\ 6L & 4L^2 & -6L & 2L^2 \\ -12 & -6L & 12 & -6L \\ 6L & 2L^2 & -6L & 4L^2 \end{bmatrix} \begin{Bmatrix} U_{i1} \\ U_{i2} \\ U_{j1} \\ U_{j2} \end{Bmatrix} \quad (2.50)$$

Thus, the stiffness matrix for a beam element is

$$[K]^{(e)} = \frac{EI}{L^3} \begin{bmatrix} 12 & 6L & -12 & 6L \\ 6L & 4L^2 & -6L & 2L^2 \\ -12 & -6L & 12 & -6L \\ 6L & 2L^2 & -6L & 4L^2 \end{bmatrix} \quad (2.51)$$

For two beam elements in a beam, the stiffness matrix becomes

$$[K]^{(G)} = \frac{EI}{L^3} \begin{bmatrix} 12 & 6L & -12 & 6L & 0 & 0 \\ 6L & 4L^2 & -6L & 2L^2 & 0 & 0 \\ -12 & -6L & 24 & 0 & -12 & 6L \\ 6L & 2L^2 & 0 & 8L^2 & -6L & 2L^2 \\ 0 & 0 & -12 & -6L & 12 & -6L \\ 0 & 0 & 6L & 2L^2 & -6L & 4L^2 \end{bmatrix} \quad (2.52)$$

In this project, the cantilever beam is used, thus the matrix is reduced first two rows and first two columns.

$$[K]^{(G)} = \frac{EI}{L^3} \begin{bmatrix} 24 & 0 & -12 & 6L \\ 0 & 8L^2 & -6L & 2L^2 \\ -12 & -6L & 12 & -6L \\ 6L & 2L^2 & -6L & 4L^2 \end{bmatrix} \quad (2.53)$$

For developing the mass matrix, the kinetic energy of a beam element is determined by adding the kinetic energy of its constituent particles according to the formula

$$T = \int_0^L \frac{\gamma}{2} \dot{y}^2 dx \quad (2.54)$$

where \dot{y} is the velocity distribution within the beam and is a function of time and position, γ is mass per unit length.

Like Equation (2.34), velocity distribution also can be represented in term of shape functions as shown

$$\dot{y} = H_{i1} \dot{U}_{i1} + H_{i2} \dot{U}_{i2} + H_{j1} \dot{U}_{j1} + H_{j2} \dot{U}_{j2} \quad (2.55)$$

Substitute Equation (3.38) into Equation (3.37),

$$T = \frac{\gamma}{2} \int_0^L (H_{i1} \dot{U}_{i1} + H_{i2} \dot{U}_{i2} + H_{j1} \dot{U}_{j1} + H_{j2} \dot{U}_{j2})^2 dx \quad (2.56)$$

It should be noted that although velocity distribution is the function of time and position, the nodal velocities are only the function of time. Equation (2.54) and Equation (2.55) have considered spatial variations.

Then, the derivative of Equation (2.55) is done as required by Lagrange's equations,

$$\frac{\partial T}{\partial \dot{U}_{i1}} = \frac{\gamma}{2} \int_0^L 2H_{i1} (H_{i1} \dot{U}_{i1} + H_{i2} \dot{U}_{i2} + H_{j1} \dot{U}_{j1} + H_{j2} \dot{U}_{j2})^2 dx \quad (2.57)$$

$$\frac{\partial T}{\partial \dot{U}_{i2}} = \frac{\gamma}{2} \int_0^L 2H_{i2} (H_{i1} \dot{U}_{i1} + H_{i2} \dot{U}_{i2} + H_{j1} \dot{U}_{j1} + H_{j2} \dot{U}_{j2})^2 dx \quad (2.58)$$

$$\frac{\partial T}{\partial U_{j1}^*} = \frac{\gamma}{2} \int_0^L 2H_{j1}(H_{i1}U_{i1}^* + H_{i2}U_{i2}^* + H_{j1}U_{j1}^* + H_{j2}U_{j2}^*)^2 dx \quad (2.59)$$

$$\frac{\partial T}{\partial U_{j2}^*} = \frac{\gamma}{2} \int_0^L 2H_{j2}(H_{i1}U_{i1}^* + H_{i2}U_{i2}^* + H_{j1}U_{j1}^* + H_{j2}U_{j2}^*)^2 dx \quad (2.60)$$

Also, $\frac{d}{dt} \left(\frac{\partial T}{\partial q_i} \right)$ is evaluated

$$\frac{d}{dt} \left(\frac{\partial T}{\partial U_{i1}^*} \right) = \gamma \left[\int_0^L H_{i1}(H_{i1}U_{i1}^{**} + H_{i2}U_{i2}^{**} + H_{j1}U_{j1}^{**} + H_{j2}U_{j2}^{**})^2 dx \right] \quad (2.61)$$

$$\frac{d}{dt} \left(\frac{\partial T}{\partial U_{i2}^*} \right) = \gamma \left[\int_0^L H_{i2}(H_{i1}U_{i1}^{**} + H_{i2}U_{i2}^{**} + H_{j1}U_{j1}^{**} + H_{j2}U_{j2}^{**})^2 dx \right] \quad (2.62)$$

$$\frac{d}{dt} \left(\frac{\partial T}{\partial U_{j1}^*} \right) = \gamma \left[\int_0^L H_{j1}(H_{i1}U_{i1}^{**} + H_{i2}U_{i2}^{**} + H_{j1}U_{j1}^{**} + H_{j2}U_{j2}^{**})^2 dx \right] \quad (2.63)$$

$$\frac{d}{dt} \left(\frac{\partial T}{\partial U_{j2}^*} \right) = \gamma \left[\int_0^L H_{j2}(H_{i1}U_{i1}^{**} + H_{i2}U_{i2}^{**} + H_{j1}U_{j1}^{**} + H_{j2}U_{j2}^{**})^2 dx \right] \quad (2.64)$$

Like nodal velocities, the lateral and rotational accelerations of nodes i and j $U_{i1}^{**}, U_{i2}^{**}, U_{j1}^{**}, U_{j2}^{**}$ are independent of coordinate x and are only depend on time. This allows to pull the nodal accelerations out of the Equations (2.60-2.63). Then the shape functions can be integrated without integrate the nodal accelerations for simplifications of works. Besides, some of the integrals are identical in Equations (2.60-2.63), thus the following shows the integrals that are needed to be evaluated .

$$\gamma \int_0^L S_{i1}^2 dx = \gamma \int_0^L \left(1 - \frac{3x^2}{L^2} + \frac{2x^3}{L^3} \right)^2 dx = \frac{13\gamma L}{35} = \frac{13}{35} m \quad (2.65)$$

$$\gamma \int_0^L S_{i1}S_{i2} dx = \gamma \int_0^L \left(1 - \frac{3x^2}{L^2} + \frac{2x^3}{L^3} \right) \left(x - \frac{2x^2}{L} + \frac{x^3}{L^2} \right) dx = \frac{11\gamma L^2}{210} = \frac{11}{210} mL \quad (2.66)$$

$$\int_0^L S_{i1}S_{j1} dx = \gamma \int_0^L \left(1 - \frac{3x^2}{L^2} + \frac{2x^3}{L^3} \right) \left(\frac{3x^2}{L^2} + \frac{2x^3}{L^3} \right) dx = \frac{9\gamma L}{70} = \frac{9}{70} m \quad (2.67)$$

$$\int_0^L S_{i1}S_{j2} dx = \gamma \int_0^L \left(1 - \frac{3x^2}{L^2} + \frac{2x^3}{L^3} \right) \left(-\frac{x^2}{L} + \frac{x^3}{L^2} \right) dx = -\frac{13\gamma L^2}{420} = -\frac{13}{420} mL \quad (2.68)$$

$$\gamma \int_0^L S_{j2}^2 dx = \gamma \int_0^L \left(-\frac{x^2}{L} + \frac{x^3}{L^2} \right)^2 dx = \frac{\gamma L^3}{105} = \frac{1}{105} mL^2 \quad (2.69)$$

$$\int_0^L S_{j2}S_{j1} dx = \gamma \int_0^L \left(-\frac{x^2}{L} + \frac{x^3}{L^2} \right) \left(\frac{3x^2}{L^2} + \frac{2x^3}{L^3} \right) dx = -\frac{11\gamma L^2}{210} = -\frac{11}{210} mL \quad (2.70)$$

Since incorporating the results of the integrations will lead to $[M]\{\ddot{v}\}$, then the mass matrix for a beam element is

$$[M]^{(e)} = \frac{\gamma L}{420} \begin{bmatrix} 156 & 22L & 54 & -13L \\ 22L & 4L^2 & 13L & -3L^2 \\ 54 & 13L & 156 & -22L \\ -13L & -3L^2 & -22L & 4L^2 \end{bmatrix} \quad (2.71)$$

Like stiffness matrix, the mass matrix for two elements is

$$[M]^{(G)} = \frac{\gamma L}{420} \begin{bmatrix} 156 & 22L & 54 & -13L & 0 & 0 \\ 22L & 4L^2 & 13L & -3L^2 & 0 & 0 \\ 54 & 13L & 312 & 0 & 54 & -13L \\ -13L & 3L^2 & 0 & 8L^2 & 13L & -3L^2 \\ 0 & 0 & 54 & 13L & 156 & -22L \\ 0 & 0 & -13L & -3L^2 & -22L & 4L^2 \end{bmatrix} \quad (2.72)$$

In this project, the cantilever beam is used, thus the matrix is reduced first two rows and first two columns.

$$[M]^{(G)} = \frac{\gamma L}{420} \begin{bmatrix} 312 & 0 & 54 & -13L \\ 0 & 8L^2 & 13L & -3L^2 \\ 54 & 13L & 156 & -22L \\ -13L & -3L^2 & -22L & 4L^2 \end{bmatrix} \quad (2.73)$$

2.6 Magnetorheological fluid damper

In recent years, Magnetorheological (MR) Fluid technology has received much attention and consequently has shown much improvement. Its adaptable nature has led to rapid growth in such varied engineering applications as the base isolation of civil structures, vehicle suspensions, and several bio-engineering mechanisms through its implementation in different MR fluid base devices, particularly in MR Dampers. The MR damper is an advanced application of a semi-active device which performs effectively in vibration reduction due to its control ability in both on and off states. The MR damper has the capacity to generate a large damping force, with comparatively low power consumption, fast and flexible response, and simplicity of design. MR fluid characterization, synthesis, and its application were presented in (Kumbhar et al., 2015; Zhu et al., 2012). An MR damper contains a type of smart fluid called a

Magnetorheological Fluid (MRF). Changes in the applied excitation current vary the strength of the magnetic flux density of the electromagnets and consequently vary the rheological properties of the MR fluid. Such fluids contain micron-sized magnetic particles (5-50 microns) such as iron, suspended in a carrier fluid - usually a kind of oil. Without an applied magnetic field, the MRF behaves as a conventional fluid and its viscosity is independent of the flow rate. However, the application of a magnetic field creates a dipole moment aligned to the field in the iron particles and the particles form linear chains parallel to it, as shown in Figure 2.16.

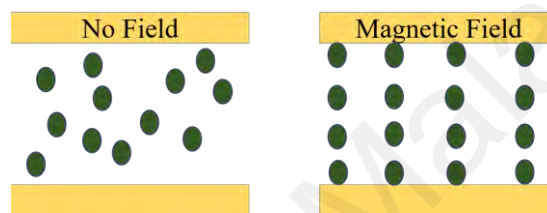


Figure 2.16: MRF magnetic particles chain-like formation with the applied magnetic field.

“A magnetorheological (MR) damper is a semi-active device which generally consists of a damper housing, piston shaft, inner and outer pistons, piston guide, floating piston, MRF and gas chamber. It has numerous advantages such as a large viscosity control range, relatively low price, low power feeding, quick response, and small size. In this device, MRF is used and its viscosity changes very quickly with the applied magnetic field, moving to semi-solid from liquid in only a few milliseconds. It results in an enormously variable and controllable damper able to provide a large resisting force (Ferdaus et al., 2014; Jiang et al., 2011; Togun et al., 2014).

The great advantages of the MR damper widen its range of application. It was used in the suspensions of heavy duty trucks and other road vehicles (Du et al., 2013; King, 2013; Sung et al., 2011; Z. Xie et al., 2013; Ali S Yildiz et al., 2013), in a seat suspension system where it is known as Motion Master (Du et al., 2013; Du et al., 2011; H Laalej et al., 2012), in haptic devices (Kameyama et al., 2014; Tsujita et al., 2012), in knee prosthetics of limbs to control the force (Bisbee III et al., 2013; Gudmundsson et al.,

2010; H.-L. Xie et al., 2010), civil structures (Billie Jr et al., 1998; Bitaraf et al., 2012; Cha et al., 2013; El-Khoury & Adeli, 2013), military equipment (Hosseini et al., 2011; Singh & Wereley, 2014), in fixing turning devices to hold turbine blades while they are being machined (Johnson & Kienholz, 1982), wind turbines (P. Martynowicz, 2017), landing gears (Atabay & Ozkol, 2013; Gharapurkar et al., 2013; Powell et al., 2013), helicopter lag dampers (Kothera et al., 2011; Norman Mark Wereley et al., 2013), and aerospace launching applications (Jean et al., 2005). This versatile applicability requires researchers to work on the optimization of the design and configuration of dampers and to optimize them with respect to their specific applications.

2.6.1 Operating principles and classifications of MR fluid damper

Conventional shock absorbers inspire the design of the MR damper. It is a semi-active damper which could control the input current for control. It generally consists of a damper housing, a piston shaft, inner and outer pistons, a piston guide, a floating piston, MR fluid and a gas chamber as shown in Figure 2.17. Inside the damper housing, piston guides contain the outer piston. The outer piston surrounds the inner piston, with a small gap between them for the MR fluid to flow. The coil is housed inside the inner piston in such a way that its induced magnetic flux can flow through the MR fluid. This magnetic field changes the viscosity of the MR fluid by the alignment of magnetic particles as shown in Figure 2.18 and thus changes the force required to move the piston through the MR fluid. As the current increases, the induced magnetic field strength increases, and a greater force is required to move the piston. The combination of these inner and outer pistons, piston housing and coil form an MR valve structure.

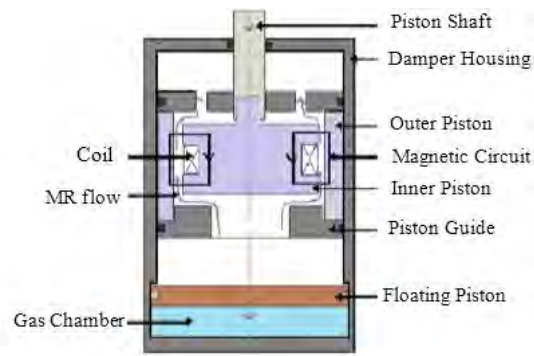


Figure 2.17: Typical MR damper configuration

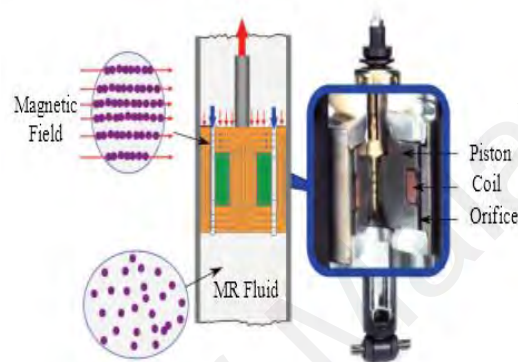


Figure 2.18: Basic operating principle of MR dampers. Reprinted from (Geldhof, 2013)

From the structure, it is seen that this MR valve divides the damper into two chambers, the lower and upper chambers, fully filled with the MR fluid. The maximum force delivered by MRD is governed by the properties of the MRF, its flow mode, and the size of the MRD. Practically all devices that use MRF are categorized as functioning in three modes: valve mode, direct shear mode and squeeze mode. When an MR damper operates in valve mode, the MRF itself hinders the MRF flow from one reservoir to another and it is the most commonly used mode among the four modes for an MR damper as shown in Figure 2.19(a) (Spencer Jr et al., 1998). MRF devices are operating in shear mode when a thin layer of MRF is sandwiched between two paramagnetic moving surfaces is shown in Figure 2.19(b). The shear mode is primarily beneficial for dampers those can provide small forces, such as for compact clutches and brakes. An MRF device is said to be operating in squeeze mode when a thin film (of the order of 0.02 inch) of MR fluid is sandwiched between pole surfaces as in Figure 2.19(c). The most recent MRF

flow mode is known as the magnetic gradient pinch mode, which is like the MRF valve mode but with a different magnetic construction. In the conventional valve mode, MRF is solidified by a uniform field throughout the valve (Yazid et al., 2014), whereas in magnetic gradient mode the MRF is only solidified near the wall by a non-uniform field. In this mode, a comparatively large opening replaces the narrow fluid flow path. In such a configuration, the magnetic gradient pinch mode operates in two control modes namely pinch mode and reversible jamming mode.

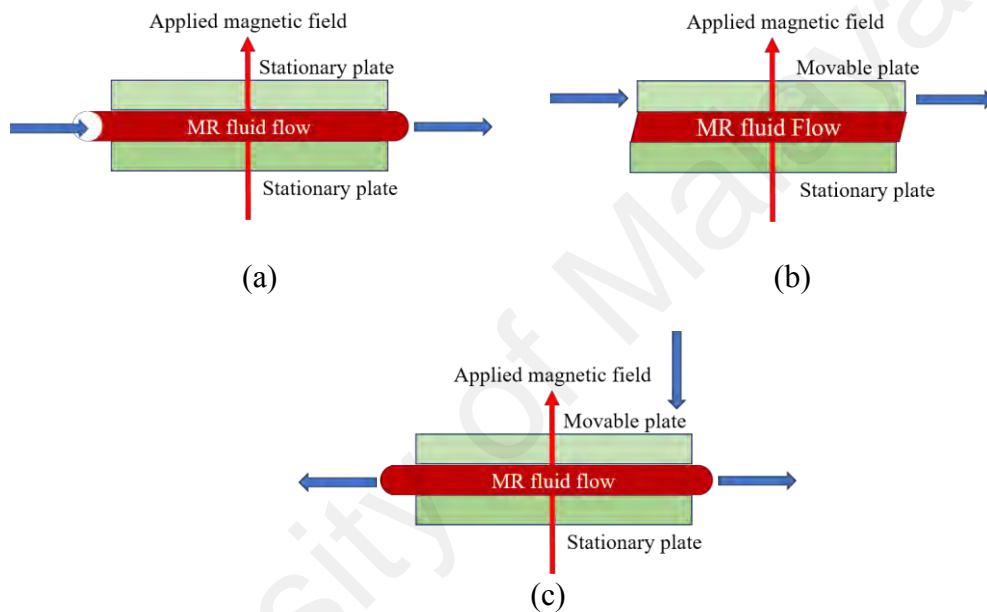


Figure 2.19: MR damper modes: (a) Valve mode (b) Direct shear (c) Squeeze mode

MR dampers are classified as linear and rotary (N. Wereley et al., 2008) with respect to their piston motion i.e. when the operation relates to the angular or rotary motion of the piston, they are called rotary MR dampers. In a rotary MR damper, the MRF operates in one or two flow modes integrally. With regard to design and configuration, there are two main types of rotary MR damper, known as continuous angle and limited angle revolution MR dampers (Imaduddin et al., 2013). The continuous angle rotary MR damper can switch with the endless rotational angle. The MR brake is a perfect example of a continuous angle MR damper. From the name, it is obvious that the MR brake reduces the motion of the rotor by altering the MRF viscosity as the rotor is absorbed in MRF. Usually, in an MR brake, the MRF operates in direct shear mode, whose operation

depends upon such factors as magnetic flux density, MRF gap, and working speed. Among these parameters, the MRF gap and working speed cannot change after the construction of an MR brake. Thus, the effective way to operate and control this device is to manipulate the magnetic flux density in the activation region. Again, regarding the position of the shear mode, the MR brake is classified as disc type and drum type MR brakes. The designs and operating principles of disc type and drum type brake were described in (Farjoud et al., 2008). In disc type MR brake, shear mode occurs in axial gap of the rotor, whereas for drum type brakes, shear mode occurs in radial gap of the rotor. On the other hand, a limited angle rotary MR damper, known as the vane type damper, cannot rotate continuously like a continuous angle damper. However, it can produce a larger damping torque compared with the continuous angle damper. Hence, it is appropriate for applications where a high damping torque with limited angular movement is required although it is not suitable for applications that require a high rotor speed. In recent decades, only limited research has been carried out on vane type MR dampers (Giorgetti et al., 2010; L. Yang et al., 2011; J. Zhang et al., 2009). The overall classification of MR dampers is presented in Figure 2.20.

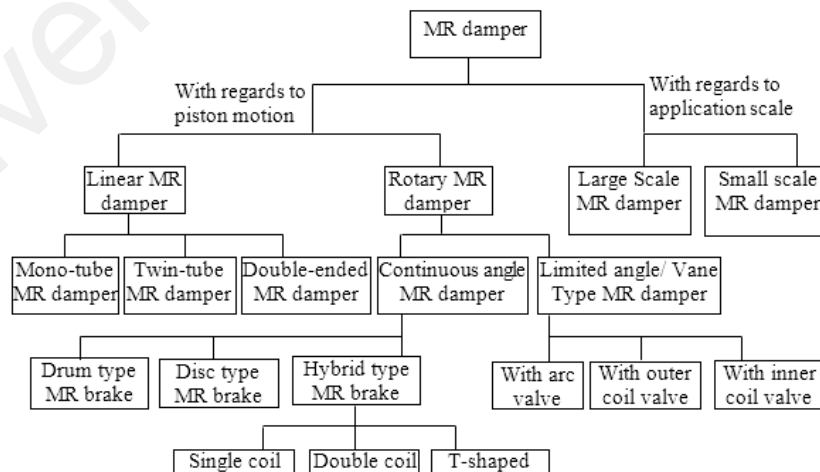
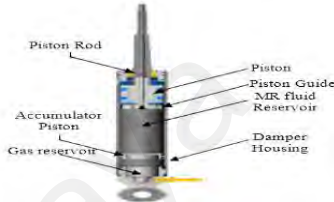
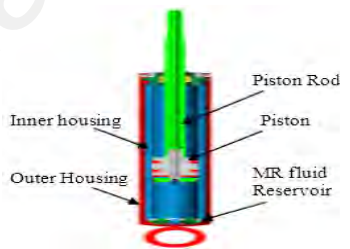
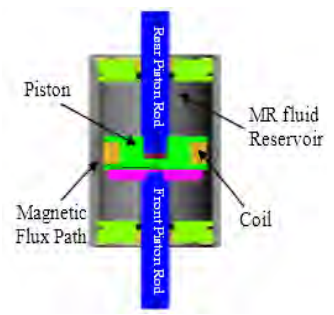


Figure 2.20: MR damper classification

According to the design and configuration of the cylinder of the MR damper, the linear MR damper can be divided into three types: Monotube, Twin-tube and Double-

ended MR damper. Various types of linear damper design, construction, and working principles are summarized in Table 2.2, with illustrations of the different dampers and their parts also presented.

Table 2.2: Various MR damper designs and working principles

Type of MR damper	Design and working principle	Figure/Reference
Mono Tube MR Damper	This MR damper consists of only one tube or reservoir and is known as a Monotube MR damper. It is the one most commonly used because of its compact size and ability to be installed in any location. The movement of the piston rod causes a volume change in the reservoir which is compensated for by an accumulator mechanism.	 <p>Mono Tube MR Damper. Reprinted from (Poynor, 2001)</p>
Twin Tube MR damper	An MR damper that contains two fluid reservoirs is called a twin tube MR damper. For two separate reservoirs, this damper has an inner and outer housing. The inner reservoir is filled with MR fluid and there no air gap. So, the outer reservoir is partially filled with MR fluid to accommodate the fluid of the inner reservoir in times of piston movement. There are two valves in the foot valve mechanism.	 <p>Twin Tube MR Damper. Reprinted from (Poynor, 2001)</p>
Double Ended MR Damper	The MR damper in which two piston rods of the same diameter enter the reservoir from both ends of the damper is known as a double-ended MR damper. In this type of damper there is no change of volume due to the piston's relative movement and as a result, the accumulator mechanism is absent here. Some common applications of this damper are in gun recoil (Ahmadian & Poynor, 2001), bicycles (Ahmadian et al., 1999), and the control of sway motion in buildings due to heavy winds or earthquakes.	 <p>Double Ended MR Damper. Reprinted from (Poynor, 2001)</p>

2.6.2 MR damper models

Controllability is a unique feature of a semi-active control system where minimum power supply can be applied and save power. To get the full advantage of the unique

features of the MR fluid damper and its nonlinear behavior, proper models must be developed that effectively depict the behavior of a typical MR damper. Different MR damper models have been proposed and the responses of the MR damper were analyzed in (Dyke et al., 1996, 1998; Qian et al., 2016; B. F. Spencer et al., 1997). In these studies, the experimental analysis was investigated and compared with a simulated response to evaluate the performance of the models. The applications of MR damper models (mainly for vehicle suspension systems) were also presented. There are also various types of developed models for the characteristics of MR dampers. According to the method of modeling, the models were classified as parametric (D. Wang & Liao, 2011) and non-parametric dynamic models (S.-B. Choi et al., 2001; Ehrgott & Masri, 1992; Jin et al., 2005; Kim et al., 2008; X. Song et al., 2007; X. Song et al., 2005). By considering the characteristics shown by the established models, they can be further classified as quasi-static models (Y.-T. Choi & Wereley, 2005; Weng W Chooi & Oyadiji, 2008; Weng Wai Chooi & Oyadiji, 2009a, 2009b; Dimock et al., 2002; Gavin et al., 1996; S.-R. Hong et al., 2007; S. Hong et al., 2008; Kamath et al., 1996; Lee et al., 2002; Lee & Wereley, 1999, 2000; Makris, Burton, Hill, et al., 1996; Makris, Burton, & Taylor, 1996; Phillips, 1969; X. Wang & Gordaninejad, 2000; Norman M Wereley & Pang, 1998) and dynamic models. Considering the reversibility of the established models, they can be classified as dynamic models (D. Wang & Liao, 2005; D. Wang & Liao, 2011) and inverse dynamic models (Tsang et al., 2006).

Among the non-parametric MR damper models, Bingham, Gamato-filisko, Li, Bouc-Wen and Modified Bouc-Wen model are well established in the various application for modeling of MR damper. Spencer et al. investigated the effectiveness of these models (J. B. F. Spencer et al., 1996) with experimental data. Also, error norms are calculated for some important models shown in Table 2.3. For each model, the error between predicted

force and measured force are calculated with respect to time (E_t), displacement(E_x) and velocity($E_{\dot{x}}$) over two complete cycles.

Table 2.3: Calculated error for MR damper models(J. B. F. Spencer et al., 1996)

Model	E_t	E_x	$E_{\dot{x}}$
Bingham	0.154	0.0398	0.133
Gamota and Filisko	0.196	0.0717	0.300
Simple Bouc-Wen	0.167	0.0585	0.135
Modified Bouc-Wen	0.0351	0.0228	0.0445

From the above tables, it is shown that the calculated error for Modified Bouc-Wen model is very small compared to other models. Moreover, only Simple Bouc-Wen and Modified Bouc-Wen model provides the hysteresis characteristics. Thus, it can be concluded that the modified Bouc-Wen model is suitable for MR damper and it is implemented in this research.

2.7 Control scheme

Controllers are designed to improve the response of the system based on desired output. For vibration problem of a structure, controllers are designed to provide stability of a structure so that unwanted vibration is minimized or mitigated. Since excitation forces are high in civil structures and wind turbines, appropriate controller design is important to avoid structural damage. The importance of controller design for wind turbines was highlighted at (Bossanyi et al., 2009). Numerous controllers were designed in the past to provide structural stability with structural vibration control. The applications and effectiveness of few widespread controllers for structural vibration control were presented in (Housner et al., 1997). H-infinity, linear quadratic regulator/Gaussian (LQR/LQG), fuzzy logic, neural network are the most applied control techniques in wind turbine to control vibration. LQR/LQG controllers are described as operating dynamic systems with providing minimum cost using quadratic function and it controls multiple input multiple output (MIMO) problem. These controllers are suitable for both linear and

non-linear problem. Eide and Karimi (2009) investigated the performance of Disturbance Accommodating Control (DAC), Linear Quadratic Control (LQR) and Linear Quadratic Gaussian (LQG) control for vibration mitigation on wind turbine systems. LQG controller was also utilized for MR damper based semi-active vibration control of an offshore platform (S. Wang & Li, 2013). In another research, Karimi et al. showed how H-infinity control law can be designed and implemented on wind turbine systems for vibration control (Karimi et al., 2010). The result shows a significant improvement in vibration reduction using the controller compared to the uncontrolled system. Robust control improves the performances and provides stability in the presence of uncertainties and the uncertainties were described probabilistically (Housner et al., 1997). The performance of a robust model predictive control (MPC) was investigated in (Staino & Basu, 2013b) to mitigate the vibration of wind turbine blades. The effectiveness of H-infinity and robust MPC control policies were shown in Figure 2.21(a) and Figure 2.23(b) respectively.

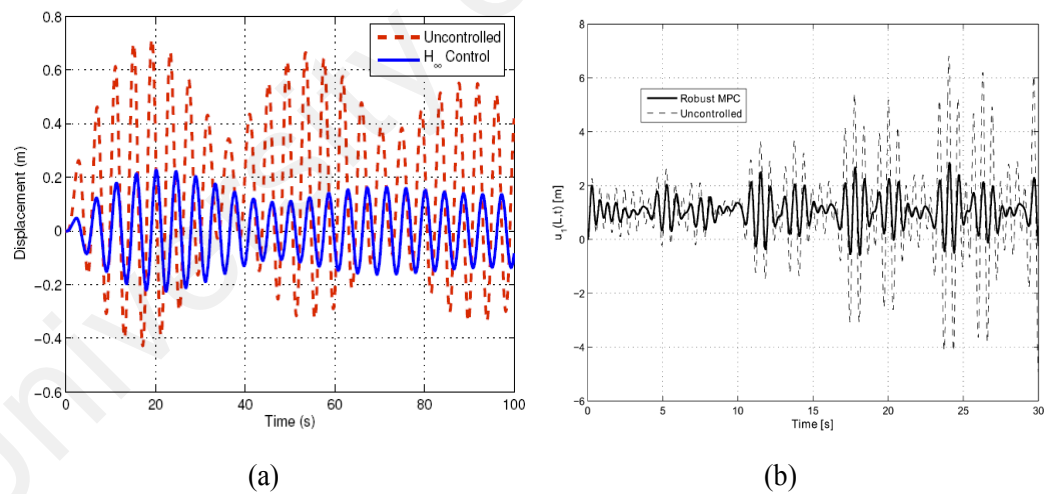


Figure 2.21: Wind turbine vibration control response using (a) H-infinity (Karimi et al., 2010) and (b) Robust MPC controller (Staino & Basu, 2013b)

To optimize the performance of wind turbines, fuzzy logic controllers were designed and implemented in (Calderaro et al., 2007). To provide an improved structural response with vibration control, the suitable controller must be designed. Researchers are giving

significant focus to design system controllers because of its usefulness to optimize wind turbine power generation with respect to vibration due to different excitation loadings.

2.7.1 Proportional integral derivative controller

PID controller is most common control scheme and becomes one the most accepted controller in industrial applications. PID controller is very simple but effective and it offers a variety of types and deigns methods. PID controller is a type of feedback control system where the controller receives a reference signal and compare it to an actual feedback. PID controller is designed to eliminate the error between a set point and an actual feedback. The controller has three control parameters such as proportional (K_p), integral (K_i), and derivative (K_d). A typical PID structure is shown in Figure 2.22.

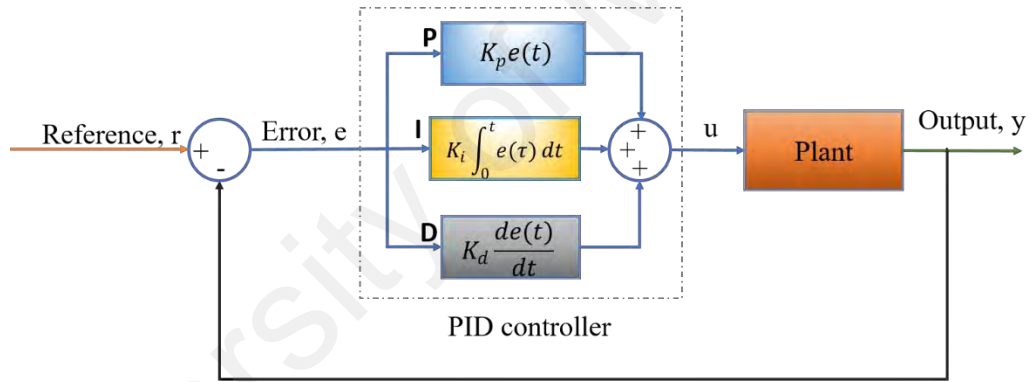


Figure 2.22: Structure of PID controller

Based on the configuration in Figure 2.24, the controlling force of PID can be expressed as below:

$$u(t) = K_p e(t) + K_i \int_0^t e(t) dt + K_d \frac{de(t)}{dt} \quad (2.74)$$

Proportional (K_p), integral(K_i), and derivative(K_d) parameters of PID controller deals with amplitude, steady-state error, and overshoot of the system respectively to achieve required response. K_p accounts for present values of error, which is if the error is large and positive, this control variable will be large and negative. A large value of this control variable causes a large change in output for a given change in error and thus the system

will become unstable. Low value, however, causes small output response to a large input error and thus the controller is less responsive or less sensitive. K_i accounts for past values of error, which is if the output is not sufficient to reduce the size of the error, this control variable will accumulate over time and cause the controller to apply the stronger action. The integral term is proportional to both magnitudes of error and duration of error. The absence of integral control variable may prevent the system reaches its desired set point. This integral term accelerates the process towards its setpoint and eliminates the steady state error. Yet, it may cause overshooting. K_d accounts for possible future values of error based on its current rate of change. This derivative term can improve settling time and stability of the system.

The response of controller can be described in terms of responsiveness to error, the degree to which system overshoots a set point and the degree of any system oscillation. The application of PID controller in a system does not guarantee optimal control of the system or its stability. In some cases, the PI controller is more common as the derivative control variable is sensitive to measurement noise.

Instability of system is caused by an excess gain which particularly in the presence of significant lag. Stability of a system can be obtained by tuning the controller. There are several tuning methods which are generally used to tune the control parameters, for example, manual tuning, Ziegler-Nichols method, Tyreus-Luyben method, software tool, Cohen-Coon method and Astrom-Hagglund method. The Z-N method is very common for PID tuning in several applications. In the Z-N method, a critical gain value is measured by increasing K_p at which the system provides sustained oscillations and the corresponding period is computed to calculate three control parameters of PID controller. However, PID controller design method enters a new era where auto-tuning, fuzzy control tuning, neural network, and nature-inspired optimization algorithm techniques are getting

much attention. For manual tuning, the effects of changes each control variable are tabulated in Table 2.4 below.

Table 2.4: Effect of increasing the PID parameters

Parameter	Rise time	Overshoot	Settling time	Steady-state error	Stability
K_p	Decreases	Increases	Minor change	Decreases	Degrade
K_i	Decreases	Increases	Increases	Eliminate	Degrade
K_d	Minor change	Decreases	Decreases	No effect	Improve if small increases

2.7.2 Ant colony optimization method

Using optimization technique for tuning PID control parameters is common in vibration control strategy. One of the most effective and simple natural inspired algorithms is Ant colony optimization (ACO) method. ACO algorithm was first implemented by Dorigo et al. where optimization problems were solved with discrete search space method. This algorithm is based on the behavior of real ants that how ants can find the shortest route from their colony to sources and get back to initial position.

A state space graph of ACO is shown in Figure 2.23. If $X = [X_1 X_2 \dots X_n]$ is defined with parameter that needs to be optimized where n is the number of parameter for optimization and the total field is divided into W subspaces with $i = [1, 2, 3, 4, \dots, W]$, the length of each subspace, $h_i = \frac{x_{i_up} - x_{i_low}}{W}$ the value of parameters X can be written as

$$[X_1 X_2 \dots X_n] = x_{1_low} + i_1 \times h_1, x_{2_low} + i_2 \times h_2, \dots, x_{n_low} + i_n \times h_n \quad (2.75)$$

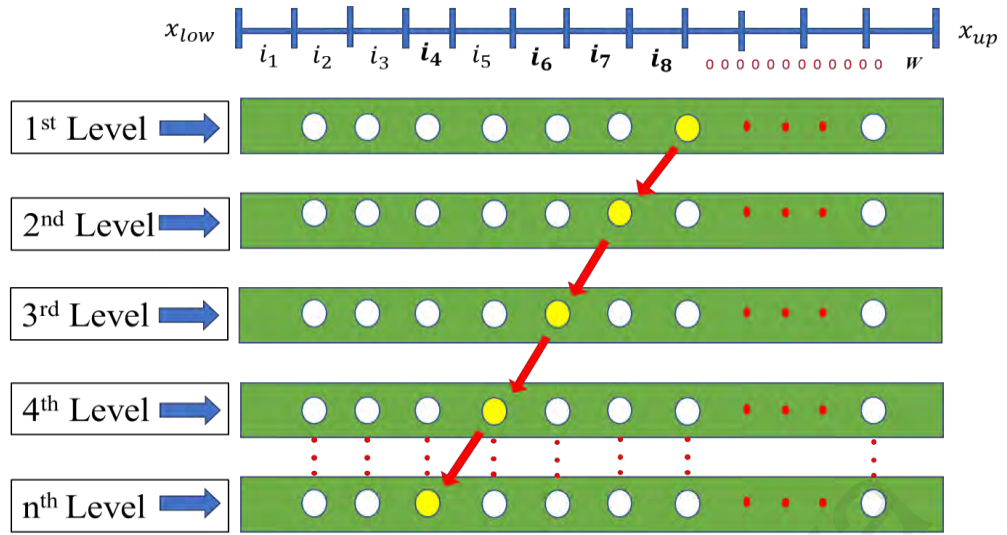


Figure 2.23: State space graph for ACO

A single ant, ($T=1,2,3,4,\dots,W_{ant}$), where W_{ant} is total number of ants, moves from one node to another node. The travel index (i_8, i_7, \dots, i_4) depends on the probability, P_{ij} , to move ant T from one node to another on the j^{th} level. The equation of the probability can be expressed as below:

$$P_{ij} = \frac{\tau_{ij}}{\sum_{i=1}^n \tau_{ij}} \quad (2.76)$$

The Equation (2.77) follows the state space rules shown in Figure 2.23 and the amount of pheromone τ_{ij} at the node is updated by

$$\tau_{ij} = (1 - \rho)\tau_{ij} + Q / f_{best} \quad (2.77)$$

where ρ is decay parameter with range (0,1), Q is the quantity of pheromone per iteration by an ant, f_{best} is the objective function value provided by the best ant after each searching period. . In the RHS, τ_{ij} is used as initialization value with τ_0 , a constant initial value.

A flow chart of ACO method to find an optimal solution is presented in Figure 2.24. ACO process starts with a new iteration of ants. The process will search for a new solution

based on the objective function. The process will be stopped if the best solution is found, otherwise, the process will continue to search for best solution until the last iteration.

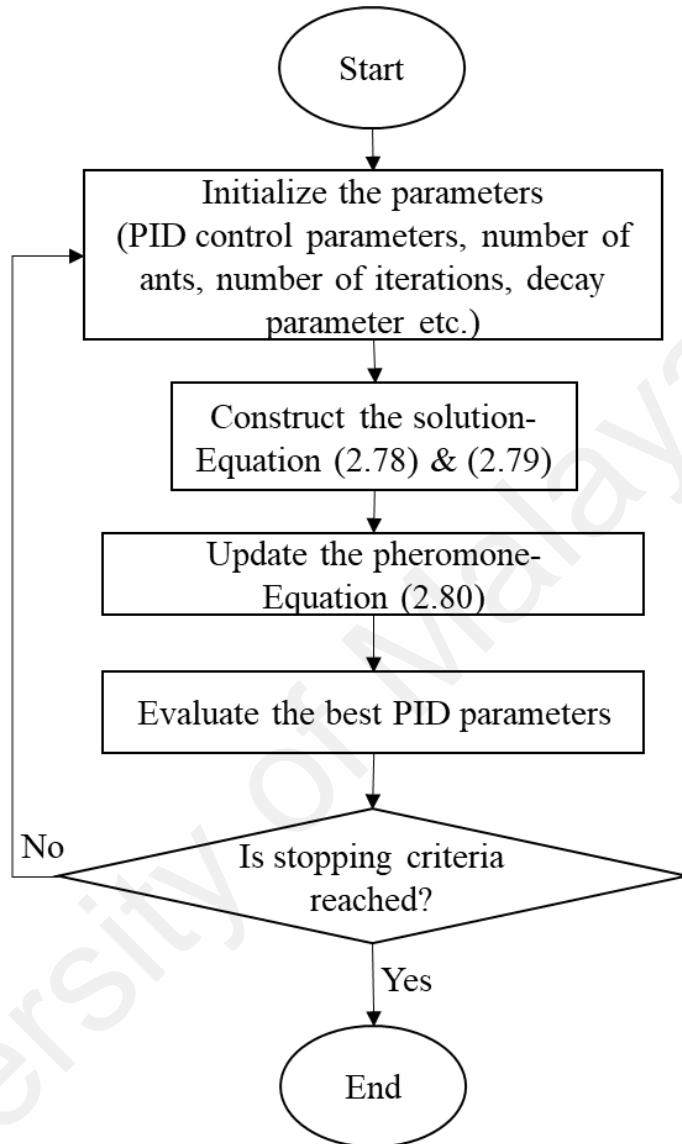


Figure 2.24: Flowchart of ACO method

2.8 Damper positioning in semi-active vibration control of wind turbine

The optimal placement of control dampers play a major role in structural vibration control and this importance was highlighted more than two decades ago (Gurgoze & Muller, 1992). Appropriate positioning of control dampers not only maximize the vibration reduction rate but also minimize design and maintenance cost. Optimal placement of control damper is investigated using a genetic algorithm in different studies previously (Askari et al., 2017; Guo & Zhang, 2004; L. Li et al., 2010). In these studies,

optimal placement of MR damper was investigated in the multi-storied building based on effective force distribution as an objective function to implement a minimum number of dampers. For wind turbines, semi-active control dampers are implemented in two positions on the wind turbine until now; one position is on top of the tower with nacelle as TLCD and TMD (Luo et al., 2012; P. Martynowicz, 2016) and at the base (Caterino et al., 2016). The implementation of MR damper in wind turbine vibration control is very limited. P. Martynowicz (2016) and Caterino et al. (2016) investigate MR damper on top of the tower and at the base respectively. However, both places have limitations for MR damper installation in terms of desired force, effectiveness of vibration control and maintenance cost. Damper on top of tower produces extra mass inside nacelle of HAWT where generators, control box etc. are installed. Moreover, in the case of heavy wind or small earthquake, vibration occurs throughout all the points of the tower including base. In this circumstance, damper on top cannot provide required counter force to reduce vibration efficiently. On the other hand, damper installed at the base can efficiently reduce the base displacement due to external disturbances, however, for tall horizontal axis wind turbines, vibration occurs from top/base and transfers to other points of the tower. Also, vibration on top of the tower due to disturbances from blades, generators cannot be reduced efficiently if the damper is installed at the base. Therefore, optimal placement of MR damper needs to be investigated on other places on MR damper such as mid-span of the tower which can work as a bracing and provide proper balance in the system to ensure maximum vibration reduction.

2.9 Summary

Most common vibration control strategies are generally classified as passive, active, and semi-active control strategies. However, for any environmental changes or structural parameter variations passive control approach cannot provide required force since it does

not involve external force. Although active vibration control is effective in vibration reduction since it requires external force, it has a limitation which is large power consumption and inability to change material properties of the actuators to adjust desired damping force. To counter this limitation, semi-active control approach was proposed for structural vibration control which also requires external forces like active control, but this system can change the material properties of the actuators under magnetic/electric field. TMD, TLCD are most widely used damping device for wind turbine vibration control. MR damper is used as semi-active vibration control device which produces high damping force with low input current. MR damper can be used as passive or active damping device where fixed current input is used. In terms of modeling of wind turbine, cantilever beam is used to represent the wind turbine tower. It was found that the most common modeling method of the beam is FEM. Equations of cantilever beam are complex, therefore, numerical methods such as FEM and FDM are often used to solve these equations to find natural frequencies and dynamic response of wind turbine model. For vibration control applications, suitable controller design is very important which gives proper control force to counter the vibration. For wind turbine application, LQR, PID and H-infinity, and Skyhook controllers are widely used. However, these controllers are often tuned with trial and error method. Also, this controller efficiency is not investigated for different range of excitation frequencies and types of loading conditions, which is very important. Automatic tuning process are not applied for wind turbine vibration control applications. Nature inspired algorithm such as ACO and PSO are not investigated to optimize the control parameters. The position of damping device on the wind turbine tower is crucial to provide maximum vibration reduction with low maintenance cost. Previously, damping device is mostly implemented either on top of the tower or at the base. Therefore, it is good opportunity to design suitable controller and optimize the parameters automatically with nature inspired algorithm and investigate the optimal position of MR damper to

reduce vibration significantly under different excitation frequency and amplitudes. Therefore, based on the previous studies, research gaps are identified. Research gaps and proposed studies to enhance the wind turbine vibration control system are summarized in Table 2.5.

Table 2.5: Research gap and proposed study

No.	Feature	Previous study	Research gap	Proposed study
1.	Vibration control under different excitation frequencies and amplitudes for wind turbine tower	Various control policies have been investigated for wind turbine vibration control such as PID, LQR, H-infinity etc. However, the effectiveness of these controllers at different frequencies (including natural frequency) is not provided.	The controller performances have not been investigated under different excitation frequencies and different types of loadings to achieve maximum vibration reduction to adapt real environments of wind turbine	The proposed controller (PID-ACO) provides optimal control parameters can overcome the limitation of low vibration reduction under excitation force at natural frequency where resonance may occur and limitation of low adaptability when excitation frequency varies.
2.	Tuning process of vibration controller	Various tuning processes have been investigated for vibration controller such as Ziegler-Nichols, Cohen Coon etc.	The controller gains are generally tuned with trial and error methods. Also, for tuning process, step input excitation is used for tracking the error between the reference and actual input. Therefore, tuning process using for harmonic force with natural frequency has not been investigated	The optimum controller gains are achieved using PID-ACO process which is an automatic process to find desired control force. Sine input is used to find the controller gains to ensure optimal control force to ensure maximum vibration reduction at 1 st mode.
3.	Position of MR damper	In the previous studies, the actuating devices have been installed mostly either on top the tower with the nacelle or at the	The investigation for optimal positioning of MR damper is limited. The MR damper at mid-point of the tower has not been	The performance of MR damper installed at different positions are evaluated in this study. Also, the damper is placed on

		base for wind turbine tower vibration control	investigated previously.	the mid-point the tower so that it can provide sufficient vibration reduction at the top of the tower, ensure structural balance, and reduce maintenance cost.
--	--	---	--------------------------	--

University of Malaya

CHAPTER 3: METHODOLOGY

3.1 Introduction

This chapter will discuss the simulation and experimental procedures of the proposed semi-active vibration control of wind turbine. The objective of this study is to minimize vibration of wind turbine tower to enhance the performance to produce maximum power. This study investigates semi-active vibration control strategy of wind turbines with ACO optimized PID controller and the suitable placement of MR damper at the mid-point of the tower. The experimental set-up for lab-scaled wind turbine tower are also presented in this chapter. The block diagram of the proposed system is shown in Figure 3.1.

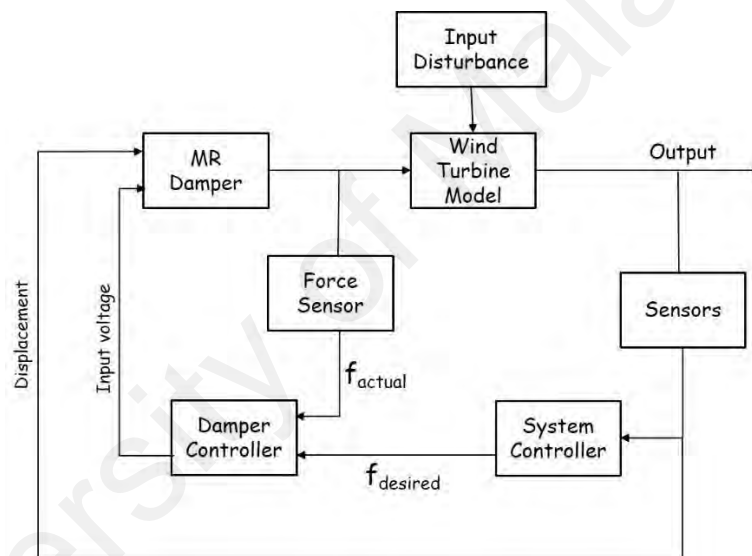


Figure 3.1: Block diagram of semi-active control system

FDM modeling and system identification process provides a suitable model for wind turbine tower. The PID-ACO controller computes required control force for MR damper to counter vibration on the tower. The controller shows that it has the ability to provide desired counter force under different excitation frequencies and loadings. Moreover, the proposed vibration controller automatically achieves optimal control force which require less computational time compare to conventional methods. Experimental validation shows that the PID-ACO vibration controller has good prospect in real life applications. A flowchart of the methodology is presented in Figure 3.2.

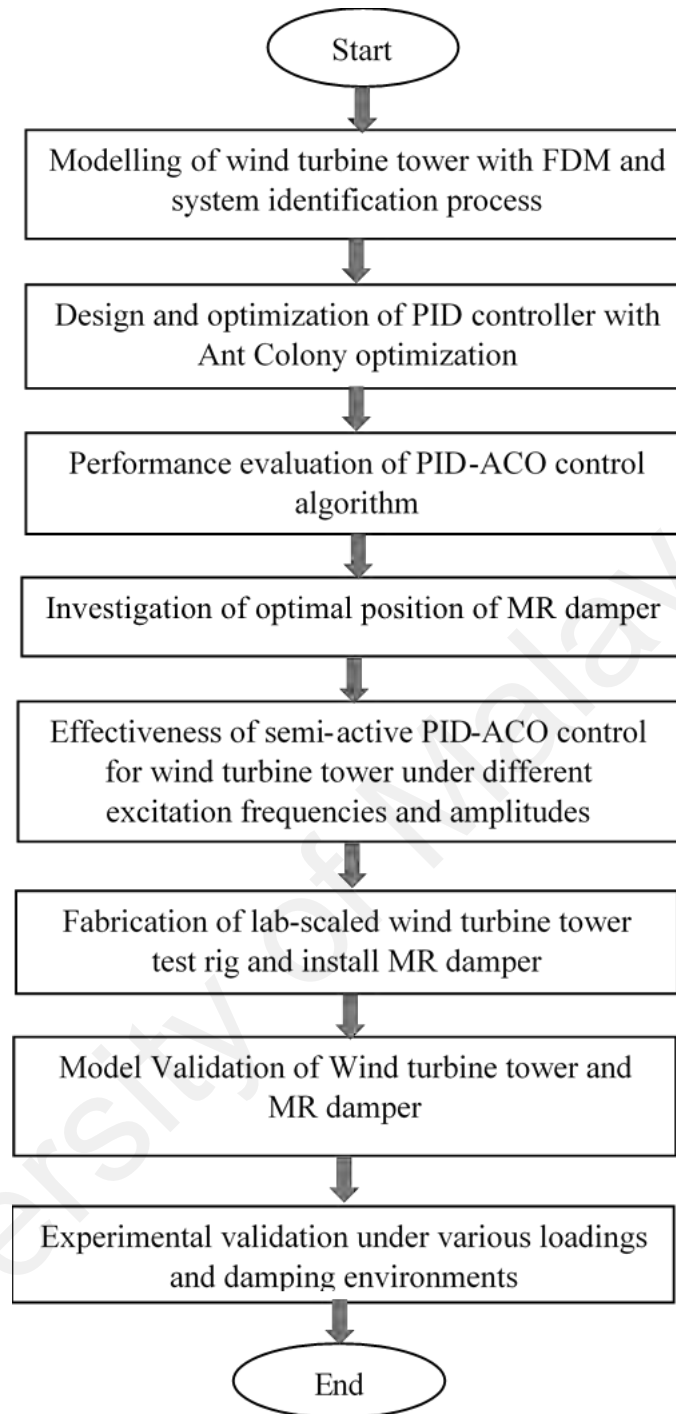


Figure 3.2: Flow chart of research methodology

3.2 Modeling and control system of semi-active wind turbine tower

Wind turbine dynamic model is important to analyze vibration in the system under different loadings and to implement vibration control system. This study developed a wind turbine tower model with FDM and verified its effectiveness with system

identification process. The estimated dynamic models from the system identification process are compared based on fit to estimation data, Cross Signature Assurance Criterion (CSAC) and Mean squared error (MSE) and best model is selected. The wind turbine tower model was simulated under sinusoidal and random excitations to analyze vibration on the tower due to wind loadings and external disturbances from the nacelle. The system controller was designed with PID controller to calculate desired force for maximum reduction of tower vibration. MR damper was used in this study as a semi-active device to provide an external force to counter vibration. Since MR damper is controllable, a PI controller was designed to find a suitable current input for MR damper based on desired and actual force of MR damper. PID controller parameters were optimized using ACO method which is very effective and user-friendly. This study investigated the effectiveness of proposed vibration control strategy for different input frequencies and amplitudes. This study also investigated the different position of MR damper on the tower to ensure structural balance and low current supply.

3.2.1 Modeling of wind turbine tower

For modeling of wind turbine tower, it was represented by cantilever beam and modeled with FDM. The cantilever beam was divided into 20 segments. The schematic diagram and properties of cantilever beam are shown in Figure 3.3 and Table 3.1. The top of the tower was represented by 20th elements of the beam. The bottom of the tower was fixed to the ground with a frame. MR damper, operated as semi-active damping device, was located at the mid-point of the tower. Sinusoidal and random input excitations are implemented on top of the tower to represent an external force from rotating blade and wind respectively to wind turbine tower. MR damper is placed on the 10th element but the damper was also investigated at 5th element.

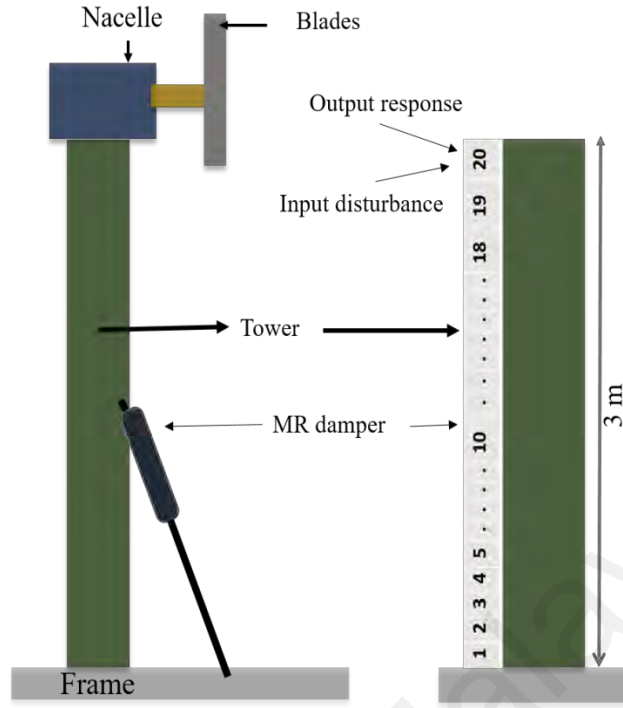


Figure 3.3: Schematic of the wind turbine tower as cantilever beam

Table 3.1: Properties of Cantilever Beam

Parameter	Aluminum Beam
Length	$L=3$ m
Width	$W=0.05$ m
Thickness	$T=0.05$ m
Modulus of elasticity	$E=7.11 \times 10^{10} \text{N/m}^2$
Density	$\rho=2700 \text{kg/m}^3$
No of elements	20

The cantilever beam is presented with Euler Bernoulli beam mathematical model. For a cantilever beam, a fourth order PDE can be generated for time response of the structure in lateral motion as below:

$$\frac{EI}{\rho S} \frac{\partial^4 y(x,t)}{\partial x^4} + \frac{\partial^2 y(x,t)}{\partial t^2} + c \frac{\partial y(x,t)}{\partial t} = \frac{L}{m} [F_{exc}(x,t) + F_{act}(x,t) * \sin \theta] \quad (3.1)$$

where, $y(x, t)$ is displacement of the structure at point x and at time, t . m is the beam mass, c is damping coefficient, F_{exc} and F_{act} is excitation force and controlled force from actuator respectively at point x and at time t , θ is the angle between the tower and the damper, ρ is the density of the beam, L is the length of the beam, and S is the cross-sectional area of the beam. The product of modulus of elasticity, E with moment of

inertia, I is the flexural rigidity of beam. The position of damping device with an angle to the tower will work as a normal bracing when no vibration control is required. Also, this angle will ensure that no additional structure/wall is required to attach the end of the damper, it can easily be placed at the base.

The dynamic equation of the structure can be generalized as below:

$$[M]\{\ddot{y}\} + [C]\{\dot{y}\} + [K]\{y\} = \{F_{exc}\}_{-top-tower} + \{F_{act}\}_{-mid-tower} \quad (3.2)$$

which can also be written as:

$$\ddot{y} + 2\zeta\omega_n\dot{y} + \omega_n^2 y = f(t) \quad (3.3)$$

where, M , C , and K are mass, damping and stiffness matrices respectively, natural frequency, $\omega_n = \sqrt{\frac{K}{M}}$, damping ratio, $\zeta = \frac{C}{2\sqrt{KM}}$, $f(t) = \frac{F_{exc} + F_{act}}{M}$. Mass and stiffness matrices are computed using FD method and damping matrix is assumed.

The modeling of FDM was verified using system identification process and the dynamic models are estimated. System identification toolbox from MATLAB used grey-box method to estimate a dynamic model of any structure. The input and output of the response were imported to the toolbox and a set of models were estimated for a different combination of poles and zeroes. The estimated models were compared based on fit to estimated data, MSE, and CSAC and the best model was selected.

Cross signature assurance criterion (CSAC) was used to evaluate the shape of the frequency response functions. The formula of CSAC is

$$CSAC(j, \omega) = \frac{\left| \left(H_j^X(\omega) \right)^H H_j^A(\omega) \right|^2}{\left(\left(H_j^X(\omega) \right)^H H_j^X(\omega) \right) \left(\left(H_j^A(\omega) \right)^H H_j^A(\omega) \right)} \quad (3.4)$$

where $H_j^X(\omega)$ is experimental frequency response function and $H_j^A(\omega)$ is analytical or numerical frequency response function. CSAC is ranged from 0 to 1 where 0 means completely different and 1 means identical between two frequency response functions. In

this project, $H_j^X(\omega)$ was used as reference frequency response function, which was obtained mass, stiffness and damping matrices using FDM and $H_j^A(\omega)$ is the frequency response function obtained from System Identification Toolbox.

MATLAB/Simulink software was used to model the wind turbine tower. Mass and stiffness matrices were used to estimate the Frequency Response Functions (FRFs). The first and second bending modes were validated with experimental model later in this study. The disturbance force was applied horizontally to the top of the tower. Tower responses due internal and external (disturbances from nacelle/blades, wind/sea waves) is observed at the top of the tower, (i.e. 20th elements) and thus reduced using the damping force of MR damper connected to the tower at the midpoint. Maximum deflection is observed at 1st mode at the top of the tower. The MR damper control force was provided by the Modified Bouc-Wen model where force is current dependent. The generated force was added to the appropriate signals of the wind turbine model to reduce the deflection.

3.2.2 Modeling of MR damper

Modified Bouc-Wen model was adopted in this study to predict better damper response. Spencer et al. first proposed a modified model of Bouc-Wen in 1997 (B. F. Spencer et al., 1997) and it is widely known as Modified Bouc-Wen model. This model constructs as a Bouc-Wen model with damper in series and spring in parallel and the structure is shown in Figure 3.4.

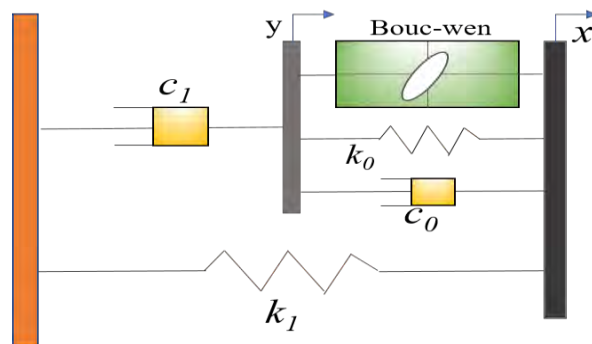


Figure 3.4: Structure of Modified Bouc-Wen model

The modified Bouc-Wen model was used to develop a controllable model for the magneto-rheological damper attached to the wind turbine tower. The model of the MR damper was assumed to be continuous in all the ranges and is numerically stable. To calculate the required force, the selected MR damper model was used for simulation and the equations are listed below:

$$F = c_1 \dot{y} + k_1(x - x_0) \quad (3.5)$$

$$\dot{y} = \frac{1}{(c_0 + c_1)} [\alpha z + c_0 \dot{x} + k_0(x - y)] \quad (3.6)$$

$$\dot{z} = -\gamma |\dot{x} - \dot{y}| |z|^{n-1} z - \beta (\dot{x} - \dot{y}) |z|^n + A(\dot{x} - \dot{y}) \quad (3.7)$$

where, k_1 is accumulator stiffness, k_0 controls stiffness at large velocities, c_1 is a dashpot, c_0 is viscous damping at large velocities, and x_0 is initial displacement, α is the evolutionary coefficient and the parameters β , γ , A and n are adjustable parameters for shaping up the hysteresis loop.

The modified Bouc-Wen model was simulated in this study to achieve MR damper force response. The Equations (3.5-3.7) were used to find damping force using MATLAB Simulink environment. The parameter α , c_0 , and c_1 are dependent on current i , and can be represented by the equations below;

$$\alpha = \alpha_a + \alpha_b i \quad (3.8)$$

$$c_0 = c_{0a} + c_{0b} i \quad (3.9)$$

$$c_1 = c_{1a} + c_{1b} i \quad (3.10)$$

In this study, MR damper RD-1005-3 manufactured by LORD Corporation is used. The parameters of this type of damper are obtained from experimental data and adopted from (Ho et al., 2013) as shown in Table 3.2.

Table 3.2: MR damper parameters

Parameter	Value	Parameter	Value
c_{0a}	672 Nsm ⁻¹	A	121
c_{0b}	3152 Ns (Am) ⁻¹	α_a	6949 Nm ⁻¹
c_{1a}	227 150 Nsm ⁻¹	α_b	60 789 N (Am) ⁻¹
c_{1b}	1050 000 Ns (Am)	β	212 114 m ⁻²
k_1	81 N m ⁻¹	γ	455 707 m ⁻²
k_0	732 Nsm ⁻¹	x_0	0 m

3.2.3 Control scheme

3.2.3.1 PID controller design and optimization

Feedback based controller is very effective in improving the dynamic response of a system. A PID controller was implemented in this study to reduce the vibration amplitude of the wind turbine tower by computing optimal control force required to be generated from MR damper. The PID controller gains are generally tuned with trial and error methods or classical methods such as Ziegler-Nichol method. These methods are time consuming and very difficult to achieve the optimal control force. Also, for tuning process, step input excitation is used for tracking the error between the reference and actual input. Therefore, tuning process using for harmonic force with natural frequency has not been investigated. ACO/PSO optimization process is an automatic process to find desired control force and it takes less time to find the desired force. In this process, Sine input can be used as input force instead of just step input to find the controller gains to ensure optimal control force to ensure maximum vibration reduction at 1st mode. The control parameters of PID were optimally tuned using ACO and compare with another nature inspired algorithm, i.e. PSO algorithm. A schematic diagram of this optimization process is shown in Figure 3.5.

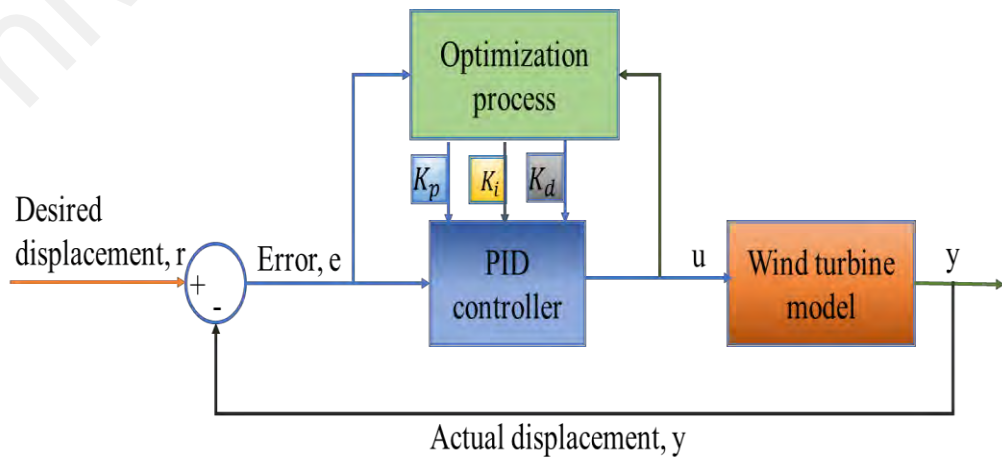


Figure 3.5: Block diagram of PID controller optimization

The equation of desired force output (u) is generated by the PID controller can be written as below:

$$u(t) = K_p e(t) + K_i \int_0^t e(t) dt + K_d \frac{de(t)}{dt} \quad (3.11)$$

where K_p , K_i , and K_d are the three control parameters (i.e. proportional, derivative, and integral respectively) of PID controller, $e(t)$ is the error between the desired displacement, $r(t)$, and actual displacement, $y(t)$, of the tower which is can be presented as below:

$$e(t) = r(t) - y(t) \quad (3.12)$$

A flow diagram of the PID control parameter optimization using nature inspired algorithm ACO/PSO is presented at Figure 3.6.

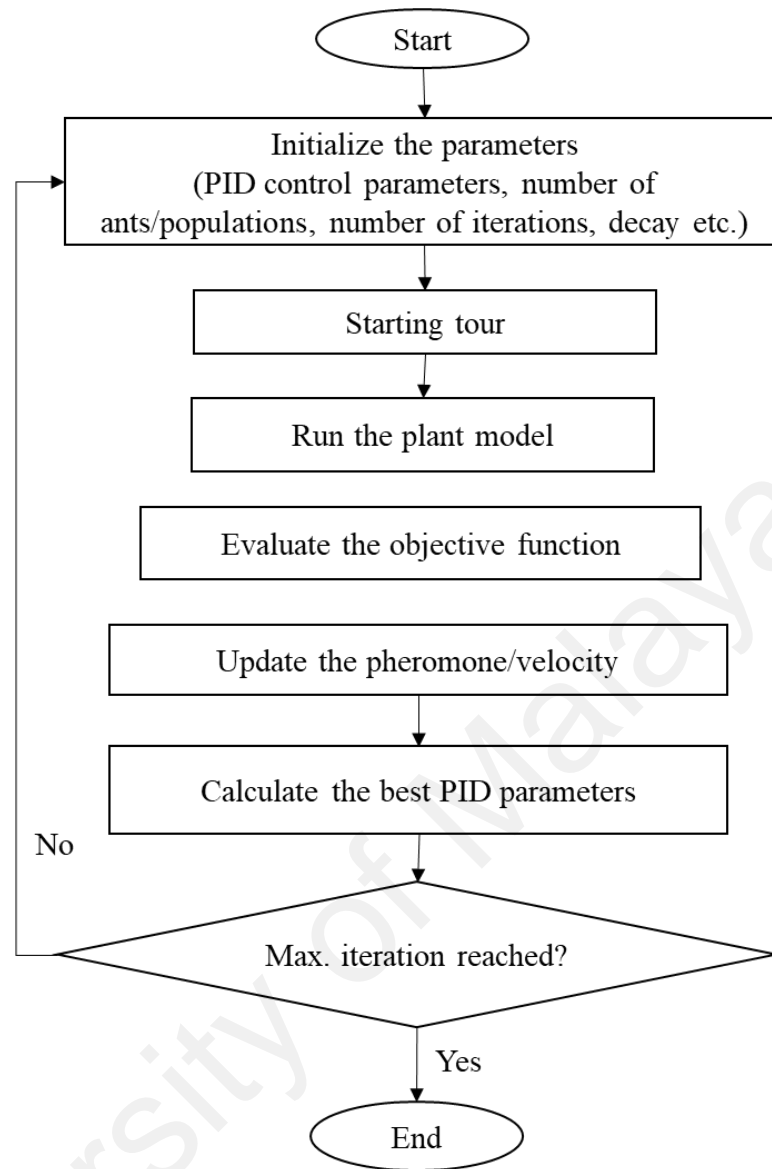


Figure 3.6: Flow chart of PID parameter optimization process

In this research, the optimal parameters of PID controller are achieved using the ACO algorithm. The initial step of the ACO process is to define the objective criteria which is used to evaluate the fitness of the algorithm. In this study the error at Equation (3.12) is defined as the objective function. This ACO method solves continuous optimization problems where objective function parameters are in continuous domain. This study computes the optimal values of PID control parameters based on the following ACO algorithm:

Begin

Step 1: Initialization

Set the range of PID control parameter (K_p , K_i , K_d) values randomly.

Initialize the number of ants, number of iterations, pheromone decay parameter, quantity of pheromone

Initialize the determinative variables to empty sets

Step 2: Construction of solution

Let n is number of ants where A is an ant at a given time.

For each iteration, an ant computes solution according to the state transition rule as below:

$$P_{ij} = \frac{\tau_{ij}}{\sum_{i=1}^n \tau_{ij}} \quad (3.13)$$

where P_{ij} is the probability of the ant n to move to the i^{th} node (ant numbers) to the j^{th} level (PID parameter), τ_{ij} is the pheromone amount at the nodes.

Step 3: Update of pheromone

After completing the tours of all the ants, the pheromone is updated as below:

$$\tau_{ij} = (1 - \rho)\tau_{ij} + Q / f_{best} \quad (3.14)$$

where ρ is pheromone decay parameter ($0 < \rho \leq 1$), Q is the quantity of the pheromone per iteration by an ant, f_{best} is the objective function value provided by the best ant after each searching periods. In the RHS, τ_{ij} is used as initialization value with τ_0 , a constant initial value.

Step 4: Evaluation of the optimal solution of objective parameters

Evaluate the best parameter of PID control parameters according to the objective function (Eqn 3.12).

Check the convergence and computational time.

Reset the number of ants/iterations, pheromone decay parameter if required.

Step 5: Imposing stopping criterion

Display the optimum values of the optimization parameters.

Update the pheromone globally according to the best solutions.

Continue from step 2 until the stopping criteria is satisfied.

End

In the process of computing optimal control force using PID-ACO algorithm, harmonic force at 1st mode was used as excitation force. This will give best solutions for vibration control of the tower to counter maximum deflections to avoid the problem of resonance. In classical tuning methods, step input force is used as excitation force, but in this study, sinusoidal force was used as excitation force since it is important to reduce vibration amplitude under natural frequency.

PID controller was designed and tuned with nature-inspired algorithm to find desired control force to counter vibration on the tower. MATLAB Simulink environment is used to simulate the system. In the block diagram in Figure 3.7, the reference was set as zero, which means that the desired displacement of the system is zero. Then the potentiometer measures the desired displacement and produces voltage provided by the controller. Different types of excitations were implemented to simulate the uncontrolled and controlled response of the model. Desired actuating force is measured using optimized PID controller.

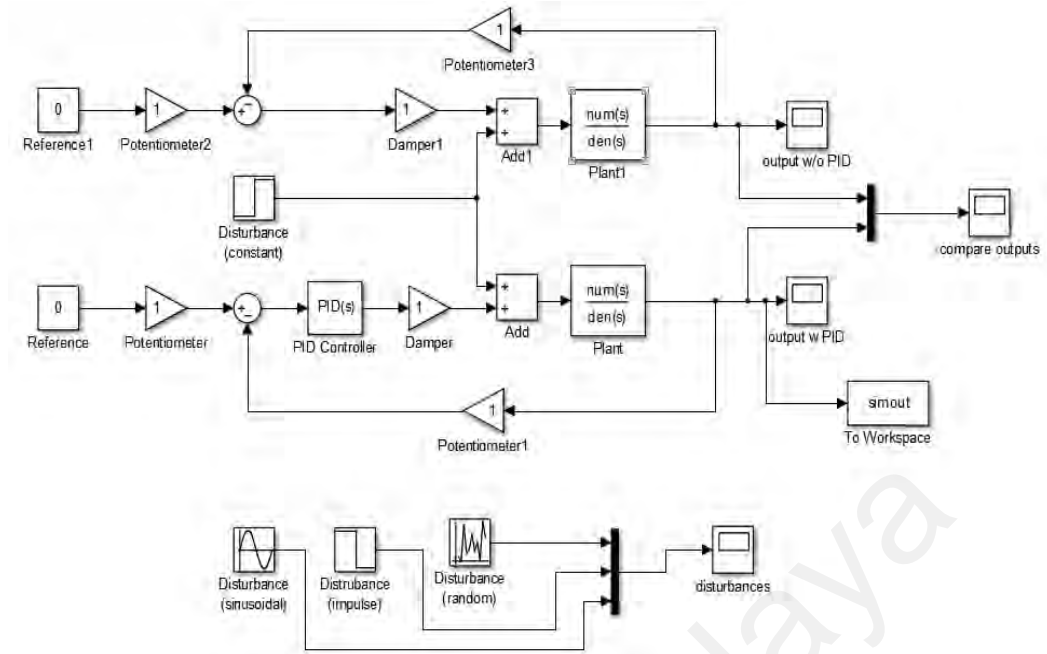


Figure 3.7: Block diagram of control system with and without PID controller in SIMULINK

Wind turbine tower model was simulated under different external disturbances at 20th elements of the tower. The vibration amplitudes were obtained using sensors. Desired force to counter vibration were calculated using PID controller. The combination of three parameters of PID controller eliminates the error between desired and actual output. The parameters were optimized using ACO method.

In this study, MATLAB was used to achieve optimize parameters of PID controller using ACO. The important input parameters for PID parameter optimization process using ACO algorithm is presented at Table 3.3.

Table 3.3: Input parameters of ACO algorithm for tuning PID controller

Input name	Values
Number of Ants	30
Number of Iterations	50
Number of evaluations	1500
Number of Nodes	10
Pheromone quantity, Q	50
Decay parameter, ρ	0.85
PID parameters search range, $[K_p, K_i, K_d]$	$[100, 5000, 0.001] \sim [20000, 25000, 1000]$

The cost/objective function for ACO algorithm is the error function between desired and actual output. Based on the selected range for three PID control parameters, ACO computes best parameters when the error is close to zero. In this process, number of ants, number of paths/iterations, the range of PID parameters were initialized at the beginning stage of ACO simulation. At first, the system will evaluate the cost function and best values are updated after each iteration. The process is automatically stopped when the cost function criterion is satisfied or when the maximum iteration number is reached. In this study, number of iterations and number of ants were selected as 10 and 50 respectively. The search range for PID parameters K_p , K_i and K_d is selected randomly between $[100, 5000, 0.001] \sim [20000, 25000, 1000]$. The basis of the selection of the range is the PID parameter values computed using Z-N method. Initially Z-N method was used to find the PID parameters and this method is compared with ACO & PSO methods.

The desired active control force was obtained for three locations on the tower which are at the 5th element, 10th element, and 15th element. These three locations will be investigated based on forces required, practicality, and design cost. The appropriate position will be used for MR damper implementation.

3.2.3.2 Current controller

A proportional-integral (PI) feedback controller was designed in this study to find suitable controller for MR damper. PI controller can properly shape the force-velocity response as expected hysteresis profile. The PI controller block diagram for current regulator which was implemented in MATLAB Simulink is shown in Figure 3.8. Using this controller, the current input, $i(t)$, can be computed using the following equation:

$$i(t) = K_p \bar{e}(t) + K_i \int_0^t \bar{e}(t) dt \quad (3.15)$$

where K_p and K_i are the proportional and integral gain of the PI controller respectively.

$$\bar{e}(t) = e(t) * \text{sign}(F_d(t)) \quad (3.16)$$

$$e(t) = F_d(t) - F_a(t) \quad (3.17)$$

where F_d and F_a is the desired and actual MR damper force respectively. The 'sign' function is used to regulate the current so that the actual force is achieved as the desired force (H. Laalej et al., 2012). PI controller finds suitable current/voltage for MR damper to produce required damping force. The limit of MR damper current is 0-2A and this limit is set with saturation block. The gain parameters, K_p , and K_i , are tuned with trial and error method. The proportional gain, K_p , is directly proportional to the controller output response. The proportional gain reduces the error between the actual and desired output by increasing or decreasing the gain. But system may become unstable if the proportional gain is too large. The integral error, K_i , helps to decrease the error over time. The integral response will increase until the error going towards zero. For tuning process, the proportional gain is increased with integral gain is kept zero until a good response is acquired. Then the integral gain is increased until the loop reached near to its reference to an acceptable value.

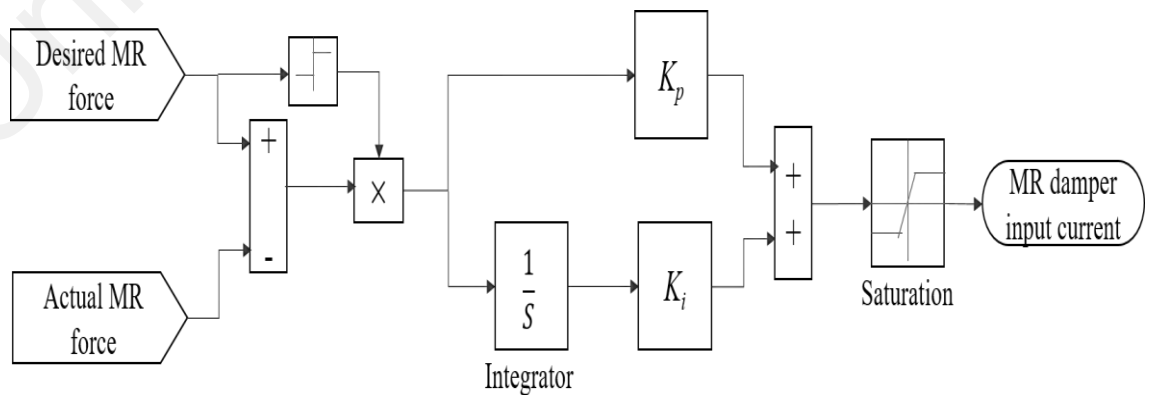


Figure 3.8: Current controller

3.3 Simulation procedures

The wind turbine tower was represented with a solid aluminum beam and divided into 20 elements. The mass and stiffness matrices are computed using FDM. MATLAB software was used to compute the FRF from the matrices. System identification toolbox is used to compute suitable dynamic models based on percentage of fit and mean squared error (MSE) with suitable poles and zeroes. The model was validated with experimental model in the result section. The MATLAB/Simulink software was used to acquire the system responses under different excitation input forces and damping environments. Therefore, the results are presented in two parts. At the beginning, a preliminary study in presented where the proposed semi-active control vibration control for wind turbine tower with PID-ACO controller was described and the respective controlled and uncontrolled responses under 1st natural frequency and random excitations was presented. The proposed control system was also investigated to check whether the same PID control parameters, which are used for first mode, can provide desired active force under different excitation frequencies and amplitudes to reduce vibration at significant level. This part also presented an investigation of the optimal position of MR damper. Then, the proposed control strategy was implemented on constructed wind turbine tower using MR damper. The simulation model was validated with experimental model based on natural frequencies, and uncontrolled response at 1st mode. Also, the optimal desired force and optimal MR damper position were implemented on the test rig. The vibration reduction rate of simulation and experimental study were compared to validate the proposed control strategy. At this stage, the output response was computed without any damper is attached, this state is called as “uncontrolled”. When damper is attached to the tower, the response was observed as passive damping system. In another state, high input current, such as 0.7A, was provided where high vibration amplitude was observed. This state is called as “Locked”. Suitable input parameters of ACO algorithm were used to adapt the tower

model to achieve the optimal parameters of PID controller. In this process, the transfer functions for the tower response at 20th elements and MR damper response at 10th elements were used. The excitation force is fed to the 20th element. During the optimization process, sinusoidal force at 1st mode was provided as excitation force because maximum vibration occurs under 1st mode. The acquired control parameters were used for all different types excitation force to verify that the proposed PID-ACO is effective for under any possible disturbances. Next, a PI controller was used as MR damper controller to find required current to feed into MR damper so that the optimal force was acquired by the damper. Modified Bouc-Wen model is used to achieve the force response due to current. The initial displacement of the damper was provided as 0 meter. The semi-active MR damper-controlled response of the tower is referred as “controlled” system. Three excitation forces are applied in this study: sinusoidal, chirp, and random. The amplitudes and the frequency of the sinusoidal force are 20 N and 1st natural frequency. For chirp signal, frequency range is 1-10 Hz. Sampled gaussian noise is used as random signal where amplitude varies from 18 N to 25 N. The semi-active controlled response with optimal control force acquired by PID-ACO was compared with the responses with passive, locked and uncontrolled system.

3.4 Equipment and experimental set up

This section will present the apparatus and test rig set up for the proposed semi-active vibration control system for a lab-scaled wind turbine with MR damper. A cantilever beam was utilized as wind turbine tower and a vertical axis wind turbine was installed on top of the tower. MR damper and its controller were attached to the tower for supplying external damping force. A shaker and power amplifier were used for providing different types of external excitation. Two accelerometers and a force sensor were used to measure response signal of tower acceleration and force applied to the tower. Data acquisition

(DAQ) hardware was used to collect data from the sensors. Sensors were connected to multi-channel DAQ and DAQ is connected to computer which provides DAQ software and data processing software such as DASyLab, ME 'Scope and MATLAB etc. The detailed list of these instruments is provided in Table 3.4.

Table 3.4: List of Instruments

Instrument Name	Description
Wind turbine tower	An aluminum beam is used as the tower Dimension: 3.175cm x 3.175cm x 150cm
Wind turbine Model: SAV-15W	Vertical axis wind turbine Weight: 2.3 Kg Working wind speed: 3-20 m/s
MR damper Model: RD-8041-1	Response time: 15 milliseconds for magnetic field changes Stroke length: 74 mm Maximum tensile strength: 8896 N Input current: 0-2 A
Wonder Box Model: RD-3002-03	MR damper controller Output current: Maximum 2 A Have both manual and external current control
PCB Accelerometer Model: 352C68	Sensitivity: 100mV/g Amplitude range: ± 50 g peak Frequency range: 0.5-36,000Hz Temperature range: -54 to 121 $^{\circ}$ C
PCB Force sensor Model: 208C03	Sensitivity: 2.248mV/N Measurement range: 2224 N Frequency range: 0.0003-10,000Hz
Data acquisition module Model: NI-9234	Number of Channels: 4 24-bit resolution Signal range: ± 5 V
Shaker Model: Tira TV 51110	Rated peak force sine/random: 100/70 N Frequency range: 2-7000Hz Max. displacement peak-peak: 13mm
Power amplifier Model: Tira BAA 120	Output power(rms): 120VA Frequency range: DC-20000 Hz Max. current: 5.5 A
DASyLab	Acquire data from sensors Channel 1: Force sensor Channel 2 and Channel 3: Accelerometer 1 and Accelerometer 2 Windows for frequency, excitation, and response signals Read data and plot
MATLAB	To process measured data, plot and compare results

3.4.1 MR damper and its controller

The purpose of this section is to introduce the MR damper that has been used in this experiment. The MR damper used in this experimental study is a product of a USA based

company; LORD Corporation. The specific model number of this MR damper is RD-8041-1. According to LORD Corporation, this MR damper improves vehicle performance by reacting and adapting to terrain and other conditions thousands of times per second. This MR damper is a type of monotube damper which contains high-pressure nitrogen gas. The MR damper has the stroke length of 74 mm and the maximum tensile strength is 8896 N. Figure 3.9 and Figure 3.10 shows the RD-8041-1 MR damper and the dimensional drawing of the damper respectively. In addition, Table 3.5 and Table 3.6 provides the typical properties and the electrical properties of this MR damper respectively.

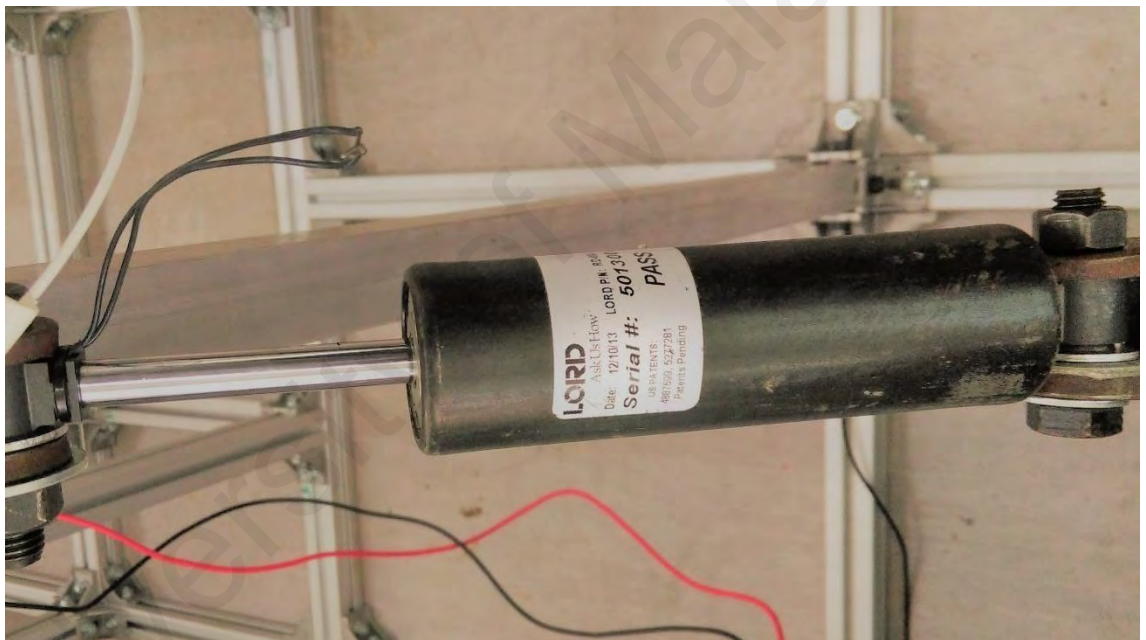


Figure 3.9: MR damper RD-8041-1

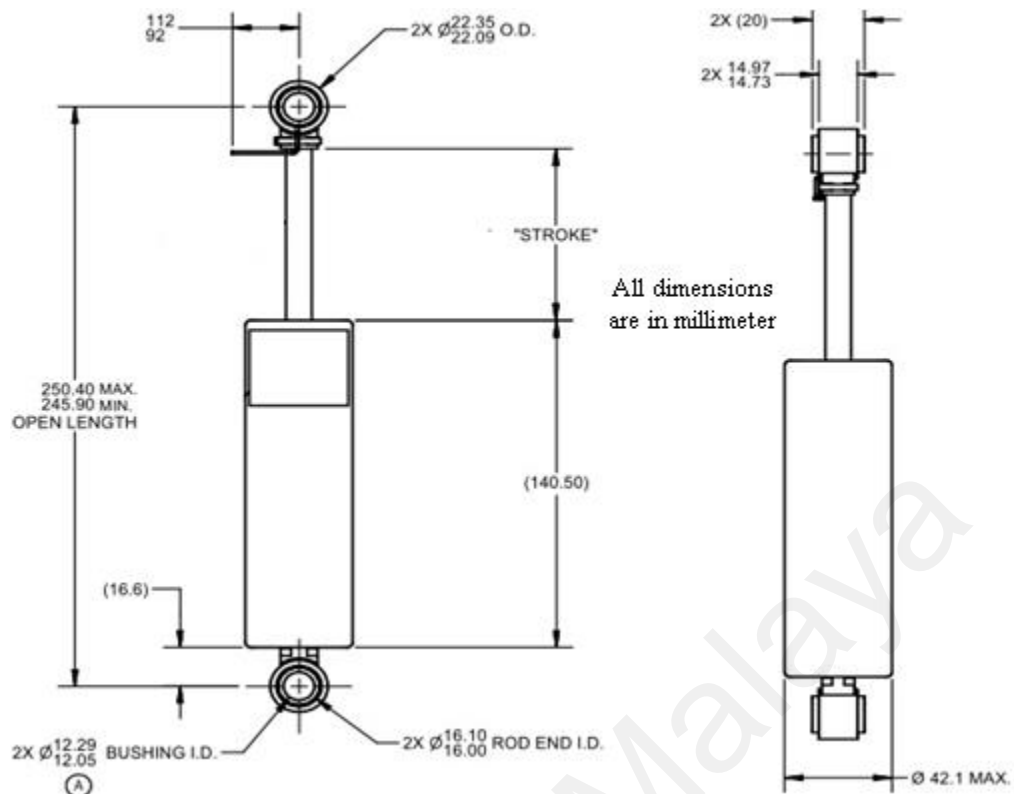


Figure 3.10: MR damper assembly drawing (courtesy: LORD technical data sheet for RD-8041-1)

Table 3.5: Typical properties of RD-8041-1 MR damper (courtesy: LORD Corporation technical data sheet for RD-8041-1)

Typical Properties		Model LORD RD-8041-1
Stroke		74 (2.91) mm (in)
Extended Length		248 (9.76), mm (in)
Body Diameter		42.1 (1.66) max, mm (in)
Shaft Diameter		10 (0.39) mm (in)
Tensile Strength		8896 (2000) max, N (lbf)
Damper Forces, Peak to Peak	5 cm/sec and 1 A	>2447 (>550) N (lbf)
	20 cm/sec and 0 A	<667 (<150) N (lbf)
Operating Temperature, °C (°F)		71 (160) max

Table 3.6: Electrical properties of RD-8041-1 MR damper (courtesy: LORD technical data sheet for RD-8041-1)

Electrical Properties		Model LORD RD-8041-1
Input Current, Amp	Continuous for 30 seconds	1 max
	Intermittent	2 max
Input Voltage, Volt		12 DC
Resistance, ohms	at ambient temperature	5
	at 71°C (160°F)	7

To control the current/voltage of MR damper, a controller device was used, and it is called wonder box in LORD Corporation. The Wonder Box provides a closed-loop current control to compensate for changing electrical loads up to the limits of the power supply. Moreover, The Wonder Box is integral to devices and systems for a wide variety of applications. (Courtesy: LORD user instructions for LORD RD-3002-03 Wonder Box Device Controller). The model of this device controller kit is LORD RD-3002-03 and it is a companion product of the MR fluid devices. The maximum output current of this controller kit is 2 Ampere. The controller device is shown in Figure 3.11.

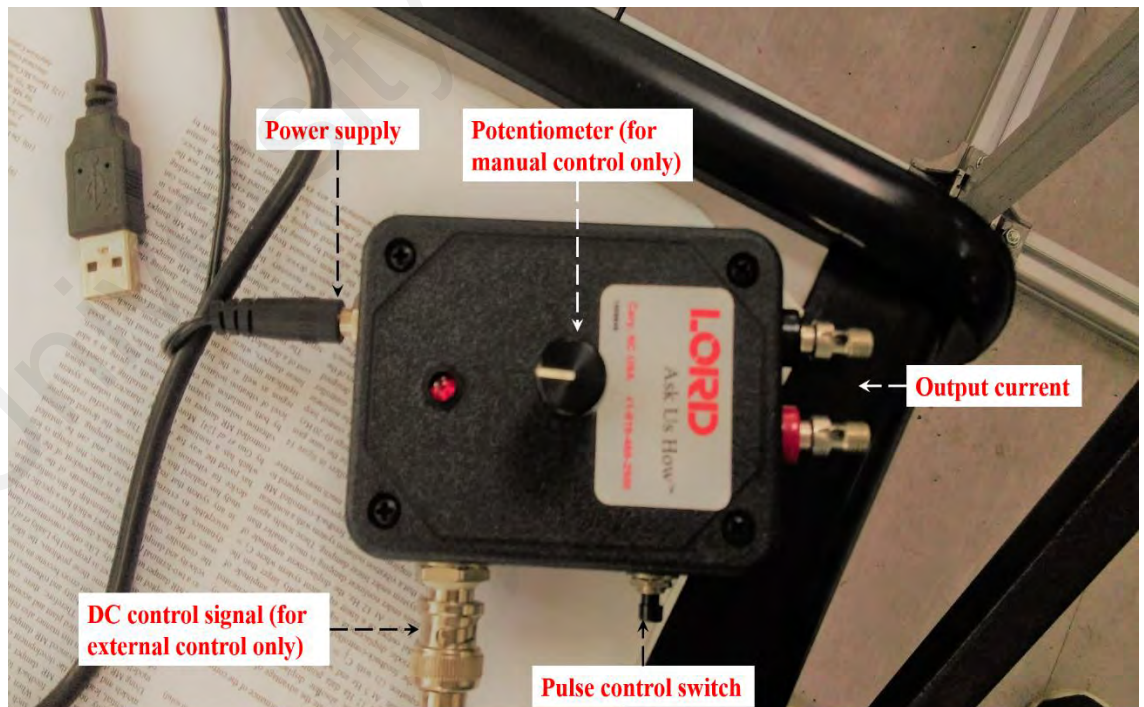


Figure 3.11: Wonder Box Device Controller- RD-3002-03

The exact current should be measured when using in the experiment from voltage and current relationship. The relationship between measured voltage and current is plotted as shown in Figure 3.12.

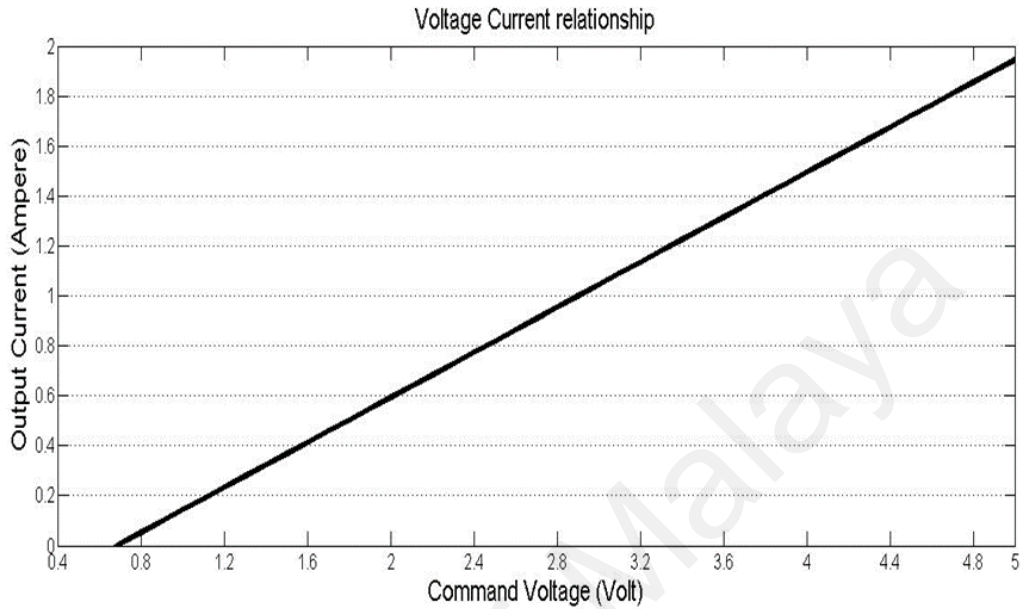


Figure 3.12: Voltage and current relationship (Measured) in the Wonder Box Device Controller- RD-3002-03

3.4.2 Optimal placement of MR damper

Three different locations (5th, 10th, and 15th elements) on the tower were investigated to find optimal positions in a simulation study using optimal PID controller based on forces required, practicality, and design cost. The optimal position for MR damper was investigated at the 10th element which is the midpoint of the wind turbine tower. For the experiment, MR damper was placed at this point and attach to the ground with an angle of 45° as shown in Figure 3.13. This configuration will act as bracing of the tower and a controllable damper to counter tower vibration under different external disturbances.

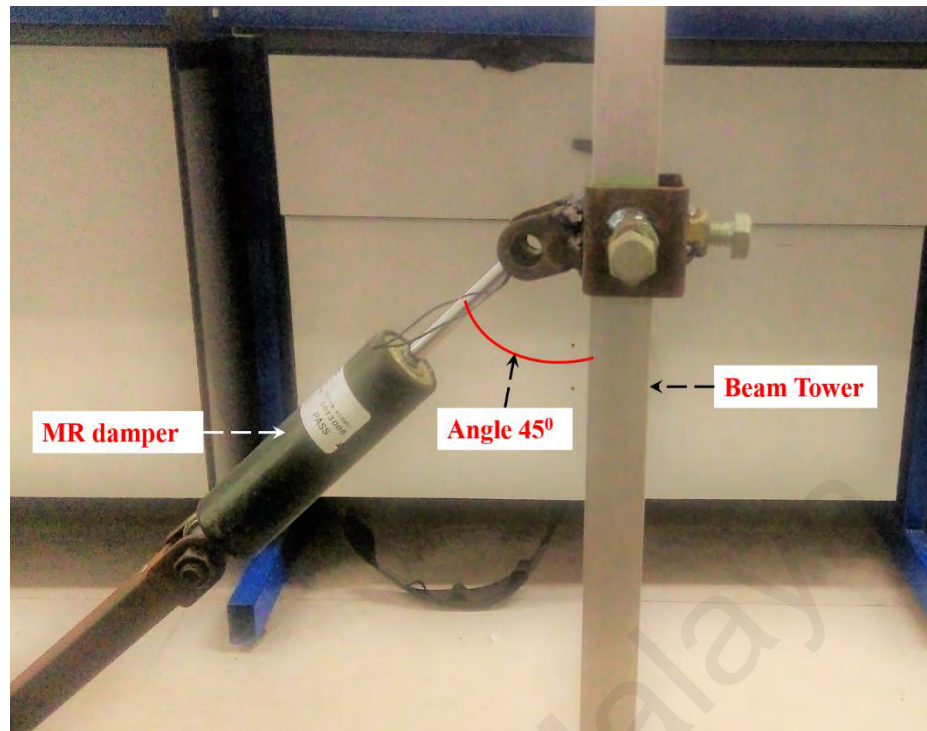


Figure 3.13: Placement of MR damper

3.4.3 Sensory information and data acquisition system

Two types of sensors were used in this experimental study which are accelerometer and force sensor as shown in Figure . The accelerometer is most commonly used the sensor in vibration applications. The accelerometer was used in this study to measure the acceleration of a certain point of movement of wind turbine tower. The model of the accelerometer is 352C68 from PCB Piezotronics. This is lightweight and small size sensor with a high-frequency range. This type of sensor can detect any signals between 0.5-10000 Hz. The sensitivity of this sensor 100mV/g whereas the measurement range of this sensor is $\pm 50g$ peak. This sensor can be operated within the temperature range of -54 to $93^{\circ}C$. The force sensor is typically known for measuring static and dynamic tensile and compressive loads. This type of sensor was used in this study to measure excitation force provided by the shaker to the vibrating system. The model of the force sensor is 208C03 from PCB Piezotronics. The sensitivity and frequency range of this sensor are 2.248mV/N and 0.0003-36000Hz respectively. This type of for sensor can measure the force up to 2224N.

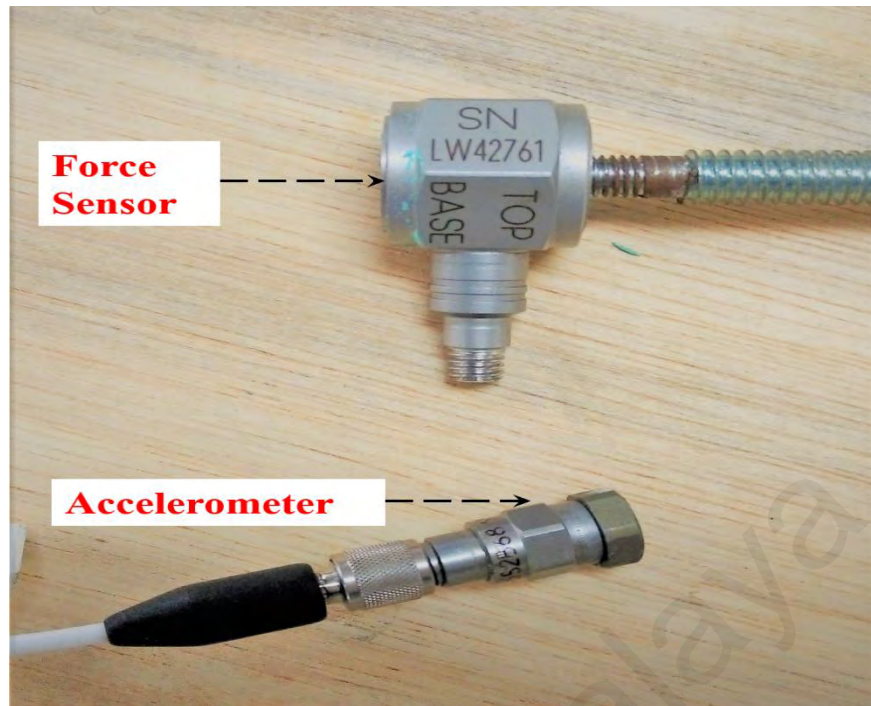


Figure 3.10: Accelerometer and Force sensor

Data acquisition hardware is a device that receives information from the accelerometer, force sensors, etc. and sends them to a computer for further processing. DAQ hardware connects the physical system to a computer for analyzing the data. In this study, NI-9234 USB type module from National instruments was used to receive signals from different sensors. It has 4 analog input channels connected with BNC cables which can receive data simultaneously, shown in Figure 3.14. The signal range of this module is $\pm 5V$. The data from the sensors is sent to the computer through DAQ software and DASyLab.

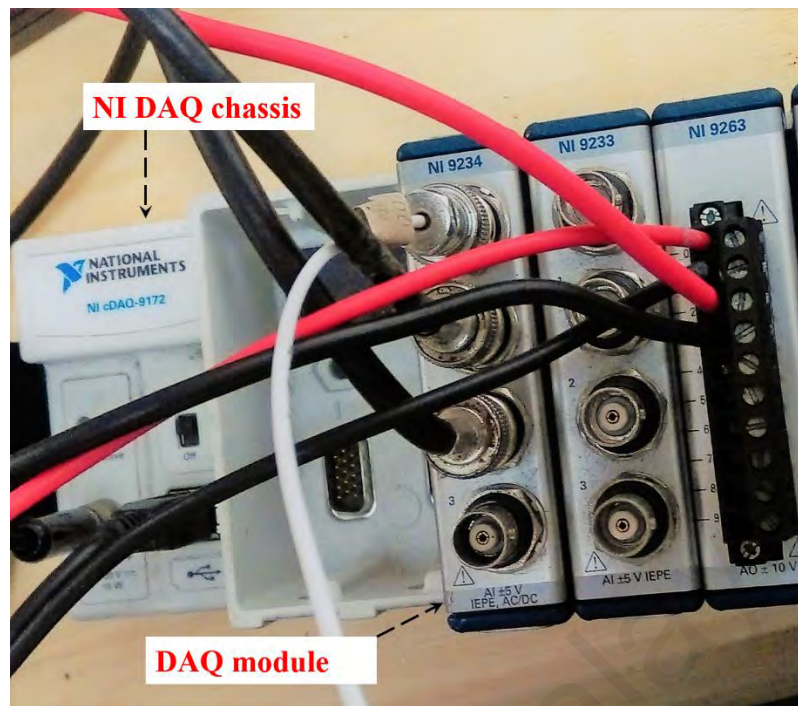


Figure 3.14: Data acquisition hardware

3.4.4 Vibration test system

To provide external excitation force to wind turbine tower, vibration test system from Tira GmbH was used in this experiment. Vibration test system consists of a shaker and a power amplifier as shown in Figure 3.15. The model of the shaker is TV 51110 which is excited by permanent magnets. The rated force of the shaker is 100N for a sinusoidal signal. The maximum peak to peak displacement of the shaker is 13mm. The shaker is attached to the tower and excites the tower with different loads. The power amplifier controls the output of the shaker by supplying rated voltage and current. The output force of the shaker was varied by varying the voltage of the amplifier. The model of the power amplifier is BAA 120. The maximum current input of the amplifier is 5.5 A.



Figure 3.15: Vibration test system

3.4.5 Experimental test rig

In this section, the experimental set-up for investigation of MR damper nonlinear characteristics and semi-active wind turbine tower vibration control system with MR damper are presented. The purpose of this study is to validate the simulation model of MR damper and wind turbine tower as well as the simulation response of wind turbine tower under different conditions.

3.4.5.1 Experimental set-up for MR damper model validation

The force/velocity of the MR damper is significantly nonlinear and proper characteristic analysis are required to be studied for optimal implementation in structural vibration control. An experimental investigation was carried out to test the damping characteristics of MR damper. This is important to validate the mathematical model of MR damper which was used to provide control force to wind turbine tower for vibration control in simulation study. Dynamic testing was performed with a long-stroke MR damper model no RD-80410-1 from Lord corporation on a universal testing machine (UTM). The experimental setup mainly includes an MR damper, a current controller, a UTM from Instron and a computer with necessary software for data acquisition and analysis. MR damper (from Lord Corporation) was tested to analyze the force characteristics for a set of inputs. The MR damper was tested using a computer-controlled

UTM. The experimental setup is presented in Figure 3.16. The upper head of the damper was attached to a hydraulic actuator that can move the damper up and down. This allows measuring the damping of the damper. UTM offers different types of grippers to attach different types of testing equipment. But these grippers were unable to attach the MR damper; therefore, rectangular aluminum sheets were attached to MR damper and the upper and lower heads of the UTM. This step help UTM upper and lower heads to grasp the MR damper easily and can provide appropriate pressure and tensile strength. The excitation signal was provided to the hydraulic actuator from the INSTRON Bluehill software. UTM has built-in sensors to measure force and displacements. The current controller was connected to the damper to provide different current inputs for measuring respected force responses.

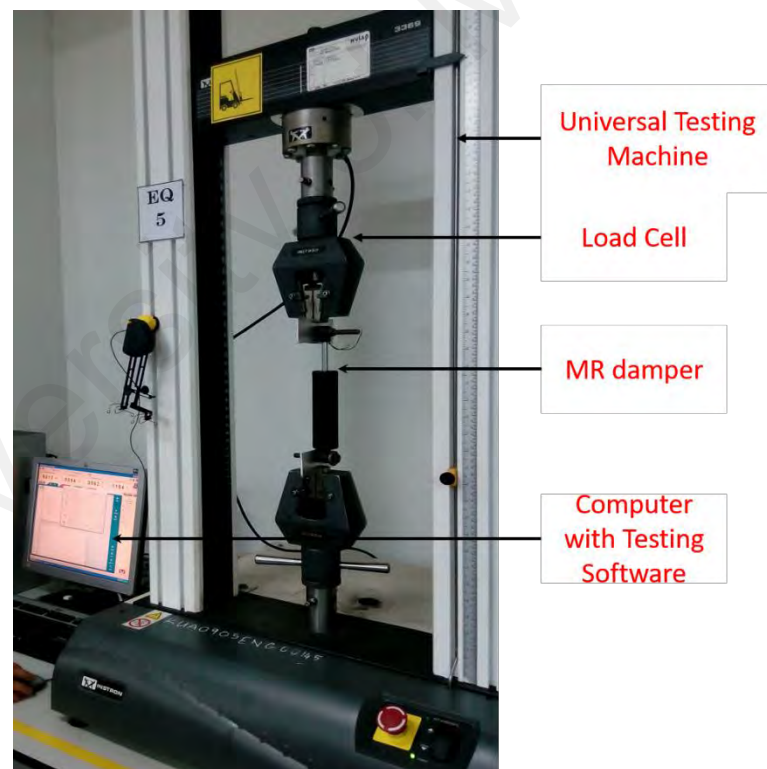


Figure 3.16: Experimental setup for characteristic testing of MR damper

3.4.5.2 Experimental set-up for wind turbine tower vibration control

The main components of the experiment are a wind turbine, MR damper, and its controller, vibration test systems, computer. First, an aluminum frame is prepared to place

the main components. The complete experimental test rig is shown in Figure 3.15. In this setup, a vertical axis wind turbine was placed on top the aluminum beam tower. The MR damper is attached to the mid-point of the tower. The other end of the damper was attached to an adjustable steel shaft and connected to frame. The connection of the MR damper to the tower can also be adjusted. The wonder box, MR damper controller, is attached to MR damper with two banana plugs. The shaker was placed nearby the tower and attached to the tower through a threaded rod. A force sensor is attached to the top of the threaded rod. DAQ hardware, a computer, and power amplifier were placed on a side of the frame.

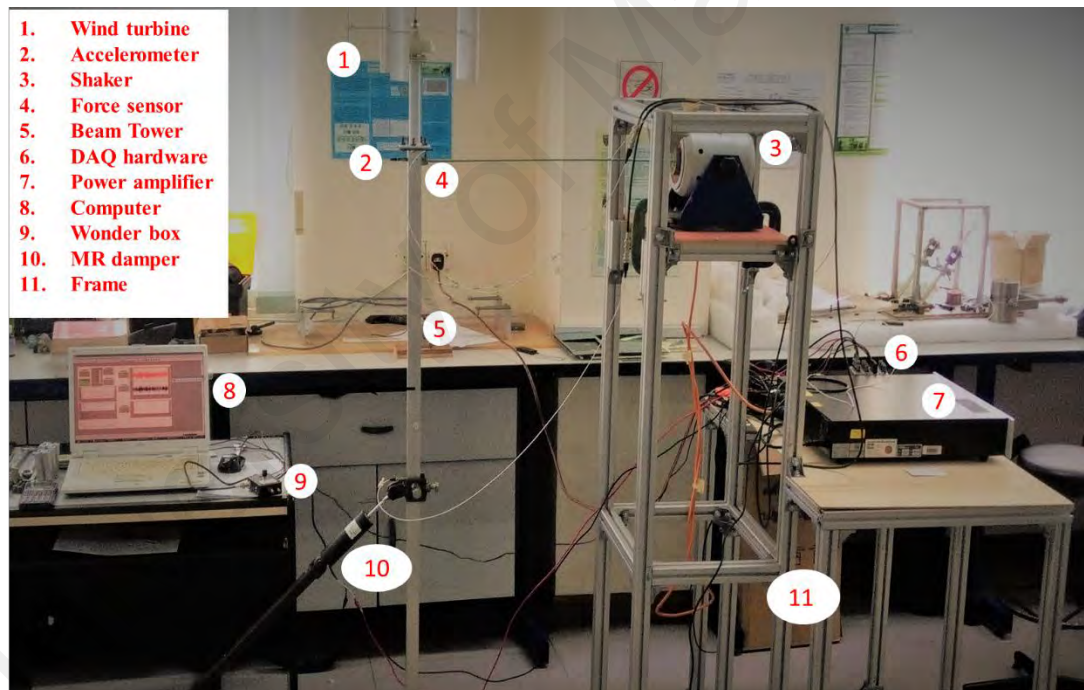


Figure 3.17: Experimental setup for wind turbine tower vibration control

3.5 Experimental procedures

In this section, the testing procedures for characteristic analysis of MR damper is presented. Also, the experimental procedures for semi-active vibration control of wind turbine tower under different loading conditions are presented.

3.5.1 Characteristics of MR damper

A series of tests were conducted under fixed displacement amplitude of the damper, velocity, and various current inputs to the damper. The testing inputs for displacement amplitude and velocity are 20mm and 200mm/min respectively. The current inputs were 0A, 0.25A, 0.7A, and 0.825A. The current inputs were supplied using Wonder Box (current controller), which converts the voltage to current supply. The resulting force was measured by the load cell. At first, resulting forces were measured without any current supply with different displacement amplitudes and velocities. Then a current was supplied to the damper and tested again. All experimental data including time, displacement and force have been recorded for analyzing the dynamic characteristics of the MR damper. To validate the simulation model of MR damper, the modified Bouc-Wen model was simulated using SIMULINK under the same inputs of displacement, velocity and current inputs and the force responses are compared with the experimental results.

3.5.2 Semi-active vibration control of wind turbine tower

After the experimental set-up is completed with all the components, the Experimental Modal Analysis (EMA) is conducted using impact hammer. EMA was conducted using impact hammer to find the modal properties of wind turbine tower before and after MR damper is attached to for model validation and implementation purpose. MR damper, in this case, will be used as passive damper. The natural frequencies were compared and used as reference for excitation frequencies during the investigation. Sinusoidal, sweep, also known as chirp and random excitation signal were generated by the power amplifier and provided by the shaker. DASYLab software was used to program the signal generator for shaker and receive signal from the sensors. The program also sends voltage signal to the wonder box, which is the MR damper controller. The voltage signal was converted to

the current by the controller and sent to MR damper. Two accelerometers were placed on the tower, first accelerometer was on top of the tower to measure the acceleration on top of the tower due to excitation and second accelerometer was attached to the mid-point of the tower where the MR damper was connected. The output responses of the tower are measured through DAQ system for four different states: First state when the damper is not attached which is called as “uncontrolled”, Second state when the MR damper is attached but no power is fed to the damper which is called as “passive”, third state when MR damper attached and maximum current is supplied, and this is called as “locked” state where high input current is provided to the MR damper and higher displacement amplitude is expected to occur, the fourth and final state when MR damper is attached and optimal current was supplied to the damper. When the excitation force is fed to the wind turbine tower via the shaker and the stinger, the tower response is measured through the accelerometer. The suitable current input was achieved from the designed PI controller based on the optimal force achieved the PID-ACO controller for the MR damper. Experimental results were measured and saved using DASyLab through accelerometers and force sensors for all types of excitation forces and damping environments as stated in simulation procedure. the tower responses were measured under different excitation forces such sinusoidal @1st mode, 20 N, chirp signal (1-10Hz, 20N), and random forces with amplitude range from 18 N to 25 N. During the experiment, it is to be ensured that all the cables were connected properly. MATLAB software was used for to process the measured data and validate with simulation results.

CHAPTER 4: RESULTS AND DISCUSSION

4.1 Introduction

Simulation and experimental results of semi-active vibration control of wind turbine are presented and discussed in this chapter. As mentioned before, wind turbine tower is represented and modeled with the cantilever beam. As explained in methodology chapter that cantilever beam is divided into 20 elements. The top of the tower is represented by 20th elements of the beam. and random input excitations are implemented on top of the tower to represent an external force from rotating blade and wind respectively to wind turbine tower. PID and PI controller are designed and tuned with nature-inspired algorithm to find desired control force to counter vibration on the tower and to find suitable current/voltage for MR damper to produce required damping force.

Results are divided into two parts: Simulation and Experimental.

4.2 Simulation Results

This section presents the simulation results for wind turbine tower modeling which includes FDM modeling and system identification. The PID control parameter optimization using ACO method is also evaluated. The optimal position of MR damper is investigated at different position to find suitable position. The effectiveness of the PID-ACO controller is also presented for wind turbine tower vibration control under different conditions.

4.2.1 Modeling of wind turbine tower

Based on the mathematical model of wind turbine tower as cantilever beam by using finite difference method, the vibration analysis of beam is studied. Mass and stiffness matrices are derived using FDM and frequency response function (FRF) is computed from the matrices. The frequency response function is plotted in Figure 4.1. Wind turbine

tower modeled with finite difference method is simulated under sinusoidal excitation on top of the tower; that is 20th element of the beam.

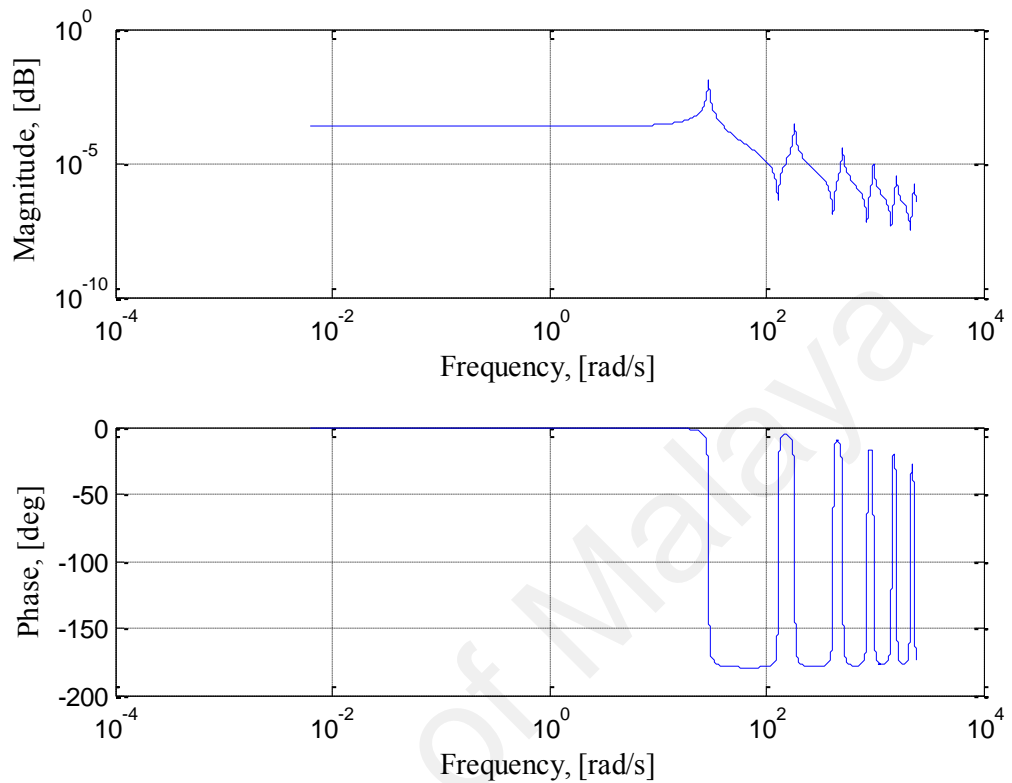


Figure 4.1: Frequency response function of wind turbine tower

Figure 4.1 shows frequency response function where it is observed that it is observed that about five natural frequencies exist around the frequency range of 0-300Hz. The first five natural frequencies are presented in Table 4.1.

Table 4.1: Modal properties of the structure

Mode	Frequency (Hz)
1	4.68
2	29
3	80.7
4	155
5	251.75

Wind turbine tower model is simulated under harmonic excitation on top of the tower; that is 20th element of the beam. Harmonic excitation is very important in vibration control because it encounters the concept of resonance. Resonance leads to large displacements and may cause the failure of the system. The amplitude and frequency of

the sine signal are 100 N and 2 Hz respectively. Input force signal and the corresponding tower response is presented in Figure 4.2.

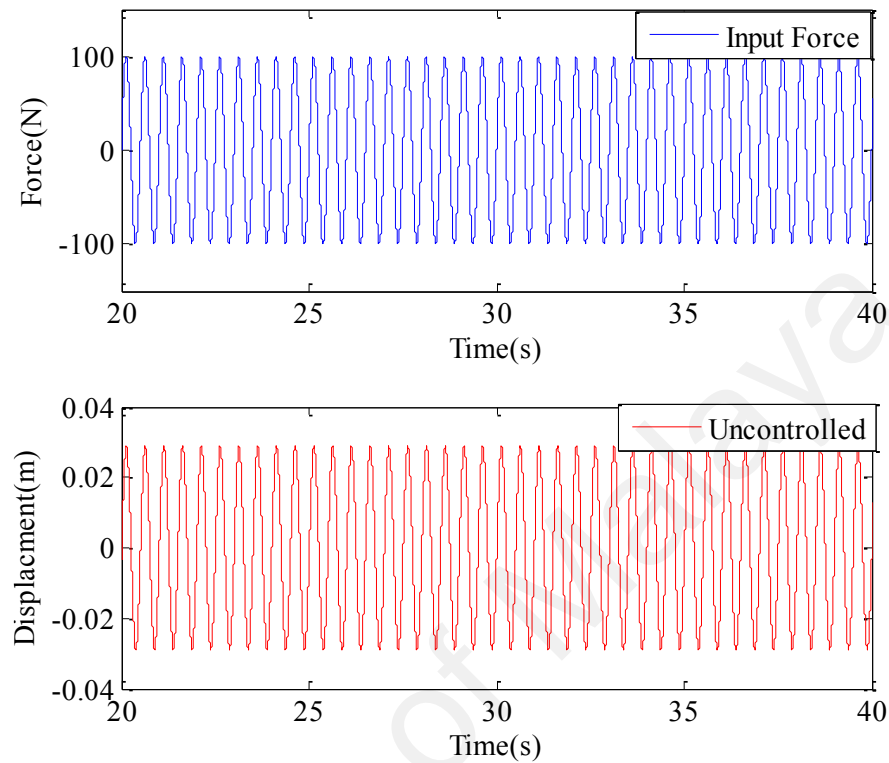


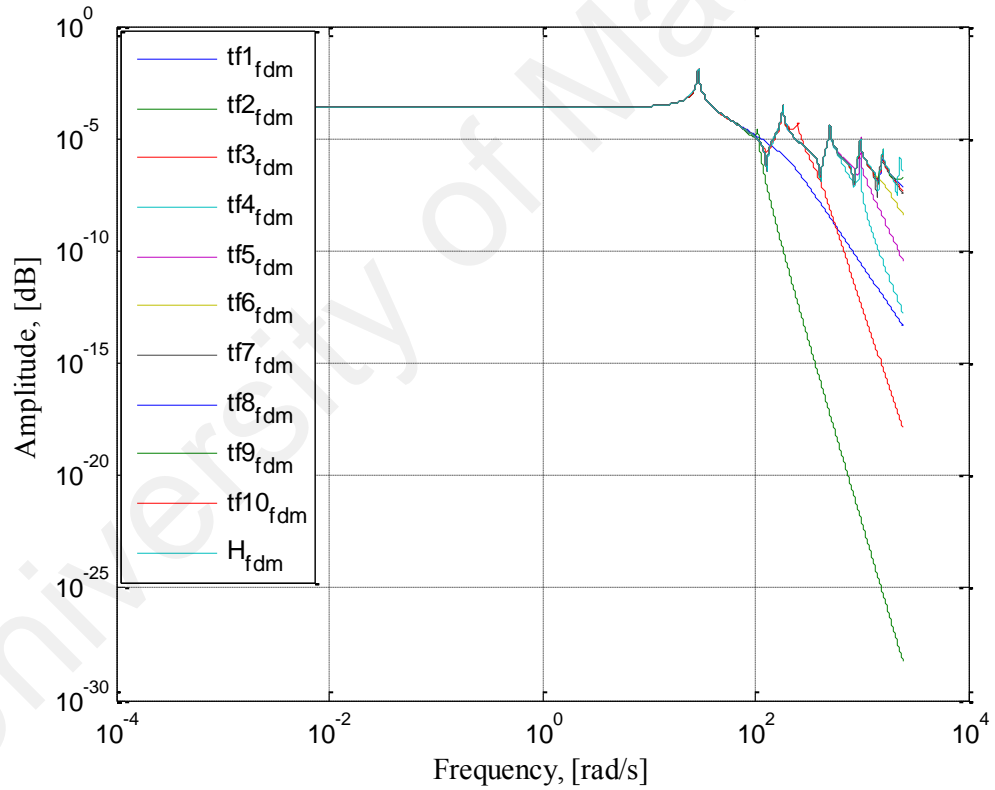
Figure 4.2: Input force and uncontrolled response of the tower under harmonic excitation

It is observed that the displacement of the tower is around 0.03m. It is important to apply control system to reduce the vibration amplitude. System identification process is used to verify the model and dynamic transfer functions are estimated for different set of poles and zeroes. The estimated transfer functions (tf) at top of the tower (i.e. 20th element) are evaluated based on fit to estimated data, MSE and CSAC. There is total number of 10 estimated transfer functions and the information of each transfer function are tabulated in

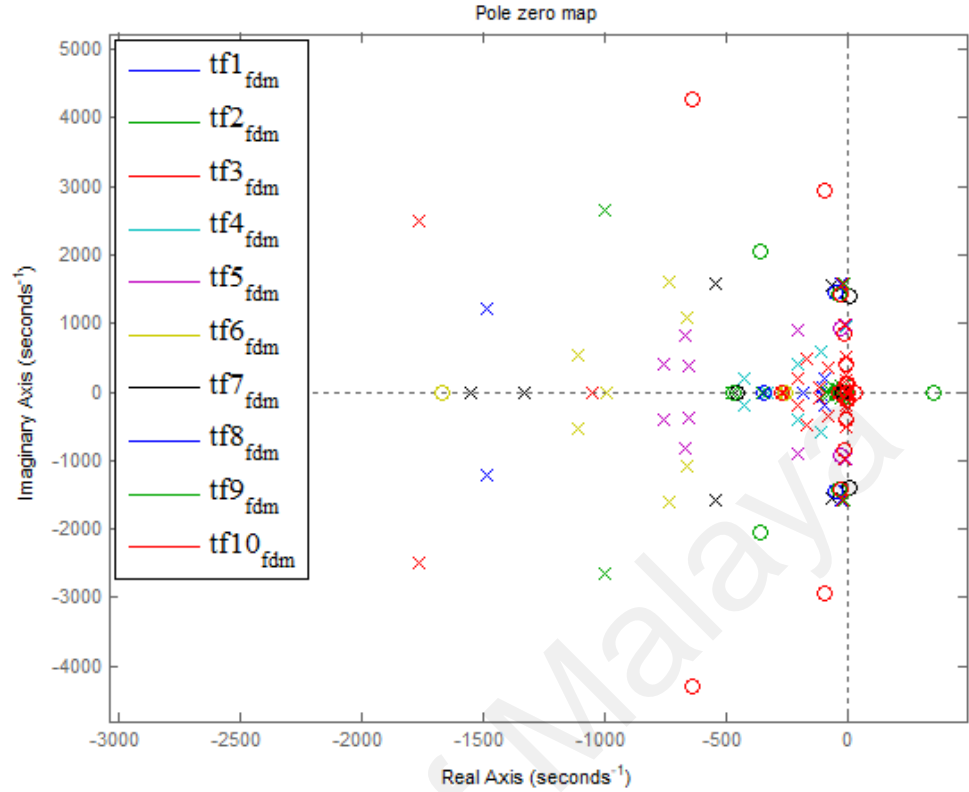
Table 4.2 4.2 and frequency response function and pole-zero map of the estimated transfer functions are shown in Figure 4.3.

Table 4.2: Evaluation of transfer functions of wind turbine tower modeled by FDM

Transfer function	No of poles	No of zeros	No of visible natural frequencies	Fit percentage, %	MSE	CSAC
Tf_1	7	0	1	97.16	2.25E-11	0.996008
Tf_2	16	0	2	-99.65	1.12E-07	0.995879
Tf_3	16	2	2	-99.99	1.13E-07	0.999578
Tf_4	16	4	4	-100	1.13E-07	0.999973
Tf_5	16	6	4	99.35	1.19E-12	0.999983
Tf_6	16	8	4	-100	1.13E-07	0.999994
Tf_7	16	10	5	-100	1.13E-07	0.999997
Tf_8	16	12	5	54.18	6.71E-08	0.999998
Tf_9	16	14	5	-63.45	7.54E-08	0.999999
Tf_{10}	16	16	5	-99.34	1.12E-07	0.999998



(a)



(b)

Figure 4.3: (a) Frequency response function and (b) pole-zero map of estimated models using FDM

The estimated transfer functions are evaluated based on fit to estimated data, MSE and CSAC. From the results obtained, it is found that for Tf_1 shows only first natural frequency is which is at about 29 rad/s. However, Tf_2 and Tf_3 , which consist 2 and 4 zeros respectively with 16 poles, can determine the first and second natural frequencies. Therefore, although they have high fit to estimation data and CSAC and low MSE, they are not chosen as they cannot simulate the response if the excitation frequency is larger than second natural frequency. Tf_4 , Tf_5 , and Tf_6 determine the first four frequencies. Their fit to estimation data are also high, MSE is low enough and CSAC is very well. These results are quite satisfactory to represent the system, but they are not chosen to represent the system because they do not show all five natural frequencies of the system. Transfer functions of Tf_7 , Tf_8 , Tf_9 , and Tf_{10} can show all five natural frequencies but Tf_8 and Tf_9 are not satisfied as they have lower than 99% fit to estimation data. Thus, they are also not

chosen to represent the system. Lastly transfer functions of Tf_7 and Tf_{10} can show all five natural frequencies, the value of fit to estimation data are higher than 99%, the value of MSE is lower than 1E-06 and CSAC value is higher than 0.999. These two transfer functions could be selected to represent the system. However, Tf_7 is chosen because it has better fit to estimation data than Tf_{10} . Also, pole-zero map in Figure 4.3(b) suggested that poles and zeroes are inside left side of the axis, therefore system is stable.

The wind turbine tower is also modeled with FEM and transfer functions are estimated using similar combinations of pole and zeros using system identification toolbox. Like FDM, the number of estimated transfer functions using FEM modeling is 10 and the information of each transfer function are tabulated in Table 4.3 and frequency response function and pole-zero map of the estimated transfer functions are shown in Figure 4.4.

Table 4.3: Evaluation of transfer functions of wind turbine tower modeled by FEM

Transfer function	No of poles	No of zeros	No of visible natural frequencies shown	Fit percentage, %	MSE	CSAC
Tf_1	7	0	1	97.18	2.35E-11	0.995996
Tf_2	16	0	1	87.02	4.99E-10	0.995192
Tf_3	16	2	3	98.02	1.16E-11	0.999799
Tf_4	16	4	4	-100	1.18E-07	0.999667
Tf_5	16	6	5	-100	1.18E-07	0.999668
Tf_6	16	8	4	98.4	7.60E-11	0.999987
Tf_7	16	10	5	-100	1.18E-07	0.999977
Tf_8	16	12	5	-98.25	1.16E-07	0.999998
Tf_9	16	14	5	-97.46	1.15E-07	0.999983
Tf_{10}	16	16	5	99.88	4.05E-14	0.999999

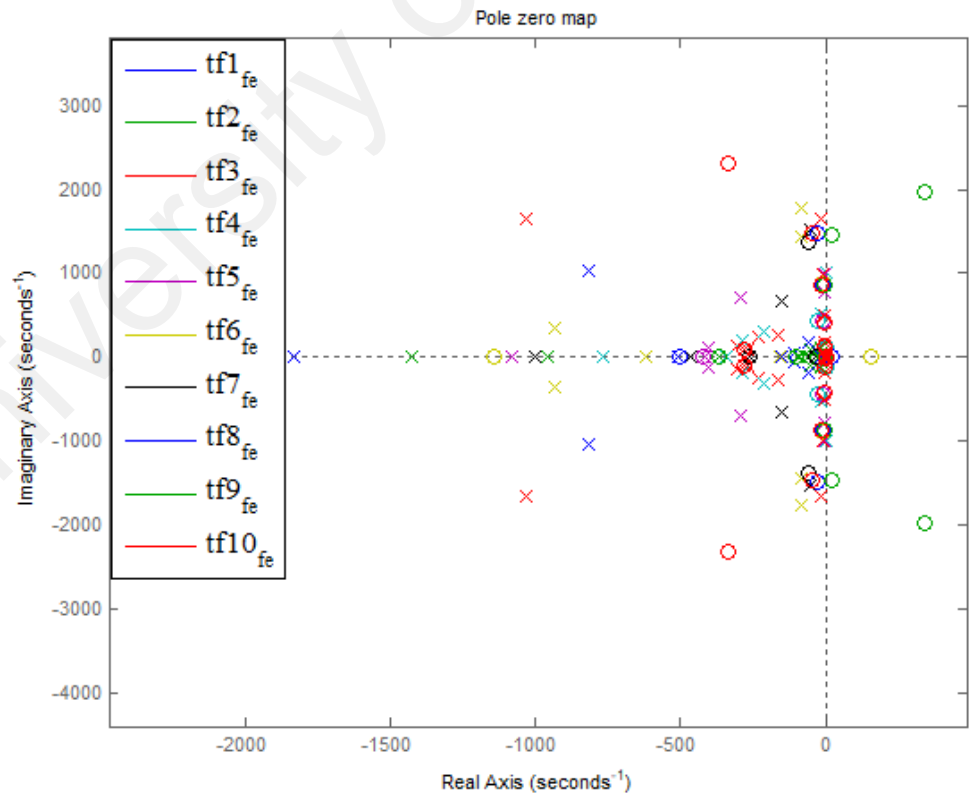
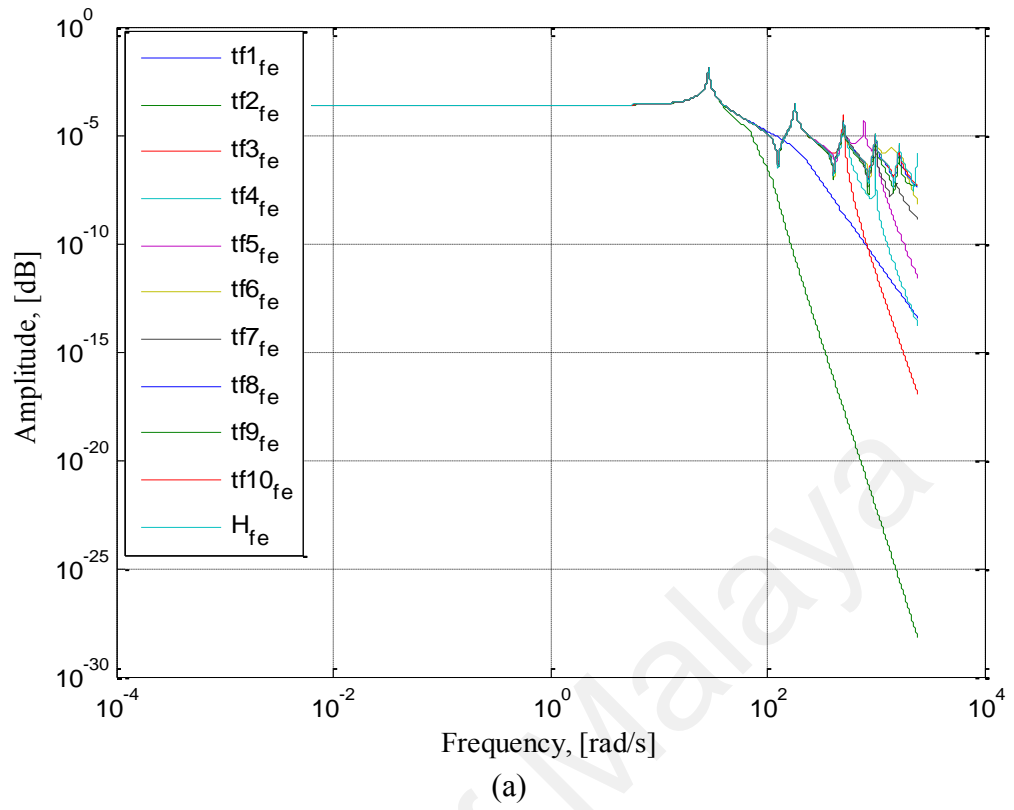


Figure 4.4: (a) Frequency response function and (b) pole-zero map of estimated models using FEM

Results show that all transfer functions using FEM have similar characteristics of FDM and Tf_7 good estimation among all combinations. A brief comparison of best transfer functions of FDM and FEM is shown in Table 4.4.

Table 4.4: Comparison of FDM and FEM modeling

Criterion \ Type of Methods	tf7 using FDM	tf7 using FEM
MSE	1.13e-07	1.18e-07
CSAC	0.999997	0.999977
Fit estimation Data (%)	-100	-100

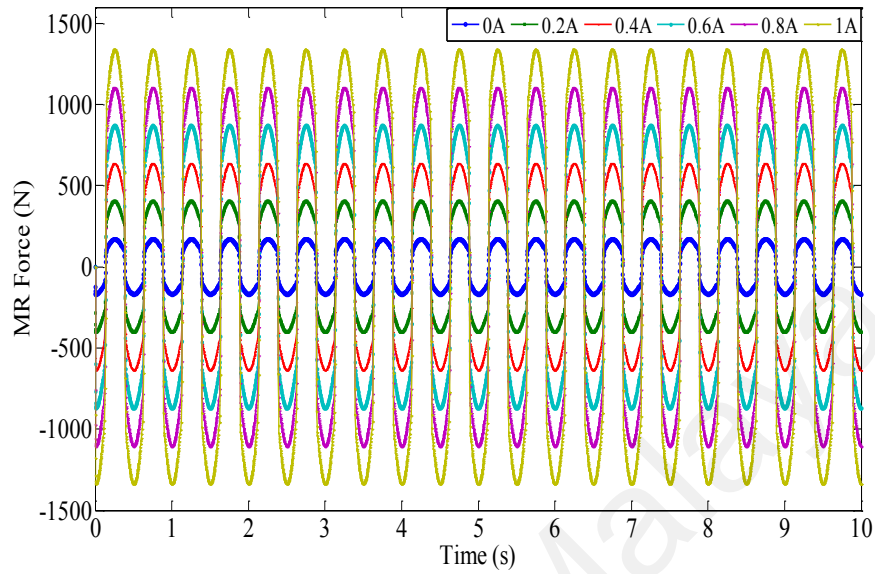
Data in Table 4.4 shows that although the percentage of fit to estimation data is 100 for both FDM and FEM but the MSE and CSAC are different. MSE for FDM is lower than FEM method and CSAC for FDM is higher than FEM which indicates better modeling with FDM over FEM. It shows the effectiveness of FDM method and therefore this is used for further investigation for vibration reduction of wind turbine tower.

$$Tf_7 = \frac{-5.943e12 s^{10} - 2.87e15 s^9 - 1.689e19 s^8 - 8.199e21 s^7 - 1.148e25 s^6 - 5.348e27 s^5 - 1.721e30 s^4 - 7.435e32 s^3 - 3.678e34 s^2 - 1.081e37 s - 1.699e38}{s^{16} + 4598 s^{15} + 1.42e07 s^{14} + 3.205e10 s^{13} + 5.32e13 s^{12} + 7.276e16 s^{11} + 7.608e19 s^{10} + 6.264e22 s^9 + 4.36e25 s^8 + 1.986e28 s^7 + 7.971e30 s^6 + 2.263e33 s^5 + 2.555e35 s^4 + 5.645e37 s^3 + 1.077e39 s^2 + 4.738e40 s + 7.171e41} \quad (4.1)$$

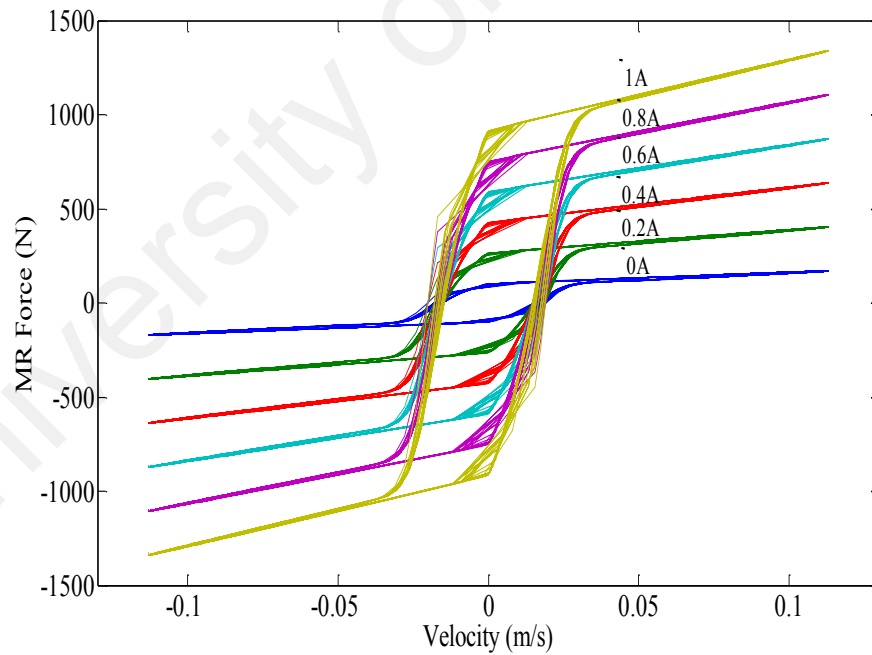
4.2.2 Simulation model of MR damper

The modified Bouc-Wen model is used in this study to find proper force response for different current input. It is found that the displacement at damper position (i.e.10th element) is 0.009m under harmonic excitation with 2 Hz and this study investigates the position of MR damper at 10th element. Thus, the model is tested under different current inputs (0-1A) and with harmonic amplitude of 0.009m and frequency of 2 Hz. The force responses with respected to time and velocity under different current input are shown in Figure 4.5(a) and Figure 4.5(b) respectively. It is observed that the force is increasing regularly with the increase of current inputs. The hysteresis loop is clearly visible force-velocity relationships which is the nonlinear characteristics of MR damper. In this study,

current input of MR damper is controlled to produce required damping force from MR damper.



(a) Force vs Time



(b) Force vs Velocity

Figure 4.5: Force characteristics under different current inputs (0-1A)

4.2.3 Optimized PID controller with ACO

PID controller is preferred in this system to find suitable active control force to be produced by MR damper. In this system, desired control force is measured at the 10th

element of the tower so that MR damper could be attached to the middle of the tower for better balancing of the tower., Design, and optimization process of the active control system with PID controller is conducted after determining the transfer function of the cantilever beam. ACO method, as discussed in the methodology, is implemented to obtain optimal PID parameter which can provide desired active control force. To evaluate the performance and its effectiveness, a classical tuning method, (i.e., Z-N method) and another nature-inspired algorithm, (i.e. PSO method) are also implemented to obtain PID parameters. These values are compared with ACO method based on acquired forces and vibration responses. Same number ants/populations (30) and number of iterations (50) are used for ACO and PSO. During tuning process, the excitation input is sine signal with amplitudes and frequency of 100 N and 2 Hz respectively. Input force signal and the corresponding tower response is presented in Figure 4.6. It is observed that the displacement of the tower is around 0.03 m. The controller PID controller is implemented and tuned with different methods to find optimal control parameters to achieve maximum vibration reduction.

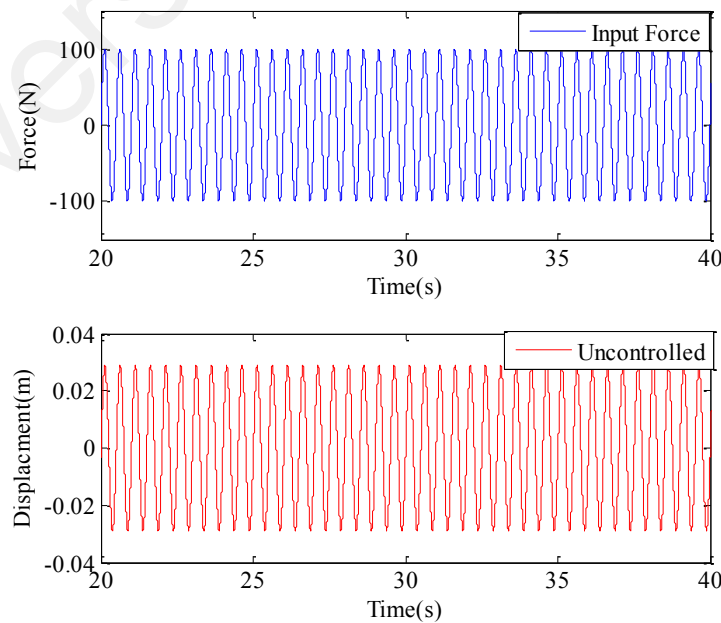
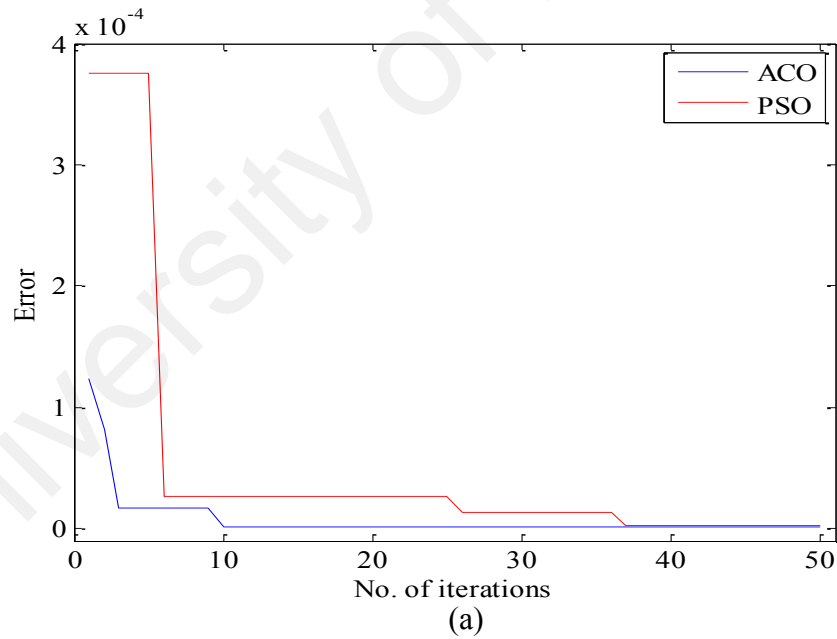


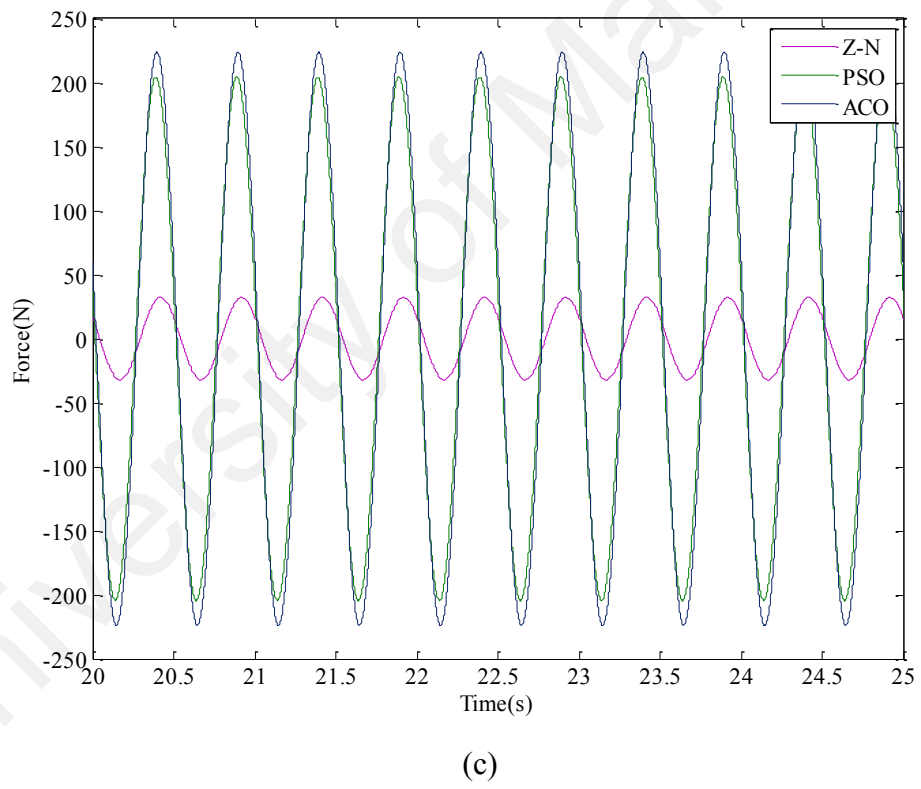
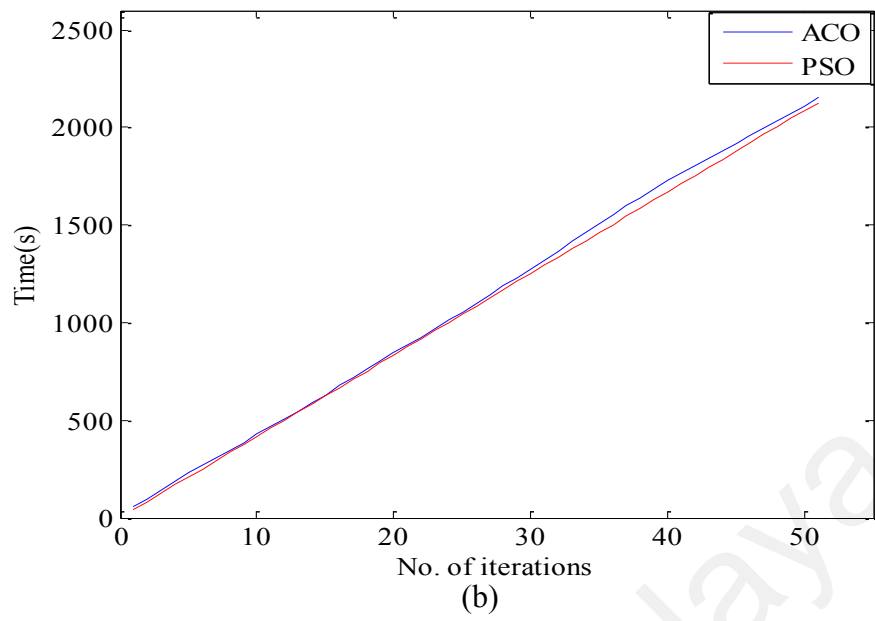
Figure 4.6: Input force and uncontrolled response of the tower

The objective function, which is the difference between the desired displacement and actual displacement is evaluated using the tuned parameters of PID controller with Z-N, PSO, ACO methods. The PID parameters for Z-N, ACO and PSO are presented in Table 4.5. Also, the error, computational time graph for ACO and PSO and the tower responses for PID controller using Z-N, PSO and ACO method are shown in Figure 4.7.

Table 4.5: PID parameters and outputs of Z-N, ACO and PSO tuning method

PID parameters	Z-N	PSO	ACO
K_p	1027.5	1.82e04	1.92e04
K_i	18870.5	9.18e04	1.78e05
K_d	38.85	2e02	1.62e02
Objective function	0.022	0.011	0.009
Tower top displacement reduction	25%	63%	67%





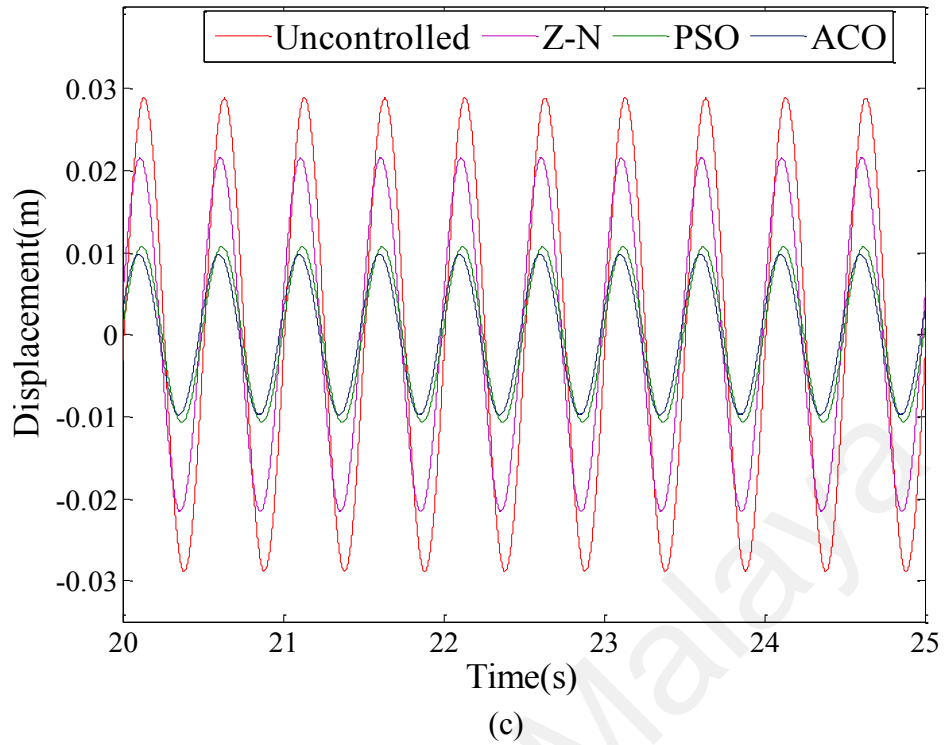


Figure 4.7: (a) Error, (b) Computational time, (c) Control force, and (d) Uncontrolled and controlled response using Z-N, PSO and ACO tuned parameter at 20th element of the tower

From the Table 4.5, it is seen that Z-N method is unable to provide required values of control parameters and lower objective function which is required to maximize vibration reduction. It is possibly because Z-N methods uses step input excitation for tuning parameters and it is also a manual process. On the other hand, sinusoidal input is used as excitation input for ACO and PSO methods. This gives advantage to find optimal desired force under harmonic force where maximum vibration may occur at natural frequency. ACO provides lowest values of objective function compared to Z-N and PSO methods. From the above results, it is also seen that with same no of populations and iterations, ACO method is better than PSO in terms of error and reduction of vibration. In Figure 4.7(a), the desired force is computed after 10 iterations with ACO, whereas, for PSO, it takes more than 35 iterations to achieve the desired force. Also, ACO method has the advantage over Z-N and PSO method in terms of computational time (Figure 4.7(b)). Z-N method finds ultimate gain using trial and error process which may take more

computational time than ACO. The control forces for all three tuning process are shown in Figure 4.7(c). It is observed that PID parameters from Z-N method provides small amount of control force, therefore provide low vibration reduction compared to both PSO and ACO method. Therefore, ACO provides better control force than PSO which gives highest reduction rate for ACO. ACO provides significant vibration reduction rate compared to Z-N and PSO as shown in Figure 4.7(d). Results show that tower displacement is reduced by 25%, 63% and 67% using Z-N, PSO and ACO method respectively under harmonic excitations. This is because Z-N and PSO method are unable to provide required damping force to achieve high vibration reduction.

Consistency test is important to check the optimization method is effective and repeatable because the optimization method provides different values of PID parameters after every test. Therefore, the coding for PID parameter optimization using ACO was tested for several times and different values of PID parameters (but very close) are found. However, there were no considerable output results, i.e. vibration amplitudes/objective function were found using those PID values. Different PID values for several tests of ACO simulation are provided at Table 4.6.

Table 4.6: Consistency test of PID parameters using ACO method

PID parameters	Test 1	Test 2	Test 3
K_p	1.92e04	1.88e04	1.91e04
K_i	1.78e05	2.40e05	2.25e05
K_d	1.62e02	1.88e02	1.82e02
Objective function	0.009	0.009	0.01

4.2.4 Optimal placement of MR damper

Placement of MR damper on the system is very important because the optimal position of MR damper maximize vibration reduction. Appropriate positioning of control dampers not only maximize the vibration reduction rate but also minimize design and

maintenance cost. However, MR damper could also be placed at top of the tower at the 5th element, and 20th element as literature suggests. Another option can be at 15th element just below the nacelle. If the damper is installed at the base, i.e. at near 5th element, it can effectively reduce the base displacement due to external disturbances, however, for tall horizontal axis wind turbines, vibration occurs from top/base and transfers to other points of the tower. Also, vibration on top of the tower due to disturbances from blades, generators cannot be reduced efficiently if the damper is installed at the base. On the other hand, but it is avoided MR damper to be placed on top of the tower, i.e. at the 20th element in this project because the nacelle consists of generator and control box of a horizontal axis with turbine are generally placed on the top of the tower. It might create more vibration and other structural problems if additional mass such as MR damper is also placed on the top. Other than the above reasons, the optimal placement of the MR damper is also investigated based on the active control force and vibration reduction rate. The desired force at 5th and 15th elements are measured as other options and compared with the result of 10th element. The desired active control force for 5th, 10th, and 15th elements are shown in Figure 4.8. The controlled and uncontrolled response at 20th element for damper at 5th, 10th, and 15th elements is shown in Figure 4.9.

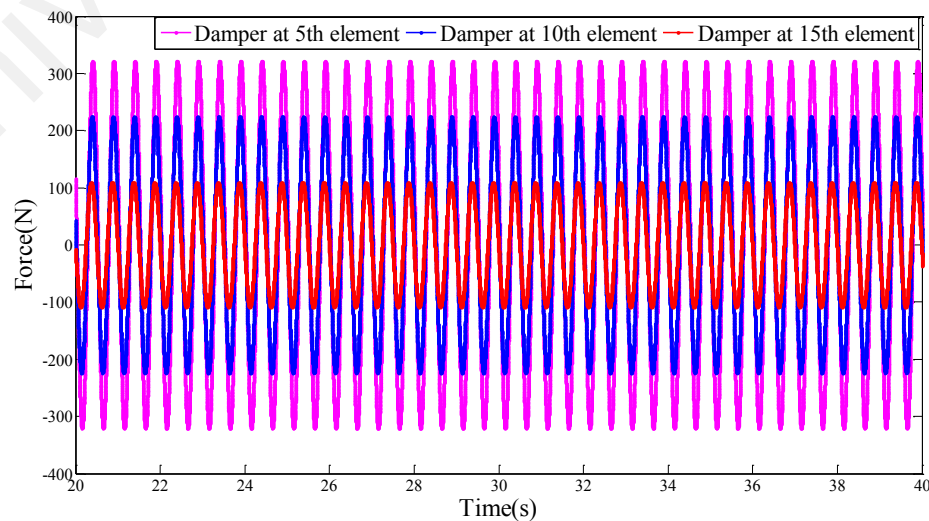


Figure 4.8: Desired force at 5th, 10th, and 15th elements of the tower

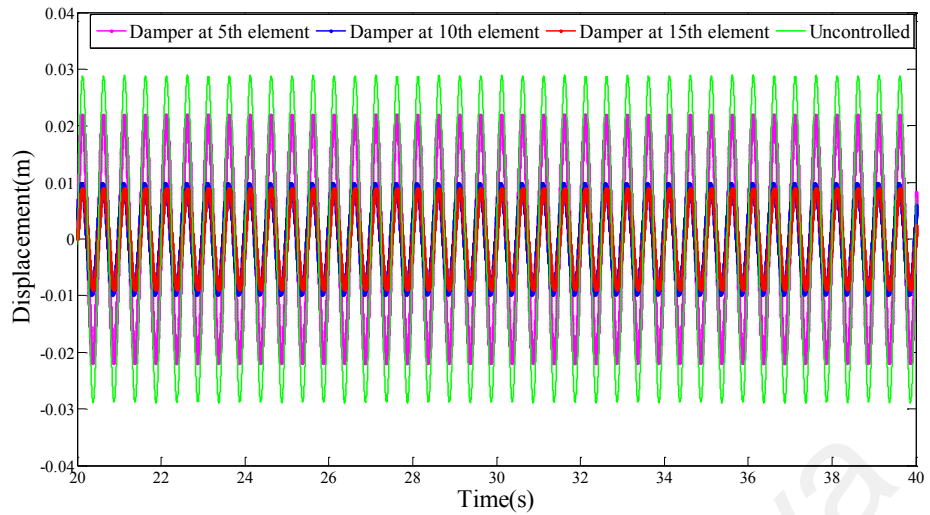
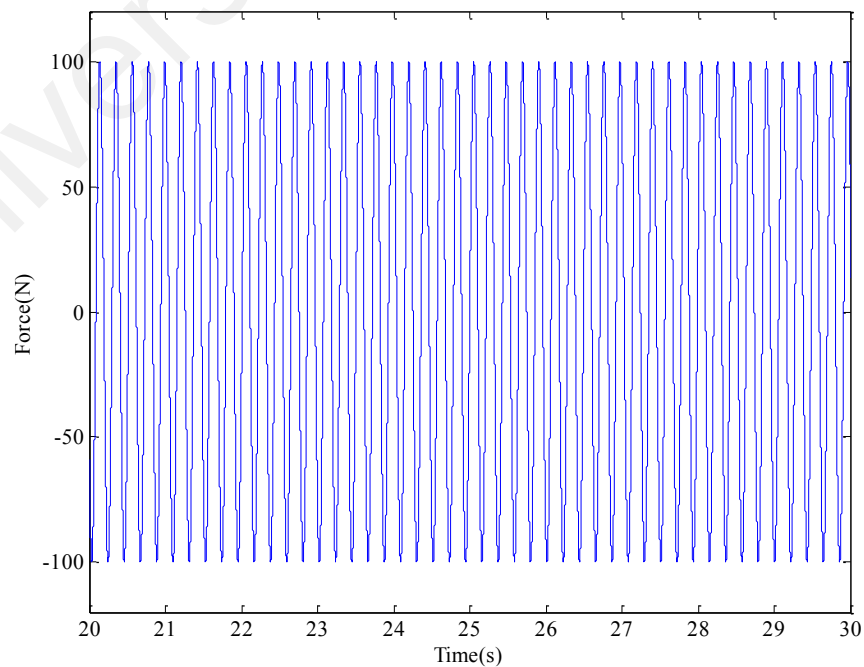


Figure 4.9: Tower Response at 20th elements for damper at 5th, 10th, and 15th elements of the tower

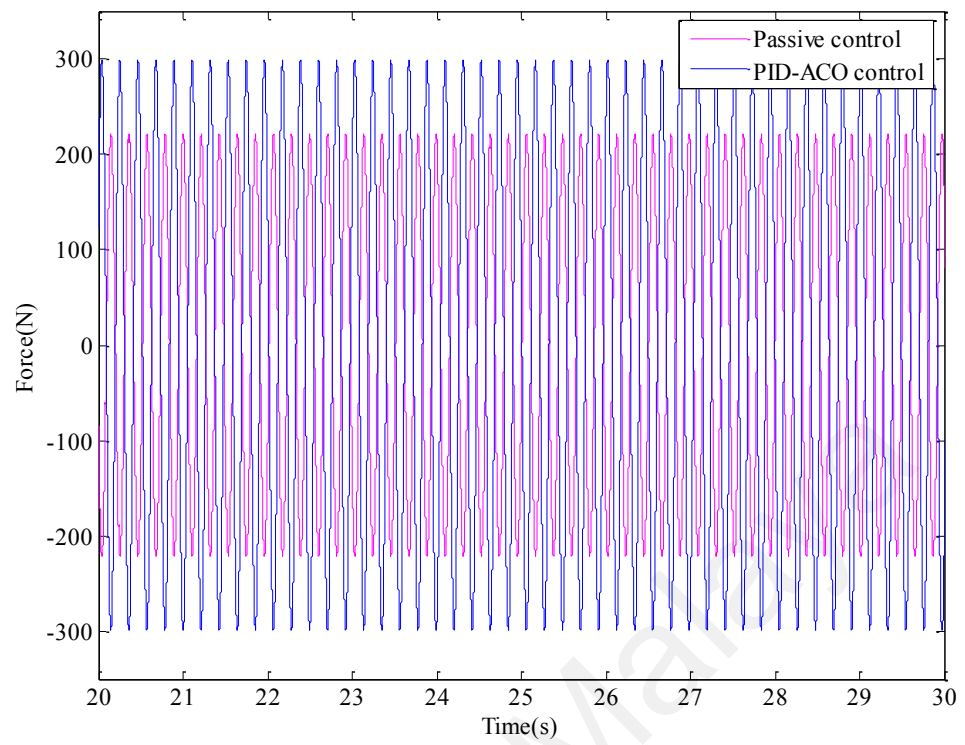
The result shows that the reduction rate of wind turbine tower response to damper at 5th, 10th, and 15th elements are 39%, 72%, and 75% respectively. From the result, it is seen that desired force at 5th element is higher compared to force at the 10th element. Also, the reduction rate of for the damper at 10th element is much higher than damper at 5th element. It can be easy to place MR damper at the relatively lower place at 5th element but higher force should be produced at this element to counter vibration at the 20th element. However, the desired force is lower at the 15th element compared to the 10th element and reduction rates are similar for damper at 10th and 15th elements. It seems 15th elements will be suitable, but it would difficult to place the damper on 15th element and maintenance cost will be higher. Moreover, the damper needs to be extended further to attach at the 15th element which can result in loss of strength and it can also affect to the damper to transfer the required force to the tower. Therefore the 10th element will be optimal for this case to ensure maximum vibration reduction and structural balance.

4.2.5 Effectiveness of optimized PID-ACO controller under different loadings

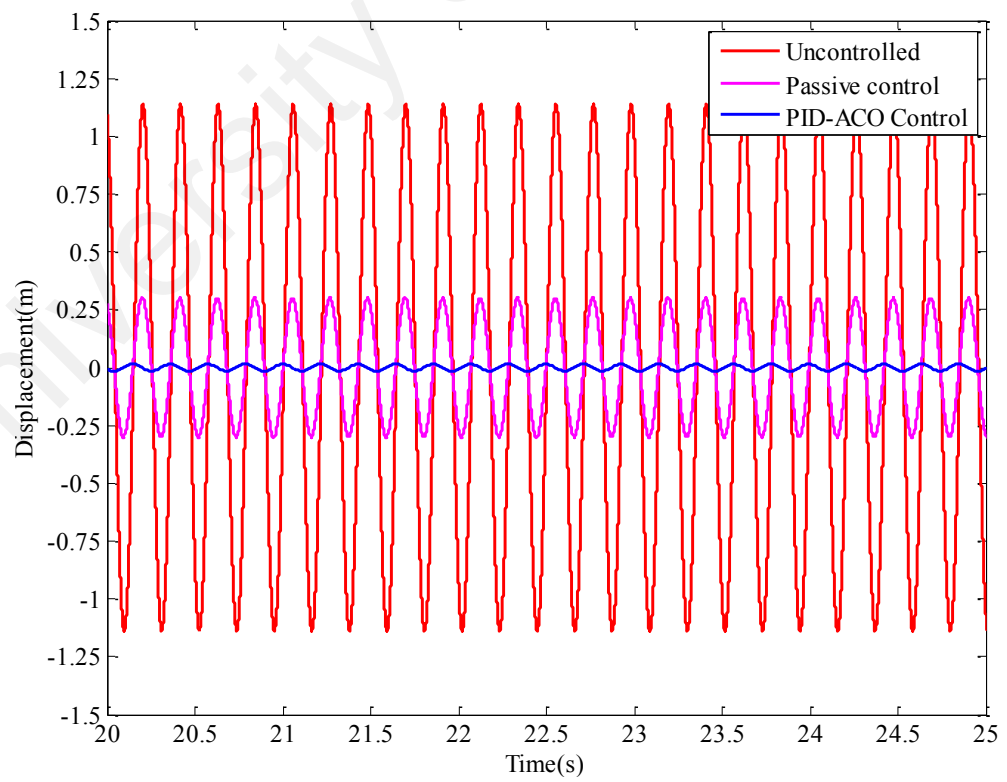
Optimized parameters of PID controller using ACO are used to measure in desired control force and provided to the system. This will be presented as PID-ACO control system and a current controller will be presented in the later part of this chapter to achieve required force from the MR damper. The PID-ACO control force is applied to the 10th elements as this is the optimal place in terms of vibrations reduction, maintenance cost etc. Wind turbine tower model under sinusoidal force at 1st mode, (i.e. 4.68Hz) and random forces, which are important loadings for wind turbine tower, are simulated to prove that the tuned PID controller can reduce or minimize the disturbance compared to an uncontrolled and a system with conventional passive damper. The passive damper is designed with damping constant of 180 Ns (Am)⁻¹ with trial and error method. The responses for sinusoidal force and random force are shown in Figure 4.10 and Figure 4.11 respectively. The effectiveness of PID-ACO controller is also computed for other loadings such as impact and negatively damped turbulent loadings (Refer to Appendix A).



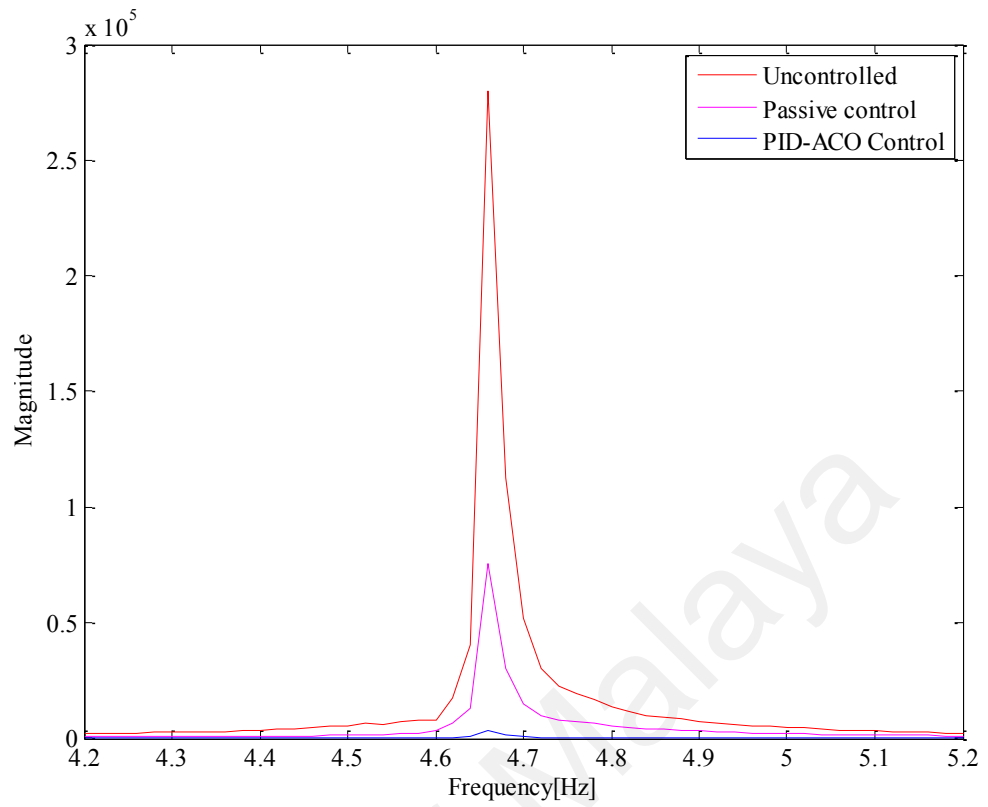
(a) Input Excitation



(b) Control force

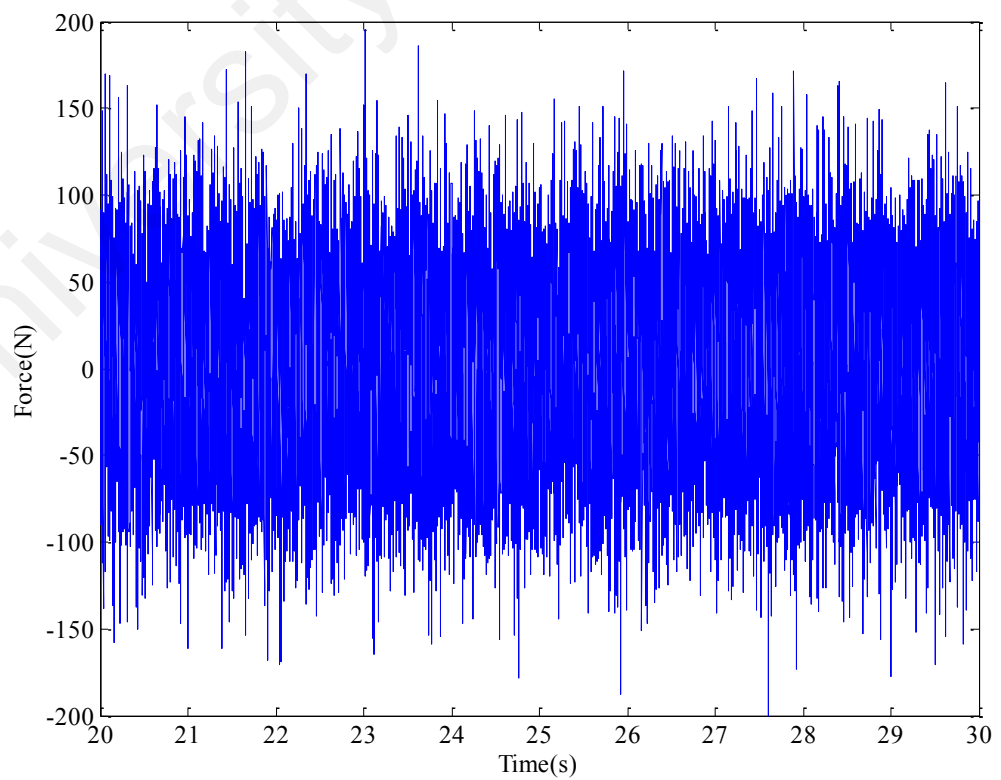


(c) Time response

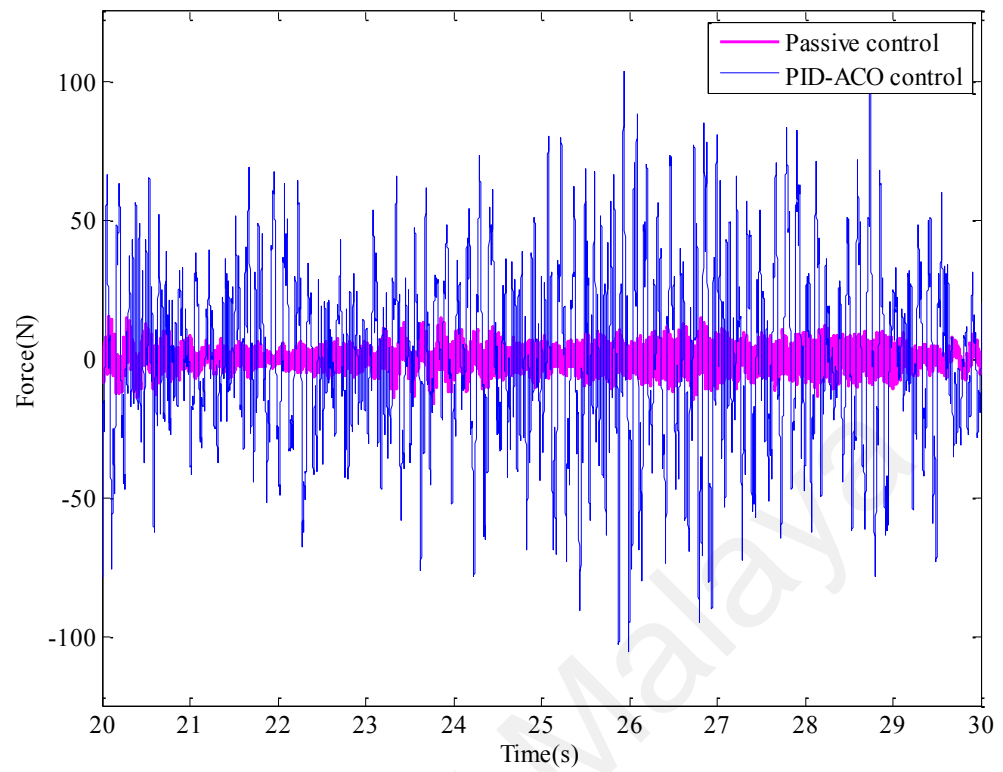


(d) Frequency response

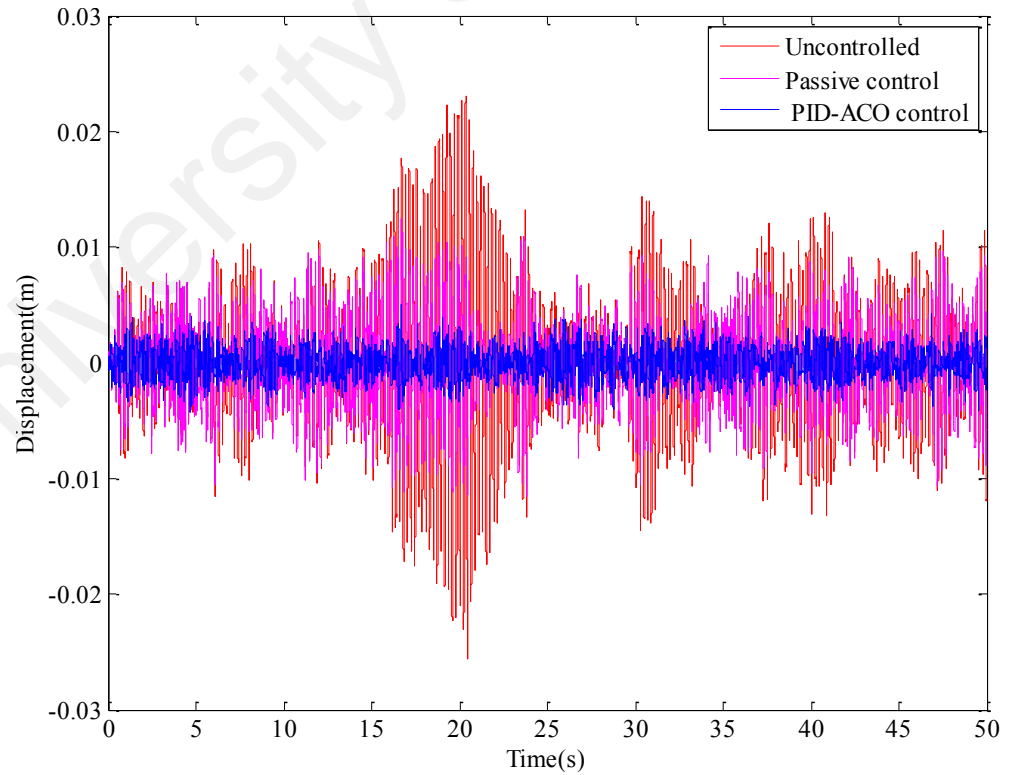
Figure 4.10: Uncontrolled, passive, and PID-ACO control response of 20th element of the tower for sinusoidal disturbance at 1st mode



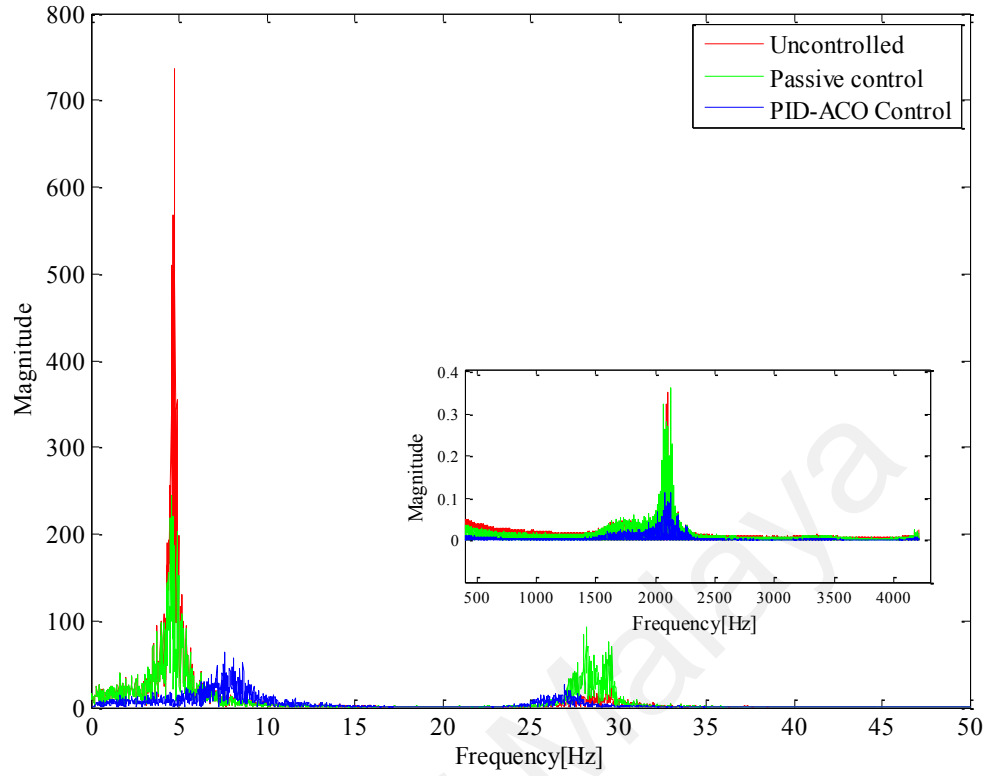
(a) Input excitation



(b) Control Force



(c) Time response



(d) Frequency response

Figure 4.11: Uncontrolled, passive, and PID-ACO control response of 20th element of the tower for random disturbance

Figure 4.10 and Figure 4.11 showed the uncontrolled and controlled response of wind turbine tower with PID controller using ACO method for sinusoidal and random disturbances respectively. The computed control force for passive and PID-ACO controller required by actuators are also provided for both cases. Under sinusoidal 1st mode, the uncontrolled peak displacement is 1.13 m. To control the vibration amplitude the passive and PID-ACO controller are implemented to observe the effectiveness of the proposed PID-ACO controller. Both passive and PID-ACO control system provides vibration reduction on the tower. However, the passive control is unable to provide suitable damping force compared to PID-ACO control system. Therefore, the peak vibration amplitude for passive control is reduced to 0.3 m, (i.e. 73% reduction), where for PID-ACO controller, the reduced peak vibration amplitude is 0.015 m, (i.e. 98% reduction). It is observed that the performance of estimated desired force by PID-ACO controller is much better compared to conventional passive control. It is also observed

that desired control force with optimized PID controller reduced more vibration compared to passive control under sinusoidal and random disturbances. Time and frequency responses for both cases showed a significant reduction of displacement at top of the tower using optimized PID controller. In summary, the tuned PID controller with ACO method for the beam system can greatly reduce the response compared to system without PID controller and passive controller.

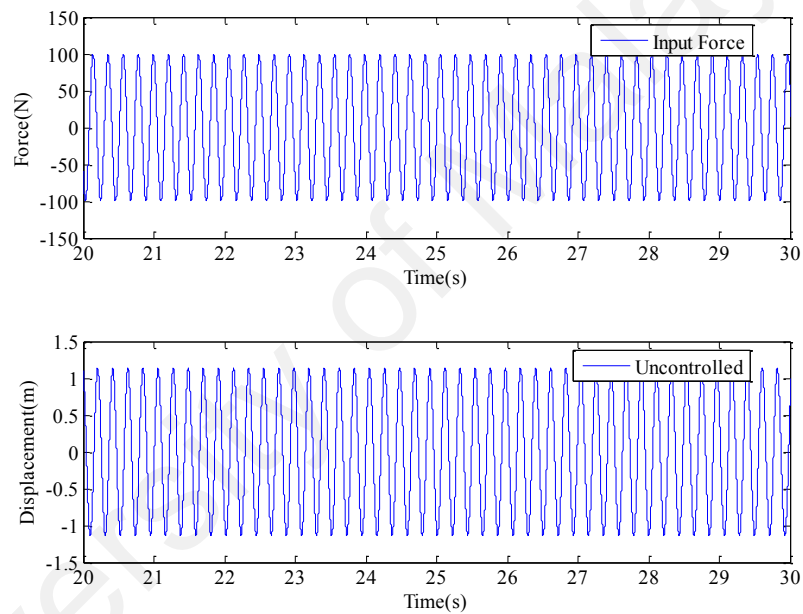
Another controller is required to find suitable current for MR damper to produce desired force required to reduce maximum vibration level and the control parameters of current controller are presented in the next section.

4.2.6 Current controller

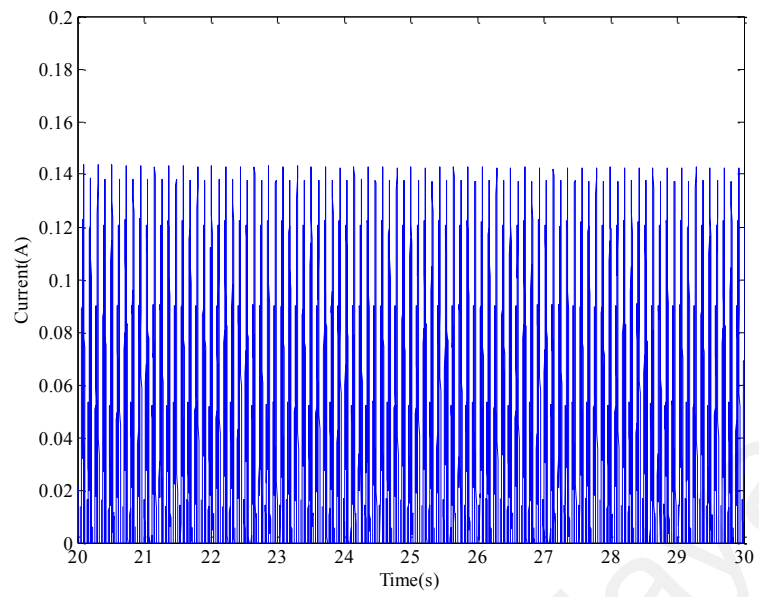
One of the important advantages of the semi-active control system is damper is controllable. In this research, the PI controller controls current input of MR damper. PI controller parameter, proportional gain, K_p and integral gain, K_i are tuned based on a comparison of desired force and actual force from MR damper using trial and error method. For the sine input mentioned above, the wind turbine tower model is simulated, and PI controller is used to find suitable current for MR damper to produce required damping force. The proportional gain is first adjusted to achieve the current input from the error between actual and desired control force. Then the integral gain is adjusted to reduce the steady state error. After the tuning process, the acquired current is 0.143 A as it is shown in Figure 4.12(b). The optimal values of PI parameters are computed as $K_p = 0.00068$ and $K_i = 0.0009$.

4.2.7 Semi-Active control response with controllable MR damper under different excitations

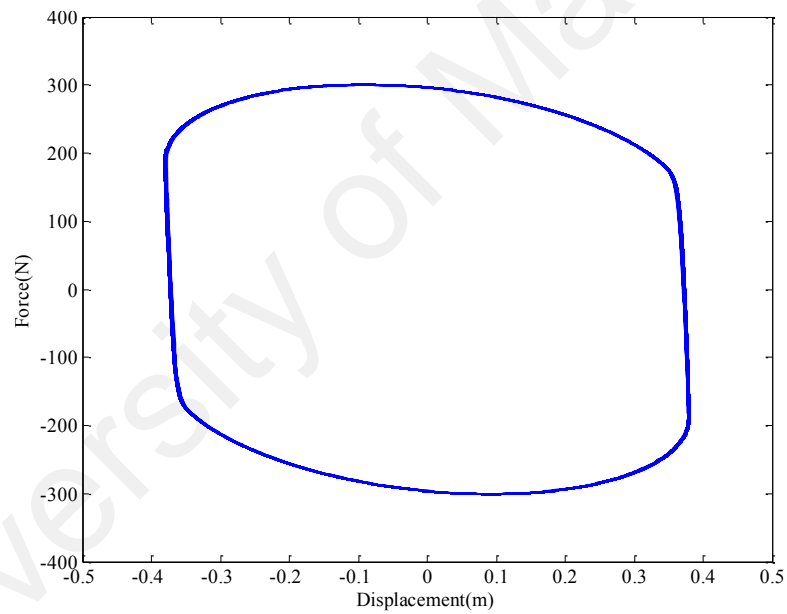
Wind turbine tower model is simulated with semi-active control strategy with system controller and current controller as presented in chapter 3. Wind turbine tower is simulated under harmonic which represents the possible disturbances from blade rotations and generators. The amplitudes of these excitations are based on the lab scaled wind turbine tower model. MR damper is simulated with Bouc-Wen model. The MR damper is placed in 10th element of the tower. The responses are shown in Figure 4.12.



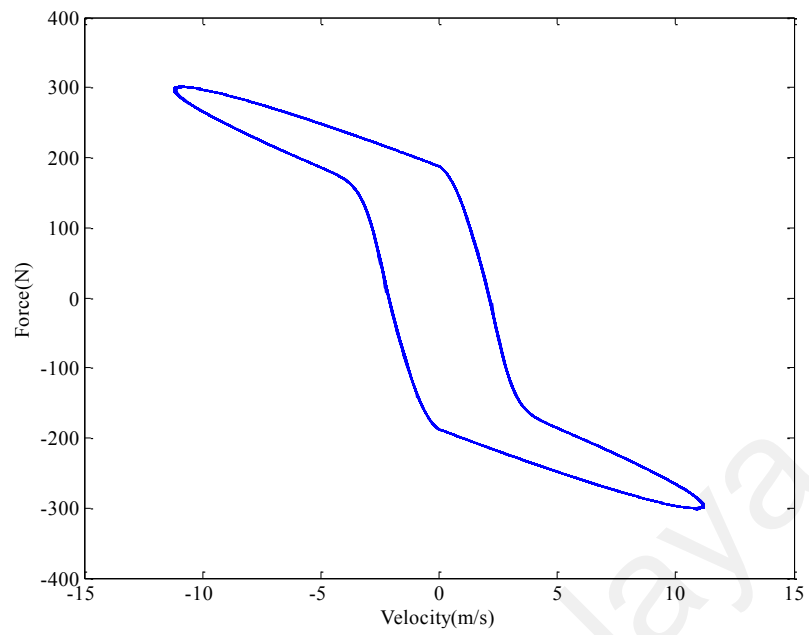
(a) Excitation force (1st mode) and uncontrolled response



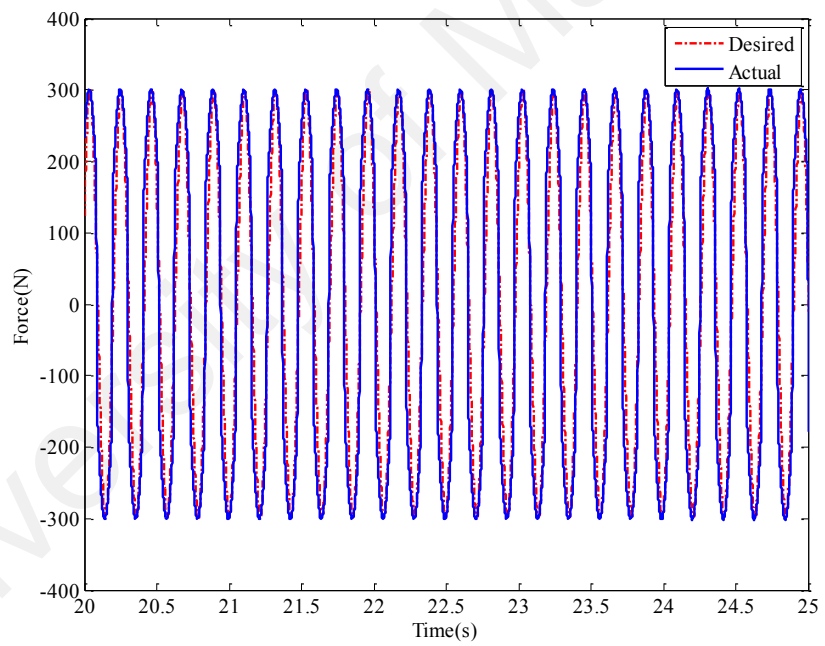
(b) Current



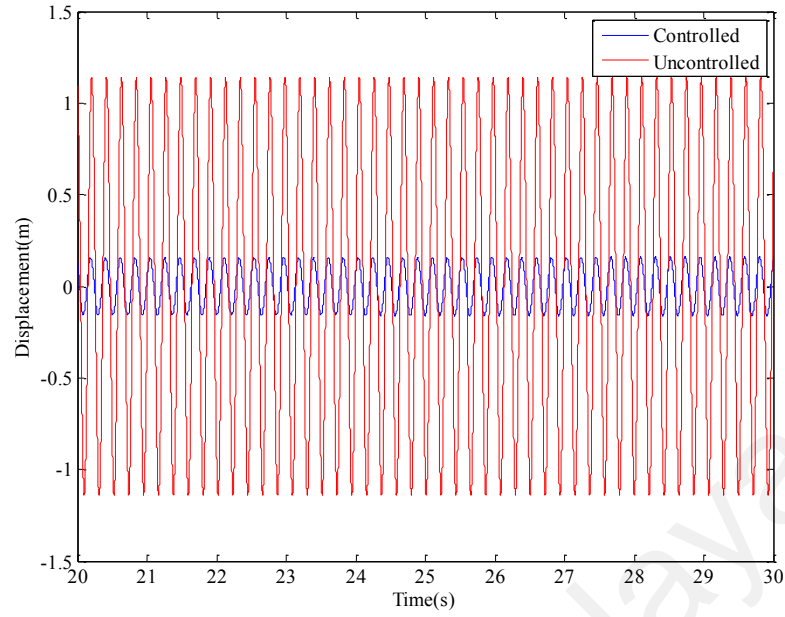
(c) Force vs Displacement



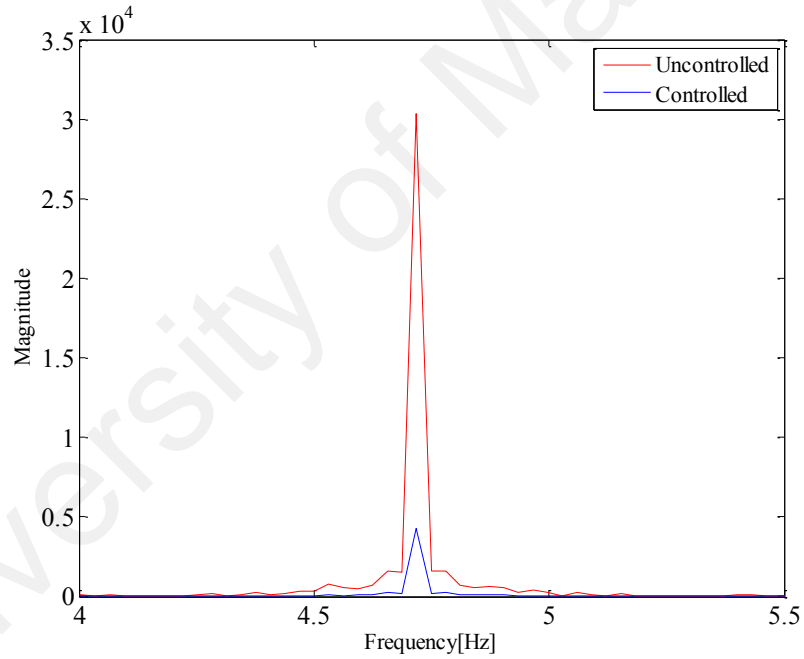
(d) Force vs Velocity



(e) Desired vs Actual control force



(f) Time response at 20th element



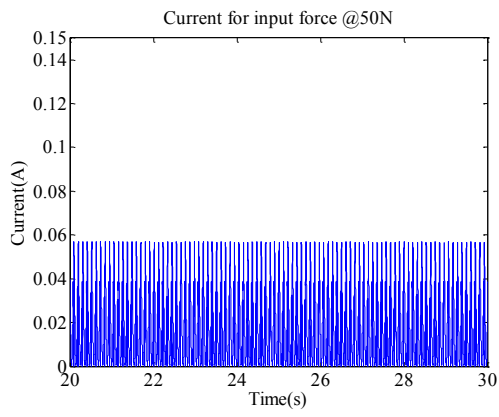
(g) Frequency response

Figure 4.12: Semi-active vibration control response of wind turbine tower

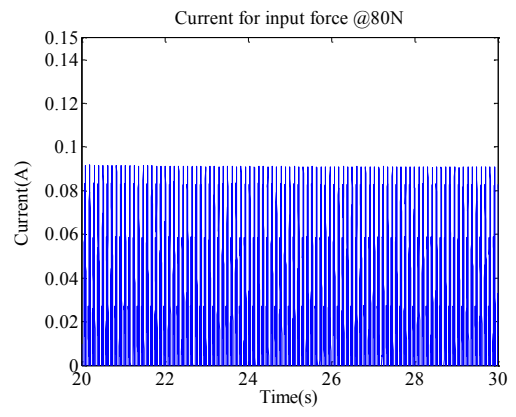
Using PID-ACO and PI controller desired force and suitable current are measured respectively. Figure 4.12(a) shows the uncontrolled response which are controlled using the MR damper which is installed at mid-point of the tower. The PI controller finds the suitable current to achieve the desired force computed using PID-ACO controller. Figure 4.12(b) shows that the required current is 0.143A. Figure 4.12(c) and Figure 4.12(d)

shows MR damper force-displacement and force-velocity relationships and hysteresis loop is clearly visible which is the characteristic of MR damper. MR damper with measured current produces required force similar as a desired force as seen in Figure 4.12(e). In Figure 4.12(f) and Figure 4.12(g), the controlled and uncontrolled responses are shown in the time domain and frequency domain respectively, where it is clearly seen that the displacement at the 20th element reduced significantly, (i.e. 83%) after implementing the semi-active control response with MR damper. The reduction rate for semi-active control compared to the reduction rate in previous section where PID-ACO control force is directly fed to the system is slightly low. This is possibly due to the phase discrepancies from the MR damper.

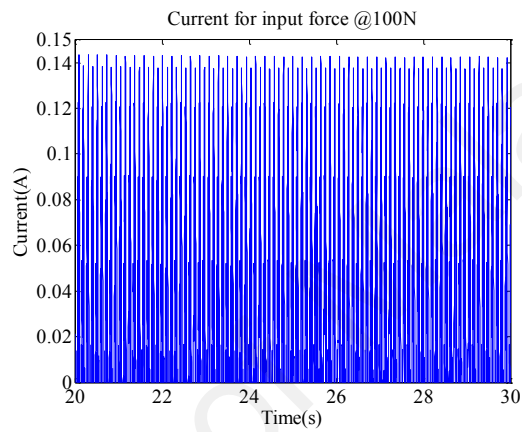
In this section, the PID-ACO control parameters are investigated under different frequencies and amplitudes to verify that the proposed control strategy reduces vibration of the tower when the excitation frequency and amplitude varies. The ACO optimized tuned parameters of PID controllers are kept same in this section. In the previous simulation, the input excitation is sine signal with amplitude of 100N and frequency of 4.68Hz. The tower model is then simulated under different amplitudes of sine signal such as 50N, 80N, and 100N but with fixed frequency of 4.68Hz to observe the effectiveness of the designed control system. The PID controller provides desired force and PI controller provide suitable current signal. The required current signals, force-displacement relationships, and controlled and uncontrolled responses for different input forces are presented in Figure 4.13, Figure 4.14, Figure 4.15 and Figure 4.16 respectively.



(a)

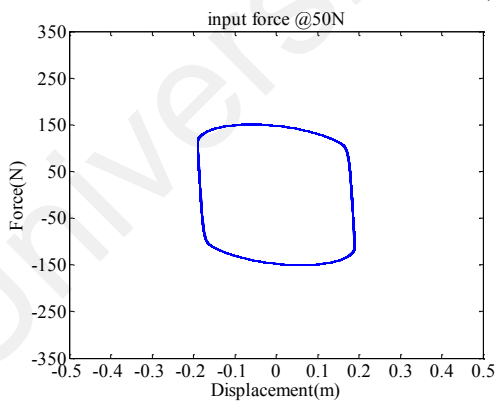


(b)

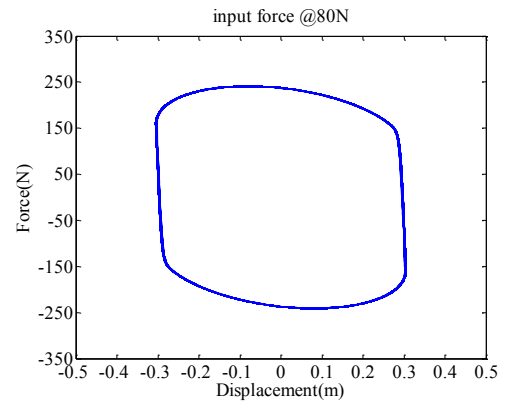


(c)

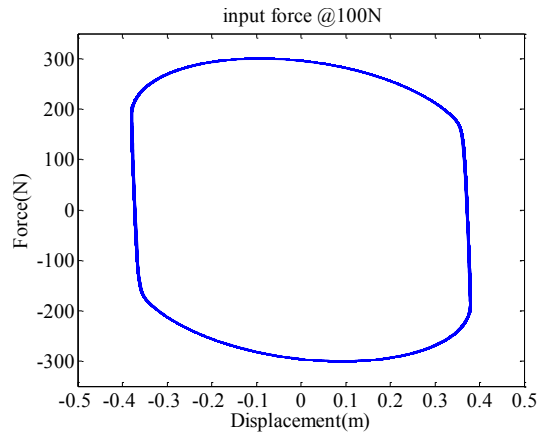
Figure 4.13: Required current for MR damper when input force at (a) 50N, (b) 80N and (c) 100N



(a)

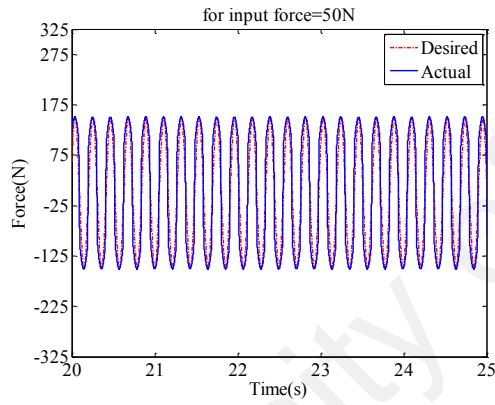


(b)

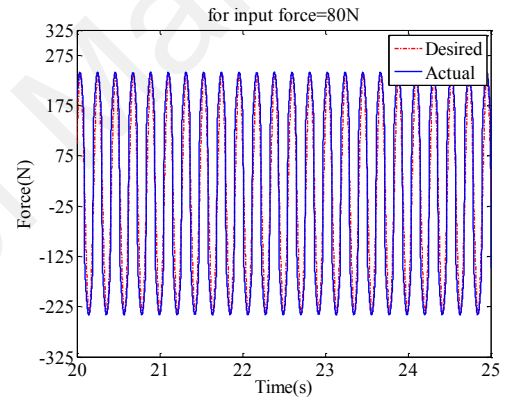


(c)

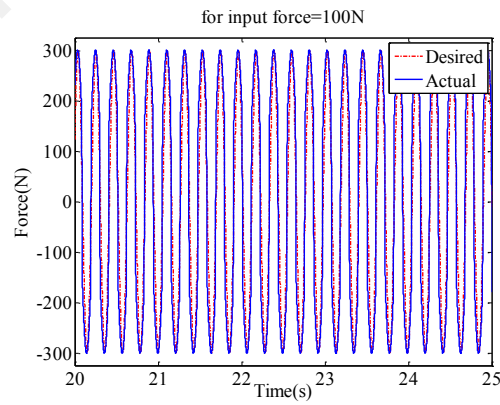
Figure 4.14: Force vs Displacement for input force at (a) 50N, (b) 80N, and (c) 100N



(a)



(b)



(c)

Figure 4.15: Desired and actual control force for input force at (a) 50N, (b) 80N, and (c) 100N

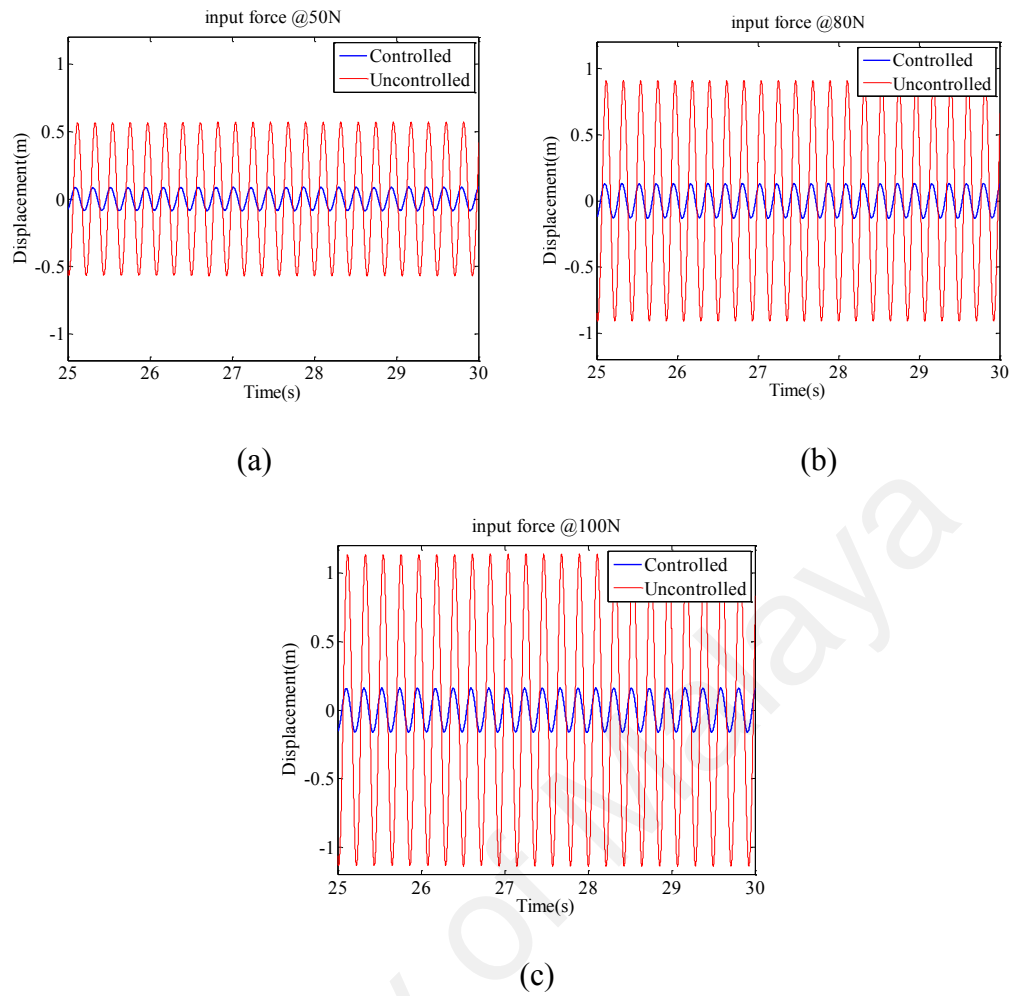


Figure 4.16: Controlled and Uncontrolled responses for input force at (a) 50N, (b) 80N, and (c) 100N

When the system is simulated under sine input with different amplitude, (i.e. 50N, 80N, 100N) but fixed frequency at 1st mode, different level of vibration amplitudes is measured. Using designed PID controller, desired forces are achieved and required current are measured for three different cases. The required current for amplitudes of 50N, 80N, and 100N are 0.055A, 0.09A and 0.143A respectively. In Figure 4.18 and Figure 4.9, it is observed that for input force of 50 N, the required current and measured damping force are lower than the corresponding value of 80N and 100N. Figure 4.15 shows the desired and actual control for all three cases and it is observed that the actual forces, which are achieved using the current controller, are same as desired force. It is also found that when the system is excited with higher force, higher current and damping

forces will be required to counter vibration and the responses for all three cases are shown in Figure 4.16. The reduction rate for amplitudes of 50N, 80N, and 100N are 84%, 85.7%, and 83% respectively.

The tower model is also simulated under sine input with fixed amplitude, (i.e. 100N) but with different frequencies, (i.e. 2Hz, 4.68Hz, 6Hz) to observe the responses of the tower vibration, therefore the control strategy is applied to spot the effectiveness of the designed control system under different frequencies. The results are shown in Figure 4.17-Figure 4.20.

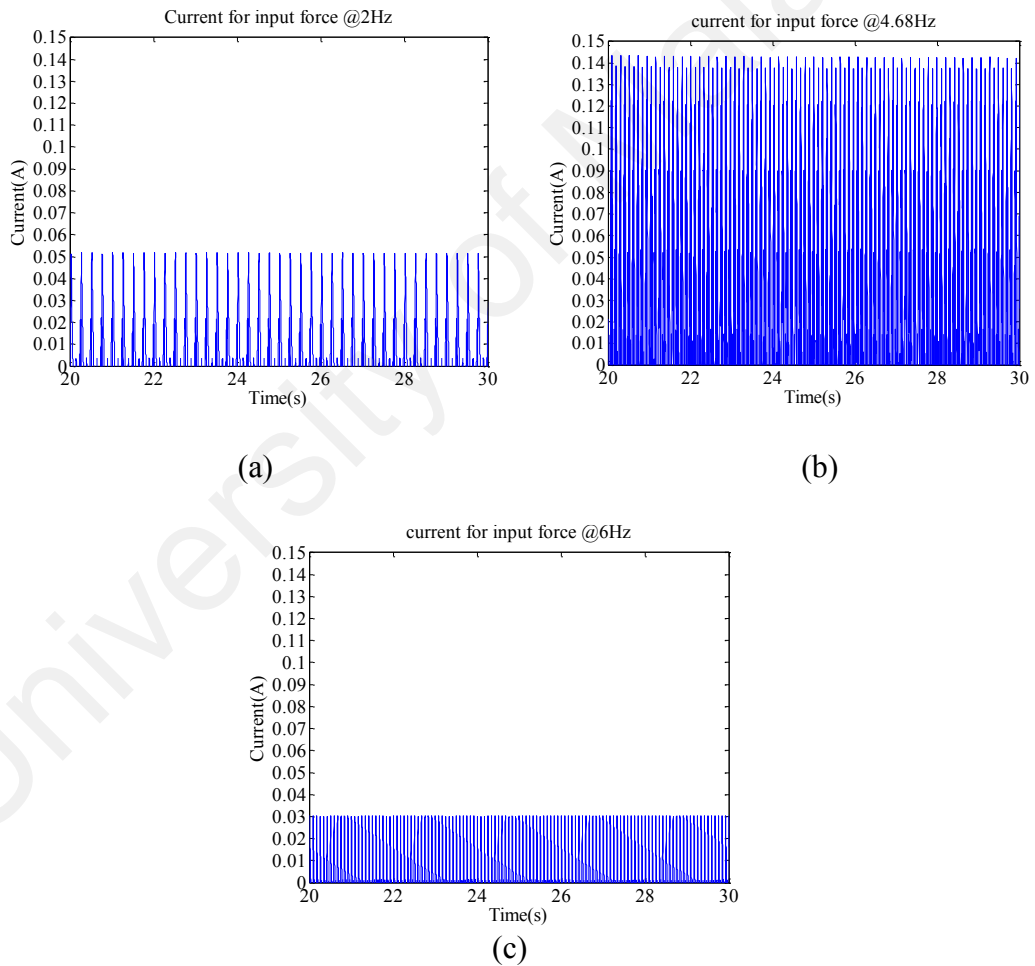
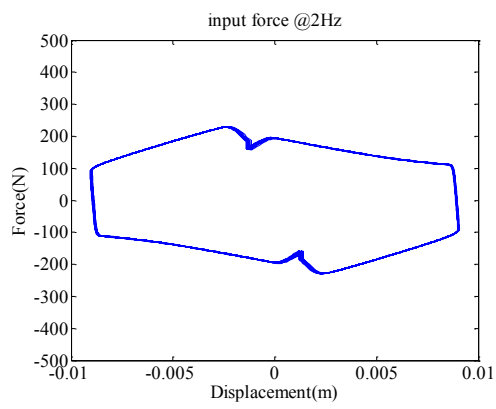
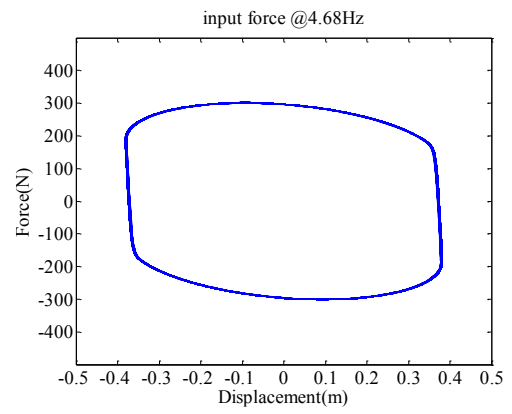


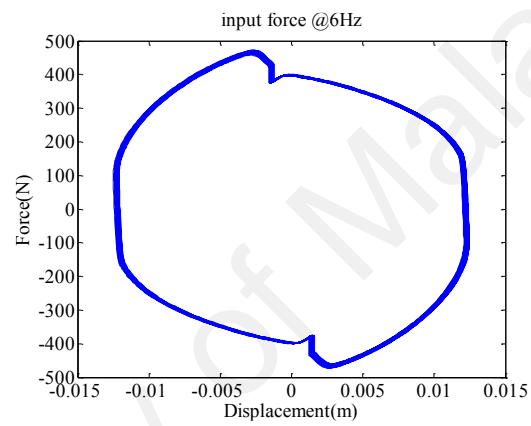
Figure 4.17: Required current for MR damper when input force at 2Hz, 4.68Hz, and 6Hz



(a)

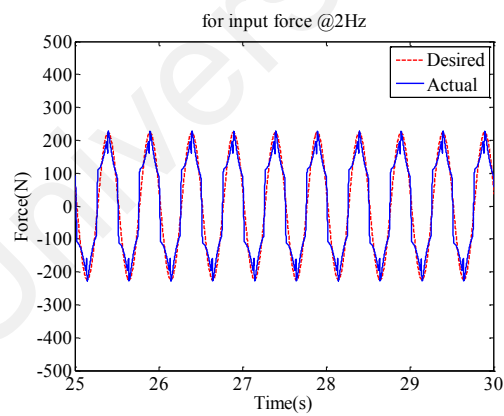


(b)

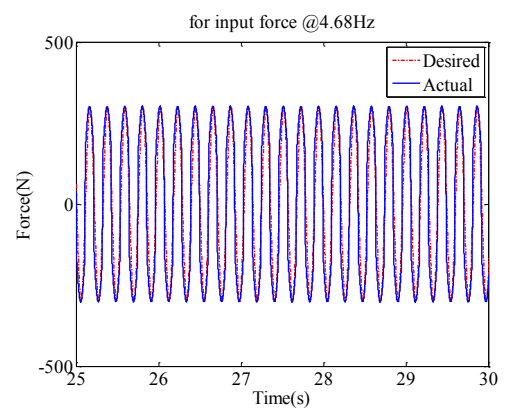


(c)

Figure 4.18: Force vs Displacement (Input force at 2Hz,4.68Hz,6Hz)



(a)



(b)

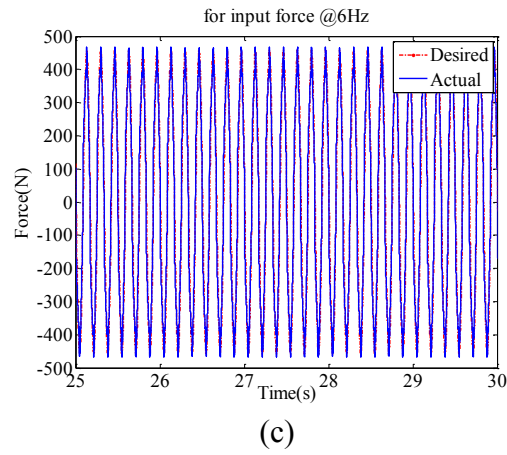


Figure 4.19: Desired and actual control force for input force at (a) 2Hz, (b) 4.68Hz, and (c) 6Hz

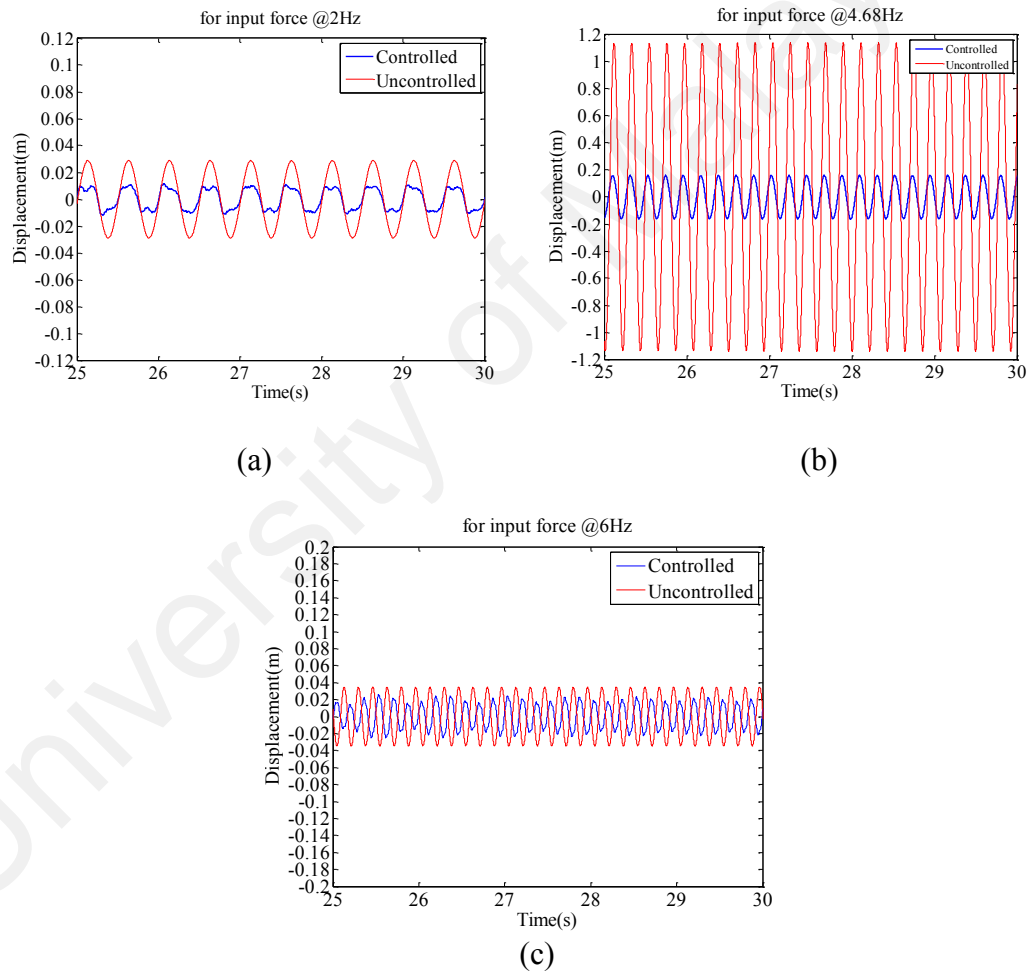
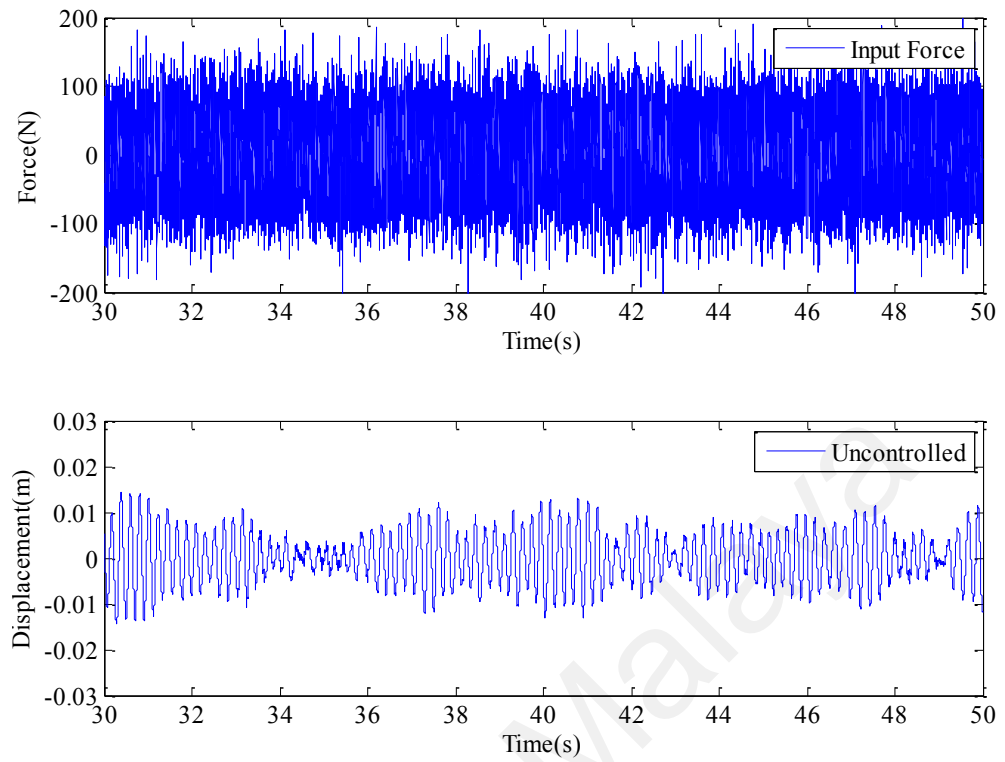


Figure 4.20: Controlled and Uncontrolled responses for input force (2Hz,4.68Hz,6Hz)

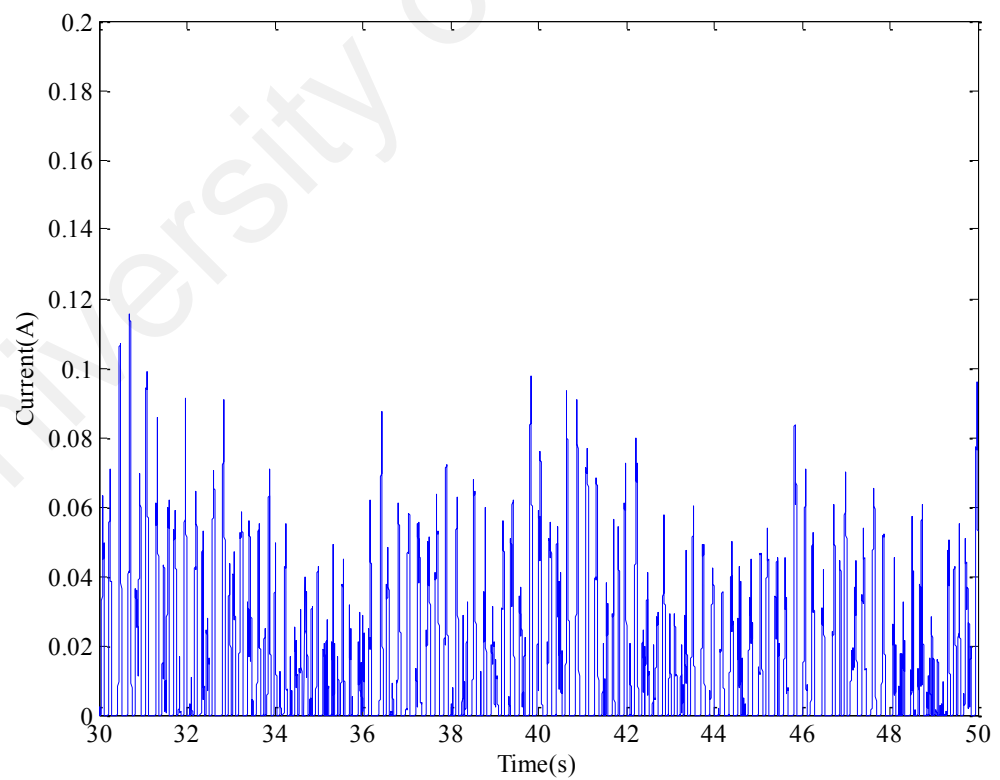
From the above results, it is seen that for different input frequencies the different vibration levels are measured. The required current for frequencies of 2Hz, 4.68Hz, and 6Hz are 0.051A, 0.143A and 0.03A as shown in Figure 4.17. At the 1st mode, (i.e.

4.68Hz), the vibration is higher at the top of the tower compared to the responses under other two frequencies. The same PID-ACO control parameter finds the required control force and the PI controller provides required current to achieve the control force for all three cases. The required force is higher for 6Hz and force is lower for 2Hz as it is seen in Figure 4.18. MR damper force depends on current supply and the displacement at the point where it is attached to. The desired and actual force for all three excitation frequencies are shown in Figure 4.19. From the response plot in Figure 4.20, in all cases vibration is reduced significantly and the reduction rates for 2Hz, 4.68Hz, and 6Hz are 67%, 83% and 34.4% respectively. The controlled response rate is different because same PID parameter values are used to find the desired force to see the effectiveness of the controller. It can be concluded that same PID parameters can handle a range of input force and frequencies.

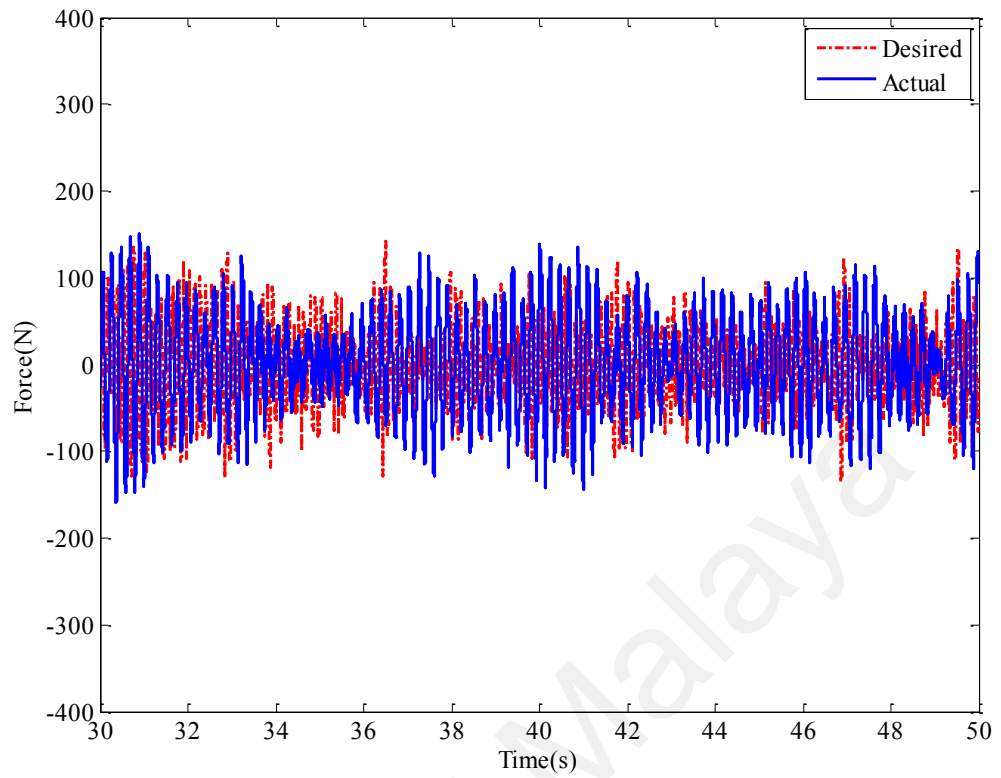
Wind turbine model is also simulated under random excitations to represent heavy wind loading on the tower. The optimized PID controller and PI controller are also implemented to find desired force and suitable current for MR damper respectively. Required current, MR damper force at the 10th element, controlled and uncontrolled responses of wind turbine tower at the 20th element are shown in Figure 4.21.



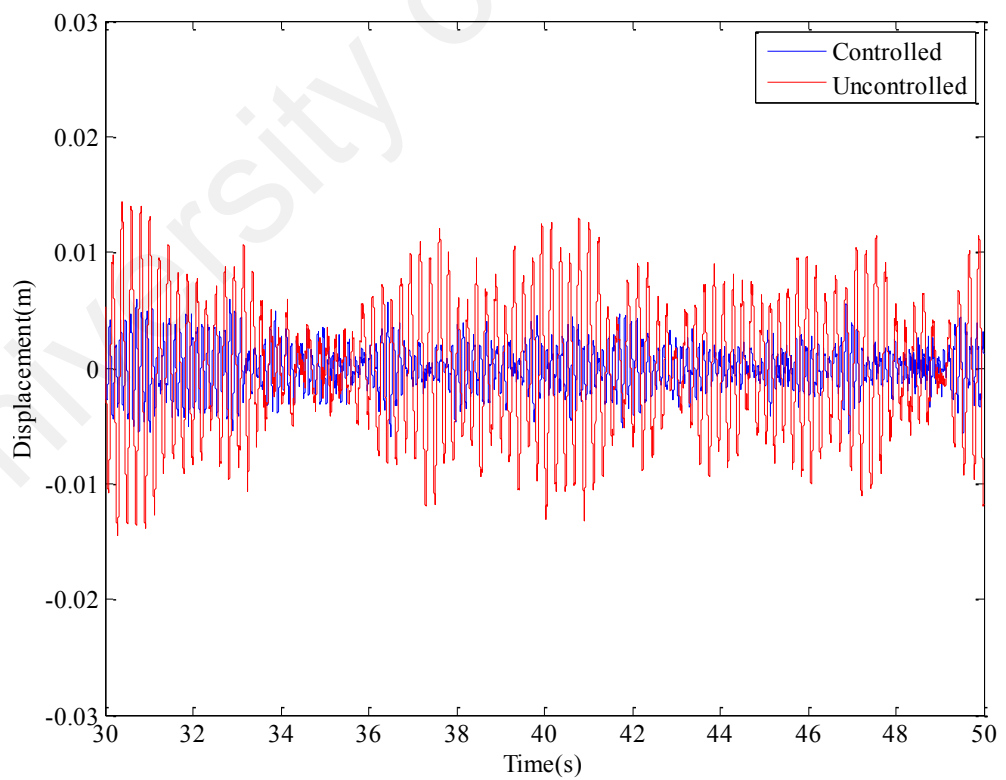
(a) Input excitation and uncontrolled response of wind turbine tower at 20th element



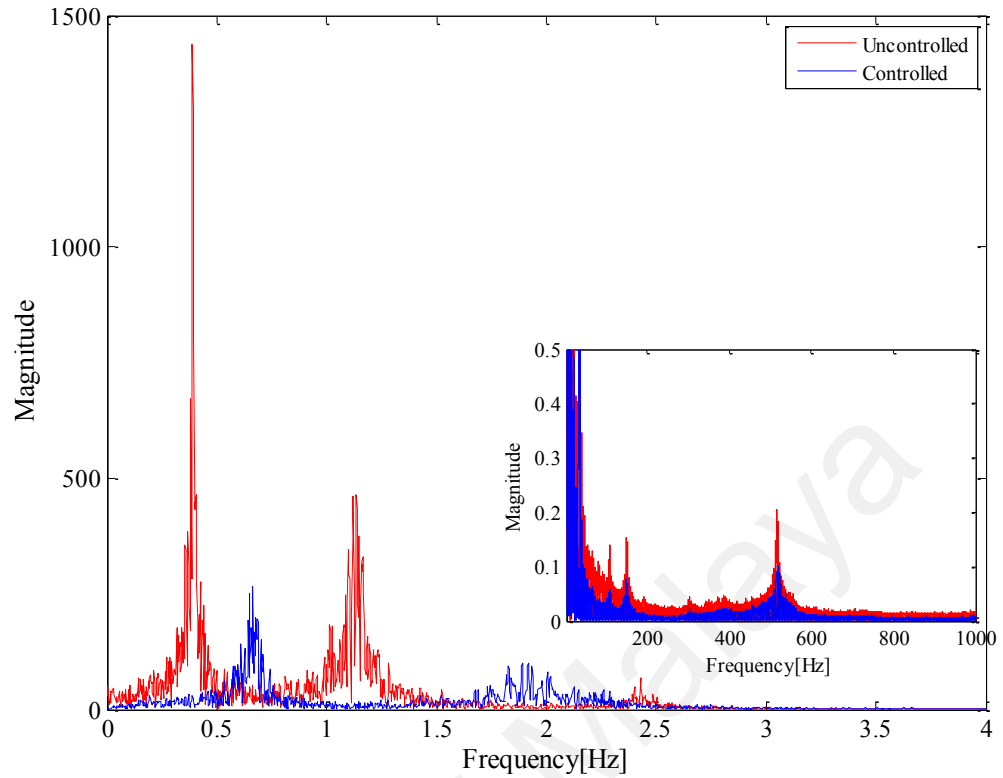
(b) Current



(c) Desired and Actual control Force



(d) Time response at 20th element



(e) Frequency response

Figure 4.21: Semi-active vibration control response of wind turbine tower under random excitation

Results show that proposed semi-active control strategy can deal with high amplitudes of random disturbances and reduces the vibration significantly. The PID-ACO control parameters are used same as for harmonic excitation to observe whether the same control system can handle different types of loading conditions. For random excitations, the vibration reduction rate at top of the wind turbine tower is 68% compared to uncontrolled system. The significance of the proposed smart semi-active control strategy for wind turbine vibration control under sinusoidal and random excitations are shown in Table 4.7. It is seen that proposed ACO optimized controller can reduce vibration on top of the wind turbine tower significantly.

Table 4.7: Comparison between uncontrolled and controlled system

Types of forces	RMS value		Reduction of amplitude, %
	Uncontrolled System	Controlled System	
Sinusoidal force	0.7523	0.1280	83%
Random force	0.0065	0.0021	68%

4.3 Experimental validation

Simulation results are validated with experimental results to verify the effectiveness of the proposed semi-active control system for wind turbine vibration reduction. The simulation results for both the wind turbine model and MR damper model are validated using the constructed experimental test rig. The simulation results using ACO optimized PID control force and current controller are verified with implementation of same input disturbances to the wind turbine tower.

4.3.1 Model validation

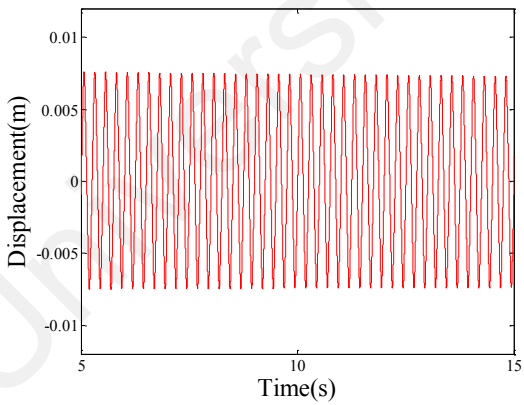
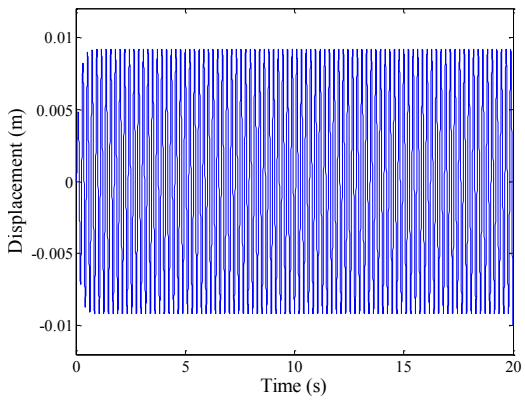
This section presents the model validation of the wind turbine tower and the MR damper. The model parameters are modified based on the specifications of the test rig. The modified models are used for simulation results and verification purpose in the following result section.

4.3.1.1 Validation of wind turbine tower model

The lab-scaled wind turbine tower including the wind turbine is 1.84 meter. The mass of the wind turbine is 2.3kg. In this section, the no of elements is increased to 23 because of the extended length of the wind turbine tower. In simulation study, the tower is represented with Euler-Bernoulli beam and the corresponding mass and stiffness matrices are computed using FDM. These matrices are used to find the natural frequencies, mode shapes and tower response under an external disturbance. On the other hand, in

experimental study, EMA is conducted to achieve the natural frequencies and mode shapes. Tower response is measured through the accelerometer for the excitation force provided by the shaker. It is found that the tower response in simulation study is higher than the experimental study. After investigation, it is understood that when the shaker is attached to tower with a stinger, the energy dissipation rate increases, and the stinger also restrict the tower to move horizontally. For this reason, the damping ratio is increased to the system and therefore the model damping ration is adjusted accordingly. The new damping ratio is used as 0.23 in the study. The simulation results are compared with experimental results for validation based on natural frequencies, mode shapes and uncontrolled response at 1st mode. The comparison is shown in Table 4.8.

Table 4.8: Comparison between experimental and simulation models

Experimental Results	Simulation Results
1 st Natural frequency: 4Hz 2 nd Natural frequency: 30Hz	1 st Natural frequency: 4.7Hz 2 nd Natural frequency: 39.8Hz
<p>Uncontrolled Response @ 20N, 4Hz</p> 	<p>Uncontrolled Response @ 20N, 4.7Hz</p> 

Results show that the first natural frequencies of experimental and simulation model are 4Hz and 4.7Hz, respectively, whereas, the respective second natural frequencies are 30Hz and 39.8Hz. The uncontrolled responses for experimental and simulation models are measured under sinusoidal excitation at 1st mode. It is seen that the uncontrolled

responses for both models are close which are 0.007m and 0.009m for experiment and simulation respectively.

4.3.1.2 Validation of MR damper model

The simulation model is validated using the experimental characteristic results of MR damper. UTM machine is used in this study to test the MR damper to analyze its nonlinear performance characteristics. MR damper is excited under different stroke lengths and velocities. The damping force increases when the stroke length and velocity increase (Refer to Appendix B). For simulation model validation, the experimental force response under stroke length of 20mm peak to peak, velocity of 200 mm/min for different current inputs, (i.e. 0 A, 0.25 A, 0.6 A, and 0.825A) are compared with simulated response under same input parameters as experiment. Figure 4.22 shows the experimental and simulation results which is indicating the relationships between force and displacement and Figure 4.23 shows the force response in the time domain for different current inputs.

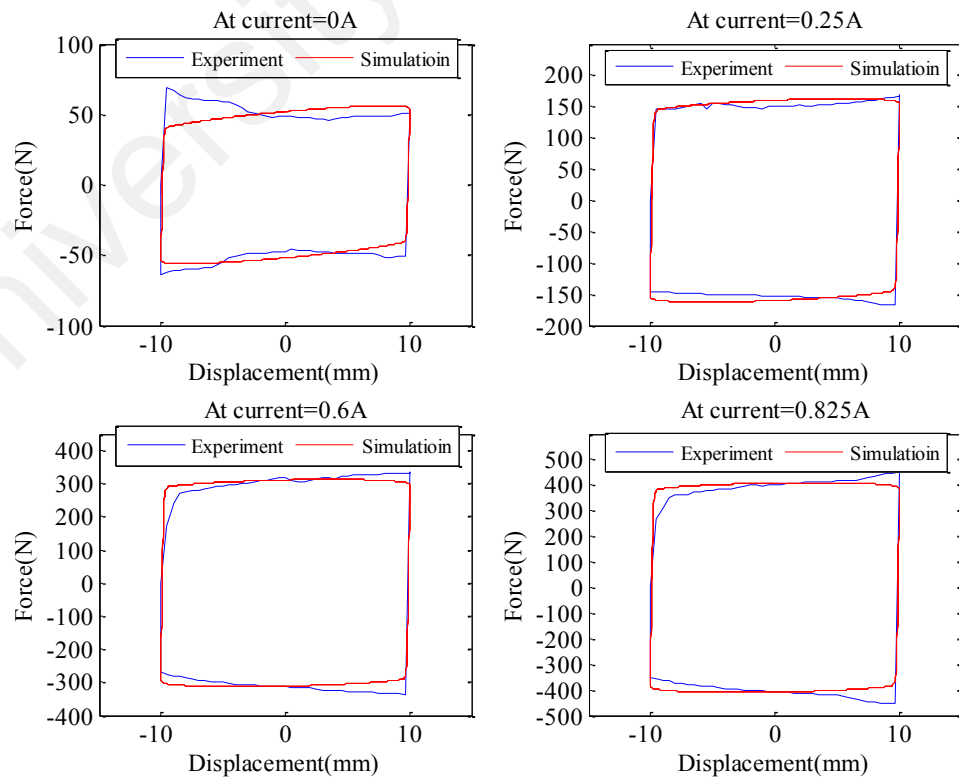


Figure 4.22: Experimental and Simulation result: force vs displacement under different current inputs

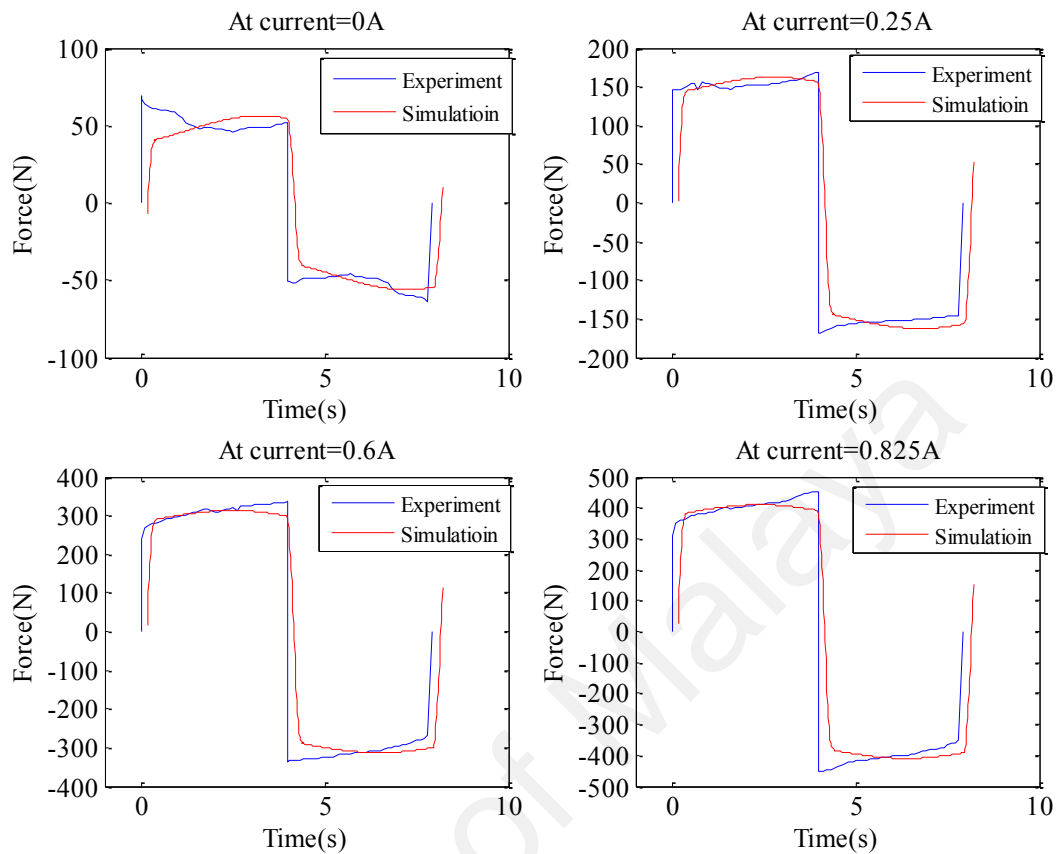


Figure 4.23: Experimental and Simulation result: force vs time under different current inputs

Figure 4.22 shows that the hysteresis loop width of force-displacement curve increases when current input increases. This means the force increase very sharply for increasing of currents. The damping force is much higher, (i.e. approx. 450 N) at 0.825 A current than the damping force at 0 A current input, (i.e. approx. 70 N). It is observed that the simulation result correlates well with experimental results under different current inputs. There are slight discrepancies appear in the data at maximum displacement. This is possibly due to the noisy input parameters during experimental tests. This problem does not occur during simulation; therefore, the curves are perfect. Figure 4.23 shows the force-time relationships where it is observed that force increases with respect to time for increment current. For a time, change from 0 to 4 seconds, force increases sharply from 0 N to 300 N for current input of 0.6 A. These experimental characteristics are also found

in simulation result. Both experimental and simulation results show that the nonlinear dynamic characteristics of the damping force responses are smooth at the full cycle and this result illustrates that smart fluid damper, (i.e. MR damper) provides the advantage of good stability, good controllability, and high damping force for low current input.

Energy dissipation is also an important criterion of MR damper to analyze its dynamic performance in a full cycle. The amount of energy dissipation, W_d , of MR damper per cycle can be computed using the following equation.

$$W_d = \int F_{mr} dx = \int_0^{2\pi/\omega_d} C_{eq} \dot{x} dt \quad (4.2)$$

where F_{mr} is damping force, ω_d is excitation frequency, x and \dot{x} indicates the stroke length and displacement of the damper respectively, and C_{eq} is damping coefficient. The amount of energy dissipation is compared for experimental and simulation data. The energy dissipation can be calculated from the force-displacement curve in Figure 4.22. The energy dissipation is computed by calculating the area under the force-displacement curve for different current inputs. The energy dissipation curve for different current inputs under 20 mm stroke length is shown in Figure 4.24 .

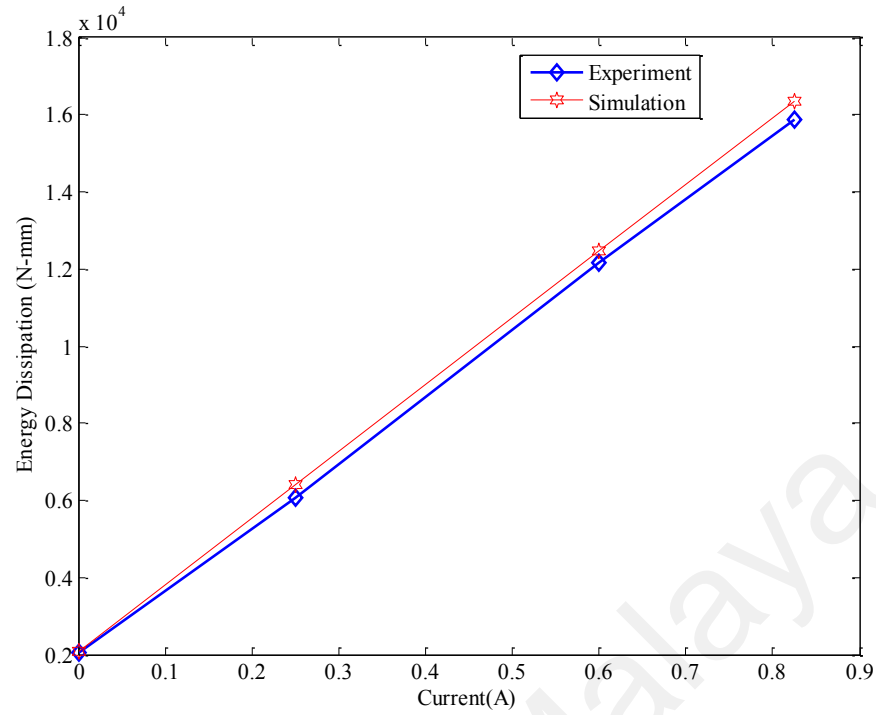
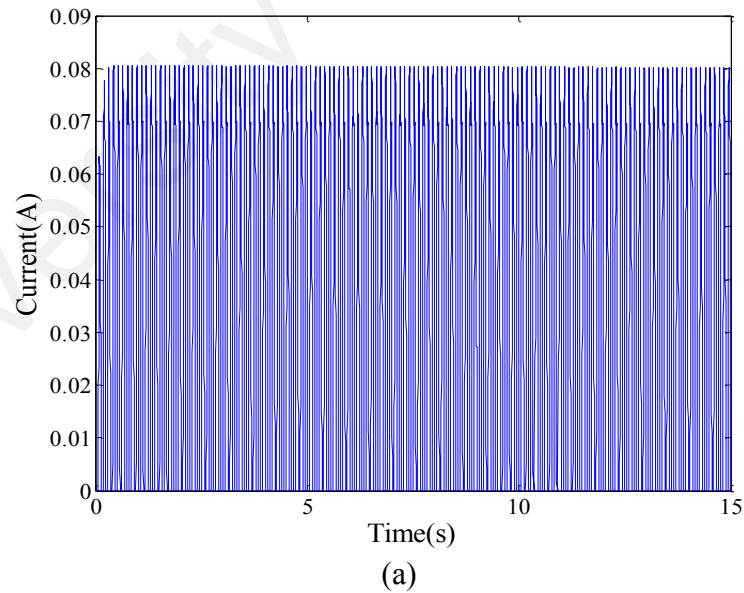


Figure 4.24: Energy dissipation of MR damper for different current inputs

It is observed that the amount of energy dissipation with the increase of current inputs. The maximum energy dissipation is obtained at 0.825 A. The energy dissipation rate becomes high mainly due to large hysteresis loop. At high current input, hysteresis loop increases, thus the energy dissipation capacity increases. The vibration reduction rate of a structure using MR damper is mainly inclined to energy dissipation capacity. The amount of energy dissipation is slightly higher for simulation model than the experimental result when current increases. This small difference may occur due to the physical conditions of the MR damper in experimental test where in simulation, the damper is assumed as perfect conditions. Therefore, the simulation model can correlate the experimental result as described above and this model is used in the simulation study for wind turbine tower vibration control.

4.3.2 Simulation results for wind turbine vibration control using PID-ACO control with MR damper under different loadings

Wind turbine model is simulated with PID-ACO controller to find the desired control force and PI controller to find suitable current for MR damper. The excitation force is selected as sine excitation at first natural frequencies, (i.e. 4.7 Hz when damper is not attached and 9.02Hz when damper is attached) to solve the problem of resonance where maximum vibration amplitudes may occur. The excitation force is fed to the tower at the top of the tower, (i.e. 20th element). MR damper is placed the mid-point of the tower, (i.e. 10th elements). The MR damper is simulated with modified Bouc-Wen model. The controlled response is computed with optimal desired force and current input of MR damper. The current input, desired force and actual force are shown in Figure 4.25. The controlled response is compared with passive, (i.e. no current supply), and locked, (i.e. high input current of 0.7A) state as stated previously and presented in Figure 4.26.



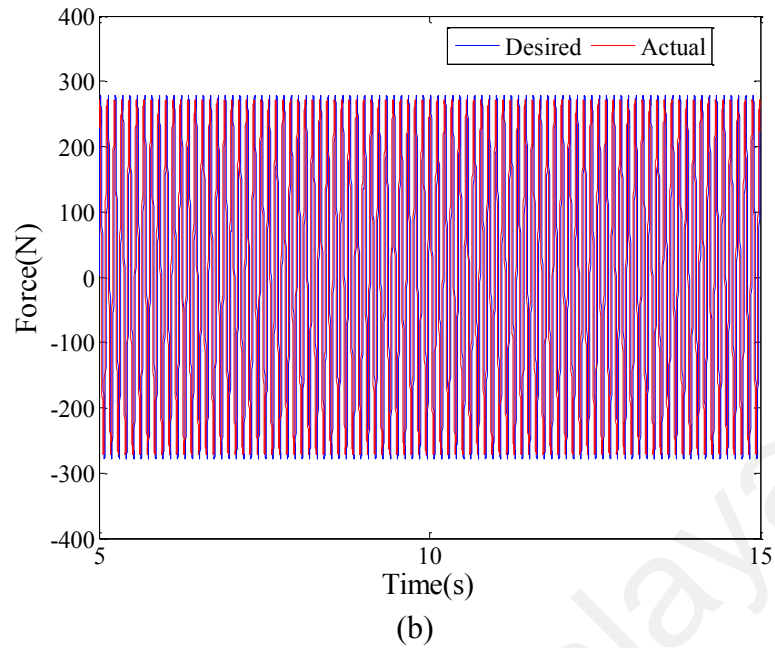


Figure 4.25: (a) Current; (b) Desired vs Actual force of MR damper

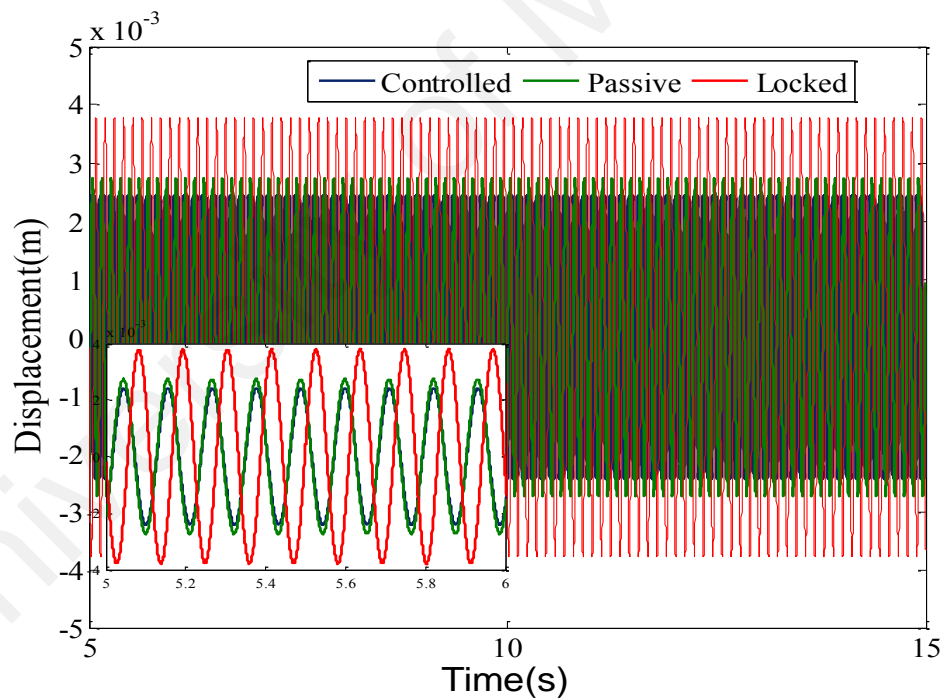


Figure 4.26: Simulation result: Tower response at 20th elements under sinusoidal force @1st mode at Controlled, passive, and locked state

The current input is found as 0.08A (Fig. 5(a)) by the PI controller and used to achieve the desired force from the MR damper (Fig. 5(b)). Result shows that controlled response provides low vibration amplitudes, (i.e. 0.0024 m) compared to passive, (i.e. 0.0028 m), locked, (i.e. 0.003785 m) and uncontrolled, (i.e. 0.009 m) state. The

controlled system reduces the tower peak displacement by 15%, 36%, and 73% compared to the passive, locked, and uncontrolled system. The tower model is also simulated under chirp excitation force where frequency varies over time. This is to verify that the proposed semi-active controller, (i.e. PID-ACO and PI) can control the vibration when frequency varies. The excitation frequency range is 1-10 Hz. The response is shown in Figure 4.27. The model also simulated under random signals, represented for wind loadings on the tower. Gaussian noise signal is used from the 'signal generator' function of Simulink to generate the random signal where the amplitude range is 18 N to 25 N. The tower responses are compared using the root mean square (RMS). The response is shown in Figure 4.28.

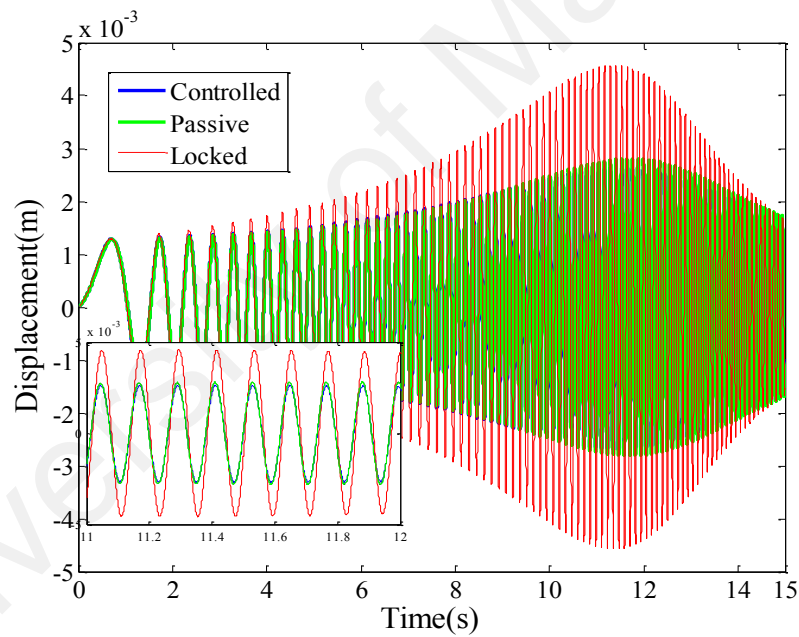


Figure 4.27: Simulation result: Tower response at 20th elements under chirp force (1-10Hz) at Controlled, passive, and locked state

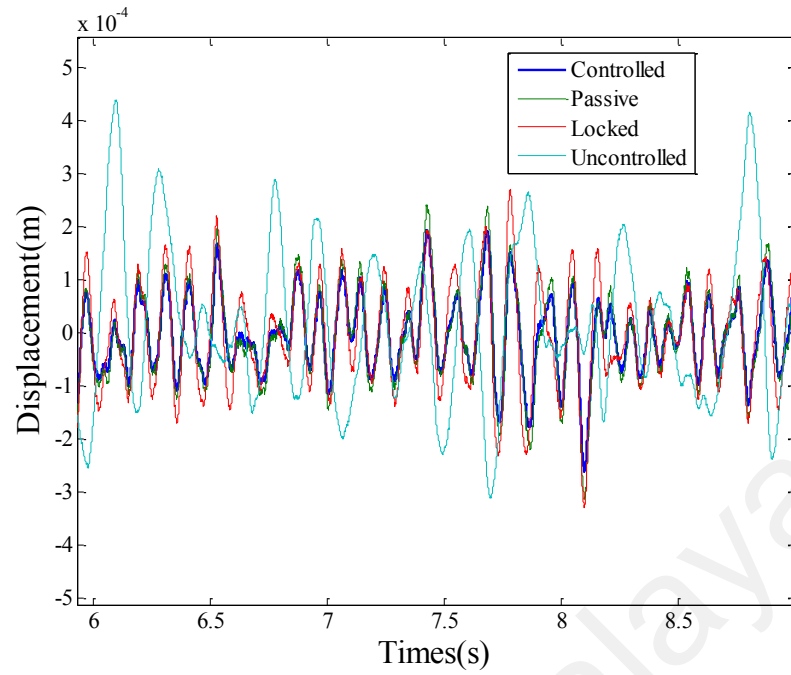


Figure 4.28: Simulation result: Tower response at 20th elements under random force at Controlled, passive, locked, and uncontrolled state

Result shows that the controlled response is lower than the response under passive state and locked state (Figure 4.27) when frequency varies especially at the frequencies closed to the natural frequency. PID controller is known limitation adapt in a system when frequency varies but the proposed PID-ACO controller can adapt this type of system. Under random excitation force, it is found that using the proposed controller, the RMS displacement is lower, (i.e. $7.3\text{e-}05$ m) compared to passive, (i.e. $8.81\text{e-}05$ m), locked, (i.e. $9.66\text{e-}05$ m), and uncontrolled, (i.e. $12.33\text{e-}05$ m). Therefore, the tower RMS displacement at the top is reduced by 17%, 25%, and 40% compared to the passive, locked, and uncontrolled system. Although the vibration amplitudes are low for random signals due to no involvement of frequency issues, the PID-ACO controlled force provides better response compared to other damping environments.

4.3.3 Experimental results for wind turbine vibration control using PID-ACO control with MR damper under different loadings

The simulation results and analyses are considered as a basis of the experimental validation studies of a lab-scaled wind turbine tower model. The model is validated in the previous section. The experimental set-up is presented in Figure 3.17. The excitation force to the tower is provided by shaker horizontally. Accelerometer and force sensors are used to measure the vibration and force amplitudes respectively. The EMA is conducted again to find new natural frequency after the MR damper is attached to the mid-point of the tower. It is found that the first natural frequency of the experimental model is 9Hz (in simulation study, the respective frequency is 9.02 Hz). Like the simulation studies, the tower responses are measured under different excitation forces such sinusoidal @1st mode, 20 N, chirp signal (1-10Hz, 20N), and random forces with amplitude range from 18 N to 25 N. The current is fed to the MR damper as suggested by the simulation study. The controlled tower responses along with passive and locked states under different excitation forces are presented in Figure 4.29-Figure 4.31.

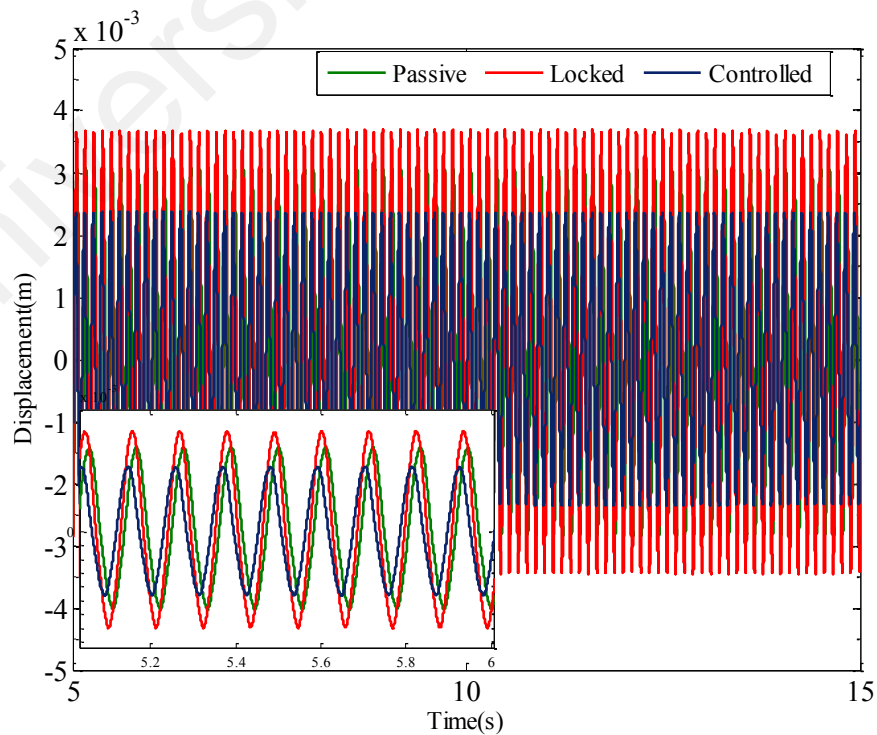


Figure 4.29: Experimental result: Tower response at 20th elements under sinusoidal force @1st mode at Controlled, passive, and locked state

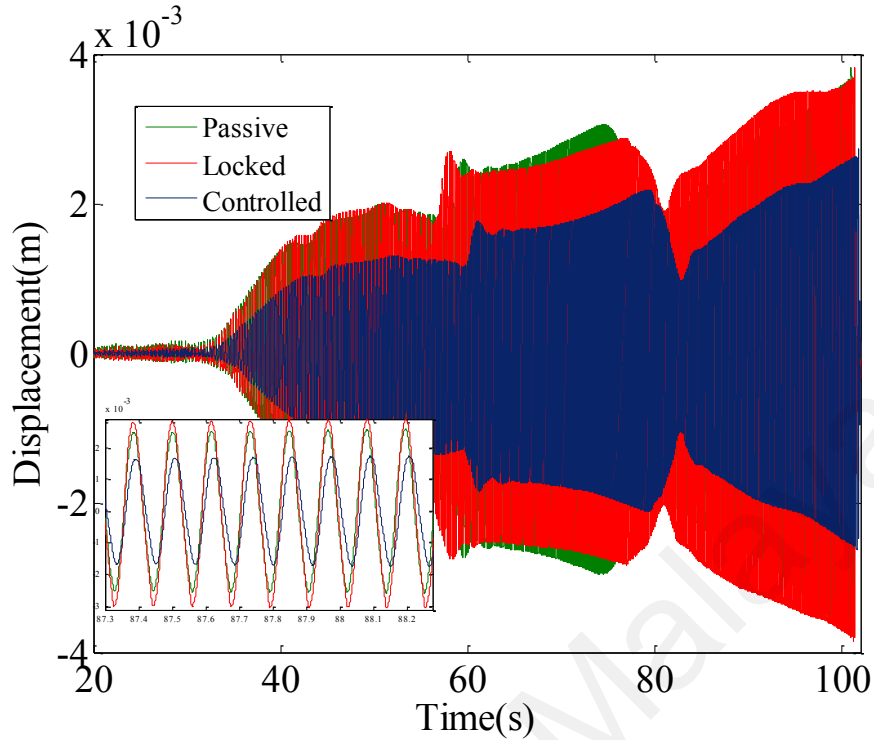


Figure 4.30: Experimental result: Tower response at 20th elements under chirp force (1-10Hz) at Controlled, passive, and locked state

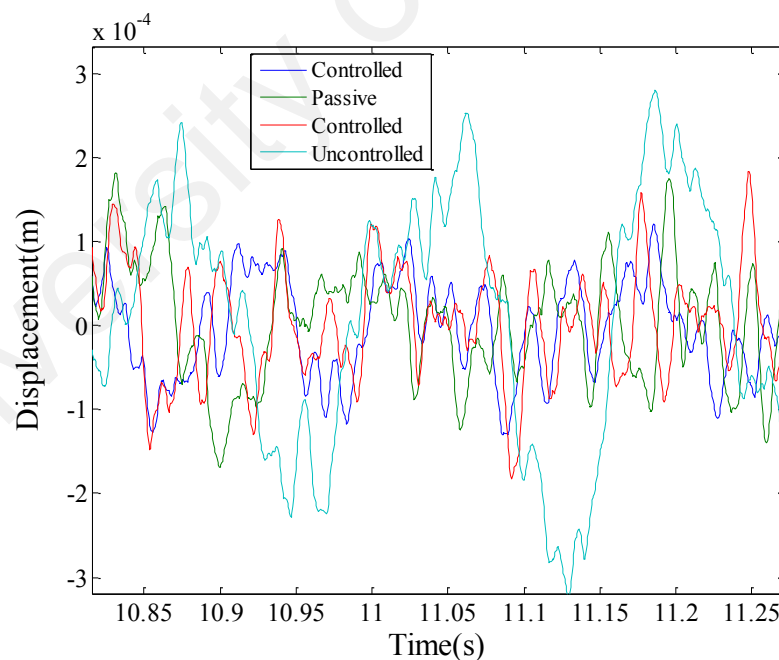


Figure 4.31: Experimental result: Tower response at 20th elements under random force at Controlled, passive, locked, and uncontrolled state

Results show that under sinusoidal force, the controlled peak displacement of the tower (Figure 4.29) is reduced by 18%, 36% and 66% compared to the passive, locked and uncontrolled system. For chirp excitation force, the experimental result shows similar

result as simulation result where the proposed controllers control the tower displacement significantly compared to the passive and locked state (Figure 4.30), the zoomed view is the response near the natural frequency. When the frequency is near or above the natural frequency, the vibration amplitudes are observed high as well. The PID-ACO controlled force can adapt quickly and control the vibration which is unlikely for PID controller tuning with conventional methods. Under the random excitation force, the proposed PID-ACO controlled RMS displacement of the tower (Figure 4.31) is low, (i.e. $6.41\text{e-}05$ m) compared to passive, (i.e. $7.88\text{e-}05$ m), locked, (i.e. $8.41\text{e-}05$ m), and uncontrolled, (i.e. $10.07\text{e-}05$ m). Therefore, the experimental result shows that the tower RMS displacement at the top is reduced by 19%, 24%, and 36% compared to the passive, locked, and uncontrolled system. The displacements of the experimental study are slightly lower than the simulation result which is possibly due to stinger misalignment from the tower. It may happen if the shaker is displaced from the actual place due to vibration of the shaker base.

4.3.4 Comparison between simulation and experimental result

This section presents a comparison between the simulation result and the experimental result for the validation purpose. The tower peak displacements under sinusoidal force and RMS displacement values under random excitation forces for both simulation and experimental studies at different states of damper attachment are tabulated in Table 4.9. The reduction rates are compared between the controlled response (damper attached, optimal force and current) and other three damping environments such as passive (damper attached, no current), locked (damper attached, high input current), and uncontrolled (no damper attached).

Table 4.9: Comparison between simulation and experimental result

Sinusoidal Excitation mode @1 st	Simulation Results		Experimental Results	
Damper environment	Peak Displacement (m)	Reduction rate	Peak Displacement (m)	Reduction rate
Controlled damper(C)	0.0024		0.00235	
Uncontrolled(U)	0.009	U → C 73%	0.007	U → C 66%
Passive damper(P)	0.0028	P → C 15%	0.0029	P → C 18%
Locked state(L)	0.003785	L → C 36%	0.0037	L → C 36%
Random Excitation	Simulation Results		Experimental Results	
Damper environment	RMS Displacement (m)	Reduction rate	RMS Displacement (m)	Reduction rate
Controlled damper(C)	7.30e-05		6.41e-05	
Uncontrolled(U)	12.33e-05	U → C 40%	10.07e-05	U → C 36%
Passive damper(P)	8.81e-05	P → C 17%	7.88e-05	P → C 19%
Locked state(L)	9.66e-05	L → C 25%	8.41e-05	L → C 24%

It is seen that the reduction rates for the simulation and the experimental studies are close. For example, the displacement difference between the simulation and experimental result for controlled damper response is only 2%. This rate for passive damper response is 3%. The reduction rates under sinusoidal excitation at 1st mode is high for both simulation, (i.e. maximum of 73% reduction from uncontrolled to controlled system) and experimental study, (i.e. maximum of 66% reduction from uncontrolled to controlled system) which is very important to counter vibration at natural frequencies where very high vibration occur due to resonance issue. This reduction rates are 68% and 58% for simulation and experimental study respectively, when passive damper response is compared with uncontrolled system. Therefore, the impact of the controlled MR damper is significant. However, since frequency issue is not involved in random signals, the vibration amplitude is low, however, the proposed method still can counter external random forces on the tower due to heavy wind forces. The PID-ACO controlled MR damper provides maximum reduction rate under random excitation force compared to

uncontrolled system, (i.e. 40% for simulation and 36% for experiment). For all the cases, it is seen that uncontrolled system, where no damper is attached, provides high vibration amplitudes. High vibration amplitude is also observed for locked state because of high input current which gives high force to the tower. The passive MR damper with zero current provides satisfactory amplitude, however, optimal controlled force with low input current provides maximum vibration reduction and can provide better results for different types of loading and at a wider operating frequency range which is very suitable for vibration control of variable speeds system like wind turbine.

CHAPTER 5: CONCLUSION AND RECOMMENDATION

5.1 Conclusions

This research investigated a semi-active PID-ACO controller for wind turbine vibration control with optimally placed MR damper to reduce vibration under different types of loading conditions and different frequency and amplitudes. To investigate **objective 1**, the complex partial differential equations of wind turbine tower are solved with FDM and the suitable dynamic transfer function is estimated using system identification process. The FDM estimated transfer function shows 100% of fit to estimation data, MSE of 1.13E-07 and CSAC of 0.999997 which is better than FEM estimated transfer function. **For objective 2**, The semi-active ACO-PID control strategy is implemented in this study for vibration control of wind turbine tower. The PID control parameters are tuned by using ACO method and the parameters of ACO are set to adapt wind turbine tower vibration problems. Comparisons among conventional Z-N, PSO and proposed ACO methods show that ACO method is better for this system in terms of vibration reduction rate, ability to adapt when frequency varies and computational time. To investigate **objective 3**, MR damper is used to obtain optimally controlled output force to counter vibration on the tower. The optimal placement of MR damper is found at the mid-span position, which is at 10th element, after comparing the response of the tower when MR damper at the 5th and 15th elements based on design complexity, vibration reduction rate and maintenance cost. Two feedback control strategy is employed as a system controller and current regulator using ACO optimized PID controller and PI controller. Different range of amplitudes and frequencies of input disturbances are also investigated to show that the proposed control method with optimal position of MR damper can deal with several conditions of disturbances. Result shows that proposed PID-ACO control method can significantly reduce the wind turbine tower vibration under

different frequencies, (i.e. 67%, 83%, 34.4% and 34.4% at 2Hz, 4.68Hz and 6Hz respectively) and different amplitudes, (i.e. 84%, 85.7%, and 83% for 50N, 80N, and 100N respectively). The result also shows that proposed semi-active vibration control method can significantly reduce the wind turbine tower vibration under sinusoidal (83%) and random (68%) disturbances using the same PID-ACO control parameters and low current input provided by PI controller. To fulfil the **objective 4**, the simulation study is validated using experimental tests. A lab-scaled wind turbine tower is build and the simulation parameter for wind turbine tower is modified based on the lab-scale model. The simulation model is validated with an experimental model based on natural frequencies, mode shapes, and tower response under 1st mode. Three different types of loadings, (i.e. sinusoidal, chirp, and random force), two different controllers to achieve a desired force, (i.e. PID-ACO controller) and current inputs, (i.e. PI controller) for MR damper are used for simulation and experimental study. The PID controller parameters are optimized using ACO algorithm where appropriate inputs were used to adapt the wind turbine tower vibration problems. Four different types of damping states, such as ‘uncontrolled’ with no damper, ‘passive’ with damper but without current supply, ‘locked’ with damper and high input current, and ‘controlled’ with controlled damper, are used to validate the controllers’ effectiveness. The controlled MR damper provides a significant result with better vibration reduction rate compared to other three damping environments based on the vibration reduction rates. The result shows that proposed semi-active vibration control method PID-ACO controller using MR damper provides maximum vibration reduction rate and reduces the vibration even when the excitation frequency varies. It is also seen that low current input, (i.e. only 0.08A) is required to reduce 73%, (i.e. for simulation), of tower top displacement. This reduction rate is higher than the passive damping system where no current is supplied. It is seen that the proposed semi-active vibration control system with MR damper, which is installed at the mid-point

rather than at the top or at the base, can provide better stability on top of the tower with low current input. Moreover, the proposed semi-active PID-ACO controlled MR damper force can reduce vibration for different possible internal/external loadings. The result shows that controlled system reduces the tower top displacements up to 73% and 40% under sinusoidal at 1st mode and random forces respectively. The simulation result is validated with an experimental result where result shows close values of displacements under different types of excitation and damping environments. Therefore, this study adds very significant values to wind turbine technology to ensure enhancement in power production.

5.2 Recommendations

Based on the results described above, the proposed study is found very effective in for wind turbine tower in terms vibration control under different loading conditions and damping environments. However, there are some limitations as well which are recommended for future work. To optimize the PID control parameters, a search range is required to set for ACO method. In this study these ranges are set based on the result on the classical method, (i.e. Z-N method). In future, some equations can be developed to find an optimal range. Also, hybrid optimization methods among ACO, PSO and/or generic algorithm can be developed to achieve better control parameters of PID controller.

The future work recommendation also includes the implementation of the proposed semi-active control on a full-scale wind turbine tower and cost-effective design of the semi-active controlled wind turbine structure. Multiple damper can also be investigated instead of single damper to improve the vibration control rate of wind turbine tower.

REFERENCES

- Adhikari, S., & Bhattacharya, S. (2012). Dynamic analysis of wind turbine towers on flexible foundations. *Shock and Vibration*, 19(1), 37-56.
- Ahmadian, M., Appleton, R., & Norris, J. (1999). Design and development of magneto-rheological dampers for bicycle suspensions. *American Society of Mechanical Engineers, Dynamic Systems & Control Division Publication, DSC*, 67, 737-741.
- Ahmadian, M., & Poynor, J. C. (2001). An evaluation of magneto rheological dampers for controlling gun recoil dynamics. *Shock and Vibration*, 8(3-4), 147-155.
- Ahmed, N. A., & Cameron, M. (2014). The challenges and possible solutions of horizontal axis wind turbines as a clean energy solution for the future. *Renewable and Sustainable Energy Reviews*, 38, 439-460.
- Argyriadis, K., & Hille, N. (2004). Determination of Fatigue Loading on a Wind Turbine with Oil Damping Device. *Proceedings of the 2004 EUROPEAN Wind Energy Conference & Exhibition*. London.
- Arrigan, J., & Basu, B. (2007). Vibration control of wind turbine blades using tuned liquid dampers. *B.H.V. Topping, (Editor), "Proceedings of the Eleventh International Conference on Civil, Structural and Environmental Engineering Computing"*. Stirlingshire, UK: Civil-Comp Press.
- Arrigan, J., & Pakrashi, V. (2011). Control of flapwise vibrations in wind turbine blades using semi- active tuned mass dampers. *Structural Control and Health Monitoring*, 18, 840-851.
- Asareh, M. A., Schonberg, W., & Volz, J. (2016). Fragility analysis of a 5-MW NREL wind turbine considering aero-elastic and seismic interaction using finite element method. *Finite Elements in Analysis and Design*, 120, 57-67.
- Askari, M., Li, J. C., & Samali, B. (2017). Cost-effective multi-objective optimal positioning of magnetorheological dampers and active actuators in large nonlinear structures. *Journal of Intelligent Material Systems and Structures*, 28(2), 230-253.
- Aslam Bhutta, M. M., Hayat, N., Farooq, A. U., Ali, Z., Jamil, S. R., & Hussain, Z. (2012). Vertical axis wind turbine – A review of various configurations and design techniques. *Renewable and Sustainable Energy Reviews*, 16, 1926-1939.

- Atabay, E., & Ozkol, I. (2013). Application of a magnetorheological damper modeled using the current-dependent Bouc–Wen model for shimmy suppression in a torsional nose landing gear with and without freeplay. *Journal of Vibration and Control*, 1077546312468925.
- Avila, S., Morais, M. d., & Barcelos, M. (2009). Vibration control of the set tower and wind turbine under the wind influence. *20th International Congress of Mechanical Engineering*. Gramado.
- Bai, C. J., Hsiao, F. B., Li, M. H., Huang, G. Y., & Chen, Y. J. (2013). Design of 10 kW Horizontal-Axis Wind Turbine (HAWT) Blade and Aerodynamic Investigation Using Numerical Simulation. *7th Asian-Pacific Conference on Aerospace Technology and Science, Apcats 2013*, 67, 279-287.
- Bekele, G., & Tadesse, G. (2012). Feasibility study of small Hydro/PV/Wind hybrid system for off-grid rural electrification in Ethiopia. *Applied Energy*, 97, 5-15.
- Bellekom, S., Benders, R., Pelgröm, S., & Moll, H. (2012). Electric cars and wind energy: Two problems, one solution? A study to combine wind energy and electric cars in 2020 in The Netherlands. *Energy*, 45, 859-866.
- Billie Jr, F., Yang, C., Carlson, J., & Sain, M. (1998). *Smart" dampers for seismic protection of structures: a full-scale study*. Paper presented at the Proceedings of the Second World Conference on Structural Control, Jun.-Jul.
- Bisbee III, C. R., Elliott, S. B., & Oddson, M. (2013). Control system and method for a prosthetic knee: Google Patents.
- Bitaraf, M., Hurlebaus, S., & Barroso, L. R. (2012). Active and Semi- active Adaptive Control for Undamaged and Damaged Building Structures Under Seismic Load. *Computer- Aided Civil and Infrastructure Engineering*, 27(1), 48-64.
- Bofares, A. M., & Elmnefi, M. S. (2014). Design and Performance of Horizontal Axis Wind Turbine Using Blade Element Momentum Theory (BEMT). *Power and Energy Systems*, 492, 106-112.
- Borg, M., Shires, A., & Collu, M. (2014). Offshore floating vertical axis wind turbines, dynamics modelling state of the art. part I: Aerodynamics. *Renewable and Sustainable Energy Reviews*, 39, 1214-1225.

- Bossanyi, E. a., Ramtharan, G., & Savini, B. (2009). The importance of control in wind turbine design and loading. *2009 17th Mediterranean Conference on Control and Automation: Ieee.*
- Braz-Cesar, M. T., & Barros, R. C. (2018). Semi-active fuzzy based control system for vibration reduction of a SDOF structure under seismic excitation. *Smart Structures and Systems*, 21(4), 389-395.
- Brodersen, M. L., Bjorke, A. S., & Hogsberg, J. (2017). Active tuned mass damper for damping of offshore wind turbine vibrations. *Wind Energy*, 20(5), 783-796.
- Buckle, I. (2000). Passive control of structures for seismic loads. *Bulletin of the New Zealand Society for Earthquake*, 1-13.
- Calderaro, V., Galdi, V., Piccolo, A., & Siano, P. (2007). Design and implementation of a fuzzy controller for wind generators performance optimisation Keywords. *Proceeding of European Conference on Power Electronics and Applications.*
- Caterino, N., Georgakis, C. T., Occhiuzzi, A., & Spizzuoco, M. (2016). Real-time monitoring and structural control of a wind turbine using a rocking system. *2016 Ieee Workshop on Environmental, Energy, and Structural Monitoring Systems (Eesms).*
- Cha, Y.-J., Zhang, J., Agrawal, A. K., Dong, B., Friedman, A., Dyke, S. J., & Ricles, J. (2013). Comparative studies of semiactive control strategies for MR dampers: pure simulation and real-time hybrid tests. *Journal of Structural Engineering*, 139(7), 1237-1248.
- Chang, C. C., Hsu, C. T., & Swei, S. M. (1998). Control of buildings using single and multiple tuned liquid column dampers. *Structural Engineering and Mechanics*, 6, 77-93.
- Chen, J. L., & Georgakis, C. T. (2013). Spherical tuned liquid damper for vibration control in wind turbines. *Journal of Vibration and Control.*
- Chen, J. L., & Georgakis, C. T. (2013). Tuned rolling-ball dampers for vibration control in wind turbines. *Journal of Sound and Vibration*, 332, 5271-5282.
- Chen, X. B., Li, J., & Chen, J. Y. (2009). Wind-induced response analysis of a wind turbine tower including the blade-tower coupling effect. *Journal of Zhejiang University-Science A*, 10(11), 1573-1580.

- Choi, S.-B., Lee, S.-K., & Park, Y.-P. (2001). A hysteresis model for the field-dependent damping force of a magnetorheological damper. *Journal of Sound and Vibration*, 245(2), 375-383.
- Choi, Y.-T., & Wereley, N. M. (2005). Nondimensional quasisteady analysis of a magnetorheological dashpot damper. *International Journal of Modern Physics B*, 19(07n09), 1584-1590.
- Chong, W. T., Fazlizan, A., Poh, S. C., Pan, K. C., Hew, W. P., & Hsiao, F. B. (2013). The design, simulation and testing of an urban vertical axis wind turbine with the omni-direction-guide-vane. *Applied Energy*, 112, 601-609.
- Chooi, W. W., & Oyadiji, S. O. (2008). Design, modelling and testing of magnetorheological (MR) dampers using analytical flow solutions. *Computers & Structures*, 86(3), 473-482.
- Chooi, W. W., & Oyadiji, S. O. (2009a). Experimental testing and validation of a magnetorheological (MR) damper model. *Journal of Vibration and Acoustics*, 131(6), 061003.
- Chooi, W. W., & Oyadiji, S. O. (2009b). Mathematical modeling, analysis, and design of magnetorheological (MR) dampers. *Journal of Vibration and Acoustics*, 131(6), 061002.
- Chu, S. Y., Soong, T. T., & Reinhorn, A. M. (2005). Active, Hybrid, and Semi-active Structural Control: A Design and Implementation Handbook.
- Collins, R., Basu, B., & Broderick, B. M. (2005). Optimal Design of Multi-Tuned Mass Damper (MTMDS) for Wind Turbine Towers Using SSA. *Proceedings of the SECED Young Engineers Conference*. Bath.
- Colwell, S., & Basu, B. (2009). Tuned liquid column dampers in offshore wind turbines for structural control. *Engineering structures*, 31, 358-368.
- Constantinou, M., Soong, T., & Dargush, G. (1998). Passive energy dissipation systems for structural design and retrofit.
- Contreras-Lopez, J., Ornelas-Tellez, F., Espinosa-Juarez, E., & Concha-Sanchez, Y. (2016). Nonlinear Optimal Control for Reducing Vibrations in Civil Structures Using Magnetorheological Dampers. *2016 Ieee International Autumn Meeting on Power, Electronics and Computing (Ropec)*.

Den Hartog, J. P. (1947). Mechanical Vibrations.

Dimock, G. A., Yoo, J.-H., & Wereley, N. M. (2002). Quasi-steady Bingham biplastic analysis of electrorheological and magnetorheological dampers. *Journal of Intelligent Material Systems and Structures*, 13(9), 549-559.

Dinh, V. N., & Basu, B. (2014). Passive control of floating offshore wind turbine nacelle and spar vibrations by multiple tuned mass dampers. *Structural Control and Health Monitoring*.

Du, H., Lam, J., Cheung, K., Li, W., & Zhang, N. (2013). Direct voltage control of magnetorheological damper for vehicle suspensions. *Smart Materials and Structures*, 22(10), 105016.

Du, H., Li, W., & Zhang, N. (2011). Semi-active variable stiffness vibration control of vehicle seat suspension using an MR elastomer isolator. *Smart Materials and Structures*, 20(10), 105003.

Dubay, R., Hassan, M., Li, C., & Charest, M. (2014). Finite element based model predictive control for active vibration suppression of a one-link flexible manipulator. *Isa Transactions*, 53, 1609-1619.

Dyke, S. J., Spencer, B. F., Sain, M. K., & Carlson, J. D. (1996). Modeling and control of magnetorheological dampers for seismic response reduction. *Smart Materials & Structures*, 5(5), 565-575.

Dyke, S. J., Spencer, B. F., Sain, M. K., & Carlson, J. D. (1998). An experimental study of MR dampers for seismic protection. *Smart Materials & Structures*, 7(5), 693-703.

Eddanguir, A., Beidouri, Z., & Benamar, R. (2012). Geometrically nonlinear transverse steady-state periodic forced vibration of multi-degree-of-freedom discrete systems with a distributed nonlinearity. *Ain Shams Engineering Journal*, 3(3), 191-207.

Ehrgott, R., & Masri, S. (1992). Modeling the oscillatory dynamic behaviour of electrorheological materials in shear. *Smart Materials and Structures*, 1(4), 275.

- Eide, R., & Karimi, H. (2009). Control design methodologies for vibration mitigation on wind turbine systems. In B.-C. Francisco (Ed.), *Vibration Analysis and Control- New Trends and Developments*, . Croatia: InTech.
- El-Khoury, O., & Adeli, H. (2013). Recent advances on vibration control of structures under dynamic loading. *Archives of Computational Methods in Engineering*, 20(4), 353-360.
- Enevoldsen, I., & Mørk, K. (1996). Effects of a Vibration Mass Damper in a Wind Turbine Tower. *Mechanics of Structures and Machines*, 24, 155-187.
- Eriksson, S., Bernhoff, H., & Leijon, M. (2008). Evaluation of different turbine concepts for wind power. *Renewable & Sustainable Energy Reviews*, 12(5), 1419-1434.
- Eriksson, S., Bernhoff, H., & Leijon, M. (2008). Evaluation of different turbine concepts for wind power. *Renewable and Sustainable Energy Reviews*, 12, 1419-1434.
- Farjoud, A., Vahdati, N., & Fah, Y. F. (2008). MR-fluid yield surface determination in disc-type MR rotary brakes. *Smart Materials and Structures*, 17(3), 035021.
- Ferdaus, M. M., Rashid, M. M., & Bhuiyan, M. (2014). *Development of an Advanced Semi-Active Damper Using Smart Fluid*. Paper presented at the Advanced Materials Research.
- Fischer, G. R., Kipouros, T., & Savill, A. M. (2014). Multi-objective optimisation of horizontal axis wind turbine structure and energy production using aerofoil and blade properties as design variables. *Renewable Energy*, 62, 506-515.
- Fitzgerald, B., & Basu, B. (2013). Active tuned mass damper control of wind turbine nacelle/tower vibrations with damaged foundations. *Damage Assessment of Structures X, Pts 1 and 2*. LAUBLRUTISTR 24, CH-8717 STAFA-ZURICH, SWITZERLAND: TRANS TECH PUBLICATIONS LTD.
- Fitzgerald, B., & Basu, B. (2016). Structural control of wind turbines with soil structure interaction included. *Engineering structures*, 111, 131-151.
- Fitzgerald, B., Basu, B., & Nielsen, S. R. K. (2013). Active tuned mass dampers for control of in-plane vibrations of wind turbine blades. *Structural Control & Health Monitoring*, 20, 1377-1396.

- Fujino, Y., Pacheco, B., Chaiseri, P., & Sun, L. (1988). Parametric studies on tuned liquid damper (TLD) using circular containers by free-oscillation experiments. *Structural Engineering/Earthquake Engineering*, 5, 381-391.
- Gao, H., Kwok, K. S. C., & Samali, B. (1999). Characteristics of multiple tuned liquid column dampers in suppressing structural vibration. *Engineering structures*, 21, 316-331.
- Gavin, H. P., Hanson, R. D., & Filisko, F. E. (1996). Electrorheological dampers, part I: analysis and design. *Journal of Applied Mechanics*, 63(3), 669-675.
- Geldhof, G. (2013). *Semi-active vibration dynamics control of multi-cart systems using a magnetorheological damper*. M. Sc. Thesis, Chalmers University of Technology, Goteborg, Sweden.
- Genov, J., Gilev, B., Slavchev, Y., & Venkov, G. Modeling and control of wind turbine tower vibrations.
- Genov, J., Gilev, B., Slavchev, Y., & Venkov, G. (2010). Modeling and Control of Wind Turbine Tower Vibrations. *Applications of Mathematics in Engineering and Economics*, 1293, 30-+.
- Gerges, R. R., & Vickery, B. J. (2005). Optimum design of pendulum-type tuned mass dampers. *The Structural Design of Tall and Special Buildings*, 14, 353-368.
- Ghaemmaghami, A., Kianoush, R., & Yuan, X. X. (2013). Numerical modeling of dynamic behavior of annular tuned liquid dampers for applications in wind towers. *Computer-Aided Civil and Infrastructure Engineering*, 28, 38-51.
- Gharapurkar, A., Jahromi, A. F., Bhat, R. B., & Xie, W.-F. (2013). *Semi-active control of aircraft landing gear system using H-infinity control approach*. Paper presented at the Connected Vehicles and Expo (ICCVE), 2013 International Conference on.
- Giorgetti, A., Baldanzini, N., Biasiotto, M., & Citti, P. (2010). Design and testing of a MRF rotational damper for vehicle applications. *Smart Materials and Structures*, 19(6), 065006.
- Goundar, J. N., & Ahmed, M. R. (2013). Design of a horizontal axis tidal current turbine. *Applied Energy*, 111, 161-174.

- Gudmundsson, K., Jonsdottir, F., & Thorsteinsson, F. (2010). A geometrical optimization of a magneto-rheological rotary brake in a prosthetic knee. *Smart Materials and Structures*, 19(3), 035023.
- Guo, H. Y., & Zhang, L. (2004). Optimal placement of MR dampers for structural control using identification crossover genetic algorithm. *Journal of Low Frequency Noise Vibration and Active Control*, 23(3), 167-178.
- Gurgoze, M., & Muller, P. C. (1992). Optimal Positioning of Dampers in Multibody Systems. *Journal of Sound and Vibration*, 158(3), 517-530.
- Gwon, T.-g. T. (2011). *Structural Analyses of Wind Turbine Tower for 3 kW Horizontal-Axis Wind Turbine*. (Master of Science), California Polytechnic State University, USA.
- Haroun, M. A., Pires, J. A., & Won, A. Y. J. (1996). Suppression of environmental induced vibrations in tall buildings by hybrid liquid column dampers. *The Structural Design of Tall Buildings*, 5.
- He, E. M., Hu, Y. Q., Zhang, Y., & Yin, G. L. (2014). Vibration and Load Suppression of Offshore Floating Wind Turbine. *Advanced Materials Research*, 1025 - 102, 891-896.
- Ho, C., Lang, Z. Q., Sapinski, B., & Billings, S. A. (2013). Vibration isolation using nonlinear damping implemented by a feedback-controlled MR damper. *Smart Materials and Structures*, 22(10).
- Hong, S.-R., John, S., Wereley, N. M., Choi, Y.-T., & Choi, S.-B. (2007). A unifying perspective on the quasi-steady analysis of magnetorheological dampers. *Journal of Intelligent Material Systems and Structures*.
- Hong, S., Wereley, N., Choi, Y., & Choi, S. (2008). Analytical and experimental validation of a nondimensional Bingham model for mixed-mode magnetorheological dampers. *Journal of Sound and Vibration*, 312(3), 399-417.
- Hosseinloo, A. H., Vahdati, N., & Yap, F. F. (2011). *Elimination of spades in wheeled military vehicles using MR-fluid dampers*. Paper presented at the SPIE Smart Structures and Materials+ Nondestructive Evaluation and Health Monitoring.
- Housner, G. W., Bergman, L. A., Caughey, T. K., Chassiakos, A. G., Claus, R. O., Masri, S. F., . . . Yao, J. T. P. (1997). Structural control: past, present, and future. *Journal of Engineering Mechanics*, vol. 123, 897-971.

- Hrovat, D., Barak, P., & Rabins, M. (1983). Semi- Active versus Passive or Active Tuned Mass Dampers for Structural Control. *Journal of Engineering Mechanics*, 109, 691-705.
- Hu, G. L., Liu, Q. J., Ding, R. Q., & Li, G. (2017). Vibration control of semi-active suspension system with magnetorheological damper based on hyperbolic tangent model. *Advances in Mechanical Engineering*, 9(5).
- Hu, Y., Chen, M. Z. Q., & Shu, Z. (2014). Passive vehicle suspensions employing inerters with multiple performance requirements. *Journal of Sound and Vibration*, 333, 2212-2225.
- Huang, D. S., Zhang, J. Q., & Liu, Y. L. (2018). The PID Semi-Active Vibration Control on Nonlinear Suspension System with Time Delay. *International Journal of Intelligent Transportation Systems Research*, 16(2), 125-137.
- Imaduddin, F., Mazlan, S. A., & Zamzuri, H. (2013). A design and modelling review of rotary magnetorheological damper. *Materials & Design*, 51, 575-591.
- Ishugah, T. F., Li, Y., Wang, R. Z., & Kiplagat, J. K. (2014). Advances in wind energy resource exploitation in urban environment: A review. *Renewable & Sustainable Energy Reviews*, 37, 613-626.
- Islam, M. R., Mekhilef, S., & Saidur, R. (2013). Progress and recent trends of wind energy technology. *Renewable & Sustainable Energy Reviews*, 21, 456-468.
- Jean, P., Ohayon, R., & Le Bihan, D. (2005). Payload/launcher vibration isolation: MR dampers modeling with fluid compressibility and inertia effects through continuity and momentum equations. *International Journal of Modern Physics B*, 19(7-9), 1534-1541.
- Jiang, W., Zhang, Y., Xuan, S., Guo, C., & Gong, X. (2011). Dimorphic magnetorheological fluid with improved rheological properties. *Journal of Magnetism and Magnetic Materials*, 323(24), 3246-3250.
- Jin, G., Sain, M. K., & Spencer Jr, B. F. (2005). Nonlinear blackbox modeling of MR-dampers for civil structural control. *Control Systems Technology, IEEE Transactions on*, 13(3), 345-355.

- Johnson, C. D., & Kienholz, D. A. (1982). Finite element prediction of damping in structures with constrained viscoelastic layers. *AIAA Journal*, 20(9), 1284-1290.
- Kamath, G. M., Hurt, M. K., & Wereley, N. M. (1996). Analysis and testing of Bingham plastic behavior in semi-active electrorheological fluid dampers. *Smart Materials and Structures*, 5(5), 576.
- Kameyama, T., Tsujita, T., Konno, A., Jiang, X., Abiko, S., & Uchiyama, M. (2014). *Displaying cutting force of soft tissue using MR fluid for surgical simulators*. Paper presented at the Haptics Symposium (HAPTICS), 2014 IEEE.
- Karimi, H., Zapateiro, M., & Luo, N. (2010). Semiactive vibration control of offshore wind turbine towers with tuned liquid column dampers using H_∞ output feedback control. *IEEE International Conference on Control Applications*. Yokohama.
- Katsanis, G. R. (2013). *Transient small wind turbine tower structural analysis with coupled rotor dynamic interaction*. (Master of Science), California Polytechnic State University, USA.
- Kim, K.-J., Lee, C.-W., & Koo, J.-H. (2008). Design and modeling of semi-active squeeze film dampers using magneto-rheological fluids. *Smart Materials and Structures*, 17(3), 035006.
- King, M. (2013). Comparison of two suspension control strategies for multi-axle heavy truck. *Journal of Central South University*, 20(2), 550-562.
- Kirkegaard, P. H., Nielsen, S. R. K., Poulsen, B. L., Andersen, J., Pedersen, L. H., & Pedersen, B. J. (2002). Semiactive vibration control of a wind turbine tower using an MR damper. In H. Grundmann, & G. I. Schuëller (Eds.), *Structural Dynamics*: Rotterdam: Balkema Publishers, A.A. / Taylor & Francis The Netherlands.
- Kothera, C., Ngatu, G., & Wereley, N. M. (2011). Control evaluations of semiactive fluid-elastomeric helicopter lag damper. *Journal of Guidance, Control, and Dynamics*, 34(4), 1143-1156.
- Krenk, S., Svendsen, M. N., & Høgsberg, J. (2012). Resonant Vibration Control of Three-Bladed Wind Turbine Rotors. *AIAA Journal*, 50, 148-161.
- Kulkarni, S., Jadhav, D., & Khadke, P. (2012). Passive Control Systems for Tall Structures. *International Journal on Theoretical and Applied Research in Mechanical Engineering (IJTARME)*, 1, 87-91.

- Kumbhar, B. K., Patil, S. R., & Sawant, S. M. (2015). Synthesis and characterization of magneto-rheological (MR) fluids for MR brake application. *Engineering Science and Technology, an International Journal*, 18(3), 432-438.
- Laalej, H., Lang, Z., Sapinski, B., & Martynowicz, P. (2012). MR damper based implementation of nonlinear damping for a pitch plane suspension system. *Smart Materials and Structures*, 21(4), 045006.
- Laalej, H., Lang, Z. Q., Sapinski, B., & Martynowicz, P. (2012). MR damper based implementation of nonlinear damping for a pitch plane suspension system. *Smart Materials and Structures*, 21(4).
- Lackner, M. A., & Rotea, M. A. (2011a). Passive structural control of offshore wind turbines. *Wind Energy*, 14, 373-388.
- Lackner, M. A., & Rotea, M. A. (2011b). Structural control of floating wind turbines. *Mechatronics*, 21, 704-719.
- Lahimer, A. A., Alghoul, M. A., Yousif, F., Razykov, T. M., Amin, N., & Sopian, K. (2013). Research and development aspects on decentralized electrification options for rural household. *Renewable and Sustainable Energy Reviews*, 24, 314-324.
- Leary, J., While, A., & Howell, R. (2012). Locally manufactured wind power technology for sustainable rural electrification. *Energy Policy*, 43, 173-183.
- Lee, D.-Y., Choi, Y.-T., & Wereley, N. M. (2002). Performance analysis of ER/MR impact damper systems using Herschel-Bulkley model. *Journal of Intelligent Material Systems and Structures*, 13(7-8), 525-531.
- Lee, D.-Y., & Wereley, N. M. (1999). Quasi-steady Herschel-Bulkley analysis of electro- and magneto-rheological flow mode dampers. *Journal of Intelligent Material Systems and Structures*, 10(10), 761-769.
- Lee, D.-Y., & Wereley, N. M. (2000). *Analysis of electro-and magneto-rheological flow mode dampers using Herschel-Bulkley model*. Paper presented at the SPIE's 7th Annual International Symposium on Smart Structures and Materials.
- Li, C., Zhuang, T. Y., Zhou, S. T., Xiao, Y. Q., & Hu, G. (2017). Passive Vibration Control of a Semi-Submersible Floating Offshore Wind Turbine. *Applied Sciences-Basel*, 7(6).

- Li, J., Zhang, Z., & Chen, J. (2012). Experimental study on vibration control of offshore wind turbines using a ball vibration absorber. *Energy & Power Engineering*, 2012, 153-157.
- Li, L., Song, G., & Ou, J. (2010). A Genetic Algorithm-based Two-phase Design for Optimal Placement of Semi-active Dampers for Nonlinear Benchmark Structure. *Journal of Vibration and Control*, 16(9), 1379-1392.
- Lignarolo, L. E. M., Ragni, D., Krishnaswami, C., Chen, Q., Simão Ferreira, C. J., & van Bussel, G. J. W. (2014). Experimental analysis of the wake of a horizontal-axis wind-turbine model. *Renewable Energy*, 70, 31-46.
- Lin, C. J., Lee, C. Y., & Liu, Y. (2017). Vibration Control Design for a Plate Structure with Electrorheological ATVA Using Interval Type-2 Fuzzy System. *Applied Sciences-Basel*, 7(7).
- Luo, N., Pacheco, L., Vidal, Y., & Li, H. (2012). Smart Structural Control Strategies for Offshore Wind Power Generation with Floating Wind Turbines. *International Conference on Renewable Energies and Power Quality*.
- Ma, G. L., Gao, B., Xu, M. L., & Feng, B. (2018). Active Suspension Method and Active Vibration Control of a Hoop Truss Structure. *ALAA Journal*, 56(4), 1689-1695.
- Makris, N., Burton, S. A., Hill, D., & Jordan, M. (1996). Analysis and design of ER damper for seismic protection of structures. *Journal of Engineering Mechanics*, 122(10), 1003-1011.
- Makris, N., Burton, S. A., & Taylor, D. P. (1996). Electrorheological damper with annular ducts for seismic protection applications. *Smart Materials and Structures*, 5(5), 551.
- Malaya, U. o. (2014). Outdoor lighting using wind-solar hybrid renewable energy sources *ScienceDaily*: Sciencedaily.
- Martynowicz, P. (2015). Vibration control of wind turbine tower-nacelle model with magnetorheological tuned vibration absorber. *Journal of Vibration and Control*, 1077546315591445.

- Martynowicz, P. (2016). Study of vibration control using laboratory test rig of wind turbine tower-nacelle system with MR damper based tuned vibration absorber. *Bulletin of the Polish Academy of Sciences-Technical Sciences*, 64(2), 347-359.
- Martynowicz, P. (2017). Control of a magnetorheological tuned vibration absorber for wind turbine application utilising the refined force tracking algorithm. *Journal of Low Frequency Noise Vibration and Active Control*, 36(4), 339-353.
- Martynowicz, P., & Szydło, Z. (2013). Wind turbine's tower-nacelle model with magnetorheological tuned vibration absorber. *14th International Carpathian Control Conference*.
- Mensah, A. F., & Dueñas-Osorio, L. (2014). Improved reliability of wind turbine towers with tuned liquid column dampers (TLCs). *Structural Safety*, 47, 78-86.
- Miah, M. S., Chatzi, E. N., & Weber, F. (2015). Semi-active control for vibration mitigation of structural systems incorporating uncertainties. *Smart Materials and Structures*, 24(5).
- Murtagh, P. J., Basu, B., & Broderick, B. M. (2005). Along-wind response of a wind turbine tower with blade coupling subjected to rotationally sampled wind loading. *Engineering structures*, 27, 1209-1219.
- Murtagh, P. J., Ghosh, A., B. Basu, & Broderick, B. M. (2008). Passive control of wind turbine vibrations including blade/tower interaction and rotationally sampled turbulence. *Wind Energy*, 11, 305-317.
- Negm, H. M., & Maalawi, K. Y. (2000). Structural design optimization of wind turbine towers. *Computers & Structures*, 74(6), 649-666.
- Nguyen, S. D., Kim, W., Park, J., & Choi, S. B. (2017). A new fuzzy sliding mode controller for vibration control systems using integrated-structure smart dampers. *Smart Materials and Structures*, 26(4).
- Nicholas, J. G., & Nakanishi, H. (Producer). (2015). Computational Physics. Retrieved from http://www.paykin.info/irina/project_1.jsp
- Okubo, H., Yano, H., & Itoh, T. (2014). Semi-active vibration suppression for smart structures with sliding-mode control. *Journal of Intelligent Material Systems and Structures*, 25 865-870.

- Oliveira, F., Brito, J. d., & Avila, S. (2013). Design criteria for a pendulum absorber to control high building vibrations. *11th International Conference on Vibration Problems*. Lisbon.
- Phillips, R. W. (1969). *Engineering applications of fluids with a variable yield stress*. University of California, Berkeley.
- Pirner, M. (2002). Actual behaviour of a Ball Vibration Absorber. *Wind Engineering and Industrial Aerodynamics*, 90, 987-1005.
- Pope, K., Dincer, I., & Naterer, G. F. (2010a). Energy and exergy efficiency comparison of horizontal and vertical axis wind turbines. *Renewable Energy*, 35(9), 2102-2113.
- Pope, K., Dincer, I., & Naterer, G. F. (2010b). Energy and exergy efficiency comparison of horizontal and vertical axis wind turbines. *Renewable Energy*, 35, 2102-2113.
- Powell, L. A., Hu, W., & Wereley, N. M. (2013). Magnetorheological fluid composites synthesized for helicopter landing gear applications. *Journal of Intelligent Material Systems and Structures*, 1045389X13476153.
- Poynor, J. C. (2001). *Innovative designs for magneto-rheological dampers*. Virginia Polytechnic Institute and State University, Blacksburg, USA.
- Qian, L. J., Liu, B., Chen, P., & Bai, X. X. (2016). *An inverse model for magnetorheological dampers based on a restructured phenomenological model*. Paper presented at the Active and Passive Smart Structures and Integrated Systems, Las Vegas, Nevada, United States.
- Rajagopalan, R. G., & Fanucci, J. B. (1985). Finite-Difference Model for Vertical Axis Wind Turbines. *Journal of Propulsion and Power*, 1(6), 432-436.
- Rao, V. (2013). Experimental and numerical studies on tuned liquid damper.
- Roderick, C. (2012). Vibration Reduction of Offshore Wind Turbines Using Tuned Liquid Column Dampers.
- Ros, N. F. M., Saad, M. S., & Darus, I. Z. M. (2015). Dynamic Modeling and Active Vibration Control of a Flexible Beam: A Review. *International Journal of Engineering & Technology*, 15(5), 12-17.

- Rotea, M., Lackner, M., & Saheba, R. (2010). Active structural control of offshore wind turbines. *48th AIAA Aerospace Science Meeting and Exhibit*. Orlando, Florida.
- Sakai, F., Takaeda, S., & Tamaki, T. (1989). Tuned liquid column damper—new type device for suppression of building vibration. *Proceedings of International Conference on High-rise Buildings*. Nanjing, China.
- Sales, T. P., Rade, D. A., & de Souza, L. C. G. (2013). Passive vibration control of flexible spacecraft using shunted piezoelectric transducers. *Aerospace Science and Technology*, 29, 403-412.
- Scheurich, F., & Brown, R. E. (2013). Modelling the aerodynamics of vertical-axis wind turbines in unsteady wind conditions. *Wind Energy*, 16, 91-107.
- Sedaghat, A., & Mirhosseini, M. (2012). Aerodynamic design of a 300kW horizontal axis wind turbine for province of Semnan. *Energy Conversion and Management*, 63, 87-94.
- Setareh, M., Ritchey, J., Baxter, A., & Murray, T. (2006). Pendulum tuned mass dampers for floor vibration control. *Journal of Performance of Constructed Facilities*, 20, 64-73.
- Shikha, Bhatti, T. S., & Kothari, D. P. (2005). Early Development of Modern Vertical and Horizontal Axis Wind Turbines: A Review. *Wind Engineering*, 29(3), 287-299.
- Singh, H. J., & Wereley, N. M. (2014). Optimal control of gun recoil in direct fire using magnetorheological absorbers. *Smart Materials and Structures*, 23(5), 055009.
- Song, B. K., An, J. H., & Choi, S. B. (2017). A New Fuzzy Sliding Mode Controller with a Disturbance Estimator for Robust Vibration Control of a Semi-Active Vehicle Suspension System. *Applied Sciences-Basel*, 7(10).
- Song, X., Ahmadian, M., Southward, S., & Miller, L. (2007). Parametric study of nonlinear adaptive control algorithm with magneto-rheological suspension systems. *Communications in Nonlinear Science and Numerical Simulation*, 12(4), 584-607.
- Song, X., Ahmadian, M., & Southward, S. C. (2005). Modeling magnetorheological dampers with application of nonparametric approach. *Journal of Intelligent Material Systems and Structures*, 16(5), 421-432.

- Soong, T. T., Reinhorn, A. M., Wang, Y. P., Lin, R. C., & Riley, M. (1992). Full scale implementation of Active structural control. *Earthquake Engineering. Tenth World Conference*. Balhema, Rotterdam: Balhema, Rotterdam.
- Soong, T. T., & Spencer Jr, B. F. (2002). Supplemental energy dissipation : state-of-the-art and state-of-the- practice. *Engineering structures*, 24, 243-259.
- Spencer, B. F., Dyke, S. J., Sain, M. K., & Carlson, J. D. (1997). Phenomenological model for magnetorheological dampers. *Journal of Engineering Mechanics-Asce*, 123(3), 230-238.
- Spencer, J. B. F., Dyke, S. J., Sain, M. K., & Carlson, J. D. (1996). Phenomenological Model of a Magnetorheological Damper. *Journal of Engineering Mechanics*, 1-23.
- Spencer Jr, B. F., Yang, G., Carlson, J. D., & Sain, M. K. (1998). *Smart dampers for seismic protection of structures: a full-scale study*. Paper presented at the Proceedings of the second world conference on structural control.
- Staino, A., & Basu, B. (2013a). Dynamics and control of vibrations in wind turbines with variable rotor speed. *Engineering structures*, 56, 58-67.
- Staino, A., & Basu, B. (2013b). A robust controller with active tendons for vibration mitigation in wind turbine rotor blades. *Proceedings of the International Symposium on Engineering under Uncertainty: Safety Assessment and Management (ISEUSAM - 2012)*. India: Springer India.
- Stewart, G. M. (2012). Load reduction of floating wind turbines using tuned mass dampers.
- Su, T. S., Hung, C. F., Chang, S. H., Wu, T. H., & Chang, L. M. (2014). Efficient Vibration Control with a Semi-Active Vibration Absorber in a Semiconductor Fab. *Applied Mechanics and Materials*, 564, 143-148.
- Sun, L. L., Hansen, C. H., & Doolan, C. (2015). Evaluation of the performance of a passive-active vibration isolation system. *Mechanical Systems and Signal Processing*, 50-51, 480-497.

- Sung, K.-G., Choi, S.-B., & Park, M.-K. (2011). Geometry optimization of magnetorheological damper for vehicle suspension via finite element method. *Advanced Science Letters*, 4(3), 805-809.
- Symans, M. D., Charney, F. a., Whittaker, a. S., Constantinou, M. C., Kircher, C. a., Johnson, M. W., & McNamara, R. J. (2008). Energy Dissipation Systems for Seismic Applications: Current Practice and Recent Developments. *Journal of Structural Engineering*, 134, 3-21.
- Symans, M. D., & Constantinou, M. C. (1999). Semi-active control systems for seismic protection of structures: a state-of-the-art review. *Engineering structures*, 21(6), 469-487.
- Tang, X., Du, H., Sun, S., Ning, D., Xing, Z., & Li, W. (2017). Takagi-Sugeno Fuzzy Control for Semi-Active Vehicle Suspension With a Magnetorheological Damper and Experimental Validation. *IEEE/ASME Transactions on Mechatronics*, 22(1), 291-300.
- Taskin, Y., Yuksek, I., & Yagiz, N. (2017). Vibration control of vehicles with active tuned mass damper. *Journal of Vibroengineering*, 19(5), 3533-3541.
- Taylor, K., Leong, C. M., & Amitay, M. (2015). Load control on a dynamically pitching finite span wind turbine blade using synthetic jets. *Wind Energy*, 18(10), 1759-1775.
- Thenozhi, S., & Yu, W. (2014). Stability analysis of active vibration control of building structures using PD/PID control. *Engineering structures*, 81, 208-218.
- Togun, H., Abdulrazzaq, T., Kazi, S., Badarudin, A., Kadhum, A., & Sadeghinezhad, E. (2014). A review of studies on forced, natural and mixed heat transfer to fluid and nanofluid flow in an annular passage. *Renewable and Sustainable Energy Reviews*, 39, 835-856.
- Tsang, H., Su, R., & Chandler, A. (2006). Simplified inverse dynamics models for MR fluid dampers. *Engineering structures*, 28(3), 327-341.
- Tsujita, T., Ohara, M., Sase, K., Konno, A., Nakayama, M., Abe, K., & Uchiyama, M. (2012). *Development of a haptic interface using mr fluid for displaying cutting forces of soft tissues*. Paper presented at the Robotics and Automation (ICRA), 2012 IEEE International Conference on.

- Velázquez, M., Carmen, M., Pacheco, L., & Eslava, G. (2014). Design and Experimentation of a 1 MW Horizontal Axis Wind Turbine. *Journal of Power and Energy Engineering*, 2, 9-16.
- Vita, L., Paulsen, U. S., Madsen, H. A., Nielsen, P. H., Berthelsen, P. A., & Carstensen, S. (2013). Design and Aero-Elastic Simulation of a 5mw Floating Vertical Axis Wind Turbine. *Proceedings of the Asme 31st International Conference on Ocean, Offshore and Arctic Engineering*, Vol 7, 383-392.
- Wang, D., & Liao, W. (2005). Modeling and control of magnetorheological fluid dampers using neural networks. *Smart Materials and Structures*, 14(1), 111.
- Wang, D., & Liao, W. H. (2011). Magnetorheological fluid dampers: a review of parametric modelling. *Smart Materials and Structures*, 20(2), 023001.
- Wang, S., & Li, N. (2013). Semi-active vibration control for offshore platforms based on LQG method. *Journal of Marine Science and Technology*, 21, 562-568.
- Wang, X., & Gordaninejad, F. (2000). *Field-controllable electro-and magneto-rheological fluid dampers in flow mode using Herschel-Bulkley theory*. Paper presented at the SPIE's 7th Annual International Symposium on Smart Structures and Materials.
- Wang, Z., & Keogh, P. (2018). Active Vibration Control for Robotic Machining. *Proceedings of the Asme International Mechanical Engineering Congress and Exposition, 2017, Vol 2*.
- Wang, Z. H., Chen, Z. Q., Gao, H., & Wang, H. (2018). Development of a Self-Powered Magnetorheological Damper System for Cable Vibration Control. *Applied Sciences-Basel*, 8(1).
- Werapun, W., Tirawanichakul, Y., Kongnakorn, W., & Waewsak, J. (2014). An Assessment of Offshore Wind Energy Potential on Phangan Island by in Southern Thailand. *Energy Procedia*, 52, 287-295.
- Wereley, N., Cho, J., Choi, Y., & Choi, S. (2008). Magnetorheological dampers in shear mode. *Smart Materials and Structures*, 17(1), 015022.
- Wereley, N. M., Hu, W., Kothera, C. S., Chen, P. C.-H., & Ngatu, G. T. (2013). United States Patent No.

Wereley, N. M., & Pang, L. (1998). Nondimensional analysis of semi-active electrorheological and magnetorheological dampers using approximate parallel plate models. *Smart Materials and Structures*, 7(5), 732.

Application of Tuned Liquid Column Dampers in Wind Turbines (2005).

Won, A. Y. J., Pires, J. A., & Haroun, M. A. (1997). Performance assessment of tuned liquid column dampers under random seismic loading. *International Journal for Non-Linear Mechanics*, 32, 745-758.

Wu, D., Huang, L., Pan, B., Wang, Y., & Wu, S. (2014). Experimental study and numerical simulation of active vibration control of a highly flexible beam using piezoelectric intelligent material. *Aerospace Science and Technology*, 37, 10-19.

Xie, H.-L., Liang, Z.-Z., Li, F., & Guo, L.-X. (2010). The knee joint design and control of above-knee intelligent bionic leg based on magneto-rheological damper. *International Journal of Automation and Computing*, 7(3), 277-282.

Xie, Z., Wong, P. K., Zhao, J., Xu, T., Wong, K. I., & Wong, H. C. (2013). A noise-insensitive semi-active air suspension for heavy-duty vehicles with an integrated fuzzy-wheelbase preview control. *Mathematical Problems in Engineering*, 2013.

Xue, X. M., Wu, X. H., & Sun, Q. (2017). Active Vibration Control of Cantilever Beam with Macro-Fibre Composite Actuator Using Time-Delayed Genetic Algorithm Controller. *International Journal of Acoustics and Vibration*, 22(3), 307-319.

Yang, L., Chen, S. Z., Zhang, B., & Feng, Z. Z. (2011). *A rotary magnetorheological damper for a tracked vehicle*. Paper presented at the Advanced Materials Research.

Yang, Z. J., Gu, Y. Z., Li, M., Li, Y. X., Lu, J., & Zhang, Z. G. (2014). Design and Analysis of Small-Scale Lift-Type Vertical-Axis Wind Turbine Using Composite Blade. *Polymers & Polymer Composites*, 22(4), 423-430.

Yazid, I. I. M., Mazlan, S. A., Kikuchi, T., Zamzuri, H., & Imaduddin, F. (2014). Design of magnetorheological damper with a combination of shear and squeeze modes. *Materials & Design*, 54, 87-95.

Yildiz, A. S., & Sivrioglu, S. (2016). Semi-active Vibration Control of Lateral and Rolling Motions for a Straddle Type Monorail Vehicle. *Ifac Papersonline*, 49(3), 279-284.

- Yildiz, A. S., Sivrioglu, S., Zergeroglu, E., & Cetin, S. (2013). *Adaptive control of semiactive quarter car model with MR damper*. Paper presented at the Control Conference (ASCC), 2013 9th Asian.
- Yu, H., Gillot, F., & Ichchou, M. (2013). Reliability based robust design optimization for tuned mass damper in passive vibration control of deterministic/uncertain structures. *Journal of Sound and Vibration*, 332, 2222-2238.
- Zhang, H., Wang, R., Wang, J., & Shi, Y. (2014). Robust finite frequency static-output-feedback control with application to vibration active control of structural systems. *Mechatronics*, 24, 354-366.
- Zhang, J., Feng, Z., & Jing, Q. (2009). *Optimization analysis of a new vane MRF damper*. Paper presented at the Journal of Physics: Conference Series.
- Zhang, X. T., Zhang, R. C., & Xu, Y. L. (1993). Analysis on control of flow-induced vibration by tuned liquid damper with crossed tube-like containers. *Journal of Wind Engineering and Industrial Aerodynamics*, 50, 351-360.
- Zhang, Z.-L., Chen, J.-B., & Li, J. (2013). Theoretical study and experimental verification of vibration control of offshore wind turbines by a ball vibration absorber. *Structure and Infrastructure Engineering*, 1-14.
- Zhang, Z., Basu, B., & Nielsen, S. R. K. (2014). Tuned liquid column dampers for mitigation of edgewise vibrations in rotating wind turbine blades. *Structural Control and Health Monitoring*, n/a--n/a.
- Zhang, Z., Basu, B., & Nielsen, S. R. K. (2015). Tuned liquid column dampers for mitigation of edgewise vibrations in rotating wind turbine blades. *Structural Control & Health Monitoring*, 22(3), 500-517.
- Zhao, S., Deng, H., Zhang, J., Sun, S., Li, W., & Wang, L. (2013). Variable stiffness and damping semi-active vibration control technology based on magnetorheological fluids. *Sixth International Symposium on Precision Mechanical Measurements*.
- Zhu, X. C., Jing, X. J., & Cheng, L. (2012). Magnetorheological fluid dampers: A review on structure design and analysis. *Journal of Intelligent Material Systems and Structures*, 23(8), 839-873.

LIST OF PUBLICATIONS AND PAPERS PRESENTED

Journals:

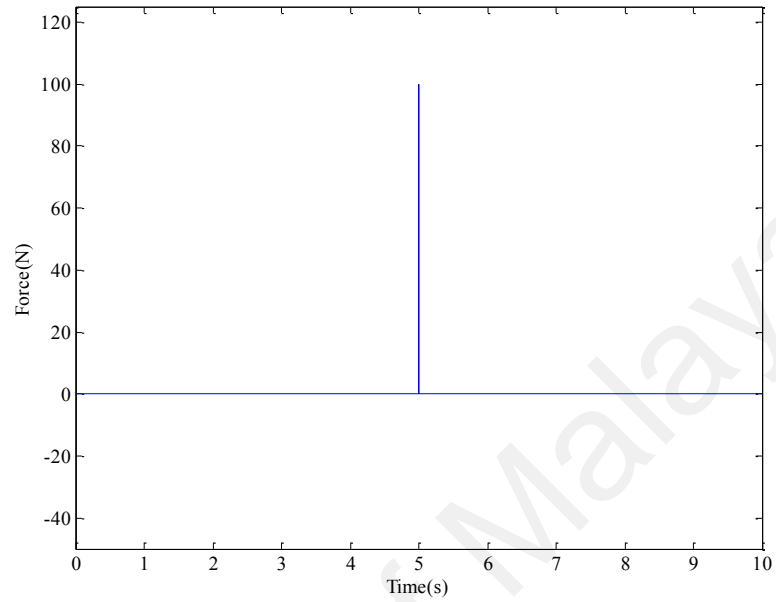
1. **M Rahman**, ZC Ong, WT Chong, S Julai, WX Ng (2018), Wind turbine tower modeling and vibration control using ant colony optimized PID controller, *Arabian Journal of Science and Engineering*, <https://doi.org/10.1007/s13369-018-3190-6> (ISI indexed journal)
2. **M Rahman**, ZC Ong, S Julai, MF Ferdaus, Raju Ahamed (2017), A Review of advances in Magneto Rheological Dampers: their design optimization and applications, *Journal of Zhejiang University-SCIENCE A*, Vol. 18(12), page 991-1010 (ISI indexed journal)
3. **M Rahman**, ZC Ong, WT Chong, S Julai, SY Khoo (2015), Performance enhancement of wind turbine systems with vibration control: A review, *Renewable and Sustainable Energy Reviews*, Vol. 51, page 43-51 (ISI indexed journal)
4. **M Rahman**, ZC Ong, WT Chong, S Julai, SY Khoo (2018), Smart Semi-active PID control strategy of tower vibration in Wind Turbines with Magnetorheological damper, *Journal of Earthquake Engineering, and Engineering Vibration*, (Under Review-manuscript no.)
5. **M Rahman**, ZC Ong, WT Chong, S Julai (2018), Implementation of semi-active MR damper to mitigate wind turbine tower vibration with PID-ACO optimized control force, *Structural control & health monitoring*. (Under Review-manuscript no.)

Conferences proceedings

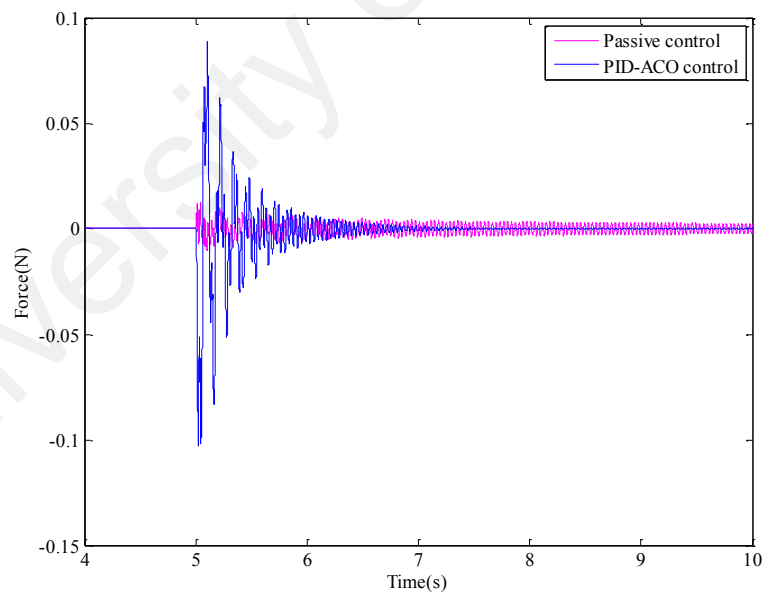
1. **M Rahman**, ZC Ong, WT Chong, S Julai, & R Ahamed (2017), Experimental Investigation of Nonlinear Characteristics of a Smart Fluid Damper, 3rd International Conference on the Science and Engineering of Materials (ICoSEM), 24-25 October 2017, Kuala Lumpur, Malaysia
2. MR Sarkar, S Julai, WT Chong, ZC Ong, **M Rahman** (2015), Mathematical modelling, and simulation of induction generator-based wind turbine in matlab/Simulink, *ARPN Journal of Engineering and Applied Sciences*, Vol. 10(22), Dec 2015 (Scopus indexed journal)

APPENDIX A

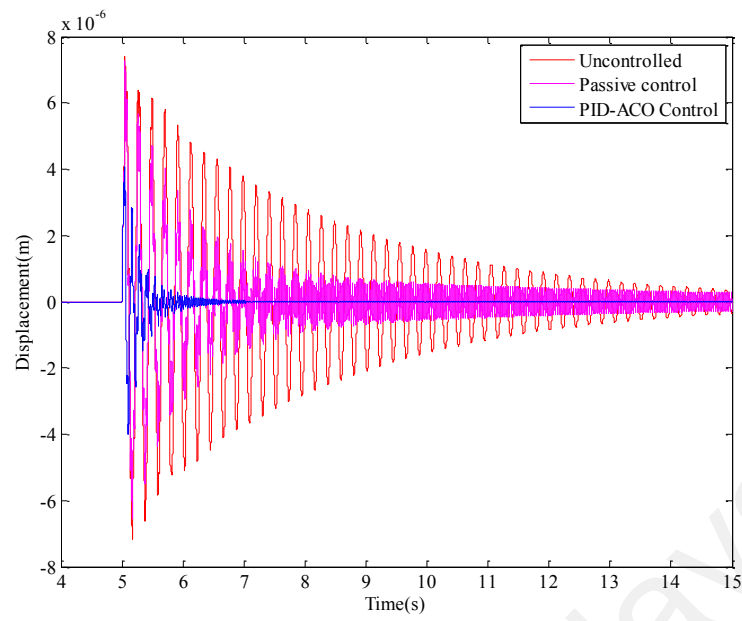
Appendix A: Effectiveness of PID-ACO controller for vibration control of wind turbine tower under different loadings.



(a)

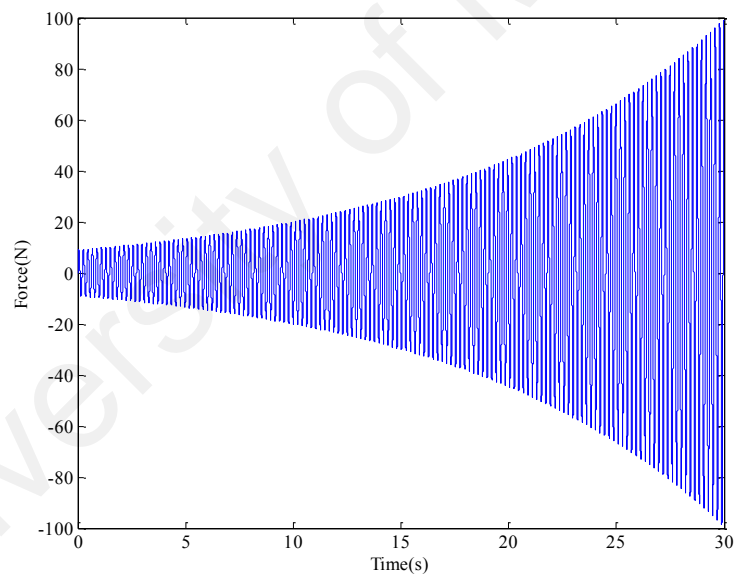


(b)

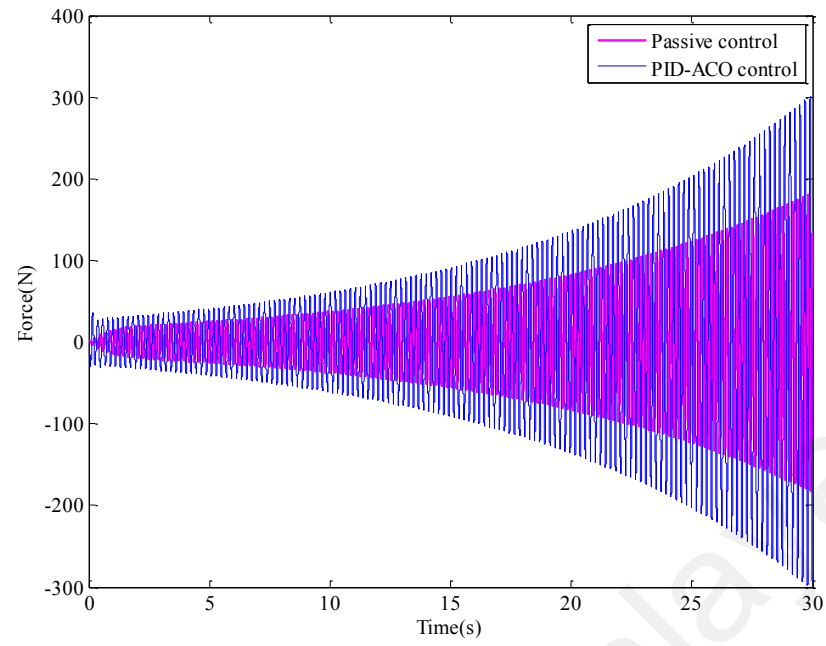


(c)

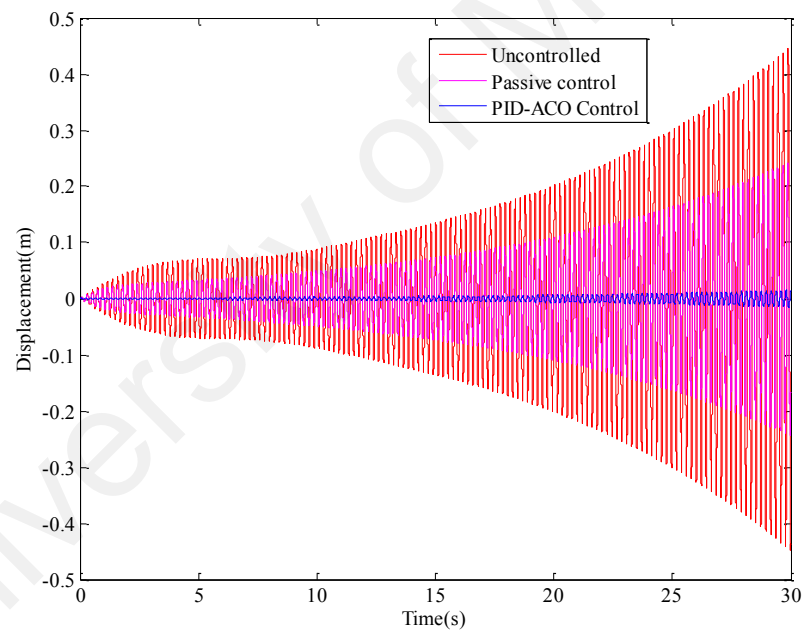
Appendix A.1: Controlled and uncontrolled response of 20th element of the tower for impulse disturbance



(a)



(b)

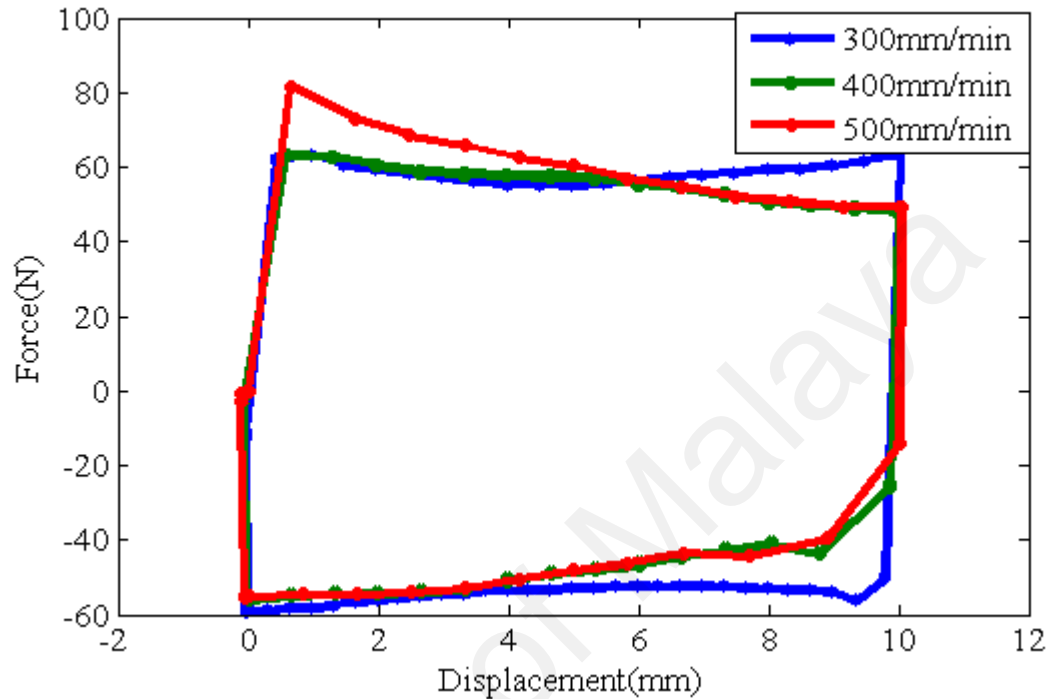


(c)

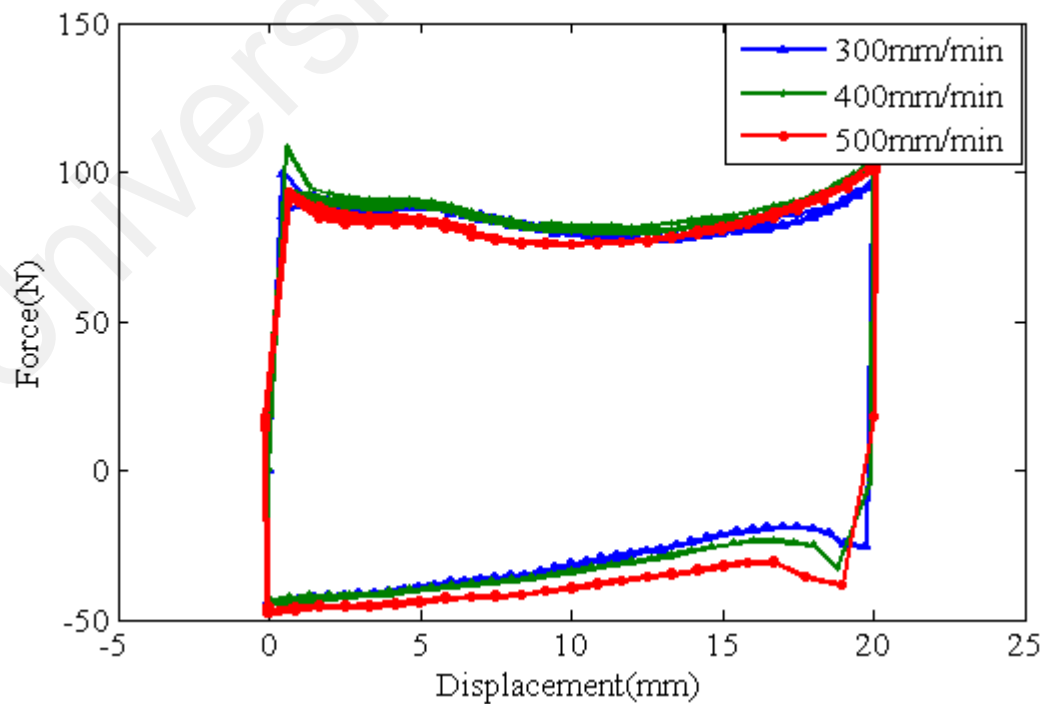
Appendix A.2: Controlled and uncontrolled response of 20th element of the tower for negatively damped sinusoidal turbulent disturbance

APPENDIX B

Appendix B: Experimental result for nonlinear characteristics of MR damper under different stroke lengths and velocities



Appendix B.1: Force-displacement curve of MR damper under 10 mm stroke length and different velocities



Appendix B.2: Force-displacement curve of MR damper under 20 mm stroke length and different velocities